Characterization of Counterion Effects of Gemini Surfactants and *In vitro* Studies of Transfection Efficiency for Gene Therapy in Epithelial Ovarian Cancer

by

Muhammad Shahidul Islam

A thesis

presented to the University of Waterloo

in fulfillment of the

thesis requirement for the degree of

Master of Science

in

Pharmacy

Waterloo, Ontario, Canada, 2015

AUTHOR'S DECLARATION

I hereby declare that I am the sole author of this thesis. This is a true copy of the thesis, including any required final revisions, as accepted by my examiners.

I understand that my thesis may be made electronically available to the public.

ABSTRACT

Gene therapy has emerged as a promising strategy for the treatment or prevention of many acquired or genetic diseases that are considered incurable at the present time. Although viral and non-viral vector approaches are the major techniques employed for somatic gene transfer, non-viral vectors (cationic liposomes, dendrimers, chitosans, polymers & surfactants) have attracted great interest recently, due to their unique properties. A number of non-viral carriers have been extensively investigated and developed in recent years for targeted drug delivery or gene therapy in various pre-clinical/clinical trials. Despite this, the quest for new non-viral carriers with improved transfection and low toxicity is still proceeding, driven by a need to overcome safety concerns associated with viral vectors. Of the non-viral vectors, an intriguing class of building blocks which has elicited extensive interest are the third generation di-cationic surfactants: a class of bis-surfactants called "gemini surfactants (GSs)". The interest is due to their unique self-assembly, hundredfold lower CMC (compared to their monomeric counterparts), thousand-fold improved surface activity, and ability to form a rich array of aggregate morphologies. In this project, the effect of various inorganic and organic counterions on micellization was studied and analyzed at air–water surfaces as well as in bulk solutions. Additionally, the size & zeta potential of the nanoparticles, and the in vitro transfection efficiency studies in human ovarian cancer cell lines were also analysed to investigate the dominant influence of the anions on the aggregation behavior and DNA delivery efficiency of eight surfactants of the ethanediyl-α,ω-bis-(dimethylhexadecyl-ammonium) type, $[C_{16}H_{33}(CH_3)_2\text{-N-}(CH_2)_2\text{-N-}(CH_3)_2C_{16}H_{33}].2X^-$ referred to as gemini 16-2-16; where X refers to the counterion were studied. Counterions of chloride (Cl^-), bromide (Br^-), ½ malate ($C_4H_4O_5^{--}$), ½ tartrate ($C_4H_4O_6^{--}$), adenosine mono phosphate, AMP ($C_{10}H_{13}N_5O_7P^-$), guanosine mono phosphate, GMP ($C_{10}H_{13}N_5O_8P^-$), cytidine mono phosphate, CMP ($C_9H_{13}N_3O_8P^-$), and uridine mono phosphate, UMP ($C_9H_{12}N_2O_9P^-$) were investigated and were classified into three different categories depending on their nature: (1) small inorganic counterions [chloride (Cl^-), and bromide (Br^-)] taken from the Hofmeister series were studied to focus on the effect of ion type; (2) Hydroxy-alkyl di-carboxylate counterions [malate ($C_4H_4O_5^{--}$), and tartrate ($C_4H_4O_6^{--}$)] were studied to focus on the effect of the hydrophilicity of counterions; and (3) heterocyclic ring containing nucleotide mono phosphate counterions were included to focus on mainly self-

assembly and other parameters. We demonstrate the influence of different anions associated with this 16-2-16 series of gemini by analyzing the effect of counterions on the micellization and aggregation behavior of these gemini surfactants, characterized by determination of the critical micelle concentration (CMC), degree of micelle ionization (α), and free energy of micellization (ΔG_M) and are discussed in terms of the hydrophilicity of anions, counterion hydration, interfacial packing of ions, and ionic morphology. Our results clearly revealed that a counterion effect on micellization and aggregate morphology, attributed to the balancing and controlling forces of the counterions to the surfactant itself. Hydrogen bonding among the –OH groups of the counterions (where applicable) and water molecules, as well as the strong hydrophobic interaction among the hydrocarbon side chains is postulated to be the main origins for the unique aggregation behaviors of these gemini surfactants. These amphiphiles can form both micelles and vesicles spontaneously with a micelle-to-vesicle transition at a concentration above the respective CMC. Furthermore, the size & zeta potential characterizations along with the in vitro transfection data manifest the significant impact of counterions on the GSs as therapeutic drug delivery carrier. Our transfection efficiency (TE) data also demonstrated that the surface charge density of the particles formed by the GSs is the predominant factor for cellular uptake and consequent TE of the respective GSs.

ACKNOWLEDGEMENTS

First and foremost, I would like to convey my profound gratitude and earnest appreciation to Dr. Shawn David Wettig, Associate Professor of the School of Pharmacy, Faculty of Sciences; University of Waterloo for his expert supervision, constant inspiration, invaluable counseling, constructive instructions and concrete suggestions throughout the research work to solve the impediments that I encountered during my graduate studies. I would not be here without his expertise and innovative input which continues to spur my inquisitiveness and incessantly crusade me as an aspiring researcher. It has been an amazing experience to catch the opportunity for personal and professional growth, and an absolute honor to have a supervisor/mentor that I can rely on for advice and support now and, hopefully, in the foreseeable future.

I would like to thank my committee members: Dr. Praveen Nekkar and Dr. Paul Spagnuolo for all their encouragement and instructions to my research. Many thanks go to Dr. Roderick Slavcev (and Shirley, from his group), for providing the opportunity to use his resources and plasmids. As well, I would like to take the opportunity to thank Dr. Jonathan Blay for making graduate studies at the school of pharmacy a welcoming environment.

I had the opportunity to work with many of my fellow colleagues in Dr. Wettig's group. I would like to thank those members of for all their support. A very special thanks goes to Chi Hong Sum for his professional help, and extraordinary guidelines to conduct experiments throughout this program. It was always a pleasure working with you, Chi.

I am grateful for the continuing support, inspiration and tremendous patience from my loving wife for all the good/tough times and for my presence in the lab for unusually extended periods. My journey would not be complete and possible without her. So, "Thank you"!! I would like to express my gratitude to my parents for their endless love and blessings. Their blessing throughout all these years has gotten me through numerous tough and stressful times. Finally, I would like to thank my family (in-laws) and friends for their support.

Lastly, I am also thankful to Janet Venne (Department of Chemistry, University of Waterloo), Eric Lee from Dr. Spagnuolo's group for the assistance of NMR and Flow cytometer analysis, respectively.

"The happiest moments of my life have been the few which I have passed at home in the bosom of my family". – Thomas Jefferson

DEDICATION

To my family (wife and daughter), my parents and all my well-wishers!

"Call it a clan, call it a network, call it a tribe, call it a family. Whatever you call it, whoever you are, you need one".

– *Jane Howard (1935-1996) US journalist, writer*

TABLE OF CONTENTS

LIST OF FIGURES

LIST OF TABLES

LIST OF ABBREVIATIONS

ζ	Zeta potential
^{0}C	Degrees Celsius
A_{600}	Absorbance at 600 nm
AAV	Adeno associated virus
Ad5	Adenovirus serotype 5
AGE	Agarose gel electrophoresis
AFM	Atomic force microscopy
AMP	Adenosine monophosphate (salt) / Adenylic acid (acidic form)
Ap	Ampicillin antibiotic
APC	Antigen presenting cells
BAM	Brewster angle microscopy
bp	base pair
BRCA1/2	Breast cancer tumor suppressor gene
CAC	Critical aggregation concentration
CCC	Circular covalently closed
CCNE1	G1/S specific cyclin-E1protein encoding gene
CMC	Critical micelle concentration
CMP	Cytidine monophosphate (salt) / Cytidylic acid (acidic form)
CMV	Cytomegalovirus
CPP	Cell penetrating peptide
CTL	Cytotoxic T lymphocyte
DC-Chol	3β-[N-(N',N'-dimethylaminoethyl) carbamoyl] cholesterol
DEAE-D	Diethylaminoethyl Dextran
DLS / PCS	Dynamic light scattering / Photon correlation spectroscopy
DNA	Deoxyribonucleic acid
DOGS	Di-octadecyl-amido-glycyl-spermine
DOPE	1,2-Dioleoyl-sn-glycero-3-phosphatidylethanolamine
DOSPA	2,3-Dioleyloxy-N-[2(sperminecarboxamido)ethyl]-N,N-dimethyl-1-propanaminium trifluoroacetate

DOSPER	1,3-Dioleoyloxy-2-(6-carboxyspermyl)-propylamide)
DOTAP	N-[1-(2,3-Dioleoyloxy)propyl]-N,N,N-trimethylammonium methyl sulfate
DOTMA	N-[1-(2,3-Dioleyloxy)propyl]-N,N,N-trimethylammonium chloride
ds	Double stranded
E. coli	*Escherichia coli*
EGFP	Enhanced green fluorescent protein
EOC	Epithelial ovarian cancer
FBS	Fetal bovine serum
FIGO	International Federation of Gynecological and Obstetrics
FQ	Fluorescence quenching
GA / GS	Gemini amphiphile / gemini surfactant
GMP	Guanosine monophosphate (salt) / Guanidylic/Guanylic acid (acidic form)
GT	Gene therapy
H_I	Hexagonal phase structure
H^C_{II}	Inverted hexagonal phase structure
HNSCC	Head and neck squamous cell carcinoma
IFN-γ	Interferon-γ
IL12	Interleukin 12
ITC	Isothermal titration calorimetry
QAS	Quaternary ammonium salt
L^C_α	Lamellar phase structure
kb	kilobases
kDa	kilodalton
LB	Luria-Bertani
LDV	Laser Doppler velocimetry / micro-electrophoresis
LMO2	LIM domain only 2 protein (cysteine rich) encoding gene
MHC	Major histocompatibility complex
MLV	Multi lamellar vesicle
mRNA	Messenger RNA
m-s-m	N,N-Bis(dimethylalkyl)-α,ω-alkanediammonium surfactants
N^+/P^-	Nitrogen to phosphate charge ratio

NK	Natural killer cells
NLS	Nuclear localization signal
NPC	Nuclear pore complex
OC	Ovarian cancer
oriC	*E. coli* origin of replication
OTC	Ornithine transcarbamylase
OVCAR-3	Ovarian cancer cell line
CPP / *P*	Critical packing parameter
PAGA	Poly-[α-(4-aminobutyl)-L-glycolic acid]
PAMPs	Pathogen associated molecular patterns
PBS	Phosphate buffer saline
PDI	Polydispersity index
pDNA	Plasmid DNA
PEG	Polyethylene glycol
PEI	Polyethylenimine
PI	Propidium iodide
PLL	Poly-L-lysine
rpm / RPM	Rotations per minute
SCID-Xl	X-linked severe combined immunodeficiency
SD / SE	Standard deviation / Standard error
ss	Single stranded
SUV	Small unilamellar vesicle
SV40	Simian vacuolating virus 40 or Simian virus 40 (a polyomavirus)
TLR9	Toll-like receptor 9
TEM	Transmission electron microscopy
TP53 or *p53*	Tumor protein-53 or tumor suppressor protein-53 encoding gene
UMP	Uridine monophosphate (salt) / Uridylic acid (acidic form)

1. Introduction

1.1 Gene therapy background

Gene therapy (GT) represents a new paradigm for not only the therapeutic treatment of human genetic diseases, but also for drug delivery. Due to its potential for treating chronic disease and genetic disorders, gene therapy has drawn increasing attention in the medical, pharmaceutical and biotechnological sciences [1]. The purpose of gene therapy is to achieve a desired therapeutic effect in the treatment of a given disease, by delivery of a gene or genes in order to enable cells to generate therapeutic proteins [2]. Commonly, gene therapy involves the administration of nucleic acids (specific gene expression cassettes) with a specific delivery vehicle (also known as a vector) for the purpose of treating diseases associated with the absence, abnormal expression, or overexpression of specific genes or genetic elements by replacing, correcting or repressing the gene of interest [3-5]. Essential components for current gene therapy includes: a) an effective therapeutic gene that can be expressed at a target site, and b) an efficient and safe delivery system (vector) that delivers the therapeutic genes to a specific target tissue or organ [6]. Globally, two major types of gene therapy applications are widely accepted: viral vector mediated and non-viral vector mediated gene delivery. Each will be described in detail in the following sections.

1.1.1 Recent advances in viral vector based GTs

Viral vectors are the most efficient vectors currently being studied [7]. There are over 1,800 approved gene therapy clinical trials with viral vectors accounting for approximately two-thirds of all trials by June 2012 [8]. As of January 2014, 1,996 clinical trials were undertaken in 34 countries where approximately 72 % of the delivery systems employed are

different viral vectors (Figure-1.1) [9]. Viral vector assisted gene therapy technique exploits the natural ability of viruses to introduce their genetic cargo to the target cells, and depends on molecular biology methods to replace essential genes for viral replication, assembly, or infection [10].

Adenoviral vectors are the most commonly used viral vector due mainly to their high transfection efficiency, high expression, and infection of non-dividing cells [8]. For instance, in 2003 the State Food and Drug Administration of China approved gene therapy treatment, *Gendicine* (by SioBiono GeneTech), which utilized a recombinant human adenovirus to deliver the *p53* tumor suppressor gene for the treatment of head and neck squamous cell carcinoma (HNSCC). *Gendicine* is the world's first approved gene therapy product that has had tremendous success for cancer treatment [4, 7]. Additionally, in 2005, China also approved *Onocorine* (Sunway Biotech Co. Ltd), a conditionally replicative recombinant adenoviral vector for the treatment of late stage refractory nasopharyngeal cancer [4]. In the same year (September 2005), the State Food and Drug Administration of China approved a second drug based on gene therapy, *Endostar*, for treatment of cancerous tumours in the lungs and other organs [11]. The only adenoviral vector that has completed a phase-III clinical trial for the first time in European Union/Commission (EU/EC) was *Cerepro* (Ark Therapeutics Group plc), in 2008 [4]. Finally, in 2012 EC approved the gene therapeutic "*Glybera"* (UniQure), an adeno-associated viral vector delivering human lipoprotein lipase gene in muscle tissue for the treatment of lipoprotein lipase deficiency [4, 12, 13].

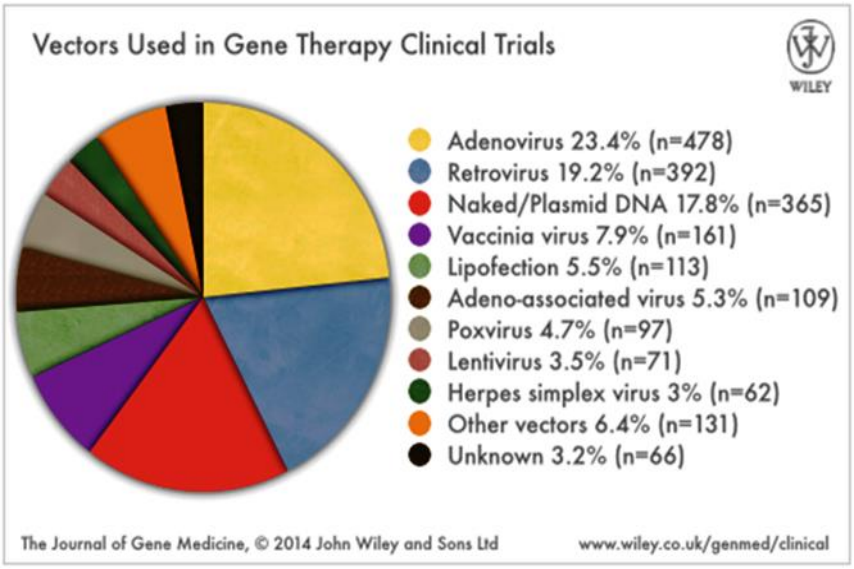

Figure-1.1: Different vectors used in GT clinical trials as of January 2014 (adapted from [9]).

1.1.2 Safety concern associated with viral vectors in GTs

Viruses are highly evolved biological machines that efficiently gain access to host cells and exploit their cellular machinery to facilitate their own replication. Ideal virus-based vectors for most gene-therapy applications harness the viral infection pathway but avoid the subsequent expression of viral genes that leads to replication and toxicity. This is achieved by deleting all, or some, of the coding regions from the viral genome, but leaving intact those sequences that are required *in cis* for functions such as packaging the vector genome into the virus capsid or the integration of vector DNA into the host chromatin [14, 15]. There are a total five types of viral vectors (Table-1.1) that are available for gene therapy pre-clinical & clinical trials [14, 16]. These five classes of viral vector can be categorized in two groups according to whether their genomes integrate into host cellular chromatin (oncoretroviruses

and lentiviruses) or persist in the cell nucleus predominantly as extrachromosomal episomes [adeno-associated viruses (AAVs), adenoviruses (Ad) and herpes viruses] [14]. Table-1.1 summarizes the advantage and disadvantages of these viral vectors for gene therapy [14, 17]. Although the viral based vectors are most widely used due to their high delivery efficiency of DNA, their usage sometimes poses severe safety concerns due to potential induction of undesired immunostimulatory responses and/or insertional mutagenesis [14]. Other limitations of viral vectors include the size of the therapeutic gene, production and packing problems, as well as high cost of production [7, 18-20].

Among the 5 classes of viral vectors, adenoviral vectors are known to be extremely efficient and unfortunately, most immunogenic [14, 21]. The majority of recombinant adenoviral vectors are based on human adenovirus serotypes 2 (Ad2) and 5 (Ad5) of species C [15, 22]. It has been reported that adenovirus-mediated cancer gene therapy showed only limited efficacy & less targeting in a number of preclinical and clinical studies [22]. Again, the use of first generation adenoviral vectors *in vivo* is associated with the induction of both innate and acquired immune responses [22, 23]. Cytotoxic T-lymphocyte (CTL) responses can be elicited against viral gene products or 'foreign' transgene products that are expressed by transduced cells [14].

Table-1.1: The main group of viral vectors (modified from [14, 17])

Vector	Genetic Material	Packaging Capacity	Particle Size	Inflammatory Potential	Main Limitations	Main Advantages
Enveloped						
Retrovirus	RNA	8 kb	100 nm	Low	Only transduces dividing cells; integration might induce oncogenesis in some applications	Persistent gene transfer in dividing cells
Lentivirus	RNA	8 kb	100 nm	Low	Integration might induce oncogenesis in some applications	Persistent gene transfer in most tissues
HSV-1	dsDNA	40 kb* 150 kb**	150 – 200 nm	High	Inflammatory; transient transgene expression in cells other than neurons	Large packing capacity; strong tropism for neurons
Non-enveloped/Naked						
AAV	ssDNA	<5kb	20 – 25 nm	Low	Small packaging capacity	Non-inflammatory; non-pathogenic
Adenovirus	dsDNA	8 kb* 30 kb***	70 – 100 nm	High	Capsid mediates a potent inflammatory response	Extremely efficient transduction of most tissues

*Replication defective. **Amplicon. ***Helper dependent. AAV: Adeno-associated viral vector; dsDNA: Double-stranded DNA; HSV-1: Herpes simplex virus-1; ssDNA: Single-stranded DNA.

The adenoviral capsid itself induces humoral virus-neutralizing antibody responses [14] and the same capsid proteins trigger an acute inflammatory response characterized by the rapid release of inflammatory cytokines, including interleukin-6 (IL-6) and IL-8, and the recruitment of immune effector cells, such as neutrophils, into the liver [22]. These inflammatory responses to the adenovirus capsid increase linearly with an escalation in vector dose. This vector dose-toxic response relationship is characterized by a 'threshold effect' in dose-escalation studies indicating that cellular toxicity occurs over a narrow dose

range and often no symptoms are observed until a slightly higher vector dose is administered, which induces severe cellular injury [14].

The potential and promising development of these viral vectors has been unfortunately overshadowed to a great extent due to these limitations as mentioned, and most importantly due to the reports of patient mortality in clinical trials that use viral vectors for gene therapy [8, 24-27]. Such an example is represented by the tragic death of Jesse Gelsinger in September 1999, a 18 year old male patient in phase-I gene therapy clinical trial (led by Dr. James M. Wilson) at University of Pennsylvania for an adenoviral (attenuated, recombinant, 3^{rd} generation) vector based therapeutic treatment for his partial ornithine transcarbamylase (OTC) deficiency [14, 16, 27-30].

OTC is a metabolic/liver enzyme that is required for the safe removal of excessive nitrogen from amino acids and proteins [14]. The genetic nature of the disease prompted a GT approach and the use of adenoviral vectors as a viable option. The vector had been infused directly into the liver through the hepatic artery, and this systemic delivery of the vector triggered a massive inflammatory response that led to disseminated intravascular coagulation, acute respiratory distress and multi-organ failure, and the eventual death of the subject [14, 29]. Autopsy reports later indicated vector induced activation of innate immunity as the main cause of death [30].

Insertional mutagenesis is another potential safety concern that has been documented in an *ex vivo* GT strategy to treat X-linked severe combined immunodeficiency (SCID-Xl) using a γ-retroviral vector [8, 25, 27, 29]. The term ‘severe combined immunodeficiency’ (SCID) was coined to indicate rare, lethal conditions in which infants die from an array of infections associated with a lack of lymphocytes in the blood [25].

A total of 20 patients suffering from SCID-Xl were treated with a γ-retroviral vector to correct the genetic defect from 1999 to 2009, achieving an impressive 85% success rate [25]. In the SCID-Xl trial, haematopoietic stem cells were genetically reconstituted with the γ-chain cytokine receptor and went through many cell divisions to generate a repopulating functional T-cell repertoire [14]. Unfortunately, a quarter (5 out of 20) of these patients were later found to have developed T-cell leukemia [25]. The development of T cell leukemia was attributed to the uncontrolled proliferation of T-cells due to vector integration near the *LMO2* proto-oncogene promoter, a phenomenon known as insertional mutagenesis leading to subsequent aberrant expression of oncogenes [8].

1.1.3 Non-viral vectors: Are they superior?

As described above, the resulting complications from the employment the viral vectors has created controversy regarding their use in human gene therapy applications [24, 26] and thus there is large body of research devoted for the quest of suitable non-viral vectors. Among the three major class of non-viral delivery systems – naked DNA, physical delivery, and chemical delivery via synthetic vectors (called non-viral vectors hereafter), the non-viral vectors, typically comprised of a mixture of cationic and neutral lipids, are generally non-toxic, non-immunogenic, are not limited in the size of gene they can encapsulate, are relatively cheap and easy to produce, and allow for specialized delivery options (such as targeted delivery, time-dependent release, and enhanced circulation times) [7, 19, 31-33].

A wide variety of commercial transfection systems based on non-viral delivery systems are available for *in vitro* cell studies [34-37]. As shown in Table-1.2, most of the commercial transfection systems employ a non-viral delivery system, rather than a viral

vector for use in transfection. From the data published in January 2014 (Figure-1.5) only 5.5 % of the vectors were lipid based (non-viral) [9]. Although in low percentage, this data reveals a promising application for non-viral gene delivery in *ex vivo* applications, instead of *in vivo* therapies as outlined in Table-1.2 [23]. A major reason for this discrepancy in the usage of viral versus non-viral vectors is the resulting transfection efficiency. Unlike viral vectors which possess inherent mechanisms to bypass the cellular defenses of the host, non-viral delivery systems do not have such mechanisms and currently have *in vivo* issues which are related to pharmacokinetics and intracellular barriers [38, 39].

Table-1.2: List of commercially available *in vitro* transfection reagents [34-37].

Name	Formulation	Manufacturer
Non-viral		
Convoy™	Cationic Polymer	ACTgene
GeneCellin™	Cationic Polymer	Bio Cell Challenge
Lipofectamine®	Cationic Lipid	Invitrogen
Effectene	Non- liposomal	Qiagen
Superfect	activated dendrimer	Qiagen
Fugene 6®	Non-liposomal	Promega
TransIT	Not disclosed	Mirus Bio
TransFast™	Synthetic cationic lipid	Promega
JetPEI®	PEI	Polyplus Transfection
ExGen 500™	Linear PEI	Fermentas/Thermo Sci
TurboFect	Cationic Polymer	Fermentas/Thermo Sci
Escort™	Cationic Liposome (DOTAP DOPE 1:1)	Sigma Aldrich Co. LLC.
NeuroPORTER™	Cationic lipid	Genlantis
HiFect®	Biochemical trasnfection agent	Lonza
X-tremeGENE	Non-liposomal reagent, synthetic	Roche
Genejuice®	Not disclosed	Millipore
Glycofect	Not disclosed	Kerafast
Viral		
SMARTvector	Lenti Virus	Thermo Sci
Virapower™	Adenovirus or lentivirus	Invitrogen
Polybrene®	Retrovirus	Millipore
rAVE™	AAV	Gene Detect

Unfortunately, this major limitation i.e. low transfection efficiency (TE) of non-viral vectors must be overcome for such systems to be recognized as the ideal vehicles for gene delivery [7, 33, 40]. The low TEs associated with non-viral delivery systems are directly attributed to the various barriers encountered by those vectors (discussed later) during the process of gene delivery. Table-1.3 illustrates a comparison of the advantages and disadvantages between viral and non-viral vectors in gene therapy. Literature suggests that cationic amphiphiles are considered to be promising alternatives for viral vectors in gene therapy [7, 41]. Thus, extensive research is necessary in this field concerning the mechanism of overcoming the delivery barriers for non-viral vectors for the rational design of suitable non-viral delivery systems for clinical use [39, 42-44].

The discussion of all the available nonviral vectors is beyond the scope of this thesis. Between the two most widely used synthetic non-viral vectors – namely cationic lipids & cationic polymers – only the cationic lipids (also known as cytofectins [45]) will be discussed in this dissertation. For non-viral gene delivery, the role of a synthetic based vector is to bind with therapeutic DNA sufficiently and rapidly, then to penetrate the target cell where the vector releases the DNA from the complex and then uptake of DNA by the nucleus [19, 46-49]. The first, key step in the whole process is the compaction of DNA into a positively charged (or neutral) particle small enough to be taken up by the negatively charged cell [18, 19, 48, 49]. This generally requires a synthetic chemical species bearing multiple positive charges to replace the monovalent counterions of DNA [48].

Table-1.3: Comparison between viral and non-viral vector mediated gene therapy [33]

Viral vectors	Non-viral vectors
High transfection efficiency	Low transfection efficiency
High production cost	Inexpensive
Limitations in scale up	Easily produced on large scale
Limited cargo size	Unrestricted by plasmid size
Immunogenic	Low immunogenicity
Potential for oncogenesis	Very low toxicity

1.1.3.1 Cationic lipid based non-viral vectors

Among the non-viral gene delivery vectors, lipid-based vectors are the most widely used non-viral gene carriers. It was first shown in 1980 that liposomes composed of the phospholipid phosphatidylserine could entrap and deliver SV40 DNA to monkey kidney cells [50]. Felgner *et al.* in 1987 was the first group who reported a synthetic species which effectively binds and delivers DNA to cultured cells; a double-chain monovalent quaternary ammonium lipid, *N*-[1-(2,3-dioleyoloxy)propyl]-*N*,*N*,*N*-trimethyl ammonium chloride (DOTMA) [6, 51, 52]. Later on, DOTMA was used in the development of the first commercialized reagent, Lipofectin^{TM} (Invitrogen), applied for lipid-based transfection or lipofection. After that initial breakthrough, many macromolecular and supramolecular cationic systems have been developed aiming to employ them as non-viral vectors to achieve better transfection efficiencies. These compounds include notably, cationic polyelectrolytes such as diethylaminoethyl-dextran (DEAE-D), polylysine, polyethylene-imine, polynorbornane, and polyamine dendrimers. The supramolecular systems of particular interest are those that form amphiphile aggregates, most commonly liposomes [48].

The amphiphilic compounds usually have two basic parts in their structural backbones – the head and the tail groups. They can differ by the number of charges on the head groups, along with differing in other structural modifications within the molecules. Generally, the hydrophilic head group of the cationic lipids commonly consists of a combination of phosphate and amine groups whereas, the hydrophobic domain is composed of two types of hydrophobic moieties including aliphatic chains, cholesterol, and/or other variations of steroid rings [19]. The linker - commonly consisting of ether, ester, carbamate, or amide bonds - determines the flexibility, stability, and biodegradability of the cationic lipid [53]. In most cases, the polar head group of a monomeric cationic amphiphiles / lipids consist of positively charged monovalent quaternary ammonium salts/ions, **QAS** [such as, in DTAB, TTAB, CTAB (Figure-1.2), and 1,2-dioleoyloxypropyl-*N*,*N*,*N*-trimehtylammonium chloride, DOTAP (Figure-1.3)]. The lipophilic moieties (tails) of the many of these lipids are connected to the hydrophilic core or the "head group" via an ether linkage rather than an ester linkage, since cationic lipids with an ether linkage – such as DOTMA, have been shown to display higher transfection efficiency *in vitro* and *in vivo* (also showing higher cytotoxicity) compared to their corresponding ester analogues, such as DOTAP [54-56].

Other commercially available transfection reagents (Figure-1.3) include *N*,*N*-dimethyl-*N*-[2-(spermine–carboxamido) ethyl]-2,3-bis(dioleyloxy)-1-propanaminium penta-hydro chloride (DOSPA), 1,3-dioleoyloxy-2-(6-carboxy–spermyl)-propyl–amide (DOSPER), dimethyl–dioctadecyl–ammonium bromide (DDAB), *N*,*N*-dioleyl-*N*,*N*-dimethyl–ammonium chloride (DODAC) usually in combination with fusogenic/helper lipids like 1,2-dioleoyl phosphatidyl–ethanolamine (DOPE) or 1,2-dioleoyl-*sn*-glycero-3-phosphocholine (DOPC) [52] (Figure-1.3). DOSPER, DOGS (Di-octadecyl-amido-glycyl-spermine), and DOSPA are

three examples of cationic lipids with modified head groups derived from the polyamine called spermine. The increased cationic groups in these multivalent lipids promote stronger DNA interaction for enhanced delivery. Modification of the alkyl tail such as replacement of the tail(s) with the application of cholesterol derived cationic lipids, DC-Chol (3β-[N-(N',N'-dimethylaminoethyl) carbamoyl] cholesterol), was shown to promote better stability and reduced cytotoxicity for improved transfection efficiencies *in vitro* [57].

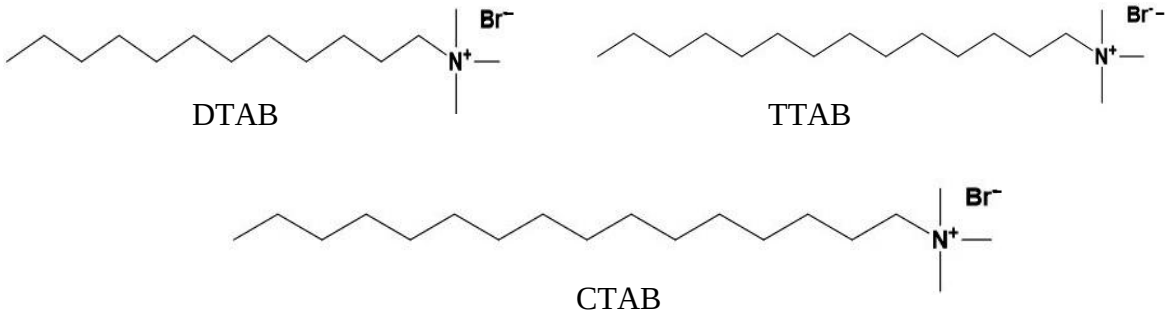

Figure-1.2: Molecular structures of DTAB, TTAB, and CTAB showing the positively charged quaternary ammonium moiety in the head groups.

Cationic lipids can compact and stabilize DNA by a combination of intermolecular attractive electrostatic interactions between the opposite charges, and intermolecular hydrophobic interactions between the apolar hydrocarbon skeletons [48, 58]. As a result of these interactions, the DNA is condensed into smaller aggregates where it is protected from endogenous nucleases; while the hydrophobic elements of the aggregate may also promote escape from the endosome by fusion or aggregation with the endosomal membrane [48]. The *in vitro* transfection efficiency of these lipids depend mainly on the structure, usage of other helper lipids (such as DOPE, for assisting endosomal escape), the N^+/P^- ratio (i.e. charge

ratio) of the lipids to DNA, the size and magnitude of the charge of the lipoplex, and the type of cell lines under treatment. Limitations of cationic lipids include low efficacy owing to poor stability and rapid clearance, as well as the generation of inflammatory or anti-inflammatory responses [50]. Recently, Allovectin-7, which is a locally administered formulation consisting of (±)-*N*-(2-hydroxyethyl)-*N*,*N*-dimethyl-2,3-bis(tetradecyloxy)-1-propanaminium bromide (DMRIE) – DOPE and a DNA plasmid, failed to meet its efficacy end points in a Phase III clinical trial for treatment of advanced metastatic melanoma [50]. Nonetheless, various liposomal formulations continue to be developed clinically, including DOTAP– cholesterol, Vaxfectin® and GL67A–DOPE– DMPE–polyethylene glycol (PEG) (Table-1.4) [50]. Notably, the new cytofectin formulation, Vaxfectin® which is composed of (±)-*N*-(3-aminopropyl)-*N*,*N*-dimethyl-2,3-bis(cis-9-tetradecenyloxy)-1-propanaminium bromide (GAP-DMORIE) and the co-lipid, 1,2-diphytanoyl-*sn*-glycero-3-phosphoethanolamine (DPyPE), has shown significant enhancement of humoral immune responses against pDNA encoded antigens compared with naked pDNA [45].

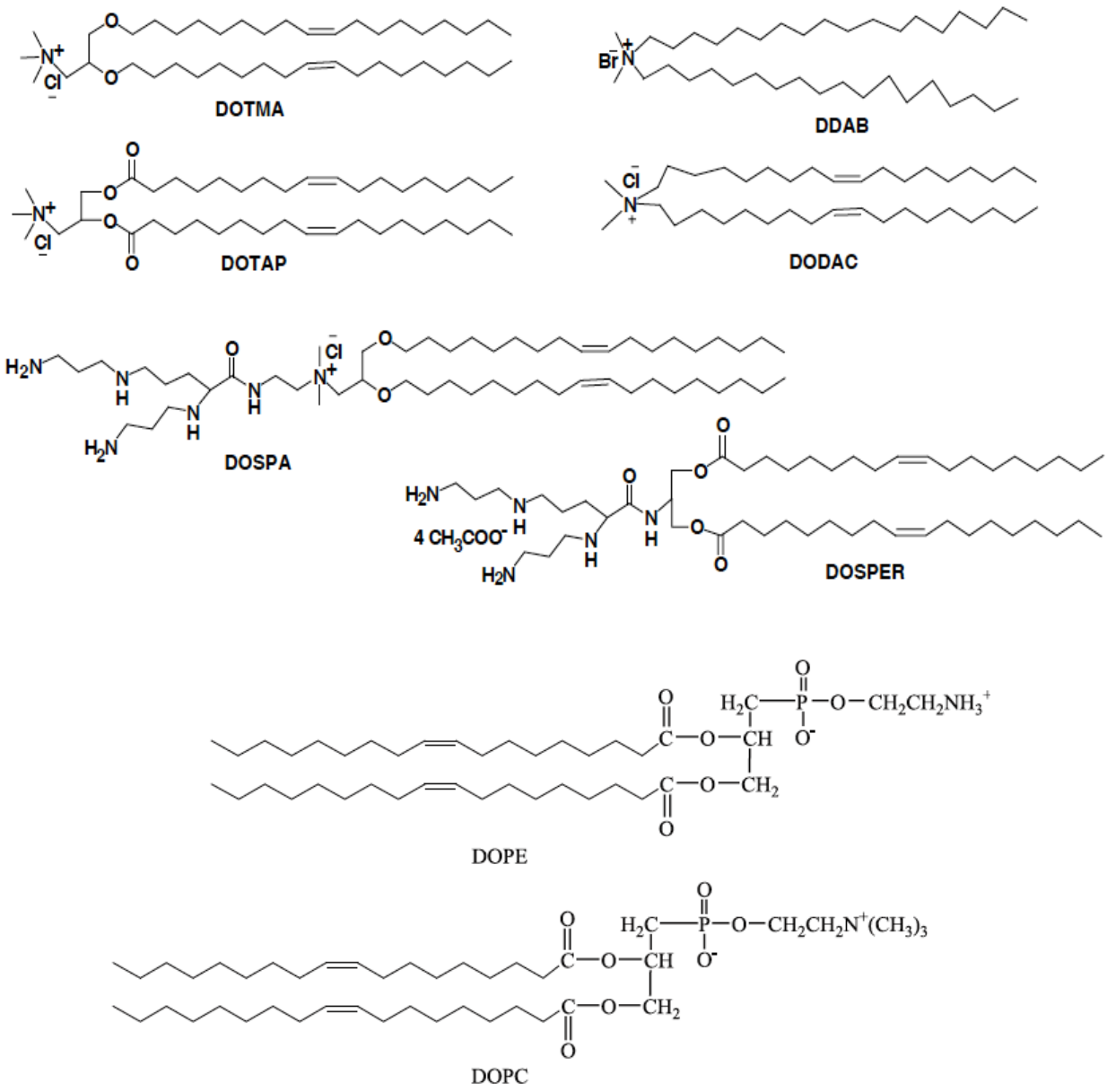

Figure-1.3: Structures of commercially available lipids DOTMA, DDAB, DOTAP, DODAC, DOSPA, DOSPER (reused with permission from [52]. Copyright [2005], Elsevier) and the neutral helper lipids DOPE & DOPC (reused with permission from [59]. Copyright [2004], Elsevier).

Table-1.4: Non-viral DNA vectors under clinical evaluation (modified from [50])

Delivery system	GT drug	Indications	Phase	Status
DOTAP– cholesterol	DOTAP–Chol-fus1	Non-small-cell lung cancer	I I/II	Completed Active
GAP-DMORIE–DPyPE	Tetravalent dengue vaccine	Dengue disease vaccine	I	Active
GL67A–DOPE–DMPE–PEG	pGM169/GL67A	Cystic fibrosis	II	Active
PEI	BC-819/PEI	Bladder cancer	II	Active
	BC-819	Ovarian cancer	I/II	Completed
	DTA-H19	Pancreatic cancer	I/II	Completed
	SNS01-T	Multiple myeloma and B cell lymphoma	I/II	Recruiting
	CYL-02	Pancreatic ductal adenocarcinoma	I	Completed
PEG–PEI– cholesterol	EGEN-001	Ovarian, tubal and peritoneal cancers	I II	Recruiting Active
	EGEN-001-301	Colorectal peritoneal cancer	I/II	Recruiting
PEI–mannose–dextrose	DermaVir/LC002	HIV vaccine	II	Active
Poloxamer CRL1005–benzalkonium Chloride	ASP0113	CMV vaccine	III II	Recruiting Recruiting
	VCL-CB01	CMV vaccine	II	Completed

1.2 Potential barriers to non-viral vector mediated GT

Generally, the process by which plasmids are delivered to targeted cells is known as transfection. Current non-viral gene therapy involves local or systemic administration of plasmid DNA (pDNA) which encodes for a transgene gene which yield expression of a therapeutic protein, thereby correcting a disease state. The non-viral DNA delivery vectors (Figure-1.4) [60] generally consist of the therapeutic nucleic acid (the pDNA), a cationic

molecule (polymer or lipid) with a neutral helper lipid (in some cases, to overcome the transfection barriers), targeting ligands, nuclear localization signals (NLS) and stealth groups [18]. As mentioned earlier, the most widely used non-viral vectors are those consisting of either cationic lipids (which form "lipoplexes" with deoxyribonucleic acid, DNA) or cationic polymers (forming "polyplexes" with DNA) [61]. There are a number of barriers (Figure-1.5) – both extracellular, and intracellular – based on several review articles [49, 62-77], that can hinder the transfection process which in turn can affect the overall efficiency of gene delivery.

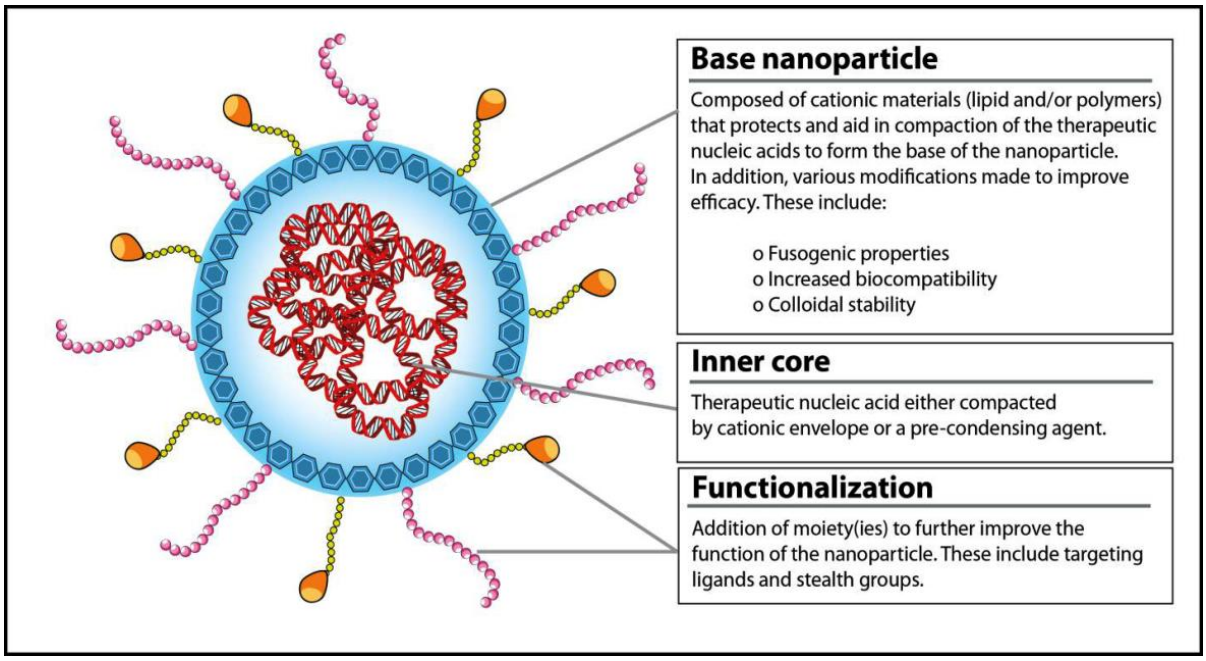

Figure-1.4: Basic building block of a non-viral gene delivery system. Non-viral delivery systems are composed of three fundamental elements. The first is the nucleic acid that forms core of the NP. Second, is the soft material that forms the basic element of the NP and encapsulate the DNA into a NP. Finally additional functional groups can be added to the base NP to augment the system and improve overall efficacy (reused from [60] through the permission of author)

Briefly, the extracellular barriers consist of vector instability due to components within the blood, adhesion to non-targeted tissues, phagocytosis of vector by macrophage, and DNA-degradation [73] In blood circulation, the vector-DNA complexes must evade uptake by macrophages, clearance by renal filtration, and must have improved ability to circumvent the RES (reticulo-endothelial system) and degradation by endogenous nuclease [78]. They need to traverse from blood vessels to target tissues followed by subsequent translocation into the cells impacting mitochondrial respiration, ATP synthesis, activity of drug efflux transporters, apoptotic signal transduction, and gene expression [78]. Despite some tissues such as tumors, inflammatory sites and the RES (e.g., liver, spleen) with leaky blood vessels, the capillary vessel walls in most organs and tissues are impermeable to large nucleic acids. Furthermore, extracellular matrix (ECM) resists the movement of gene medicines to target cells due to its dense polysaccharides and fibrous proteins [73]. The intracellular barriers include cellular internalization of the vector (cell membrane itself is a major barrier), escape from the endosome and delivery in the cytoplasm, dissociation of the nucleic acid-vector complex, cytosolic trafficking of nucleic acid, and nuclear entry of the DNA cargo [18, 73].

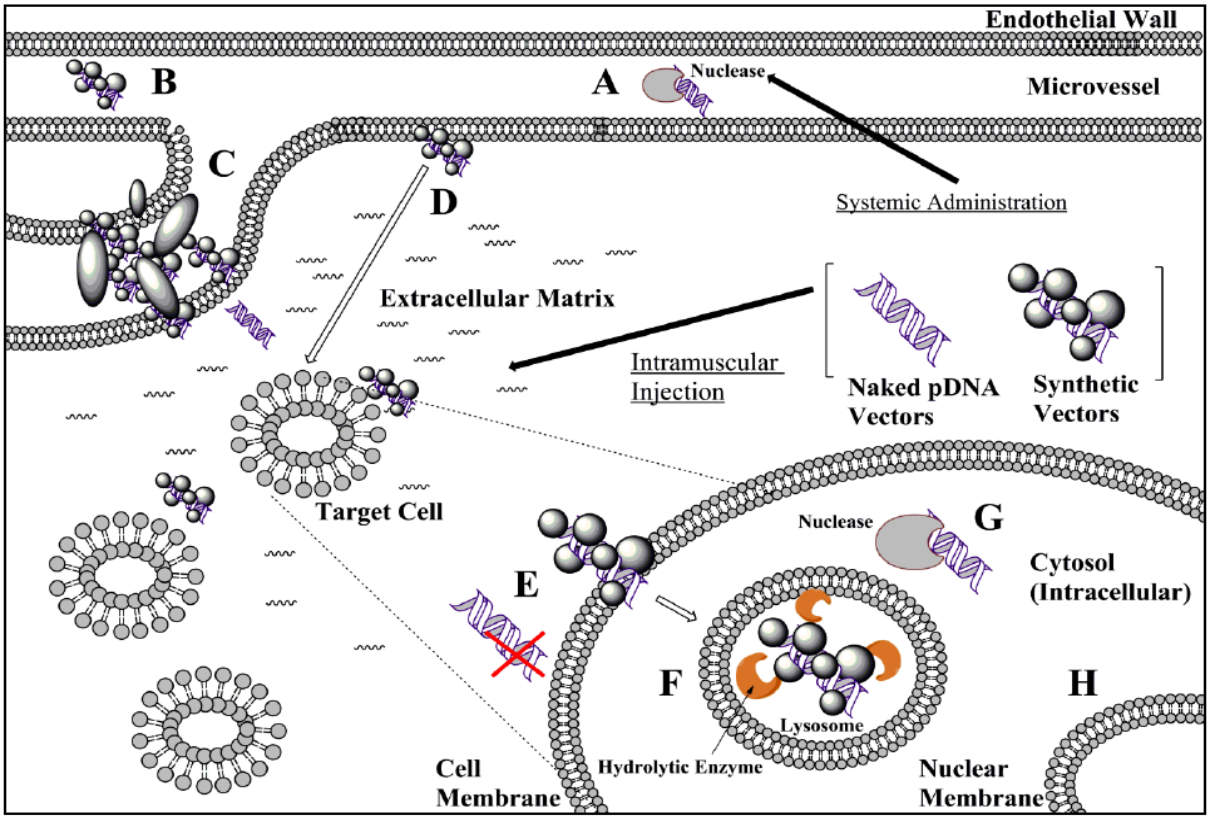

Figure-1.5: Extracellular and intracellular barriers to gene delivery: **A)** Degradation of unprotected, naked pDNA vectors by nucleases upon systemic delivery; **B)** Removal of synthetic vectors by the reticuloendothelial system; **C)** Significant aggregation with blood components leading to vessel obstruction; **D)** Extravasation of naked pDNA and synthetic vectors across the endothelial wall and extracellular matrix; **E)** Repulsive forces between naked pDNA vectors and cell membrane inhibit effective cellular uptake and internalization; **F)** Lysosomal degradation of synthetic vectors and DNA cargo in absence of endosomal escape; **G)** Degradation of released DNA cargo by intracellular nucleases; **H)** Nuclear membrane obstructing nuclear entry and transgene expression (reused from [79] through the permission of the author).

1.3 Gemini surfactants as non-viral vectors

Surface active agents, commonly called “surfactants” are a special class of amphiphilic compounds possessing characteristic physicochemical properties at two immiscible interfaces and in bulk solution [80]. Surfactants (cationic, anionic, or non-ionic)

are versatile materials used in numerous products for purposes including motor oils, pharmaceuticals, detergents and petroleum, as floating aids for applications, and in high-technology areas like mining, petroleum, chemical, biochemical research, electronics, printing, magnetic recording, biotechnology and microelectronics [81, 82]. As surfactants are utilized extensively throughout the world every day, the quest for high-efficiency, environment friendly novel surfactants is ongoing.

Classic surfactant molecules are generally composed of two distinct parts in their molecular structure: one polar head group and a nonpolar alkyl chain or tail. Due to this dual polar-non polar character, surfactant molecules are often termed as "amphiphiles" [80, 81]. When surfactants are dissolved in water, their hydrophobic groups are directed away from the water and the free energy of the solution is minimized through a phenomenon called the "hydrophobic effect" [83]. Due to their amphiphilicity, surfactant molecules tend to also be adsorbed at the interface of two immiscible phases (Figure-1.6) to decrease the surface and interfacial tension. Alternatively they can self-aggregate to form well-developed supra-molecular assemblies, called micelles (if present above a certain concentration, known as the critical micelle concentration, CMC) as a means of minimizing unfavorable energies [80, 81, 84].

From extensive investigations of bis-surfactants a synthetic amphiphile called "gemini surfactants" (GSs), was developed. In 1991, Menger *et al.* first coined the term "Gemini" meaning "twin or dimer" to describe these bis-surfactants having a rigid spacer such as benzene or stilbene [48, 85, 86]. The terminology has since been extended to encompass any other bis or double tailed (dimeric) surfactants, irrespective of the nature of the spacer [7, 87], as well as surfactants with two or more head groups with any number of

tails [88, 89]. These dimeric gemini surfactants are composed of two monomeric amphiphilic moieties connected at or near the head group by a spacer or linker group. The spacer can be short or long, composed of methylene groups, rigid (stilbene), polar (polyether) or non-polar (aliphatic, aromatic) groups. The polar head group can be positive (ammonium), negative (phosphate, sulphate, carboxylate) or non-ionic and may be polyether or sugar [6, 7, 48, 55, 85, 86, 89-94].

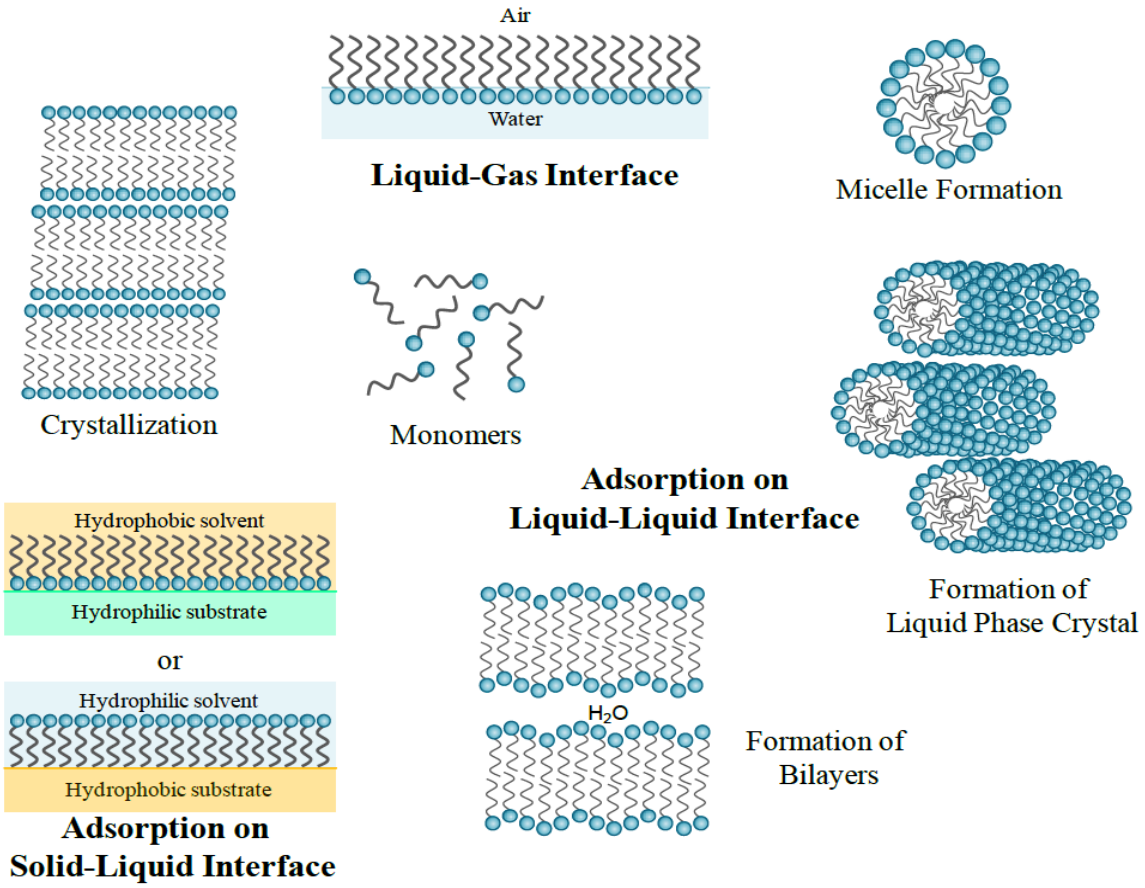

Figure-1.6: Schematic representation of typical adsorption and formation of aggregates by self-assembled amphiphiles (adapted from [83]).

In addition to structural variables associated with simple surfactants (such as tail length and degree of branching, ionic nature of the head group, and counterion type), GSs are

also characterized by the number of heads (dimer, trimer, tetramer, etc.), and spacer solubility (i.e., hydrophilic or hydrophobic) [6, 88, 89]. Gemini analogues of lipids (also called gemini lipids) have also been reported, which possess multiple head groups and at least four or more hydrophobic chains as shown in Scheme-1.1 [6, 88]. The great majority of gemini structures are symmetric with two identical polar groups and two identical chains. The most commonly studied series of GS is the *N,N'*-bis (dimethylalkyl)-alkane-diammonium-dibromide series, or "*m*-*s*-*m*" DMA type gemini surfactants (DMA=dimethyl ammonium, the *m* in this notation refers to the number of carbon atoms in the alkyl tails, while *s* refers to the number of atoms making up the spacer group) [6, 7, 48, 55, 85, 91, 95]. However, unsymmetrical gemini molecules and GS with three or more polar groups or tails have also been reported [6, 96, 97].

Gemini surfactants possess unique properties that directly result from their novel structure, such as a critical micelle concentration (CMC) that is 10 – 100 orders of magnitude lower than their monomeric counterparts, a thousand-fold increase in surface activity, greater efficiency in lowering the surface tension, lower Kraft temperature, better solubilization, better wetting, viscoelasticity, gelification, and shear thickening than the corresponding conventional monomeric surfactants [7, 80, 81, 84, 92, 94, 98-100].

Due to their unique properties, gemini surfactants have wide applications in skin care formulations, templates for the synthesis of nanoparticles, biomedical application including gene delivery, drug entrapment/release, soil remediation, enhanced oil recovery, and antimicrobial activity as effective emulsifiers, dispersants, bactericidal agents, antifoaming agents, and detergents. [92, 101, 102]. The extremely low CMC of GSs means reduced toxicity *in vivo* as well as minimized cost since less surfactants is required [7, 55].

Furthermore, as the GSs provide a higher positive charge per mass ratio than the monomeric counterparts, a relatively lower amount is sufficient to rapidly complex a given aliquot of DNA in a more compact fashion leading to smaller sized nanoparticles (a critical factor for cellular uptake and intracellular trafficking) [6].

The general structure of gemini surfactants is shown in Scheme-1.1 [7, 103]. The long hydrocarbon chain of the GS tends to increase the surface activity. Increasing the hydrophobicity may make the molecule water-insoluble, whereas increasing the hydrophilicity of the head group may impart water solubility. Hydrophilic groups in the spacer also increase the aqueous solubility. An increase in carbon number in the nonpolar chain increases both lipophilicity and surface activity [6, 89]. Hence, the molecular structure of the GSs provides significant opportunities to vary their structure compared to their monomeric counterparts by independently modifying the spacer, one or both head-groups, and one or both hydrophobic tails or the associated counterions to obtain an extremely wide range of compounds. This ultimately opens a new horizon to fine tune the self-aggregation of GSs based liposomes to obtain a better control on biological activity (DNA delivery) and other solution properties [7, 55].

Owing to their remarkable properties, considerable attempt has been made for the design and synthesis of novel GSs of various categories to study the relationship between their molecular structures and their aggregation morphologies in aqueous solution [104]. In comparison of the monomeric counterparts of the GSs, the spacer group has been known to strongly affect the self-assembly of gemini surfactants in aqueous solution, and thus considered as a unique component in gemini structure. So far, the various gemini surfactants

containing different spacers, for example, a flexible hydrophilic, flexible hydrophobic, or rigid hydrophobic, have been investigated [104, 105].

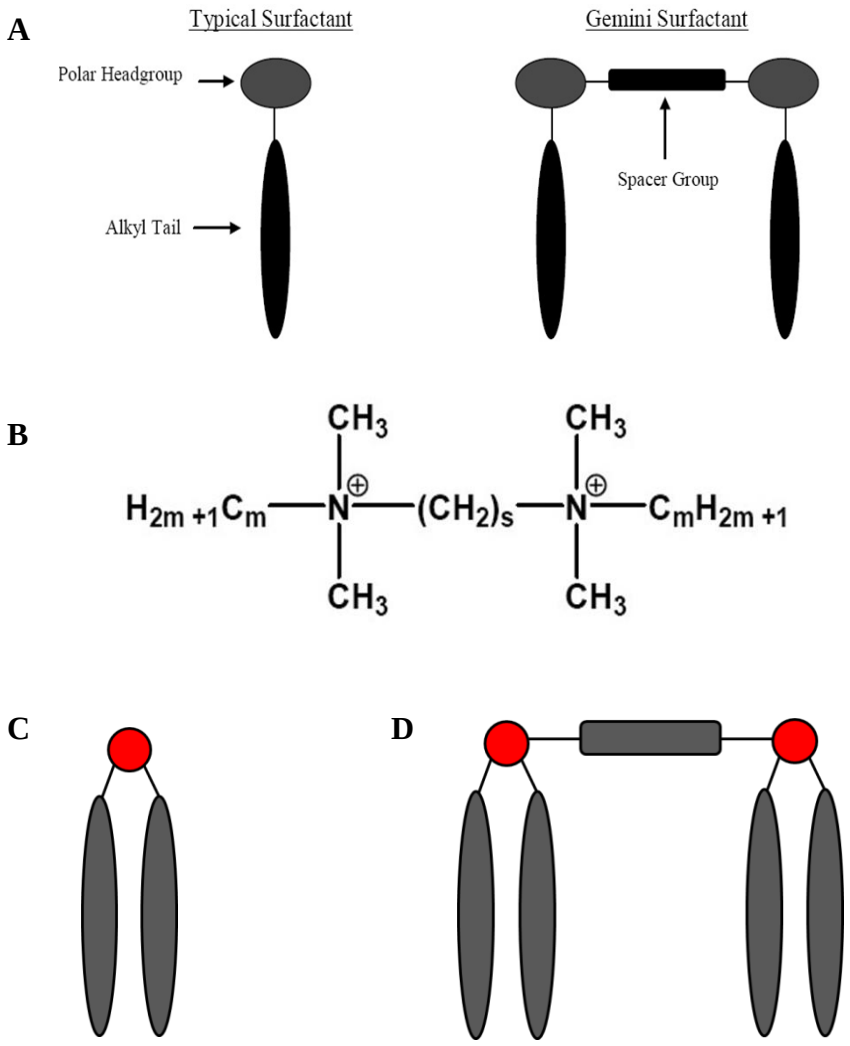

Scheme-1.1: (**A**) General structure of a conventional and gemini surfactant (without the associated counterions); (**B**) Structure of m-s-m GSs (**C**) Model representing simple lipids, and (**D**) Gemini lipids {**A & B** – adapted from [7]}.

Numerous studies reveled that gemini surfactants are able to compact DNA efficiently when the spacer length s is <4 or >10. Besides, the spacer lengths correspond to

conditions where cylindrical micelles (s < 4) or bilayer structures (s > 12) are known to form. Conversely, intermediate length spacers in gemini were found to be less effective [7, 106, 107]. Now, in case of hydrophobic tail lengths, a general rule for ionic surfactants is that, in aqueous medium, the CMC decreases as the number of carbon atoms in the hydrophobic group increases and it is halved by the addition of one methylene group to a straight-chain hydrophobic group attached to a single terminal hydrophilic group. Due to the coiling of the long chains in water, when the number of carbon atoms in a straight-chain hydrophobic group exceeds 16, the CMC no longer decreases so rapidly with increase in the length of the chain, and when the chain exceeds 18 carbons it may remain substantially unchanged with further increase in the chain length [108, 109].

1.3.1 Gemini Surfactants (GSs) for DNA transfection in GT

Compaction of DNA by gemini surfactants is affected by both the nature of the head group (effective head group area, valence) and the length and saturation of the hydrophobic tail. The optimal structure(s) formed by self-aggregation of these surfactants can be predicted by the surfactant packing parameter or critical packing parameter, *CPP or P* (Figure-1.7), which can be calculated by the following equation –

$$P = v / (a_0 * l) \qquad 1.1$$

where v = volume of alkyl tail, l = length of alkyl tail, and a_0 = surface area occupied by the head-group. The P value indicates the preferred curvature of the structure and a value of 0.3 is typical for spherical micelle organization (highly curved), whereas $P = 1$ represents planar bilayer formation and $P > 1$ applies to inverted micelles [7, 108, 110].

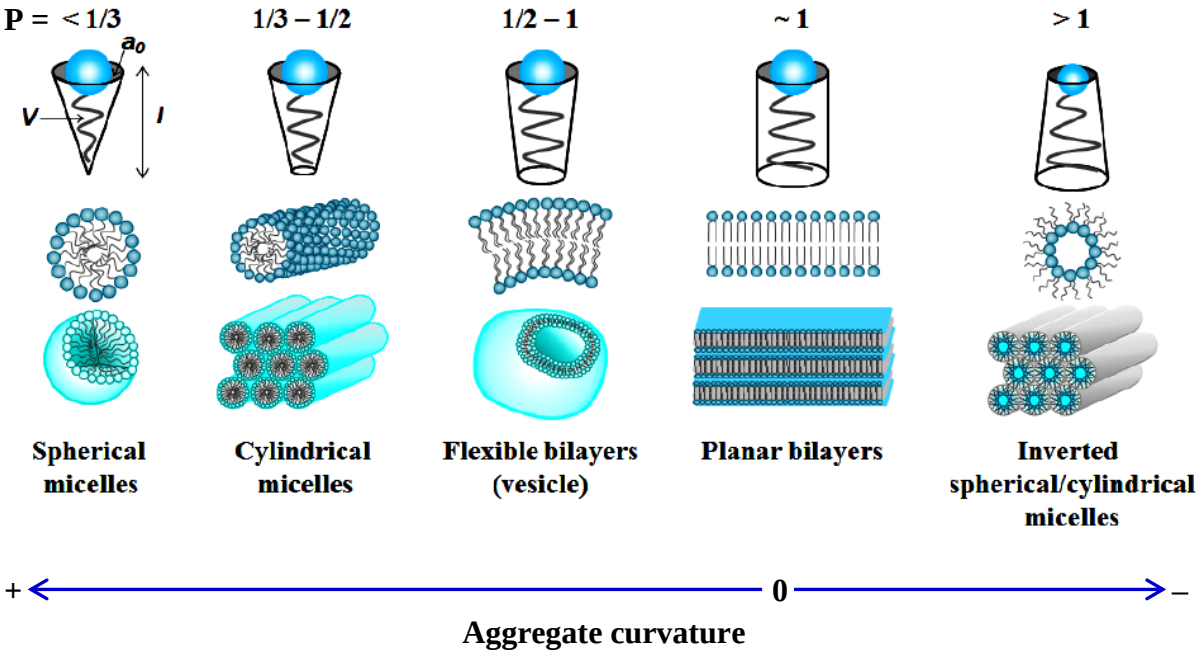

Figure-1.7: Packing parameter showing different morphologies of amphiphilic aggregates defined by Israelachvili (adapted from [83]).

When binding with negatively charged DNA the packing parameter for vesicle systems ($P > 0.5$) is larger than that of micelle systems ($P < 0.5$), and therefore it is easier for a vesicle system to form non-lamellar structures such as inverted hexagonal and cubic morphologies ($P \geq 1$). When lipoplexes interact with anionic lipids it makes DNA release easier from the lipoplexes and the low curvature phases (inverted hexagonal and cubic morphologies) are the controlling factors in lipid-mediated delivery [110].

Electrostatic forces along with attractive hydrophobic interactions, hydrophobic hydration, and the repulsive forces existing between DNA – DNA and surfactant – surfactant molecules trigger the formation of DNA – surfactant complexes for gene delivery [93, 110]. These interactions change the shape and size of macromolecular DNA without the loss of

therapeutic (biological) properties of the genetic material, into various morphological shapes that are readily taken up by cells [103].

As mentioned previously, the cationic gemini surfactants effectively complex and condense the DNA and provide an overall positive charge to the transfection complex (depending on the charge ratio used) to allow interaction with the negatively charged cell membrane. Studies on transfection efficiencies of gemini-DNA complexes with respect to charge ratio suggested that transfection was optimum with excess cationic gemini where the gemini/DNA charge ratio is approximately 10 [110]. After the rapid uptake of the DNA-vector complexes by the cell, it is thought that the transfection complexes will escape the endosome by their ability to form different morphological shapes such as inverse hexagonal (H^{C}_{II}) or cubic phases (Pn3m). Gemini surfactants that are capable of forming vesicle (lamellar) structures in aqueous solution have improved transfection efficiencies than those with micelle structures due to higher surfactant packing parameter, *P* value [110].

The total volume of hydrophobic tails of typical cationic surfactant molecules increase faster than that of the head group areas, because of the existing electrostatic attraction between the positive head groups and other oppositely charged moieties (such as counterions). Lamellar lipoplexes generally bind with anionic lipids of cellular membranes and increase the packing parameter of the cationic surfactants which allow the formation of inverted hexagonal or cubic structures [110]. However, these non-lamellar structures are not favorable for binding DNA; instead they are favorable for releasing DNA after cellular internalization.

1.3.1.1 Role of DOPE lipid in gemini mediated DNA transfection for GTs

To achieve better transfection efficiencies 1,2-dioleoyl-s*n*-glycero-3-phosphatidyl ethanolyamine, DOPE (Figure-1.3), an important neutral helper lipid is often added to gemini surfactant-based gene delivery formulations to facilitate the endosomal escape – a crucial barrier for GT [110].

Endosomal escape by DOPE mediated lipoplexes has shown that the escape mechanism is independent of membrane charge density. Inside the cell membrane, generally when the endosome matures to lysosome, its pH reduces to acidic condition. This drop in pH triggers lamellar (L^{C}_{α}) to inverted hexagonal phase (H^{C}_{II}) transitions of DOPE lipids in the lipoplexes. The negative curvature of this inverted hexagonal lipoplexes results in an elastically frustrated state with the outer lipid monolayer, possessing a positive curvature, that surrounds the lipoplexes; this establishes the driving force for rapid fusion with cell and endosomal membranes [111, 112] (Figure-1.8), hence the DOPE is sometimes termed as "fusogenic lipids". The ability of DOPE mediated lipoplexes to adopt inverted hexagonal phase structures for rapid fusion and endosomal escape is a significant contributing factor [110] to higher transfection efficiency when compared to lipoplexes with lamellar phase structures.

Studies have shown that the presence of the helper lipid DOPE increased the transfection efficiency about 10 fold [103, 113]. Addition of pure DOPE causes formation of mixed aggregates with higher (greater than unity) packing parameter value of the systems; shifting micelle systems towards vesicles, and vesicle systems toward the inverted hexagonal or even cubic phase. In addition, DOPE has a positive role to increase the fluidity of cellular membranes and thus facilitates the penetration of genetic materials into the cell. Furthermore,

it also helps in disruption of the endosomal membrane at the endosomal escape phase leading to increased transfection efficiency [110].

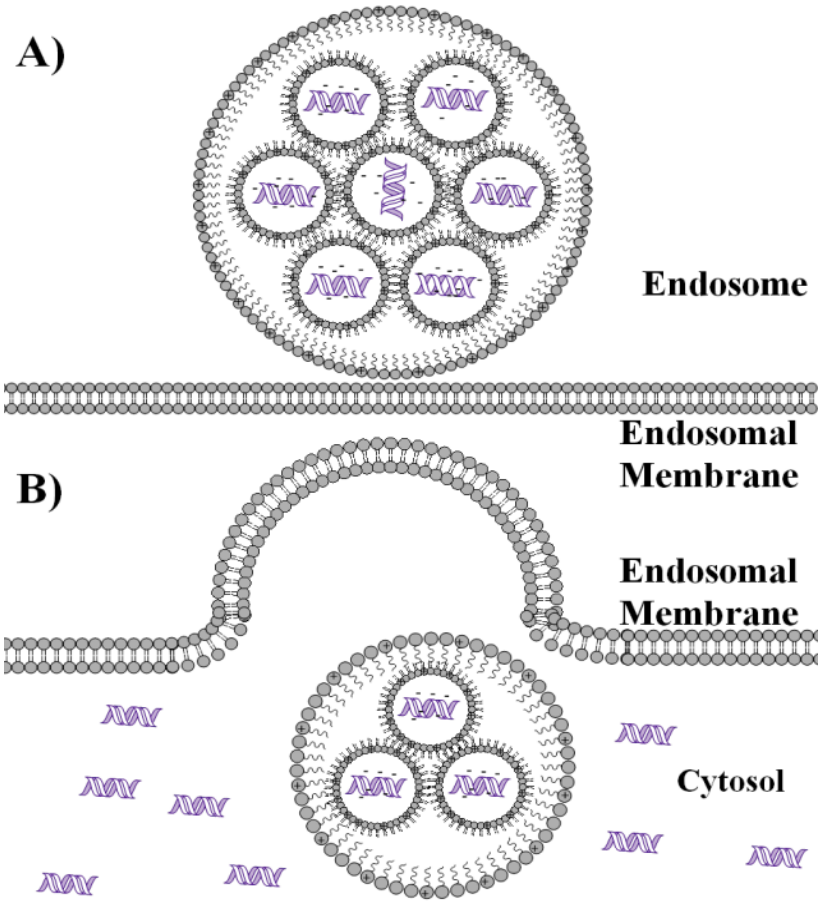

Figure-1.8: Schematic illustration of endosomal escape of fusogenic DOPE mediating lipoplexes. Consistent reduction in pH trigger lamellar to inverted hexagonal phase transitions **(A)**, prompting an elastically frustrated state that drives rapid fusion with endosomal membrane and endosomal escape **(B)** (reused from [79] through the permission of author).

1.3.2 Effects of Counterions

1.3.2.1 Counterion effects on gemini surfactant aggregation

Many attempts have been made to investigate the effect of salts on micelle formation in light of the Hofmeister (lyotropic) series and other numerous counterions (organic/inorganic, monoatomic/polyatomic, nucleotides, peptides etc.) [84, 114-122]. Unfortunately, despite the structural diversity of gemini surfactants, only a few studies have focused on the effect of the gemini surfactant counterions on the micellization properties other than bromide or chloride [123]. As the specific properties (solubility, CMC, aggregation behaviour, richer morphology, and other solution properties) [97, 124] of gemini varies depending on the associated counterions (along with their chain lengths and spacer groups), the focus of this section will be to discuss those solutions properties of gemini surfactants with different inorganic and organic counterions.

The effects of salts on aggregation behaviors of ionic surfactants in aqueous solutions are vital to many applications for detergency and emulsification in industry as well as in biotechnological fields [115]. Oda *et al.* (2010) investigated and analyzed the effect of counterions to probe the principal ionic effects influencing the micellization behavior of the dimeric 14-2-14 gemini surfactants [123]. The critical micelle concentration (CMC), ionization degree of micelle (α), free energy of micellization (ΔG_M), and aggregation numbers (N) of the gemini surfactant (14 – 2 – 14) were used to demonstrate the effect of different anion properties. In their study, among various groups of counterions (Figure-1.9), they include nitrate (NO_3^-), iodide (I^-), bromide (Br^-), chloride (Cl^-), fluoride (F^-), dihydro-phosphate (PH^-) and acetate (C_2^-) ions within the "small counterions group"; and the

methoxyacetate (MeOAc), lactate (LACT), trifluoroacetate (TFA), diphenate (DIPH), sulphate (SO_4^{2-}) and tartrate (TART) ions were included in the "orphan group".

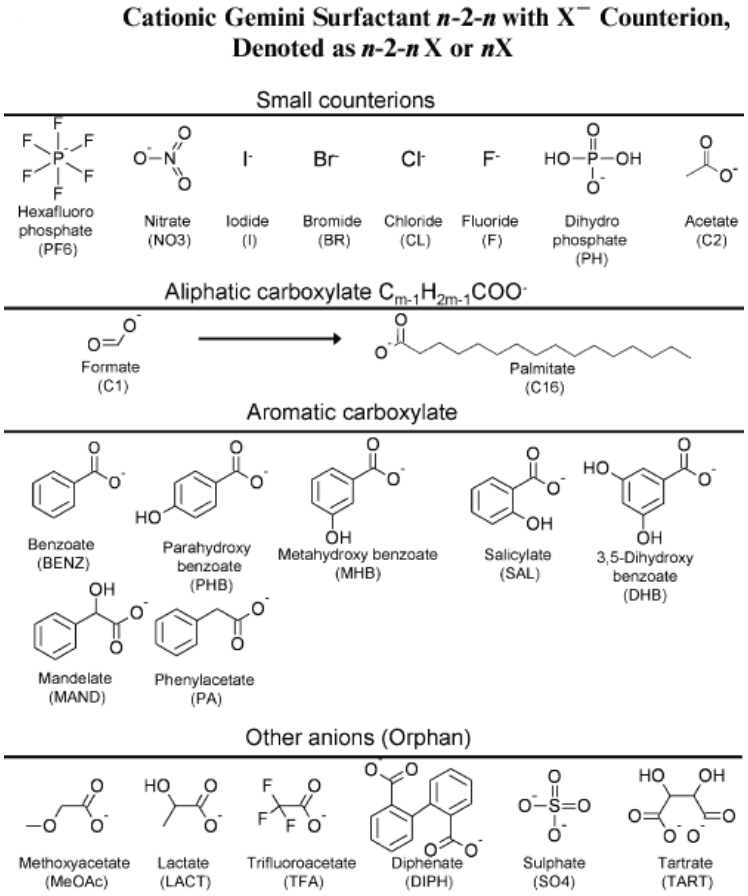

Figure-1.9: Various groups of counterions in the study of Oda *et.al* (reused with permission from [123]. Copyright [2010], American Chemical Society).

The hydrophilicity of the anions is the primary factor determining micellization and is inversely related to micellization process. The higher hydrophilicity of a counterions leads to high CMCs of the GS (Figure-1.10: Table-1) [123]. Studies showed that the smaller counterion groups generally follow the Hofmeister series in terms of CMC: the CMC of the GS 14-2-14.X^- was found to increase according to the Hofmeister series: $I < NO_3^- \sim Br^- < Cl^-$

< F^- ~ C_2^- < PH^-. Among the halide ions of this group, the most polarizable and least hydrated iodide (I^-) ion has a large negative energy transfer value (ΔG_{HB}) indicating that it is a very chaotropic anion which destroys the structure of water in its vicinity leading to the lowest CMC value.

Table 1. CMC, α_a, $\alpha_{b,25}$, $\Delta G_{M,25}$ of 14-2-14 with Small Counterions at 30°C unless Indicated Otherwise

gemini	CMC (mM)	ionization degree α_a	ionization degree $\alpha_{b.25}$	$\Delta G_{M.25}$ ($kJ \cdot mol^{-1}$)
14BR	0.14	0.27	0.23	−27.05
$14NO_3$	0.14	0.25	0.23	−27.09
14CL	0.26	0.29	0.26	−24.39
$14C_2$	0.61	0.48	0.33	−20.65
14F	0.64	0.55	0.33	−20.58
14PH	1.23	0.58	0.38	−17.87
14I	0.10 (60 °C)	0.49		

Figure-1.10: Table-1 describing the CMC and other parameters of 14-2-14 gemini associated with the Hofmeister series counterions in the head group (reused with permission from [123]. Copyright [2010], American Chemical Society).

Although two other halides Br^- and Cl^- have intermediate properties, the fluoride (F^-) ion displays opposite properties compared to iodide (I^-) ion since it is the smallest anion, the least polarizable, the most hydrated, and the most Kosmotropic. Overall, for monatomic anions, the hydration number is directly related to the hydrophilicity: the more hydrophilic anions have smaller polarizability and higher hydration number leading to higher CMC values. On the other hand, due to entropic reasons the micellization is disfavored for large and polyatomic anions with lower hydration number but with similar hydrophilicity of the monoatomic anions (Figure-1.11: Table-2 & Table-3) [123].

Table-2: CMC, α_a, ΔG_M, and $\Delta G_t(CH_2)$ of Gemini 14-2-14 with alkyl-carboxylate counterions

Gemini	CMC (mM)	Degree of ionization (α_a)	ΔG_M (kj/mole)	$\Delta G_t(CH_2)$ (kj/mole)
14C1	0.58	0.43	– 20.88	– – – – –
14C2	0.61	0.48	– 20.65	0.23
14C3	0.42	0.54	– 20.99	– 0.34
14C4	0.35	0.52	– 21.46	– 0.47
14C6	0.23	0.37	– 24.24	– 1.39
14C8	0.12	0.10	– 30.39	– 3.08

Table-3: CMC measured at 30^0C unless otherwise noted, Ionization degrees (α), and Free energy of micellization (ΔG_M), at 30^0C of 14-2-14 with aromatic and orphan carboxylate counterions

Gemini	CMC (mM)	Degree of ionization (α_a)	ΔG_M (kj/mole)
14SAL	0.09 (60^0C)	0.14	– – – – –
14BENZ	0.14 (60^0C)	0.47	– – – – –
14MHB	0.18 (60^0C)	0.45	– – – – –
14PA	0.19 (60^0C)	0.43	– – – – –
14MAND	0.23 (60^0C)	0.44	– – – – –
14PHB	0.32 (60^0C)	0.41	– – – – –
14DHB	0.37 (60^0C)	0.42	– – – – –
14TART	0.06	0.42	– 20.47
14PA	0.12	0.46	– 26.07
14MAND	0.13	0.47	– 25.95
14TFA	0.14	0.50	– 23.95
14LACT	0.19	0.40	– 24.96
14MeOAc	0.61	0.68	– 18.70

Figure-1.11: Table-2 & Table-3 describing the various solution properties of 14-2-14 gemini with various organic and polyatomic counterions in the head group (modified from [123]).

In case of aliphatic carboxylates counterions, the CMC of the GS was found to decrease with increasing chain length (increasing hydrophobicity) of the carboxylate ions except for the acetate ion (Figure-1.12). But in case of aromatic carboxylates, the CMC of the gemini increases with higher hydrophobic property of the aromatic carboxylate counterions although the solubility is very low. For the same reasons as described above for the

Hofmeister series ions, among the orphan counterions, the CMC was found to be lowest for the tartrate ion and highest for the methoxy acetate [115, 123]. In summary, the counterions has a marked influence on both micellization and aggregation of the GS and these effects of counterions depends on the complex interplay between hydrophobicity of anions and other ion properties such as counterion hydration, interfacial packing of ions, and ionic morphology [123].

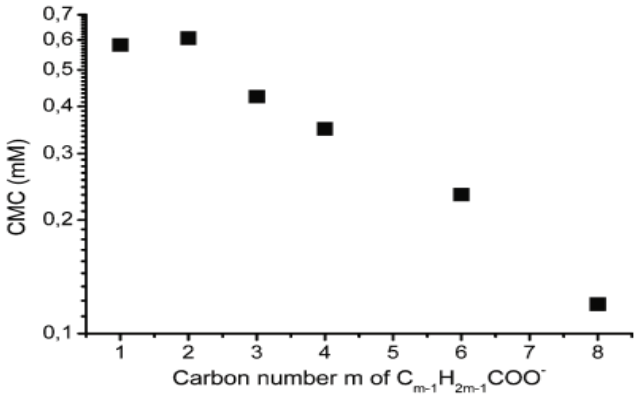

Figure-1.12: CMC of the 14-2-14 with aliphatic carboxylate counterions at 30^0C (reused with permission from [123]. Copyright [2010], American Chemical Society).

1.3.2.2 Counterion effect of amphiphiles on transfection

Until recently, there were no investigations done on the effects of counterions of gemini surfactants on *in vitro* transfection efficiencies. Thus, due to lack of published papers on the effect of counterions on transfection, this section will discuss the effect of counterions on transfection done through cationic lipids, or cationic polymers in cancer cell lines.

The effect of counterions (chloride, bromide, methyl sulfate, bisulfate, and triflate) on the *in vitro* transfection of the DOTAP emulsion system was investigated in one of the study

by Young *et.al* [125]. From this study it was revealed that the counterions associated with the lipid head groups significantly affect the binding of the DNA and carrier system. Here, the bisulfate ($H_2SO_4^-$) and triflate counterions (trifluoromethanesulfonate, $CF_3SO_3^-$) promoted significant water dislocations and re-structuring via different orientations, and this extensive water organization are mainly responsible for cationic lipid head group dehydration [125]. According to thermodynamic rules, generally cationic lipids' head group dehydration promotes greater amphiphile packing, leading to smaller aggregates that are destabilized through charged head group repulsions. While increased electrostatic repulsions give rise to metastable particles whose free energies are reduced upon DNA-induced amphiphile re-organization.

The methyl sulfate counterions encouraged the lowest levels of transfection activity (Figure-1.13), presumably due to the stronger electrostatic interaction of sulfate di-anion that supersedes the predicted Hofmeister series of neutral salts. The halogens were more closely associated with the alkyl ammonium head group (charge shielding), in the order of chloride to bromide. An increase in charge shielding leads to water exclusion and closer inter-chain packing, consequently leading to an average increase in the transfection activity from chloride to bromide (Figure-1.13) [125, 126].

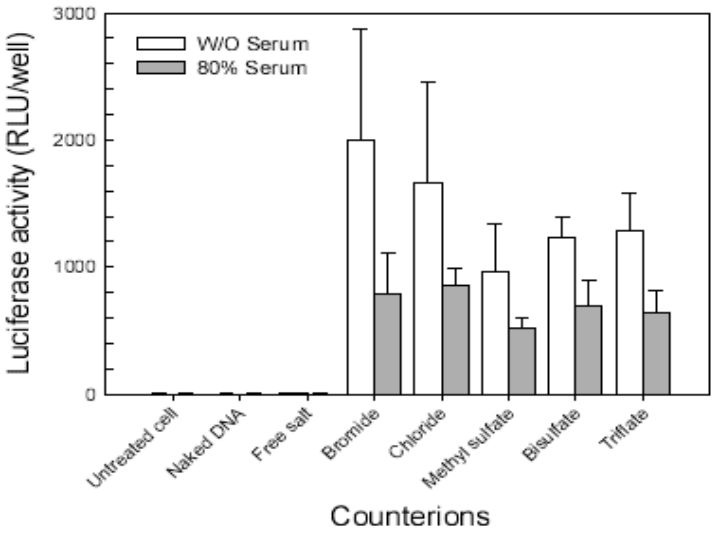

Figure-1.13: Effect of DOTAP with counterions for *in vitro* transfection in COS-1 cell lines (reused with permission from [125]. Copyright [2001], Springer).

From the literature review, it is evident that, the nature and the type of the counterion associated with the head group of an amphiphile has an important influence on the conformation of the amphiphile in solution, and also on the size and the stability of the complexes with DNA [127-129]. In 2004, Saaida *et al.* used chloride, acetate and lactobionate counterions for the poly-norbornene based cationic amphiphile (Figure-1.14) in their work, where the DNA is not only complexed by electrostatic interactions, but also by the hydrophobic effect and packing of the poly-norbornene based polymeric units (cationic) [130]. It was reported that the polymer with the chloride counterion is a fully quarternized polymer and they can form only stretched chains within the polymer seen from TEM images. Chloride is a counterion strongly bonded to the ammonium group, leading to a shielding of the electrostatics repulsions between the units and the formation of large aggregates. Consequently, the interaction/complexation with DNA involves essentially the electrostatic

interactions and gives rise to weakly complexed aggregates with large toroidal or spherical morphologies, which can be easily displaced by the heparin and degraded by DNase I, except only at high NH_3^+/PO_4^- ratios (>2) (Figure-1.15) [130].

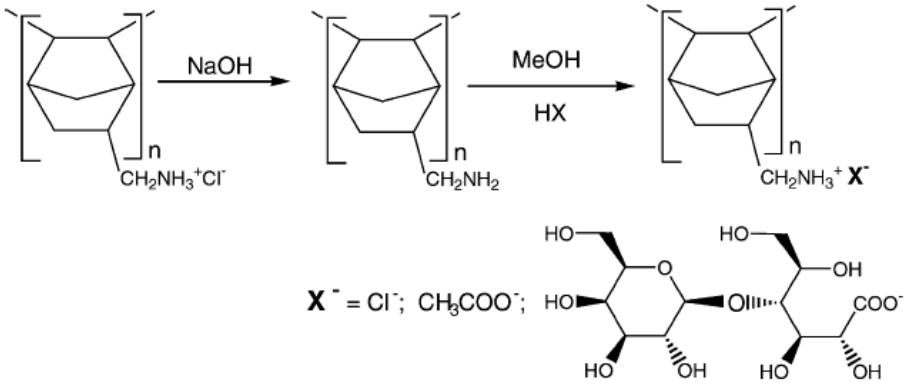

Figure-1.14: Poly-norbornene based cationic amphiphiles based on different counterions (X^-), where X^- = Chloride, Acetate, and Lactobionate anions respectively (reused with permission from [130]. Copyright [2004], Elsevier).

On the other hand, with acetate counterions (CH_3COO^-), the poly-norbornene is able to produce latex particles with packed cores formed by the non-quarternized polymeric units, surrounded by hydrophilic moieties (ammoniums) [128]. The acetate counterion is loosely bonded to the ammonium group leading to the strengthening of the electrostatic repulsions between the ammoniums, but at the same time this effect increased the hydrophobic interactions between the norbornene units. In this case, the interactions with DNA are both electrostatic and hydrophobic, strengthening the stability of the complexes leading to only small spherical aggregates; which in turn affect the *in vitro* transfection efficiency (Figure-1.15). Also, this high affinity and strong interactions explain why this complex is not easily displaced by heparin [130].

Lastly, the lactobionate counterion (lactobionic acid, $C_{12}H_{22}O_{12}$) is a sugar, weakly bonded to the ammonium group, and promotes water organization by a kosmotropic effect. For this polymer, electron microscopy image showed that these latex particles consisted of a packed core, formed by the non-quarternized norbornane units, surrounded by the methylene-ammonium units and a shell of hydrated lactobionate counterions [130]. Here, the kosmotropic effect leads to dehydration of the ammonium group increasing their repulsion and promoting a greater hydrophobic packing of the norbornane units. The conjunction of these two effects gives rise to very small (with a diameter of around 10–20 nm) but metastable particles. Finally, the metastable nature of these complexes explains that the DNA is easily displaced by the heparin [130]. Thus, the transfection efficiency for all the polymers increased with the NH_3^+/PO_4^- ratio (Figure-1.15), possibly due to an increasing interaction of the different polymers/DNA complexes with the cell surface, and also due to the positive charge on the complexes, which partly depends on the nature & type of the counterions.

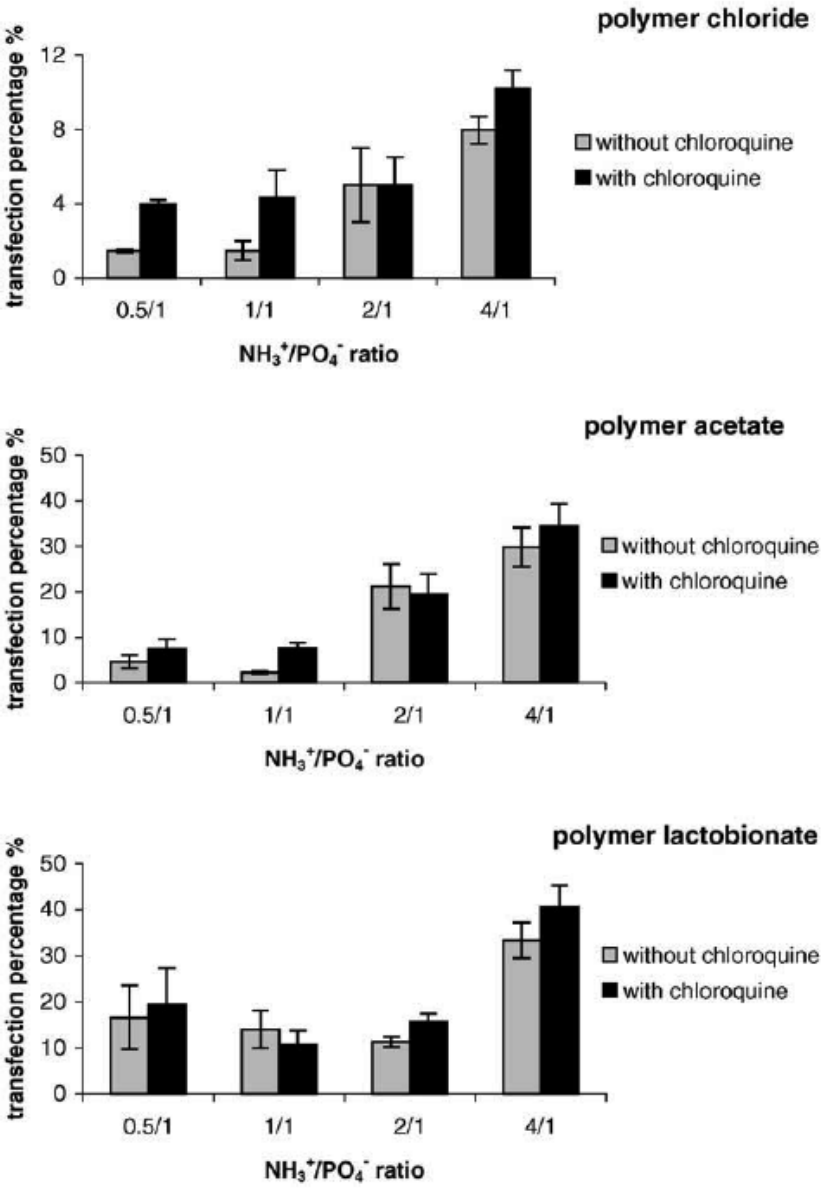

Figure-1.15: Transfection efficiencies of methylene-ammonium poly-norbornene polymers into CHO cell lines. The cells were incubated with poly-norbornene polymers/DNA complex containing 5 μg of plasmid DNA and poly-norbornene polymers at different NH_3^+/PO_4^- ratios. Cells were harvested and GFP activity determined 48 hour after transfection (reused with permission from [130]. Copyright [2004], Elsevier).

1.3.3 Selected counterions of the gemini surfactants for this project

In this work we present a study of 16-2-16 gemini surfactants coupled with 8 different counterions (Chart-1.1) classified into three general groups: (1) small inorganic counterions, which are mainly taken from the Hofmeister series, (2) organic hydroxy-alkyl-di-carboxylate counterions, in which the hydrophilicity of the anion can be modified by inserting hydroxyl group, while keeping the same carbon length and net charge, and (3) the four nucleotide mono-phosphate counterions where ribose sugar and heterocyclic rings (purine/pyrimidine) are present in their structures. The following figure (Figure-1.16) shows the association of monovalent and divalent counterions with one 16 – 2 – 16 GS molecule.

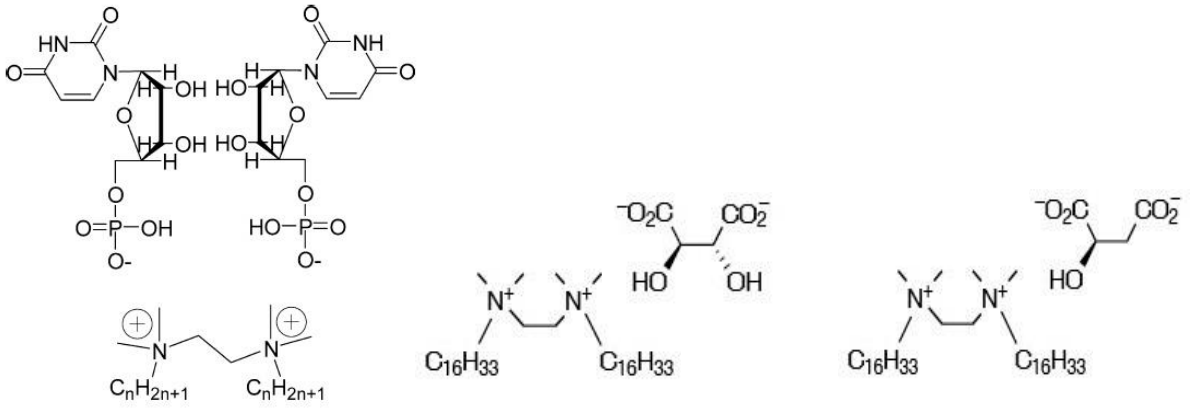

Gemini-UMP Gemini-Tartrate Gemini-Malate

Figure-1.16: Structure of Gemini-UMP, Gemini-tartrate, and Gemini-malate (reused with permission from [121, 131] respectively. Copyright [2005], Elsevier and copyright [1998], John Wiley and Sons respectively).

Chart-1.1: The counterions (X^-) associated with 16-2-16 series of gemini: 16-2-16.2X^-

Group-1: Small counterions from Hofmeister series

Br^-	Cl^-
Bromide	Chloride

Group-2: Hydroxy-di-carboxylates (aliphatic, organic)

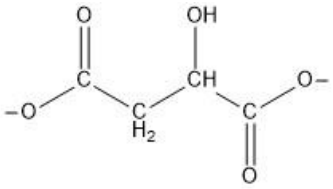

Malate

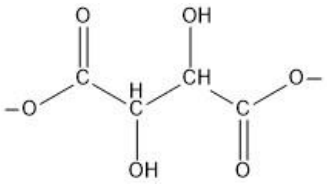

Tartrate

Group-3: Nucleotide mono phosphates, NMPs (organic)

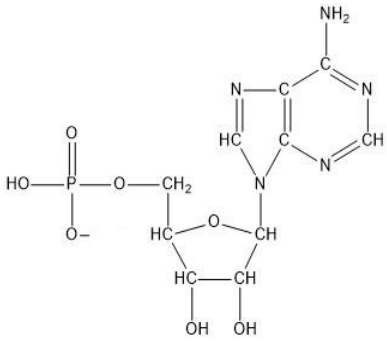

Adenosine 5´mono phosphate (AMP)

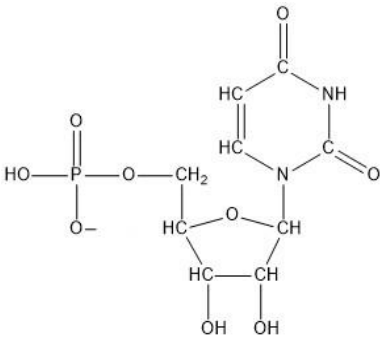

Uridine 5´mono phosphate (UMP)

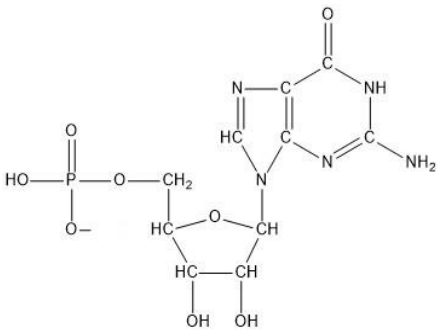

Guanosine 5´mono phosphate (GMP)

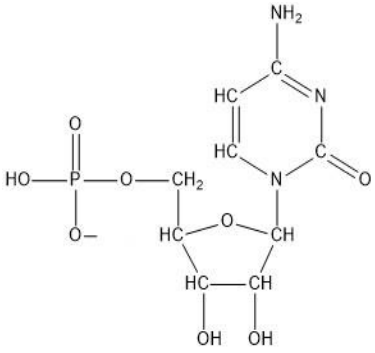

Cytidine 5´mono phosphate (CMP)

2. Objectives & Hypothesis

2.1 Overview of the project

Success of GT relies on having efficient vectors for the transfer and expression of the genetic material at the desired location in the living organism. As discussed earlier, exploitation of the inherent ability of viruses to infect cells has produced the most efficient delivery vectors in gene therapy, but limitations in the safety of viral vectors restrict the application of this method. These limitations have motivated our group in the development of an effective non-viral vector, which uses synthetic, self-assembling gemini surfactants to deliver the DNA. Our goal is to develop new non-viral systems with high transfection efficiencies through the modifications of different counterions of gemini surfactants. As previously mentioned (section 1.3), earlier studies have focused on the effect of variations in the chemical structure of the surfactant itself. It has been previously established that significant modification in the shape of nanoparticles, formed from gemini surfactants, can be achieved through variations in the counterions. We believe that appropriate selection of counterion will allow for better control of nanoparticle size/shape in our non-viral gene therapy vectors.

This work will focus on the characterization of cationic gemini nanoparticles formulated with GSs associated with hydrophilic/hydrophobic anions (mono-atomic or organic) and will investigate the effect of counterions on transfection efficiency by modifying micellization process of DNA-GS complexes. The study will also outline the effects of counterions on micellization of GS in terms of interaction between hydrophobicity of the anions and other ion properties (hydration number, polarizability, ionic morphology etc.).

Methods that will be used to study the self-aggregation, solution properties, and interaction behavior of DNA with GS having different anions are: Tensiometry, Conductometry, Krafft Temperature & Solubility measurements, Densitometry, pH measurements, Viscometry, Dynamic Light Scattering (DLS), Laser Doppler Velocimetry (LDV), and lastly *in vitro* transfection in human epithelial ovarian cancer cell lines (OVCAR-3, ATCC). The recombinant plasmid DNA (pDNA), pNN9 (a circular covalently closed, double stranded helix DNA molecule encoding for an enhanced green fluorescence protein gene, EGFP) will be extracted from *Escherichia coli* and can be used in the nanoparticle formulations for all *in vitro* transfection assays. Transfected cells will express EGFP once the pDNA is transcribed in the nucleus of the cancer cells, and the resultant messenger ribonucleic acid (mRNA) will be translated. The possible outcome will be the development of less toxic non-viral DNA transfection agent based on different counterions of the gemini surfactants with improved transfection efficiency for human ovarian cancer cells.

2.2 Hypothesis statement

Nanoparticles formulated from gemini surfactants having different counterions will enhance the DNA transfection efficiencies for epithelial ovarian cancer cells**.**

2.3. Objectives: short-term goals

The specific objectives of this project include:

1. Syntheses of all the GSs with selected counterions

2. Physiochemical characterization of GSs and gemini nanoparticles by studying:

a. Tensiometry

b. Conductometry

c. Krafft Temperature measurements

d. Densitometry & pH measurements

e. Viscometry

f. Zeta potential (LDV) and Particle size (DLS) [for nanoparticles].

2.4. Objectives: long-term goals

Investigation of the *in-vitro* transfection efficiency, in OVCAR-3 examining:

a. Effect of concentration of gemini

b. Effect of different counterions associated with the gemini

c. Effect of charge ratio of surfactant to DNA

d. Effect of helper lipid along with gemini

3. Materials & Methods

3.1 Materials

3.1.1 Materials for GS syntheses

The raw materials used for the synthesis of gemini surfactants (GSs) were 1-bromohexadecane (99.5 %, Fisher Scientific), 1-chlorohexadecane (99.5 %, Fisher Scientific), *N,N,N′,N′*-tetramethylethane-1,2-diamine, TMEDA (99%, Fisher Scientific), L-(–) malic Acid (98%, Sigma-Aldrich), L-(+) tartaric Acid (98%, Sigma-Aldrich), silver Acetate (99%, Fisher Scientific), silver carbonate (98%, Fisher Scientific), adenosine 5′-monophosphate, AMP (99.8%, mono-hydrate & acid form, Sigma Aldrich), cytidine 5′-monophosphate, CMP (99.9%, acid form, Sigma Aldrich), uridine 5′-monophosphate, UMP (99.9%, acid form, Sigma Aldrich), and guanosine 5′-monophosphate, GMP (99.8%, acid form, Fisher Scientific). These materials were purchased from the specified companies and used directly without any further purification. All solvents used in the syntheses of GS were of HPLC grade (99.99%) and were purchased from Fisher Scientific, USA. Deuterated chloroform (chloroform-D, 99.8 atom % D), DMSO-d_6 (99.9 atom % D), and deuterated water (heavy water, 99.9 atom % D) were purchased from Sigma Aldrich (USA) and directly used for ^{1}H NMR analysis (AVANCE 300 MHz, BRUKER, USA) of raw materials (where applicable) and synthesized GSs. For all experimental analyses, GS solutions were prepared by using fresh ultrapure Milli Q water (Filtered through 0.22 μm Millipak 4.0 Filter, TOC (Total Organic Carbon) = 1 ppb, Specific resistance = 18.2 MΩ.cm @ 25^{0}C) dispensed from Gradient A-10 Milli Q water system (Millipore, Canada) as required.

3.1.2 Materials for *in vitro* transfection

3.1.2.1 Chemicals / Reagents for transfection

DOPE [1,2-di-(9Z-octadecenoyl)-*sn*-glycero-3-phosphoethanolamine] solution (99%), 25 mg/mL in $CHCl_3$ ($C_{41}H_{78}NO_8P$, **M.W.** = 744.05 g/mole) was purchased from Avanti Polar Lipids Inc. (USA) and stored at – 20°C. (±) α-Tocopherol (95%, synthetic, ACROS Organics™) [**F.W.** =430.72, S.G. = 0.95] used as membrane stabilizer for DOPE liposome preparation, was purchased from Fisher Scientific (USA) and used as received.

The following materials were also purchased from Fisher Scientific (USA):

- DPBS (Dulbecco's Phosphate-Buffered Saline, 1 X, without Ca^{2+} & Mg^{2+}, pH 7.2)
- RPMI 1640 1X with L-Glutamine + Phenol Red
- Fetal Bovine Serum [FBS, 20% (v/v)]
- Trypsin [0.25% (w/v) Trypsin (1X) + 0.53mM EDTA; w/o Ca^{2+} & Mg^{2+}] solution
- TrypLE™ Express [animal origin free (AOF), recombinant enzyme] solution
- Penicillin/Streptomycin antibiotics (10,000U/mL Penicillin, 10,000μg/mL Streptomycin in 0.85% NaCl)
- Trypan Blue 0.4% (w/v, pH = 7.5 ± 0.5) in DPBS, and
- Propidium Iodide Solution in DPBS

Opti-MEM® I (1X) Reduced-Serum Medium w/o Phenol Red, and Lipofectamine™ 2000, 1 mg/mL was purchased from Gibco® and Invitrogen™, Life technologies (NY, USA) respectively. Bovine Pancreas Insulin (10 mg/mL insulin in 25 mM HEPES, pH 8.2) solution was purchased from Sigma Aldrich (USA). All these materials mentioned in this section were used as received without any further purification.

3.1.2.2 pDNA

The recombinant plasmid DNA pNN9 (Figure-3.1) was a generous gift from Dr. Roderick Slavcev (School of pharmacy, University of Waterloo). After subsequent amplification, extraction, and confirmation of the extracted DNA by gel electrophoresis and size determination, these pNN9 plasmids were used for all size and zeta potential characterizations and for all transfection assays. K-12 strains of *Escherichia coli* (a Gram-negative, anaerobic, rod-shaped bacterium) were used in the generation of the recombinant cell constructs and **JM109** strains of the same bacterium were employed as hosts for plasmid amplification for extraction. For the extraction of pNN9 plasmids intended for size & zeta potential characterization, centrifugation protocol of the E.Z.N.A.® Plasmid DNA Maxi Kit (OMEGA bio-tek, Georgia, USA) was used. To eliminate the resulting endotoxins, on the other hand, E.Z.N.A.® Endo-Free Plasmid DNA Maxi Kit was used for extraction of the plasmids that are intended to be used for all transfection assays.

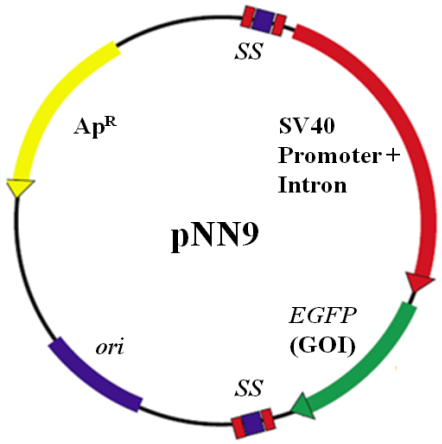

Figure 3.1: The pDNA vector (pNN9) used in this project. This 5.6 kb pDNA vector (pNN9) possesses two Super Sequences (SS, a multipurpose target site) flanking the eukaryotic expression cassette. SV40 enhancer sequences serve as DNA-targeting sequences (DTS) for improved nuclear entry during gene delivery. The EGFP (enhanced green fluorescence protein) gene is the gene of interest used for confirmation of successful transfection (reused with permission of BioMed Central from [132] through the Creative Commons Attribution License).

3.1.2.3 Cell Line

The adherent cell line that was used for transfection assay in this project is human epithelial ovarian cancer (NIH:OVCAR-3) cell line (HTB161™) from ATCC® (Manassas, VA; USA) which is androgen, estrogen, and progesterone receptor positive.

3.2 Methods

3.2.1 Synthesis of 16-2-16 series of GSs $[C_{16}H_{33}(CH_3)_2\text{-}N^+\text{-}(CH_2)_2\text{-}N^+\text{-}(CH_3)_2C_{16}H_{33}].2X^-$

3.2.1.1 Synthesis of 16-2-16 with bromide and chloride counterions

The gemini surfactants with bromide and chloride counterions were synthesized according to the method of Menger and Littau with minor modification (Scheme-3.1) [90, 133-135]. An excess (10 – 50%) of two molar equivalents of the appropriate hexadecyl-halide, $C_{16}H_{33}\text{-}X^-$ (X^- = bromide, chloride) and one molar equivalent of *N,N,N′,N′*-tetramethylethane-1,2-diamine (TMEDA) in acetonitrile was refluxed with continuous stirring for 6 – 12 days, in order to obtain one molar equivalent of corresponding 16-2-16 gemini-halide (halide = bromide, chloride). After reaction, the solvent was removed via rotary evaporation with the resulting product being dissolved in a minimum volume of chloroform ($CHCl_3$) : methanol (CH_3OH) (9 : 1, v/v) and recrystallized with excess acetone. Recrystallization was repeated 2 – 3 times [134, 135] in order to obtain pure (confirmed by ^1H NMR analysis and Tensiometry) gemini surfactants. The white crystals of gemini surfactant were collected via vacuum filtration through grade-41 filter paper (Whatman™ routine quantitative ashless filter paper, Fisher Scientific, USA), and then dried under vacuum at a temperature of 35 – 40^0C for 5 – 6 days until a constant weight was attained. The chemical structure and purity of the gemini surfactants was verified by ^1H-NMR (in

$CDCl_3$). The 16-2-16-bromide was used as the parent compound for the syntheses of the remaining categories of GSs.

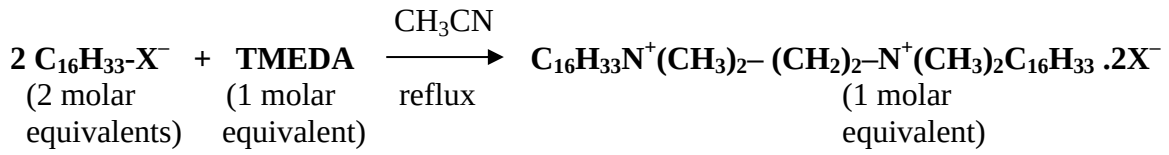

Scheme-3.1: Synthesis reaction for the preparation of 16-2-16-halides

3.2.1.2 Synthesis of 16-2-16 with tartrate and malate counterions

The tartrate and malate salt of the 16-2-16 surfactant were prepared according to Scheme 3.2.

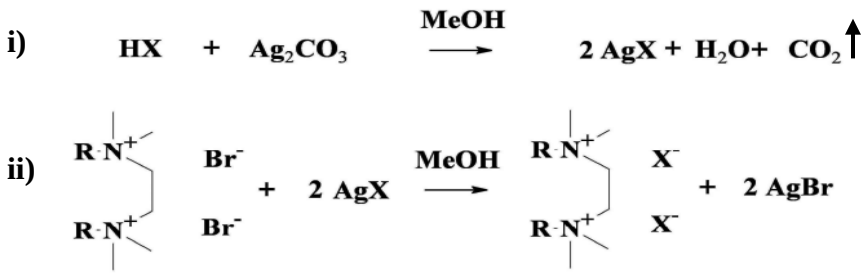

Where, R = Hexadecyl Group ($C_{16}H_{33}$ –); HX = Malic Acid / Tartaric Acid

Scheme-3.2: Synthesis reactions for the preparation of 16-2-16-malate and 16-2-16-tartrate

A solution of the silver salt of tartaric or malic acid in methanol was prepared (scheme-3.2, reaction-i) freshly by adding silver carbonate Ag_2CO_3 (10% excess) to the stoichiometric amounts of tartaric or malic acid solution (in CH_3OH) followed by constant vigorous stirring at 50^0C under slight vacuum to remove carbon dioxide for 90 minutes. A methanol solution of the 16-2-16.2Br^- surfactant (stoichiometric amount) was added to the freshly prepared silver tartrate or malate solution, and the mixture was stirred for 3 hours at 50^0C. A black precipitate of the silver bromide (Ag-Br) was observed within 3 hours,

indicating complete exchange of counterions. Celite was added and mixed via constant stirring for 30 minutes. After cooling to RT, the solution was filtrated over Celite, ensuring the complete removal of Ag-Br. The filtrate was rotary evaporated to remove the methanol solvent leaving a liquid that was dissolved in a chloroform ($CHCl_3$) **:** methanol (CH_3OH) (9 **:** 1, v/v) mixture. The resulting gemini-tartrate or gemini-malate surfactant was precipitated with excess acetone or ethyl acetate [117, 136]. The surfactants were recrystallized from the same solvent system three times to ensure purity. The off white crystals were collected by vacuum filtration dried under vacuum at 35 – 40^0C until constant weight was attained. Structure and purity of the gemini-tartrate and gemini-malate surfactants was verified via ^{1}H NMR (in D_2O).

3.2.1.3 Synthesis of 16-2-16 with nucleotide mono phosphate (NMP) counterions

16-2-16.2NMP gemini surfactants were prepared in two steps: **i)** exchange of bromide ions with acetate (Scheme-3.3), followed by **ii)** exchange of acetate counterions with the corresponding nucleic acids (Scheme-3.4).

i) Gemini (16-2-16) bromide-acetate exchange:

$$C_{16}H_{33}N^{+}(CH_3)_2\text{–}(CH_2)_2\text{–}N^{+}(CH_3)_2C_{16}H_{33}\ .2Br^{-} + 2.CH_3\text{-}COO^{-}\text{–}Ag^{+} \xrightarrow{MeOH} C_{16}H_{33}N^{+}(CH_3)_2\text{–}(CH_2)_2\text{–}N^{+}(CH_3)_2C_{16}H_{33}\ .2Ac + 2\ AgBr\downarrow$$

Scheme-3.3: Ion exchange reactions for 16-2-16-bromide to 16-2-16-acetate

To 100 mL of 16-2-16-bromide solution (in MeOH), silver acetate (Ag-Ac) (10% excess) was added followed by constant stirring at 55 – 60^0C for 4 hours. Silver bromide

(AgBr) precipitate appeared within 4 hours, indicating complete exchange of counterion. The solution was filtrated over Celite, and the remaining filtrate was rotary evaporated to remove the solvent. The resulting dense liquid was dissolved in chloroform ($CHCl_3$) **:** methanol (CH_3OH) (9 **:** 1, v/v) mixture, and the gemini-acetate powder was obtained by precipitating with excess acetone (or ethyl acetate) followed by 3 recrystallizations in the same solvent system [137]. The off white crystals were collected by vacuum filtration, dried under vacuum at 35 – 40^{0}C until constant weight was attained. Structure and purity of the gemini-acetate surfactant was verified via ^{1}H NMR (in D_2O).

ii) Gemini 16-2-16.2Ac to 16-2-16-nucleotides:

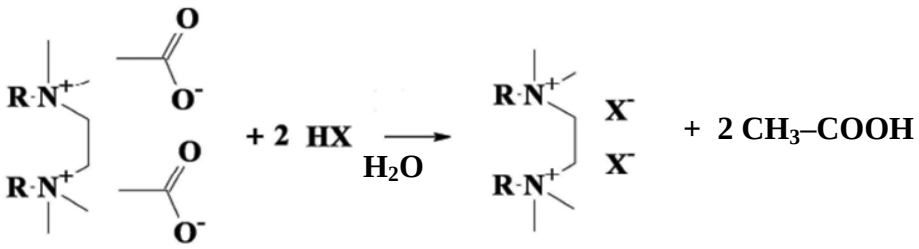

Where, R = Hexadecyl Group ($C_{16}H_{33}$ –); HX = Nucleotide Mono Phosphates, NMPs (AMP, GMP, CMP, UMP)

Scheme-3.4: Ion exchange reactions for 16-2-16-acetate to 16-2-16-NMP

Approximately 50 mL of aqueous solution of the gemini-acetate was added to an aqueous solution (80–100 mL) of the desired nucleotide mono phosphate, NMP (10% excess) followed by constant stirring for 3 – 4 hours at 45 – 50^{0}C. Upon completion, the mixture was cooled to room temperature and then allowed to freeze at –80^{0}C overnight before lyophilization. The frozen GS-NMP samples were lyophilized for 4–6 days with a FreeZone® 2.5 L Freeze Dry System (Labconco Corporation; Kansas City, Missouri) at an

operating temperature of -86^0C. Consecutive lyophilisation and dissolution in water were repeated until the total evaporation of acetic acid occurred (confirmed by ^{1}H NMR) [137].

3.2.2 ^{1}H NMR characterization

All ^{1}H NMR measurements were carried out at 25.0 ± 0.1^{0}C on a Bruker Avance NMR spectrometer operating at 300 MHz with the field strength of 7.0 Tesla. D_2O and CD_3OD (99.9 atom % D) were used to prepare stock solutions (7-10 mg/mL) of the synthesized surfactants for ^{1}H NMR study. The peaks were referenced with respect to tertamethylsilane, TMS (δ = 0.00 ppm) when CD_3OD was used as a solvent and to 4,4-dimethyl-4-silapentane-1-sulfonic acid, DSS (δ = 0.00 ppm) when D_2O and/or DMSO was used as a solvent. In all NMR experiments, the number of scans (16 on average) was adjusted to achieve good signal-to-noise, and was recorded with a two seconds relaxation delay in a digital resolution of 0.04 Hz/data point at a flip angle of 30^0 of the pulse program. The following notation was used for the ^{1}HNMR splitting patterns: singlet (s), doublet (d), triplet (t), multiplet (m), and double doublet (dd).

3.2.3 Measurement of CMC

Critical micelle concentrations (CMC) of all the synthesized GSs were determined using surface tension and specific conductance measurement methods.

3.2.3.1 Surface Tension measurement

Surface tension measurements were carried out using the du Noüy ring method [84, 94, 105, 138] on a Lauda TE3 automated Tensiometer (Lauda, Germany) equipped with a Platinum-Iridium (Pt–Ir) alloy du Noüy ring with a circumference of 6.001 cm (radius =

0.955 cm). The ring was thoroughly cleaned and flame dried before each experiment. Concentrated stock solutions (0.3 mM, and 0.01 mM) of the surfactant of interest were added to 50 mL of freshly dispensed Milli-Q water (kept within the Simax 80 vessel, Fisher Scientific, USA) using a model 765 Dosimat auto-titrator (Metrohm, USA) and surface tension readings were taken after thorough mixing and temperature equilibration. The measured surface tension values were automatically corrected according to the procedure of Harkins and Jordan [139, 140] using the instrument software. All measurements were carried out in replicates with a minimum of five successive measurements having a standard deviation that did not exceed 0.10 mN/m. Temperature was maintained at a constant value (25 ± 0.05^0C) using a Lauda Ecoline RE 304 (Lauda, Germany) circulating water bath. All CMC determinations were carried out in duplicate for each of the gemini surfactants studied.

3.2.3.2 Conductivity measurements:

Electrical conductivity was used to determine the critical micelle concentration (CMC) and the degree of micelle ionization (α) of the GSs. Since the conductivity is strongly influenced by the presence of any metastable or kinetically controlled aggregates [118], care was taken so that all samples were treated in the same manner. Specific conductance, κ (in μS/cm) of all the surfactant solutions was measured as a function of concentration with a SevenEasy^{TM} S30 Conductivity Meter (METTLER TOLEDO, Switzerland). All measurements were performed in a double-walled glass titration cell (Fisher Scientific, USA) with the temperature being controlled at 296.15 K (23 ± 0.05^0C) using Lauda Ecoline RE 304 (Lauda, Germany) circulating water bath. Concentrated surfactant solution was successively added to 40 mL of Milli Q water contained in the titration cell. Sufficient time was allowed between consecutive additions for the system to equilibrate. The specific conductance (κ) as

a function of surfactant concentration was measured using an InLab® 730 conductometer probe (electrode) with a cell constant of 0.56 cm^{-1} and with inbuilt automatic temperature compensation (ATC). The conductometer was initially calibrated with standard solutions of specific conductivity 1413 μS/cm. All the conductometric titrations were carried out in duplicate for each of the gemini surfactants studied.

3.2.4 Krafft Temperature measurement

Saturated aqueous solutions (~1.5 mM, >> CMC for all surfactants) were prepared, separately, for each gemini surfactant, by sonication at 55^0C. After cooling at room temperature (25 – 30^0C) they were held at 4^0C in a refrigerator for at least 45 – 48 hours [81, 94], until precipitates of the hydrated surfactant crystals appeared. The precipitated solutions were then introduced into conductivity titration cell described in the previous section. Temperature was controlled to ± 0.05^0C with a Lauda Ecoline RE 304 (Lauda, Germany) circulating water bath. The initial temperature was set to 5^0C and then was gradually increased by 1^0C in every 10 minutes up to 55^0C. The temperature point where the precipitated (hydrated crystals of gemini) gemini solution became completely clear was detected by visual inspection through the transparent titration cell and recorded as the Krafft temperature (T_K). Krafft temperature determinations were carried out in duplicate for each gemini surfactant.

3.2.5 Density and pH measurement

To measure the density and pH of the GS solutions, stock solutions for each gemini surfactant, by sonication at 55^0C were prepared at a specific concentration (~1.5 mM, >> CMC for all surfactants). The density was measured in triplicate using a 2 mL pycnometer

(Fisher Scientific, USA) at 55^0C (as this temperature is above the T_K for all the eight GSs) using the equation for specific gravity (Equation-3.1) as the following:

Density of a liquid (in g/mL units), $D_L = (M_L \times D_W) / M_W$ 3.1

Where,

M_L = Mass of the liquid at experimental temperature

D_W = Density of Milli Q water at experimental temperature (0.98 g/mL @ 55^0C)

M_W = Mass of of Milli Q water at experimental temperature

pH measurements were made in triplicate at 55^0C using an Accumet XL 60 dual channel pH meter (Fisher Scientific, USA) through the AccuCap™ Combination pH electrode (13-620-130) carrying the inbuilt ATC probe (13-602-19).

3.2.6 Bacterial growth and extraction of plasmid

Before the extraction process of plasmids, a single colony of bacterial strain JM109 **[pNN9]** (JM109 of *Escherichia coli* is a generous gift from Dr. Slavcev's research group) was grown overnight (18 – 20 hours) in 5 mL of growth media **[**Luria-Bertani (LB) broth + Ampicillin (Ap) antibiotic (100 μg/mL)**]** in a temperature controlled bench-top shaker (New Brunswick Scientific Excella™ E24, Fisher Scientific, US) at 250 rpm and 37^0C with circulating air supply. A new batch of cells were grown overnight from that last day culture at 1:100 dilution in 50 mL of growth media (within a 250 mL Erlenmeyer flask), at the same temperature and rpm. After the overnight treatment, final culture was taken out from the shaker when the $A_{600} \approx 0.8 – 0.9$, at which point indicates the exponential bacterial growth of

mid logarithmic phase [132]. As already mentioned, E.Z.N.A.® Endo-Free Plasmid DNA Maxi Kit and E.Z.N.A.® Plasmid DNA Maxi Kit (OMEGA bio-tek, Georgia, USA) were used for extraction of DNA for transfection and Zetasizer studies respectively. In both of the cases, standard centrifugation protocol was followed to extract the plasmids.

An aliquot of 200 ng/μL plasmid solution (in Milli Q water) was prepared from the extracted plasmid stock and the pH of that solution was measured in duplicate while the average is reported (pH = 6.1 ± 0.2). The pH value of the plasmid solutions will help to extrapolate an assumption on the compatibility of the transfection complexes/nanoparticle formulation mixtures. The extracted plasmid stock was then immediately stored at – 20^0C freezer as recommended in the protocol. The estimated bacterial cell concentration in the extracted culture was calculated according to optical density readings where, OD_{600} (= 2 x A_{600}). The DNA production efficiency and confirmation of the DNA size was assessed by agarose gel electrophoresis (AGE) (Alpha-Imager HP, Alpha Innotech, Cell Biosciences, USA). Finally, the concentration of the extracted plasmid were analysed by UV spectrophotometry (NanoDrop 2000, Fisher Scientific, USA).

3.2.7 Confirmation of extracted plasmids: Agarose Gel Electrophoresis (AGE)

The protocol followed for AGE was as described by Lee *et al.* (2012) with minor modification [141]. After casting the AGE tray and initial setup of the apparatus, the required volume (for ≥ 500 ng of plasmid) of the extracted plasmid sample, 1 **μL** of the DNA-ladder standard (aka, control, 500 μg /μL, 1 kb size), and 6X Sample Loading Buffer/Dye solution (in glycerol) at a ratio of (Loading Buffer : Plasmid =) 1 : 5 was carefully pipetted, and separately mixed in appropriate combination (Ladder + Dye, and Samples + Dye) on

parafilm sheets (Curwood Parafilm M™ Laboratory Wrapping Film, Fisher Scientific, USA). After adjusting the final volume of the individual mixture(s) by adding Milli Q water, 10 μL of each mixture was separately pipetted into the designated wells before running the power.

The electrophoresis power (potential difference of 100 volts, and 3 amperes of current) was allowed to run until the blue dye approaches the end of the gel (generally >1.5 hr, until clear band separation). As DNA diffuses within the gel over time, very light bands are difficult to see, and thus, the UV imaging (provided in the "Appendix" section) was done, shortly after cessation of electrophoresis, through an UV transilluminator at 302 nm. The pNN9 plasmid has a size of 5.6 kb in its normal covalently closed circular (CCC) form [132], and from the UV image of the AGE, the size of the pNN9 plasmid was confirmed. Experimentally extracted plasmid DNA mainly has two different forms of DNA: a closed circle supercoiled form (SC), and a nicked circular form (NC) as in small fractions [142]. In the UV images, the observed bands of closely similar intensity of the pNN9 plasmid near 5 kb and 9 kb (approximately) region corresponding to the DNA ladder control suggested the existence of both topological form of plasmids within the extracted sample. Lastly, to confirm the purity of the extracted plasmid, $A_{260/280}$ values from the NanoDrop 2000 spectrophotometer were also recorded (provided in the 'Appendix' section) and confirmed with the values given in the extraction kit (within 1.8 – 2).

3.2.8 Measurement of Particle size (diameter) and Zeta potential (ζ)

Particle size and zeta potential were measured for all gemini surfactant solutions, as well as for nanoparticles prepared from gemini surfactant/DOPE, gemini surfactant/Plasmid DNA, and gemini surfactant/DOPE/Plasmid DNA combinations at various charge ratios. All

particle size & zeta potential measurements were made using a Malvern Zetasizer Nano ZS instrument (Malvern Instruments, Worcestershire, UK).

3.2.8.1 Preparation of GS based nanoparticles

3.2.8.1.1 Preparation of GSs stock solution

For both the size and zeta potential measurements for all the eight GS, 1.5 mM solution were prepared after constant sonication at or above their respective Krafft temperature and then the solutions were filtered through 0.2 μm syringe filters (Thermo Scientific™ Nalgene™ Syringe Filters, US) immediately after solubilizing them to prepare the final stock solution for use. The following table (Table-3.1) enlists the molecular mass of all the GS with different counterions.

Table-3.1: Molecular mass of 16 – 2 – 16 series of GS with eight different counterions

16 – 2 – 16. 2Br $^-$	=	726.86 g/mole	16 – 2 – 16. 2GMP $^-$	=	1289.50 g/mole
16 – 2 – 16. 2Cl $^-$	=	638.05 g/mole	16 – 2 – 16. 2UMP $^-$	=	1211.40 g/mole
16 – 2 – 16. 2AMP $^-$	=	1257.50 g/mole	16 – 2 – 16. Malate $^{--}$	=	699.124 g/mole
16 – 2 – 16. 2CMP $^-$	=	1209.42 g/mole	16 – 2 – 16. Tartrate $^{--}$	=	715.12 g/mole

3.2.8.1.2 Preparation of 1 mM DOPE liposomal solution

DOPE vesicles (1 mM) were prepared in Dulbecco's Phosphate Buffer Saline (PBS) with modification of the procedures outlined according to Wettig *et al*. [143]. Here, lipid film hydration method (the most widely used method) was followed for the preparation of multi lamellar vesicles (MLVs) for a lipid, and the method consist of two [144] major steps –

a) Formation of a Lipid Film

b) Hydration of the Lipid Film/Cake

3.2.8.2 Formulation of nanoparticles and measurement of size and ζ-potential

The prepared stock solutions of GSs and DOPE was sonicated for 30 minutes at the Krafft temperature of GSs and then filtered through Nalgen 0.20 μm and 0.45 μm syringe filters (Thermo Scientific, USA) respectively before using to formulate the nanoparticles. The same applies to the preparation of nanoparticles for *in vitro* transfections except that, the GS stock solutions and the DOPE-vesicle solution were prepared aseptically to avoid unforeseen contamination.

Different aliquots of the 16 – 2 – 16 stock solution (0.8 µl, 2 µl and 4 µl per 0.4 µg DNA) were used to generate GS/DNA lipoplexes at 2:1, 5:1, and 10:1 N^+/P^- charge ratios respectively. After 15 minutes of incubation at room temperature, different aliquots (3 µl, 7.6 µl and 15.2 µl) of 1 mM DOPE vesicle solution (in DPBS) were added and then subsequent mixtures were further incubated for 20 minutes at room temperature to generate lipoplexes, of varying charge ratios, with a constant GS to DOPE ratio of 2 **:** 5. The following table (Table-3.2) was used as a blueprint for the formulation of nanoparticles.

As mentioned earlier, particle sizes for plasmid, GS solutions, and the resulting plasmid-gemini (G+P) complexes & plasmid-gemini-DOPE (G+P+D) lipoplexes were measured by dynamic light scattering (DLS, where θ = 173°) using Malvern Zetasizer Nano ZS instrument (Malvern instruments, UK). A minimum of 700 μL sample volume was taken into DTS 1070 folded capillary cells / cuvette to measure both sizes and ζ-potentials of the respective samples, and Zetasizer software of version 7.11 was used for machine operation. Here, both the sizes & zeta potentials (ζ) values for all the samples mentioned in Table-3.2 were measured at 25^0C in quintuplicate and the averages (n = 5) were reported.

Table-3.2: Mapping of nanoparticles formulation based on GSs

Formulation Compounds*	**GS + D + P (+/- =10:1)**	**GS + D + P (+/- =5:1)**	**GS + D + P (+/- =2:1)**	**GS + D**	**GS**	**P**	**D**
Plasmid (P)	0.4 µg	0.4 µg	0.4 µg	–	–	0.4 µg	–
Gemini (GS) (1.5 mM)	4 µL	2 µL	0.8 µL	4 µL	4 µL	–	–
DOPE (D) (1 mM)	15.2 µL	7.6 µL	3 µL	15.2 µL	–	–	15.2 µL
Milli Q Water	50 µL	50 µL	50 µL	50 µL	50 µL	50 µL	50 µL

** GS: Gemini Surfactant with 8 different counterions; D: DOPE SUV solution; P: pNN9 Plasmid solution*

3.2.9 *In vitro* Transfection Assay

3.2.9.1 *In vitro* transfection assay in OVCAR-3 cells

In vitro transfection experiments were carried out over 4 consecutive days, following a standard optimized protocol for OVCAR-3 transfection previously developed in our lab [145]. Cryopreserved OVCAR-3 cells from the liquid nitrogen (-196^0C) cryopreservation storage system (Locator™ 6 Plus Thermolyne Rack and Box Systems, Thermo Scientific, US) were directly seeded in 75cm^2 Nunc EasYFlask with filter cap (Thermo Scientific, US) in standard growth media [RPMI-1640 (HyClone, Thermo Scientific, US) supplemented with 20% Fetal Bovine Serum (FBS) (HyClone, Thermo Scientific, US), 1% Bovine pancreas insulin solution in HEPES buffer (Sigma Aldrich, US), and 1% penicillin-streptomycin (Fisher Scientific, USA)]. The cells were grown at 37^0C with 5% CO_2 in a Thermo Forma II series water jacketed incubator (Fisher Scientific, USA), and maintained at 70-80% (< 80% is recommended) confluency prior to transfection.

On the first day of the experiment cells were detached and seeded at a concentration of 50,000 cells/well into a BioLite 24-well cell culture plate (Thermo Scientific, US), and

were allowed to grow and to get adhered upon the surfaces of each well for ~24 hours. On day 2, the seeded cells were washed with DPBS and fresh RPMI-1640 (without FBS or antibiotics) to which 1 % insulin was added. Transfection lipoplexes were prepared in Opti-MEM (Gibco, Invitrogen) and the resulting lipoplexes were added drop-wise at amounts corresponding to 0.4 μg of DNA per well. Transfection with 1.2 μl of Lipofectamine^{TM} 2000 (1 mg/mL, Invitrogen) per 0.4 μg of DNA, was also carried out according to the manufacturer's protocol and served as a positive control. Cells were also transfected with naked plasmid, plasmid complexed with gemini surfactant alone, DOPE only, and DOPE complexed with gemini surfactants (Table-3.3 was used as a template), as controls. The mapping for transfection mixtures is given in Table-3.4. After adding transfection formulations, cells were incubated at 37^0C with 5% CO_2 for 5 hours before the transfection medium was replaced by fresh RPMI-1640 supplemented with 20% FBS & 1% insulin. Cells were further grown until 24 hours post-transfection at which point the cells were collected, washed, and re-suspended in DPBS in Nunc 15mL Conical Sterile Polypropylene Centrifuge Tubes (Thermo Scientific, US) for flow cytometry analysis (Day 4). All the experiments for each transfection formulation were done in triplicate; each experiment was done twice in parallel, for which average (n = 6) transfection efficiencies and cell viabilities are reported.

3.2.9.2 Flow cytometry

Transfection efficiency (TE) was determined 24 hours after transfection by determination of EGFP fluorescence using a Guava easyCyte™ 8HT benchtop flow cytometer (EMD Millipore, Merck KGaA, Billerica, MA) which is a part of Dr. Spagnuolo's lab in the School of Pharmacy. Flow cytometry analysis gives information about the comparative expression of green fluorescence which serves as an indicator of transfection efficiency in terms of % GFP (green fluorescence protein) expression. The % GFP expression indicates the percentage of cell population expressing GFP over residual fluorescence of non-transfected cells (no treatment category) or transfected with only pDNA and lipid mixture alone [146].

Briefly, cells were detached by trypsinization, and then centrifuged at $0 - 4^0$ C and 1800 rpm for 10 min. The resulting cell pellets were washed and suspended with 1000 µL of DPBS, followed by another centrifugation step, and finally resuspended in 200 µL of DPBS. The resuspended cells were then seeded again in a flat bottom 96 well plate (SARSTEDT, Fisher Scientific, USA) as per machine specifications. To determine the cytotoxicities after transfection by detecting dead cells, 2.5 µL of propidium iodide (PI, 50 mg/mL) was added to each sample and incubated in an ice bath for at least 30 min before the flow cytometer analysis. The analyzed data are expressed as Mean (n = 6) ± SD (standard deviation)

Table-3.3: Transfection formulation template for each well

Formulation Compounds	Plasmid (P)	Gemini GS (1.5 mM)	DOPE (D) (1 mM)	Opti-MEM (1X)	Lipofec--tamine 2000	# of wells
GS + D + P (+/- =10:1)	0.4 µg	4.04 µL	15.2 µL	50 µL	–	7, 7, 7 (Inc. 1 extra for each GS)
GS + D + P (+/- =5:1)	0.4 µg	2.02 µL	7.6 µL	50 µL	–	
GS + D + P (+/- =2:1)	0.4 µg	0.81 µL	3.03 µL	50 µL	–	
GS + D (+/- =10:1)	–	4.04 µL	15.2 µL	50 µL	–	7, 7, 7 (Inc. 1 extra for each GS)
GS + D (+/- =5:1)	–	2.02 µL	7.6 µL	50 µL	–	
GS + D (+/- =2:1)	–	0.81 µL	3.03 µL	50 µL	–	
GS + P For (+/- =10:1)	0.4 µg	4.04 µL	–	50 µL	–	7, 7, 7 (Inc. 1 extra for each GS)
GS + P For (+/- =5:1)	0.4 µg	2.02 µL	–	50 µL	–	
GS + P For (+/- =2:1)	0.4 µg	0.81 µL	–	50 µL	–	
D (Lipid only) For (+/- =10:1)	–	–	15.2 µL	50 µL	–	7, 7, 7 (Inc. 1 extra)
D (Lipid only) For (+/- =5:1)	–	–	7.6 µL	50 µL	–	
D (Lipid only) For (+/- =2:1)	–	–	3.03 µL	50 µL	–	
P (Plasmid only)	0.4 µg	–	–	50 µL	–	7 (Inc. 1 extra)
L (Lipofectamine 2000) + Plasmid	0.4 µg	–	–	50 µL	1.2 µL	13 (Inc. 1 extra)
NT (No Treatment)	–	–	–	50 µL	–	13 (Inc. 1 extra)

Table-3.4: Mapping for BioLite 24-well multidishes for transfection

Plate I: GDP Plate:

	1	2	3	4	5	6
A (10:1)	D + G + P	D + G + P	D + G + P	D + G + P	D + G + P	D + G + P
B (5:1)	D + G + P	D + G + P	D + G + P	D + G + P	D + G + P	D + G + P
C (2:1)	D + G + P	D + G + P	D + G + P	D + G + P	D + G + P	D + G + P
D	–	–	–	–	–	–

Plate II: GD Plate:

	1	2	3	4	5	6
A (10:1)	D + G	D + G	D + G	D + G	D + G	D + G
B (5:1)	D + G	D + G	D + G	D + G	D + G	D + G
C (2:1)	D + G	D + G	D + G	D + G	D + G	D + G
D	–	–	–	–	–	–

Plate III: GP Plate:

	1	2	3	4	5	6
A (10:1)	G + P	G + P	G + P	G + P	G + P	G + P
B (5:1)	G + P	G + P	G + P	G + P	G + P	G + P
C (2:1)	G + P	G + P	G + P	G + P	G + P	G + P
D	P	P	P	P	P	P

Plate IV: D Plate:

	1	2	3	4	5	6
A (10:1)	D	D	D	D	D	D
B (5:1)	D	D	D	D	D	D
C (2:1)	D	D	D	D	D	D
D	–	–	–	–	–	–

Plate V: Control Plate:

	1	2	3	4	5	6
A (10:1)	NT	NT	NT	NT	NT	NT
B (5:1)	NT	NT	NT	NT	NT	NT
C (2:1)	L + P	L + P	L + P	L + P	L + P	L + P
D	L + P	L + P	L + P	L + P	L + P	L + P

Here, P = Plasmid, L = Lipofectamine™ 2000, G = GSs @ 1.5 mM, D = DOPE @ 1 mM, NT = no treatment

4. Results & Discussion

4.1 Syntheses and ^{1}H NMR Characterization of GSs

The average yields for the synthesis of the gemini surfactants examined in this work are provided in Table 4.1, although we were not really concerned about the actual yield from the syntheses. The yield obtained for the synthesis of the chloride salt is markedly low compared to the other surfactants prepared; especially given that this synthesis involved only a single synthetic step as compared to the organic counterion salts. This low yield for the 16-2-16 surfactant is attributed to the lower reactivity of 1–chlorohexadecane relative to 1–bromohexadecane in an S_N2 type reaction [147]. Confirmation of the gemini surfactant structures was obtained by ^{1}H NMR (all the spectra have been provided in the "Appendix" section). Assignment of protons in the ^{1}H NMR spectra for the 16-2-16 surfactant is illustrated in Figure 4.1. Chemical shift data for each surfactant is summarized below.

Table-4.1: Average yield of the gemini surfactants after syntheses

Name of the final products	Name of the reactants	Purification	Average yield*of final products (%)
16 – 2 – 16 . 2Br $^-$	Cetyl Bromide, TMEDA	Recrystallization	65
16 – 2 – 16 . 2Cl $^-$	Cetyl Chloride, TMEDA	Recrystallization	30
16 – 2 – 16 . 2Ac $^-$	Gemini-Br $^-$, Ag-Acetate	Recrystallization	70
16 – 2 – 16 . 2AMP $^-$	Gemini-Ac $^-$, AMP.H_2O	Lyophilization	75
16 – 2 – 16 . 2CMP $^-$	Gemini-Ac $^-$, CMP	Lyophilization	85
16 – 2 – 16 . 2UMP $^-$	Gemini-Ac $^-$, UMP	Lyophilization	85
16 – 2 – 16 . 2GMP $^-$	Gemini-Ac $^-$, GMP	Lyophilization	80
16 – 2 – 16 . Tartrate $^{--}$	Gemini-Br $^-$, Ag-Tartrate	Recrystallization	50
16 – 2 – 16 . Malate $^{--}$	Gemini-Br $^-$, Ag-Malate	Recrystallization	55

Yield = (Actual yield / Theoretical yield) x100

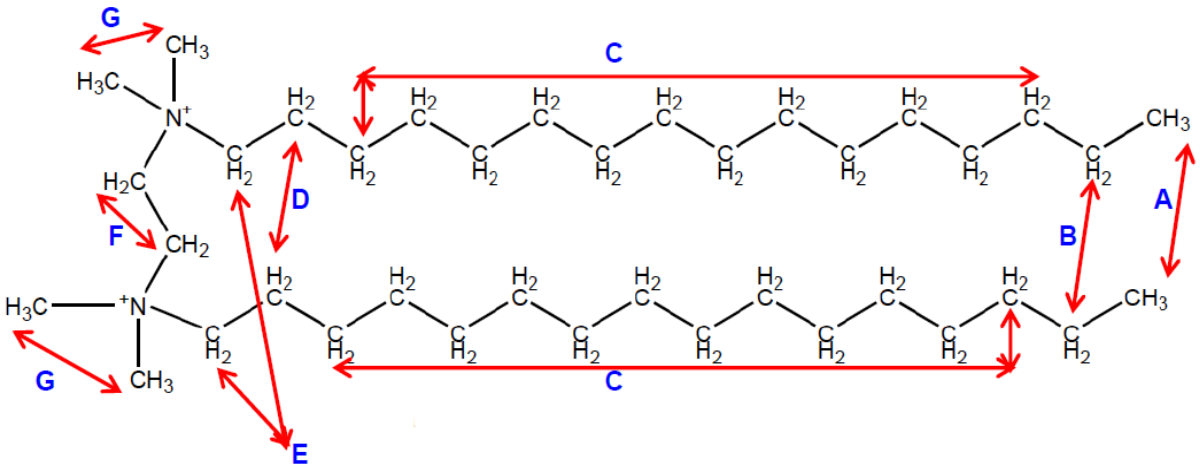

Figure-4.1: Assignment of protons in 16-2-16 gemini surfactant structure used in the interpretation of ^{1}H NMR spectra.

Chemical shift data for each surfactant:

a) 16-2-16.2X $^{-}$ (X $^{-}$ = Br $^{-}$ or Cl $^{-}$). ^{1}H NMR (300 MHz, CD_3OD, 25 °C, δ ppm):

4.75 (4H, t); 3.69 (4H, t); 3.49 (12H, m); 1.78 (4H, m); 1.35 (4H, m); 1.23 (48H, m); 0.83-0.87 (6H, t).

b) 16-2-16.2AMP $^{-}$. ^{1}H NMR (300 MHz, D_2O, 25 °C, δ ppm):

8.36 (1H, s); 8.07 (1H, s); 5.98 (2H, d); 4.66 (4H, t); 4.38 (2H, m); 4.22 (2H, m); 4.03 (4H, m); 3.81 (4H, t); 3.35 (4H, t); 3.17 (12H, m); 1.61 (4H, m); 1.19 (4H, m); 1.05 (48H, m); 0.67 (6H, t).

c) 16-2-16.2UMP $^{-}$. ^{1}H NMR (300 MHz, D_2O, 25 °C, δ ppm):

7.95 (1H, d); 5.91 (1H, d); 5.86 (1H, s); 4.29 (2H, m); 4.17 (2H, m); 4.05 (4H, m); 3.87 (4H, t); 3.46 (4H, t); 3.23 (12H, m); 1.75 (4H, m); 1.34 (4H, m); 1.19 (48H, m); 0.79 (6H, t).

d) 16-2-16.2CMP $^{-}$. ^{1}H NMR (300 MHz, D_2O, 25 °C, δ ppm):

7.99 (1H, t); 6.08 (1H, d); 5.90 (2H, d); 4.25 (2H, m); 4.18 (2H, m); 4.09 (4H, m); 4.02 (4H, t); 3.39 (4H, t); 3.21 (12H, m); 1.70 (4H, m); 1.32 (4H, m); 1.22 (48 H, m); 0.82 (6H, t).

e) 16-2-16.2GMP $^{-}$. ^{1}H NMR (300 MHz, D_2O, 25 °C, δ ppm):

7.99 (1H, d); 5.79 (1H, d); 4.64 (2H, t); 4.38 (2H, m); 4.16 (2H, m); 3.98 (4H, m); 3.81 (4H, t); 3.36 (4H, t); 3.15 (12H, m); 1.63 (4H, m); 1.14 (4H, m); 1.11 (48H, m); 0.72 (6H, t).

f) 16-2-16.Tartrate $^{--}$. ^{1}H NMR (300 MHz, D_2O, 25 °C, δ ppm):

4.20 (2H, d); 3.84 (4H, t); 3.39 (4H, t); 3.18 (12H, m); 1.68 (4H, m); 1.28 (4H, m); 1.23 (48H, m); 0.81 (6H, t).

g) 16-2-16.Malate $^{--}$. ^{1}H NMR (300 MHz, D_2O, 25 °C, δ ppm):

4.11 (1H, t); 3.81 (4H, t); 3.35 (4H, t); 3.14 (12H, m); 2.22-2.26 (2H, m); 1.65 (4H, m); 1.27 (4H, m); 1.19 (48H, m); 0.77 (6H, t).

4.2 Physicochemical characterization of Gemini Surfactants

As mentioned in the "Objective" section 2.3, various techniques were employed for physicochemical characterization the gemini surfactants. Tensiometry and conductometry were used to characterize the aggregation behavior of gemini surfactants. Krafft temperature, solubility of organic counterions, density, pH, viscosity, and foamability measurements were done as a part of physicochemical characterization for all the gemini surfactants. The data for solubility, viscosity and foamability measurements have been provided in the "Appendix" section of this dissertation.

4.2.1 Characterization of Gemini Surfactant Aggregation using Tensiometry and Conductometry

We employed the tensiometric and conductometric method to study the micellization of the 16-2-16 series of gemini associated with eight different counterions in the structure.

The majority of literature studies in which the impact of counterion on surfactant aggregation is examined use added salt as opposed to exchange of the counterion [114, 115, 134, 138, 148-162]. It should be noted that the effects of added salt, as opposed to the exchange of counterion can result in dramatic differences in aggregation properties, in part due to the increase in ionic strength which has a major effect to dissociate the counterions of the GSs, and partly because the incomplete removal of the original counterion may still affect the surface and aggregation properties [134].

4.2.1.1 CMC and head group area determinations by Tensiometry

The micellization behavior and surface activity of an ionic surfactant is mainly dependent on the associated counterion [108]. The variations of the surface tension, γ with the semi-log concentration, Log C (molar) at 298.16 K (for gemini-tartrate, T=308.16 K) for 16-2-16 series of gemini surfactant are shown in Figure-4.2. From the figure, it can be clearly observed that the surface tension decreases sharply with an increase in surfactant concentration until the critical micelle concentration is reached.

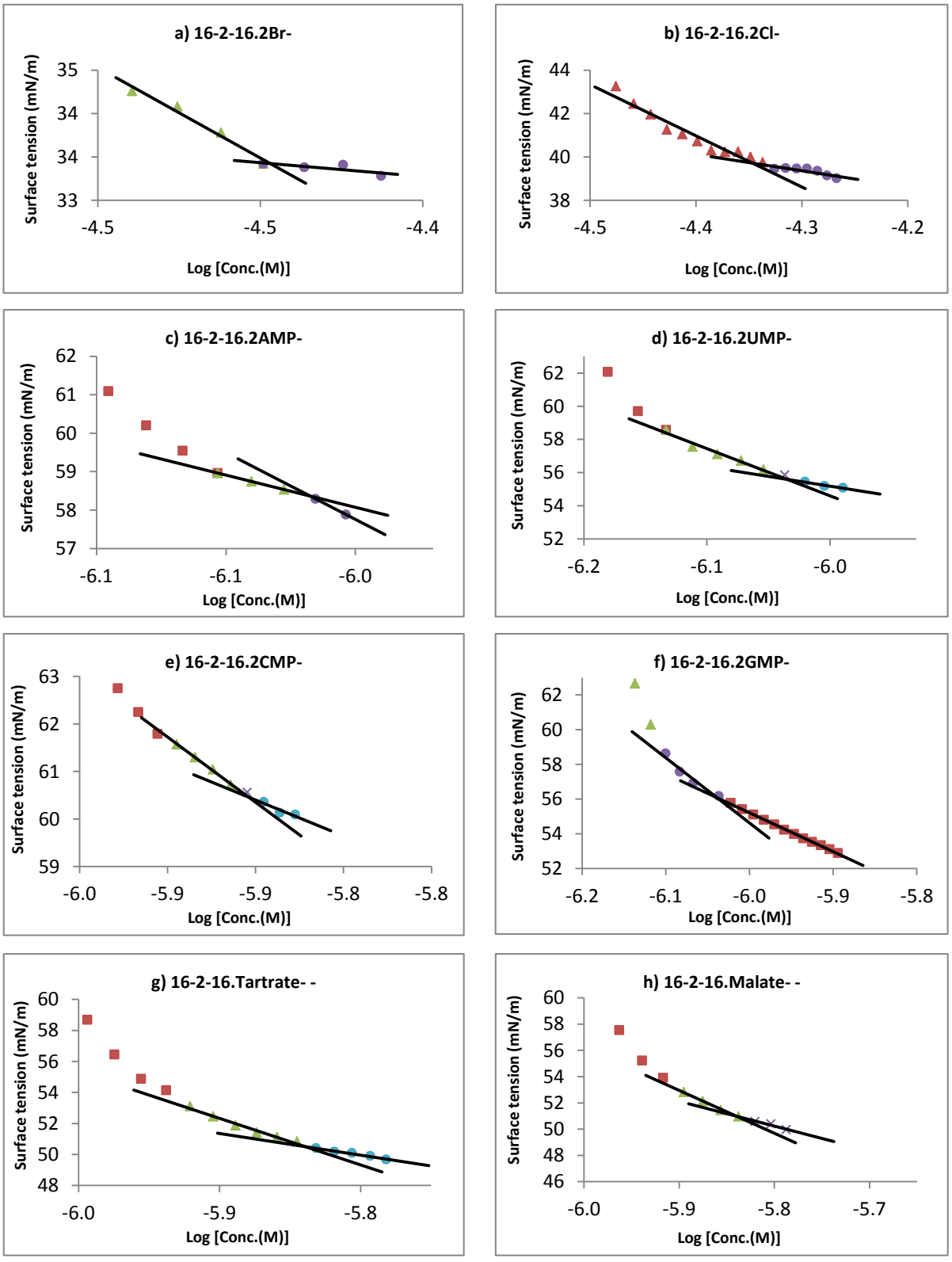

Figure-4.2: Surface tension vs Log (Conc.) plots of 16-2-16 series of surfactants

The measured CMC and other parameters of these gemini surfactants in solution are listed in Table-4.2 From the results, it can be seen that for the inorganic counterions (Br^- and Cl^-) 16-2-16 has a low CMC, the magnitude of which is dependent on the hydrophobicity of the halide. Specifically, since the bromide is more hydrophobic than chloride, the CMC for the 16-2-16 bromide gemini surfactant (30.8 μM) is lower than that observed for the 16-2-16 chloride surfactant (44 μM). For the small organic counterions (malate and tartrate), this trend is reversed, with the more hydrophobic malate ion (having one fewer hydroxyl substituents) having a higher CMC as compared to the less hydrophobic tartrate ion.

Table-4.2: Measured CMC and other parameters of gemini surfactants associated with different counterions

Gemini Surfactants	**γ_{cmc} (mN/m)**	**Π_{cmc} (mN/m)**	**CMC (μM)**	**$10^6\Gamma_{max}$ (molecules / m^2)**	**A_{min} (nm^2 / molecule)**	**ΔG^0_{mic} (KJ / mole)**	**ΔG^0_{ads} (KJ / mole)**
*16-2-16.2Br^-	39.6	30.8	30.8 ± 7	1.4	1.23	-35.7	-59.0
16-2-16.2Cl^-	42.6	28.1	44.0 ± 9	1.3	1.28	-34.9	-56.3
16-2-16.2AMP$^-$	55.5	13.4	1.1 ± 0.2	1.3	1.36	-45.6	-55.7
16-2-16.2CMP$^-$	59.9	10.7	1.3 ± 0.0	1.6	1.03	-43.5	-50.2
16-2-16.2UMP$^-$	55.9	14.5	1.1 ± 0.0	1.4	1.25	-44.1	-55.0
16-2-16.2GMP$^-$	55.8	14.7	0.9 ± 0.0	2.1	0.78	-44.5	-51.4
16-2-16.Tartrate^{--}	50.4	19.9	1.5 ± 0.1	1.7	0.95	-43.2	-54.7
16-2-16.Malate^{--}	52.3	18.2	1.6 ± 0.2	2.0	0.82	-43.0	-52.1

A_{min} for the 16-3**-16.2Br^- was found to be 1.21 nm^2/molecule [163]*

According to Collins and Washabaugh [164], the ions which exhibit strong interactions with water are known as kosmotropic ions (structure makers). On the other hand, the ions which are less hydrated and thus less effective in organizing surrounding water

molecules are termed as chaotropic ions (structure-breakers) [164]. For inorganic counterions, ions with low charge density and larger radii (e.g. bromide) typically have a stronger chaotropic effect. Hydrophobic inorganic counterions are more polarizable and are least hydrated in aqueous solution; and being chaotropic in nature, they destroy the structure of water in the vicinity of the counterion leading to reduced CMC values, favoring micellization [123].

At the end of 19^{th} century, Hofmeister proposed that the influence of ions on the precipitation of proteins in salt solutions followed a particular pattern, leading to the commonly referred to "Hofmeister series" of ions [164, 165]. Although Hofmeister effects for macromolecules in aqueous solution are ubiquitous (for example enzyme activity, protein stability, protein–protein interactions, optical rotation of sugar and amino acids, as well as bacterial growth) [166], this pattern of behavior is also observed in many physico-chemical mechanisms including the phenomena of micellization of charged surfactants [167]. Cremer *et al.* (2006) reported that the direct interactions existing between the ions and macromolecules are predominantly responsible for most aspects of this pattern [166]. Furthermore, Warr *et al*. (2004) reported a study to evaluate the affinity of some anions (Br^-, Cl^-, I^-, NO_3^-) to the head groups of gemini surfactants at the air/water interfaces and their subsequent effects on gemini aggregation. The order of affinity of the counterions for gemini surfactant descends $I^- > NO_3^- > Br^- > Cl^-$, which follows to the Hofmeister series [168].

Similarly, Manet *et al*. (2010) reported that the CMC of gemini surfactants with monatomic counterions generally increases according to the Hofmeister series: $I^- < NO_3^- \sim Br^- < Cl^- < F^- \sim C_2^- < PH$. On the other hand, due to entropic reasons, micellization is disfavored for large polyatomic anions, although they have a lower hydration number, and

similar hydrophobicity to the monatomic counterions [123]. Our results for the gemini halides were in agreement with the previously reported trends.

The packing densities of surfactants at the air-water interface are important to the interpretation of the surface activities of surfactants [80, 84, 169, 170]. The surfactant molecule occupies an area at the air/water interface (i.e. A_{min}) which should reflect their packing densities [80, 170, 171]. The surface excess concentration Γ_{max} (also known as the Gibbs surface free excess) and the minimum surface area occupied/molecule, A_{min} at the air-water interface can be calculated according to the Gibbs adsorption isotherm [108, 172].

$$\Gamma_{max} = \frac{-1}{2.303nRT}\frac{d\gamma}{dlogC} \quad 4.1$$

and, the equation

$$A_{min} = (N_A\Gamma_{max})^{-1} \times 10^{18} \quad 4.2$$

where, R = 8.314 J·mol^{-1}·K^{-1}, T = 298.15 K with surface tension (γ) expressed in N/m, N_A is Avogadro's number (6.023 × 10^{23} mol^{-1}), and n is the number of species the surfactant dissociates into. For monovalent counterions in combination with the gemini surfactant, a value n = 3 generally used, for the case of divalent counterions combined with the gemini, a value of n = 2 is used [94, 170, 172-174].

The CMC, average surface tension at the CMC (γ_{cmc}), average surface pressure (Π_{cmc}) Γ_{max}, A_{min}, the average Gibbs free energy of micellization (ΔG^0_{mic}), and the standard free energy of adsorption (ΔG^0_{ads}) have been determined from the tensiometry measurements and are listed in Table-4.2. ΔG^0_{mic} and G^0_{ads} can be calculated according to [80, 175] –

$$\Delta G^0_{mic} = RT \ln X_{CMC} \quad 4.3$$

$$\Delta G^0_{ads} = \Delta G^0_{mic} - \Pi_{CMC} / \Gamma_{max} \quad 4.4$$

where, X_{CMC} is the CMC in mole fraction units [i.e. CMC / (CMC + 55.6), where 55.6 is the number of moles of water per litre], Π_{CMC} is the surface pressure at CMC ($\Pi_{CMC} = \gamma_0 - \gamma_{cmc}$: γ_0 is the surface tension of pure water).

Both ΔG^0_{mic} and G^0_{ads} are strongly negative, indicating that micelle formation and adsorption at the air-water interface are spontaneous processes. From our results, it is clear that a change in the counterion impacts the aggregation of the gemini surfactant, rather dramatically. The trends in ΔG^0_{mic} and G^0_{ads} as well as A_{min} are similar to that observed for the CMC, again likely related to the relative hydrophobicity of the counterions.

Although the presence of hydroxyl groups in their structures makes the NMP counterions hydrophilic in nature, from the solubility data (in Appendix section) it was found that the solubility of the NMP counterions follows the sequence: UMP > AMP > CMP > GMP. Overall, these four counterions affect the CMC of 16-2-16, reducing it by almost 40-fold compared to that for the gemini halides. Although no conclusion can be drawn from our data based on the hydrophilicity of these counterions (i.e. the CMC values along with the other parameters does NOT follow the trend of increasing hydrophobicity), all the gemini-NMPs have approximately the same energies of micellization and adsorption. Again, the negative values of both ΔG^0_{mic} and ΔG^0_{ads} signify that the adsorption of these 16-2-16 series of surfactants at the air/water interface as well as micellization in the aqueous solution is spontaneous.

4.2.1.2 Electrical Conductivity Measurements: Conductometry

The CMC and degree of micelle ionization for an ionic surfactant can be determined from a plot of the electrical conductivity (κ) of the solution as a function of surfactant concentration. The conductance increases linear with increasing concentration, as the number of ions present in solution also increases. At the CMC, aggregation takes place, at which point the ions no longer move independently from one another, resulting in a dramatic decrease in slope for the conductivity vs. concentration curve. A linear fit [82, 176-178] of the conductivity above and below the CMC is used to determine the value of the CMC; the point of intersection of the two linear fits is equal to the CMC [134, 179]. The degree of micelle ionization of the micelles, α can be calculated from the ratio of the slopes of the linear regions above and below the CMC [134]. The degree of ionization α can also be replaced by the degree of counterion association to micelle, β obtained by the relationship $\alpha = 1 - \beta$. Both the terms α and β are used to reflect the extent of counterion binding to the micelles. A larger value of α, corresponds to greater dissociation of the counterions from the surface of the micelle, and indicates weaker binding of the counterions to the micelles [134].

The conductance plots for all surfactants are shown in Figure 4.3, and calculated values of the CMC and α are provided in Table-4.3. Excellent agreement is observed between the CMC determined from conductivity measurements and those determined from surface tension. Again, we see a pronounced effect of counterion exchange on the CMC and Gibbs free energy of micellization, although surprising, the effect of counterion exchange on α was minimal.

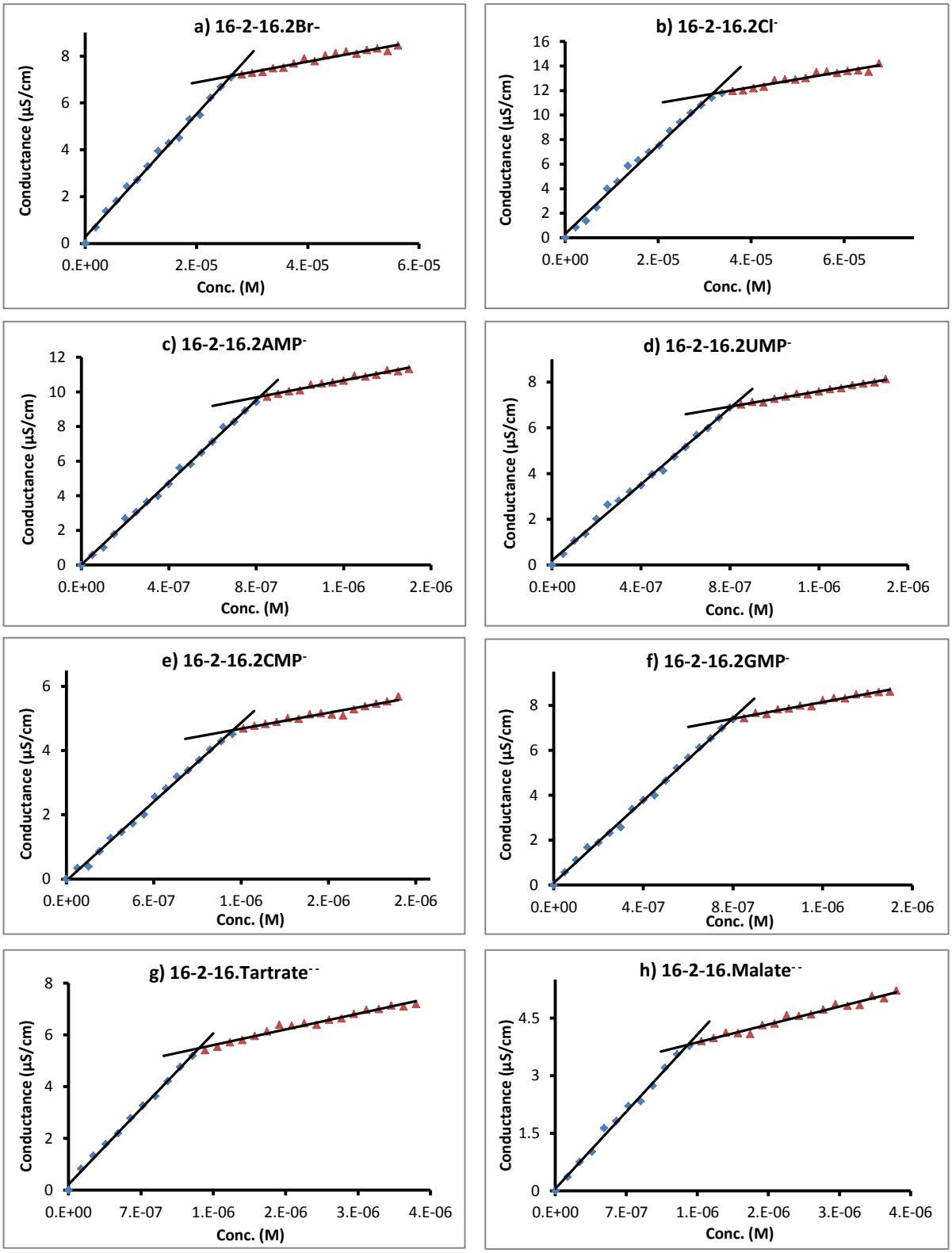

Figure-4.3: Specific conductance vs Concentration for the 16-2-16 gemini surfactants with various counterions. The intersection of the lines of best fit give the CMC, and the ratio of the slopes above and below the CMC (S_2/S_1) provides the degree of micelle ionization, α.

Generally, a higher degree of micelle ionization indicates that head group repulsion would play an important role in determining the structure of the micelle aggregates [94, 180]. The head groups of the monomer molecules in a micelle formed from ionic surfactants are charged by a fraction, 1 – α, of the counterions that are condensed onto the surface of the micelle [181]. A cationic gemini surfactant with a higher α would be a better candidate to condense proteins or other polyelectrolytes, such as DNA, as anionic molecules may more easily be able to replace the counter ions at the surface of the micelle to form compact complexes of much smaller size [94]. Being highly polarizable, the organic counterions enhance their binding at the micellar surface, and also decrease the electrostatic repulsion between the head groups of the surfactant molecules in the micelle, thus lowering both CMC and α [134].

Table-4.3: CMC and degree of micellization values of GSs associated with eight different counterions measured by conductometric method

Gemini Surfactants	Average CMC (μM)	Average Degree of Micelle Ionization (α)	Average Gibb's Free Energy of Micellization (KJ/mole)
*16-2-16.2Br $^-$	26.8 ± 0.8	0.17 ± 0.002	-70.7 ± 0.3
16-2-16.2Cl $^-$	31.4 ± 1.2	0.22 ± 0.013	-67.2 ± 0.5
16-2-16.2AMP $^-$	0.8 ± 0.01	0.21 ± 0.001	-90.8 ± 0.2
16-2-16.2CMP $^-$	1.1 ± 0.01	0.20 ± 0.001	-89.2 ± 0.1
16-2-16.2UMP $^-$	0.8 ± 0.003	0.20 ± 0.001	-91.5 ± 0.2
16-2-16.2GMP $^-$	0.8 ± 0.02	0.19 ± 0.010	-92.2 ± 0.9
16-2-16.Tartrate $^{--}$	1.3 ± 0.01	0.21 ± 0.003	-63.2 ± 0.1
16-2-16.Malate $^{--}$	1.3 ± 0.02	0.24 ± 0.015	-61.8 ± 0.5

** Degree of micelle ionization (α) for 16-**3**-16.2Br $^-$ was found to be 0.35 [163]*

The Gibbs free energy of micellization (ΔG_{mic}) was calculated from the following equations [134]. As the degrees of micelle ionization of the micelles (α) values are readily available directly from the conductometric plots, literature suggests using these equations [134] to calculate the ΔG_{mic} more accurately, instead using the equation-4.3 used in case of tensiometry:

$\Delta G_{mic} = RT\ (1+2\beta)\ \ln (CMC) - RT \ln 2$ [For monovalent counterions] 4.5

$\Delta G_{mic} = RT\ (1+\beta)\ \ln (CMC / 2)$ [For divalent counterions] 4.6

where, T = 298.16 K; R = 8.314 J/mole/K; β = (1 – α); α = (Slope–2 / Slope–1); from Specific conductance (μS/cm) **vs.** Concentration (M) curve. The CMC values obtained from tensiometry and conductometry methods were approximately close and in good agreement, but the free energy of micellization was drastically different due to application of different equations [94, 108] and experimental technique.

4.2.2 Krafft Temperature

Generally for cationic and anionic surfactants, the solubility in water undergoes an abrupt increase at a particulate temperature. This temperature is known as the Krafft temperature (T_K) and is the minimum temperature at which point the hydrated surfactant becomes soluble and is judged visually to be the point of complete clarification of a turbid saturated solution of surfactant [181-184]. Below T_K, a gel or precipitate is formed [118] and the surfactants remain in crystalline (hydrated crystals) form [80]. Hydrophobic tail lengths, the nature of the surfactant head group and the nature of the associated counterions are all key parameters in determining T_K. Generally, the T_K of a conventional monomeric and ionic

surfactant is found to increase with increasing the length of the alkyl chain and decrease with increasing the size of the head group [182]. As such, the double tailed gemini surfactants with longer chain lengths have higher T_K [137].

The inorganic bromide and chloride counterions are more polarizable, less hydrophilic and as a result less hydrated [123]. As such the more hydrophobic bromide counterion results in a Krafft temperature higher than that for the chloride counter ion (Table 4.8). Tartaric acid has one additional hydroxyl group in its structure as compared to malic acid, resulting in increased hydrogen bonding in an aqueous solution of tartaric acid leading to decreased solubility of tartrate ions at room temperature. As the temperature increases, the Brownian motion of the water molecules increases exponentially and thus, the existing intermolecular hydrogen bonds disrupts leading to the solubility of tartaric acid at a higher temperature. Consequently, the T_K for gemini-tartrate was found higher than the gemini-malate. The solubilities of the NMPs at different temperatures decreases according to this sequences: UMP > AMP > CMP > GMP, found from the solubility test (see "Appendix" section). With the exception of AMP and CMP, the Krafft temperatures follow the same trend (Table 4.4), with the Krafft temperature of GMP being the highest at 55^0C.

4.2.3 Determination of pH, and density

Table-4.4 also summarizes the average values for pH, and density measurements for our series of gemini surfactants. Counterions associated with the gemini structure clearly impact the pH of the gemini surfactant in solution. Among the eight gemini surfactants examined, the UMP counterion makes the resulting gemini solution most acidic whereas chloride ions render the gemini solution almost neutral. The optimum pH required for

mammalian cell growth is pH 6.9 – 8 [185] but, it has been reported that the transfection efficiency of the non-viral vector, chitosan in human-lung carcinoma A549 cells was higher at pH 6.9 than that at pH 7.6 [186]. In this project, both the media (RPMI 1640 and Opti-MEM® I) that we employed for transfection assays utilize a sodium bicarbonate buffer system which was provided from the 5–10% CO_2 environment of the incubator to maintain the physiological pH for cell growth. Considering this bicarbonate buffer as a weak system and given the pH data of the 16-2-16 series of gemini surfactants in hand, it is suggested that the change in pH of the overall transfection nanoparticles due to change of pH for the presence of gemini will probably affect the transfection efficiency as well as cell viability. Although the quaternary ammonium head group of the surfactants undoubtedly contributes to cytotoxicity [187], alteration of pH could be another factor contributing to cytotoxicity. Generally, surfactant intercalation into the cell membrane leads to changes in the membrane's molecular organization and increases membrane permeability that results in cell lysis [187], and decreased cell viability.

Table-4.4: Krafft temperature, pH, and density measurements data for GSs.

Liquid / Solution	**Krafft Temp (^{0}C)**	**pH**	**Average Density (Kg/m^3)**
Milli Q Water	N/A	6.9	986.0
16 – 2 – 16 . 2Br $^-$	55	3.8	987.1
16 – 2 – 16 . 2Cl $^-$	40	6.3	987.5
16 – 2 – 16 . 2AMP $^-$	45	3.4	988.4
16 – 2 – 16 . 2CMP $^-$	35	3.6	1026.4
16 – 2 – 16 . 2UMP $^-$	4	3.1	987.9
16 – 2 – 16 . 2GMP $^-$	55	4.6	988.9
16 – 2 – 16 . Tartrate $^{--}$	50	3.8	990.3
16 – 2 – 16 . Malate $^{--}$	25	5.0	991.6

Variations in counterions have a less prominent effect on the average density of the 16-2-16 series of surfactants, again shown in Table-4.4. Comparatively very subtle increase in density was observed for the gemini-CMP solution probably due to their actual morphological shapes and packing densities. The rest of the gemini surfactants have comparable densities (all approximately that of pure water), likely due to their similarities in packing and self-assembly behaviour. No notable patterns of changes in densities based on variation of counterions were found to correlate with the solubility data of the counterions, although there is no direct or inverse relationship exists between the density and solubility.

4.3 Characterization of 16-2-16 GS aggregates by size and zeta potential measurements

4.3.1 Size and zeta potential of extracted plasmid

It has already been confirmed the presence of supercoiled pNN9 plasmid (CCC) in our extracted samples, mentioned in the section 3.2.8. Despite the fact that pNN9 was the larger sized plasmid [79], the DNA supercoiling reduced the overall size and the average size of the pNN9 plasmid solution was found at 414 (± 15) nm with a polydispersity index (PDI) of 0.52. Although the DNA supercoiling can mask a fraction of the negative charges attained from the intramolecular phosphate groups, resulting to a lower effective negative charge [188, 189] for pNN9 (CCC), our results of measured zeta potential values were found at –33 (± 0.5) mV. These negative zeta potentials of the pNN9 plasmids (CCC) denoted significant surface charges for extensive electrostatic interaction with the cationic 16-2-16 gemini surfactant, leading to complete counterion release and reduced head group repulsions. Reduced intermolecular head group repulsion between the surfactant molecules will ensure better DNA encapsulation leading to more uniform aggregates.

4.3.2 Size and zeta potential of DOPE vesicles

The average size of the DOPE vesicles was found to be 124 ± 8 nm with a PDI of 0.46. This value was in excellent agreement with the value reported by Wettig *et al.* [143]. The average zeta potential for the DOPE vesicles was found to be –30 ± 2 mV.

4.3.3 Size and zeta potential of 16-2-16 gemini surfactants in solutions

The average aggregate size and the average zeta potential of the gemini surfactants are reported in Table-4.5 and illustrated graphically in Figure-4.4. Due to high concentrations of the stock solution (1.5 mM, well above the CMC of all the eight surfactants), all the 16-2-16 gemini surfactants were able to rapidly self-assemble into micelles within the experiment conditions.

From both the size and zeta potential data, it is evident that counterions play a significant role on the aggregate hydrodynamic radius and zeta potential for the gemini surfactants. Comparing the gemini-halides, 16-2-16-bromide forms smaller aggregates (211 ± 5) with a more homogenous size (as indicated by the lower polydispersity index) than the 16-2-16-chloride (274 ± 24). This trend followed the CMC pattern of inorganic counterions (for example, Br^- and Cl^-) with the sequence mentioned in Hofmeister series based on hydrophobicity of inorganic counterions. Both the 16-2-16-Bromide and 16-2-16-Chloride aggregates have strong positive zeta potential (ζ) values which indicate that the aggregates possess colloidal stability, but also have sufficient positive charge for interaction with and compaction of the negatively charged DNA molecules.

Table-4.5: Average size, PDI, and Zeta potential for GSs with eight different counterions

Name of the GS solution (1.5 mM)	Average Size (nm) (±SD)	Average PDI	Average Zeta (ζ) potential (±SD)
16 – 2 – 16 . 2Br $^-$	211 ± 5	0.23	60 ± 1
16 – 2 – 16 . 2Cl $^-$	274 ± 24	0.45	53 ± 1
16 – 2 – 16 . 2AMP $^-$	145 ± 13	0.48	36 ± 3
16 – 2 – 16 . 2CMP $^-$	110 ± 18	0.37	28 ± 2
16 – 2 – 16 . 2UMP $^-$	141 ± 13	0.59	27 ± 2
16 – 2 – 16 . 2GMP $^-$	**68** ± 4	0.58	44 ± 5
16 – 2 – 16 . Tartrate $^{--}$	184 ± 29	0.42	**110** ± 3
16 – 2 – 16 . Malate $^{--}$	**297** ± 45	0.43	**22** ± 3

Between the 16-2-16-Malate and 16-2-16-Tartrate solutions, the malate counterion resulted in surfactant aggregates having the largest size among all 8 counterions investigated, with the zeta potential (22 ±3 mV) indicating a less colloidally stable system. Interestingly with one additional hydroxyl group in the counterion, 16-2-16-Tartrate formed smaller aggregates (185 ± 29 nm), with the largest measured zeta potential (110 ± 3mV) among all 8 counterions, mainly due to having lower pK_a value of tartaric acid than that of malic acid.

Lastly, among the four gemini-NMPs, surprisingly the 16-2-16-GMP formed the smallest aggregates (68 ± 4 nm) among all the surfactants, despite being the most intractable to get solubilized. Among the NMP counterions, the 16-2-16-GMP aggregates had the highest ζ value (44 ± 5mV) indicating colloidal stability of the system. These strong positive ζ values will also help the researchers to put an assumption on the probable electrostatic interactions between the gemini systems and the negatively charged DNA molecules. The remaining NMP counterions resulted in 16-2-16 aggregates of comparable sizes.

A)

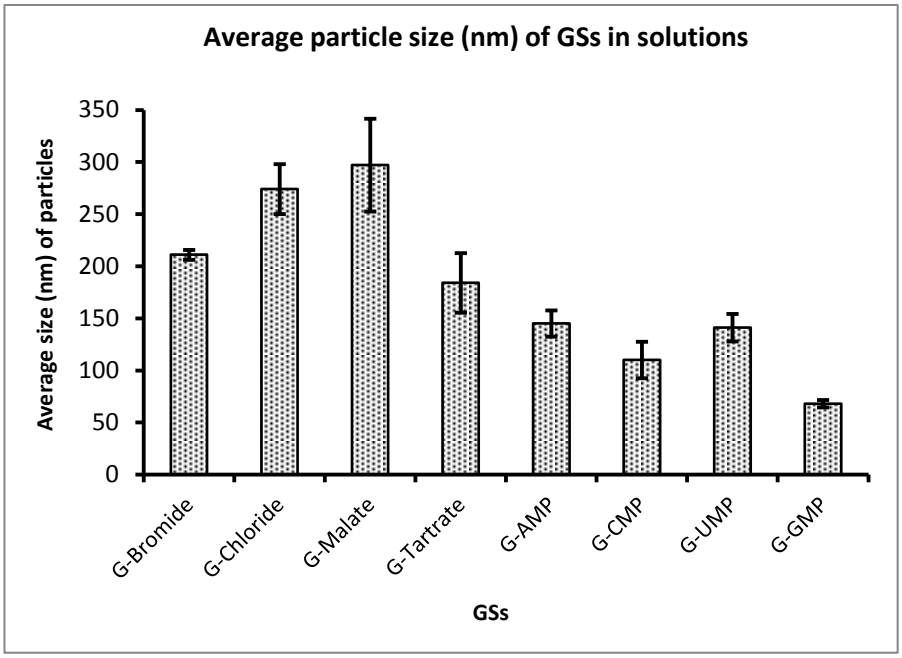

B)

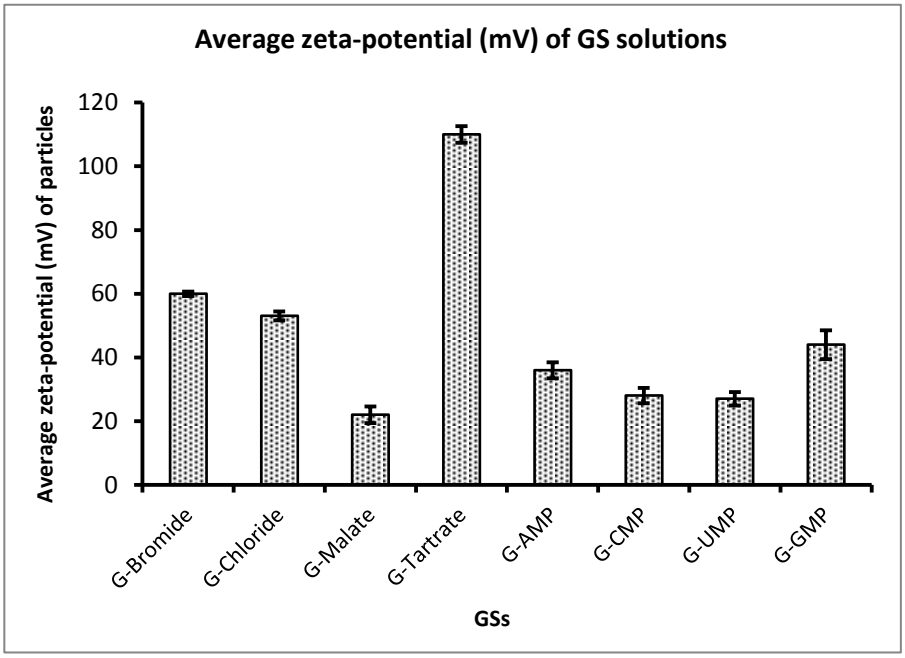

Figure-4.4: Graphical representation of variation of particle sizes **(A)** and zeta potentials **(B)** with the change of different counterions of 16–2–16 series of gemini surfactants (n = 3, error bar = standard deviation).

4.3.4 Size and zeta potential of 16–2–16 gemini based nanoparticles

4.3.4.1 Size and zeta potential of 16–2–16/Plasmid (GP) nanoparticles

Nanoparticles containing both 16-2-16 and plasmid were prepared following the procedure as described in Section 3.2.9.2 of this dissertation. Three different charge ratios of 16–2–16 to DNA (10:1, 5:1, and 2:1) were used to prepare the G+P nanoparticles; these nanoparticles have been prepared and characterized as controls for the complete 16–2–16/Plasmid/DOPE (GDP) used in the *in vitro* transfection assays.

Usually, for a higher charge ratio, more surfactant molecules are available to compact the plasmids, which intuitively should result in smaller sized GP aggregates with larger, positive, ζ values. In reality, it was very difficult to draw such a conclusive relationship for the GP nanoparticles produced using 16-2-16 surfactant with various counterions. From Table-4.6, and Figure-4.5 it is clearly manifested that some of the 16-2-16 gemini surfactants can produce much smaller sized aggregates after complexation with the plasmids than the sizes of the GSs itself. In majority of the cases, the large particles exhibited at the charge ratio of 2:1 were likely the result of aggregation upon charge neutralization of 16-2-16 head groups and DNA, and in the case of 5:1 and 10:1 charge ratios, subsequent addition of more gemini surfactants resulted in a dramatic decrease in particle sizes (except the GP nanoparticles formulated from 16-2-16-Malate).

Here, based on the hydrophobicity of inorganic counterions (for example, Br^- and Cl^-), 16-2-16-Bromide produced smaller aggregates than the 16-2-16-Chloride, and this trend is in agreement with the CMC pattern for inorganic counterions as in the Hofmeister series. Although no notable pattern, based on either solubility or CMC, was seen on the sizes of the gemini-NMP–plasmid aggregates, the aggregate sizes with the gemini-tartrate and gemini-

malate followed the CMC trend mentioned in the Hofmeister series based on the hydrophilicity of organic counterions. Whereas, the zeta potential values (Table-4.6) for the GP nanoparticles formed from all the charge ratios were strongly positive, indicating the existence of colloidal stability of the nanoparticles formed. The data presented in the tables also reinforced that strong electrostatic interactions are responsible to compact the larger sized DNA molecule to yield smaller nanoparticles, a crucial factor to obtain desired transfections. In all the cases, the PDI values were found by < 0.4 indicating homogeneity of the nanoparticles for all the eight GSs, and the SD values were found within ± 20 nm. This is mainly due to the presence of strong electrostatic as well as hydrophobic interactions between the 16-2-16 gemini surfactants and the negatively charged pNN9 molecules.

Table-4.6: Average sizes, polydispersity indices (PDI) and Zeta potentials (ζ) of 16–2–16 gemini/Plasmid (GP) nanoparticles

Gemini Surfactants	Nanoparticle charge ratio (+/–)	Size (nm)	PDI	ζ (mV)
16–2–16.2Br $^{-}$	G + P (10 :1)	109 ± 9	0.24	43 ± 2
	G + P (5 :1)	225 ± 13	0.31	37 ± 1
	G + P (2 :1)	260 ± 10	0.29	38 ± 2
16–2–16.2Cl $^{-}$	G + P (10 :1)	223 ± 8	0.23	38 ± 1
	G + P (5 :1)	291 ± 11	0.24	33 ± 2
	G + P (2 :1)	325 ± 17	0.40	41 ± 1
16–2–16.Malate $^{--}$	G + P (10 :1)	211 ± 11	0.21	37 ± 2
	G + P (5 :1)	237 ± 7	0.37	31 ± 1
	G + P (2 :1)	193 ± 12	0.32	43 ± 2
16–2–16.Tartrate $^{--}$	G + P (10 :1)	112 ± 8	0.31	55 ± 1
	G + P (5 :1)	129 ± 6	0.28	53 ± 2
	G + P (2 :1)	143 ± 14	0.36	45 ± 1
16–2–16.2AMP $^{-}$	G + P (10 :1)	81 ± 12	0.29	33 ± 1
	G + P (5 :1)	106 ± 10	0.23	31 ± 2
	G + P (2 :1)	197 ± 8	0.26	30 ± 1
16–2–16.2CMP $^{-}$	G + P (10 :1)	87 ± 16	0.27	32 ± 1
	G + P (5 :1)	164 ± 9	0.33	30 ± 1
	G + P (2 :1)	209 ± 12	0.31	29 ± 1
16–2–16.2UMP $^{-}$	G + P (10 :1)	116 ± 8	0.36	35 ± 1
	G + P (5 :1)	129 ± 15	0.41	32 ± 1
	G + P (2 :1)	138 ± 11	0.29	31 ± 2
16–2–16.2GMP $^{-}$	G + P (10 :1)	76 ± 10	0.42	36 ± 1
	G + P (5 :1)	112 ± 17	0.36	31 ± 1
	G + P (2 :1)	172 ± 9	0.28	29 ± 1

A)

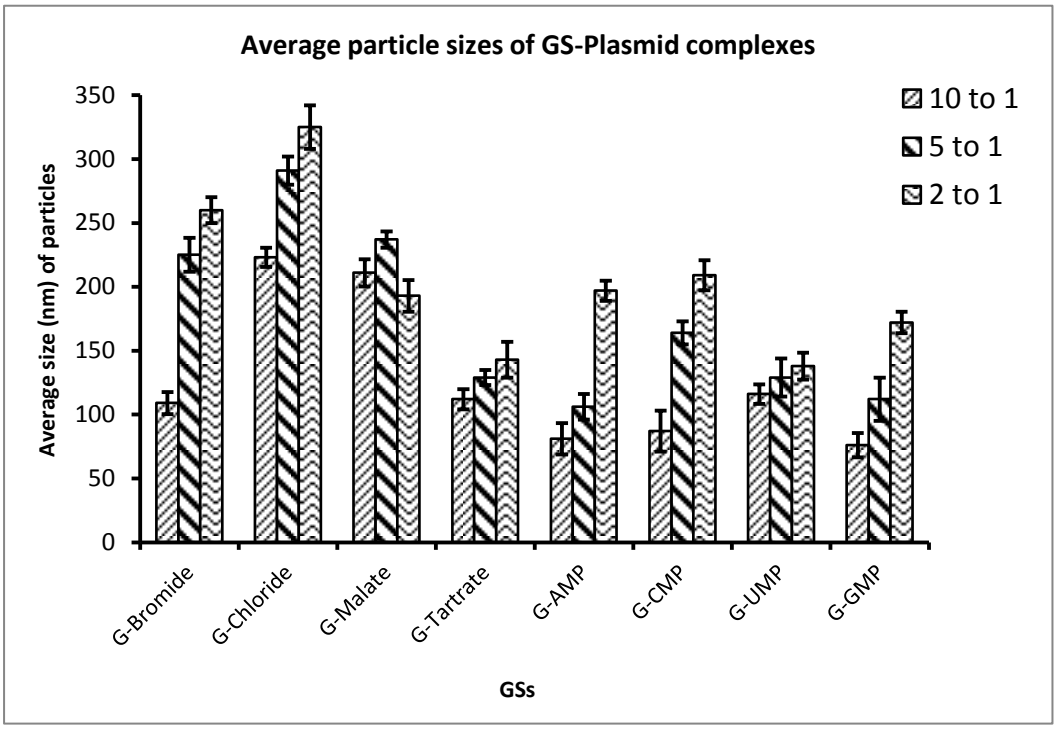

B)

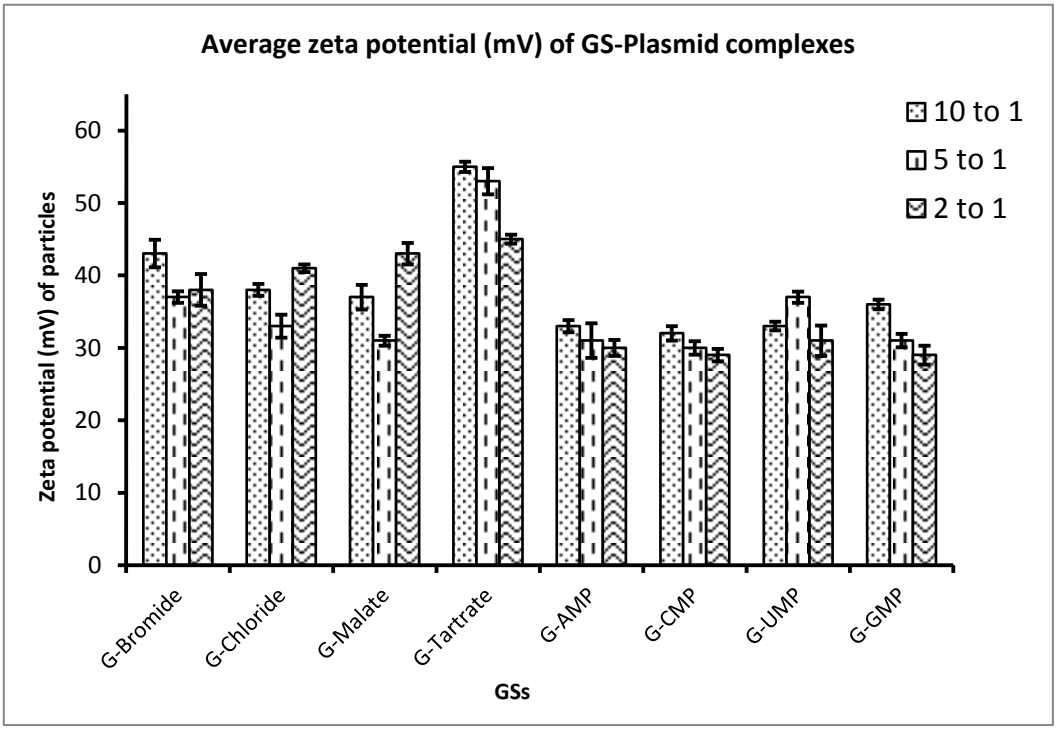

Figure-4.5: Graphical representation of variation of particle sizes **(A),** and zeta potentials **(B)** of GP nanoparticles at 3 different charge ratios of 16–2–16 gemini to Plasmid with the change of different counterions (n = 3, error bar = standard deviation).

4.3.4.2 Size and zeta potential of GDP and GD nanoparticles

Nanoparticles prepared for the actual transfection of our cells were prepared using DOPE as a helper lipid. As described in the introduction of this thesis, the addition of DOPE is observed, phenomenalogically to increase the transfection efficiencies of many cationic lipids. This is thought to be due to the fact that DOPE is known to be a fusogenic lipid, as well as having a preference for membranes with a high degree of curvature, both of which tend to be destabilizing effects (antagonistic effects [190]) when DOPE is incorporated into endosomal membranes. Table-4.7 summarizes the average size, polydispersity index and zeta potential for the 16-2-16/Plasmid/DOPE (GDP) nanoparticles at three 16-2-16:DNA charge ratios, with a 16-2-16:DOPE ratio of 2:5, for the various counterions studied. The column charts in Figure-4.6 illustrate the average sizes and zeta potentials of GDP nanoparticles at three charge ratios of 16-2-16 : DNA respectively.

From the evaluation of the particle size variations for lipoplexes across different charge ratios, it is assumed that the varying sizes of the GDP lipoplexes, irrespective of post incubation time after mixing with DOPE, may be attributed to supercoiled nature of the pNN9 plasmids. Because, the supercoiled form of DNA had notable effects on the interactions between DNA and gemini surfactant in terms of counterion release during lipoplex formation [188, 189]. Literatures suggest that the compact conformation of supercoiled CCC pDNA inhibit complete counterion displacement as well as altered gemini/DNA interactions leading to subsequent varying size of aggregates [188, 189]. Overall, the differences in GDP sizes may be attributed to the existing antagonistic interactions between 16-2-16 gemini and DOPE [190] in combination with incomplete

counterion release for GP complexes, leading to more prominent DOPE induced instabilities that prevented the generation of stable, uniform GDP lipoplex particles.

Table-4.7: Average sizes, polydispersity indices (PDI) and Zeta potentials (ζ) of 16–2–16 gemini/Plasmid/DOPE (GDP) nanoparticles

Gemini Surfactants	Nanoparticle charge ratio (+/–)	Size (nm)	PDI	ζ (mV)
16–2–16.2Br $^{-}$	G + P + D (10 :1)	521 ± 7	0.47	34 ± 2
	G + P + D (5 :1)	351 ± 15	0.17	47 ± 1
	G + P + D (2 :1)	178 ± 2	0.26	25 ± 1
16–2–16.2Cl $^{-}$	G + P + D (10 :1)	207 ± 31	0.62	39 ± 1
	G + P + D (5 :1)	149 ± 2	0.60	45 ± 4
	G + P + D (2 :1)	228 ± 1	0.38	22 ± 2
16–2–16.Malate $^{--}$	G + P + D (10 :1)	121 ± 11	0.28	37 ± 1
	G + P + D (5 :1)	111 ± 2	0.53	35 ± 3
	G + P + D (2 :1)	105 ± 1	0.22	29 ± 1
16–2–16.Tartrate $^{--}$	G + P + D (10 :1)	201 ± 45	0.27	31 ± 1
	G + P + D (5 :1)	172 ± 20	0.35	47 ± 2
	G + P + D (2 :1)	135 ± 30	0.27	24 ± 1
16–2–16.2AMP $^{-}$	G + P + D (10 :1)	83 ± 3	0.32	34 ± 4
	G + P + D (5 :1)	94 ± 3	0.33	55 ± 2
	G + P + D (2 :1)	139 ± 2	0.32	24 ± 1
16–2–16.2CMP $^{-}$	G + P + D (10 :1)	106 ± 4	0.44	49 ± 2
	G + P + D (5 :1)	127 ± 11	0.56	42 ± 2
	G + P + D (2 :1)	427 ± 22	0.47	19 ± 0
16–2–16.2UMP $^{-}$	G + P + D (10 :1)	426 ± 24	0.21	33 ± 4
	G + P + D (5 :1)	92 ± 3	0.35	33 ± 2
	G + P + D (2 :1)	173 ± 7	0.47	23 ± 1
16–2–16.2GMP $^{-}$	G + P + D (10 :1)	810 ± 40	0.63	–33 ± 5
	G + P + D (5 :1)	519 ± 28	0.44	–29 ± 3
	G + P + D (2 :1)	523 ± 22	0.53	–17 ± 1

From the table-4.7, it was found that, for 16-2-16-Bromide, 16-2-16-UMP, and 16-2-16-GMP, the GDP complexes formed are very large (~ 500-1000 nm size range), at the charge ratio of 16-2-16 : Plasmid of 10:1; for 16-2-16-GMP being the largest size (810 nm). At lower charge ratios (5:1 or 2:1), the transfection mixtures formed acceptable sized nanoparticles (~ 80-230 nm range) in terms of relatively higher intracellular uptake and efficient gene transfer [191, 192], with the exception of the GDP complexes based of 16-2-16-bromide, 16-2-16-CMP, and 16-2-16-GMP. Apparently, 16-2-16-Bromide, 16-2-16-Malate, 16-2-16-Tartrate, and 16-2-16-GMP produced nanoparticles of sizes from larger to smaller as the charge ratios decreases from higher (10:1) to lower (2:1). The reverse pattern was seen in case of the GDP complexes based on 16-2-16-AMP and 16-2-16-CMP; whereas, no conclusive trend was seen for the 16-2-16-Chloride and 16-2-16-UMP. Surprisingly, at the charge ratio of 2:1, the GDP transfection mixture based on all the 16-2-16 gemini surfactants (except 16-2-16-Chloride, 16-2-16-CMP and 16-2-16-GMP) produced average particle sizes of < 200 nm range. Moreover, aggregation of the resulting GDP lipoplexes and interference with light scattering measurements, upon charge neutralization, contributed to large standard deviations and populations of highly variable particle sizes [110] in majority of the 16-2-16 systems.

It is evident from the table-4.7 that, except for the 16-2-16-GMP, all the other GS based transfection complexes possess positive zeta potential values for all the three charge ratios. Usually, charged cationic nanoparticles tend to adsorb proteins from the biological environment through electrostatic interaction, causing precipitation of the particles, and thus often display poor stability in cell culture conditions [193]. Hence, colloidal stability in biological environments is a challenging issue in clinical application of any nanoparticle-

based delivery system due to the large surface area to volume aspect ratio of nanoscale materials. For these delivery systems, zeta potential is an important physicochemical parameter that influences the stability of nanodispersions [193]. Moderate to extremely positive or negative zeta potential values cause larger repulsive forces which prevent time dependant aggregation of the particles in resting condition, and thus ensure good stability. Thus, in the case of a combined electrostatic and steric stabilization, a minimum zeta potential of ± 20 mV is reasonable [193, 194], although the stability range of ± 25 mV is widely acceptable, as mentioned in the Zetasizer Nano ZS instrument's manual.

Although, among the 16-2-16-NMPs, 16-2-16-GMP possesses the highest positive ζ value (+44 mv, Table-4.5), the negative zeta potential values of 16-2-16-GMP based transfection complexes here for all the three charge ratios were very surprising and unexpected. Although, after compaction of DNA, the reason for the overall negative charge of these nanoparticles is unknown, it is predicted that the self-staking nature [123] of this gemini molecule itself can cause some sort of morphological changes in the resulting nanoparticles which contribute to the possession of the overall negative charges. Now, among the three contributing forces for cellular uptake of nanocarriers, namely the electrostatic interactions (for oppositely charged surfaces), hydrophobic interaction, and hydrophobic hydration [108], the first attractive force has the predominance over the other mechanisms for cellular internalization via endocytic pathway, having the biological membranes as negatively charged. Hence, considering these phenomena, the resulting negative zeta potential values of the 16-2-16-GMP based GDP nanoparticles, render them as the less effective candidates for transfection assays due to potential role of predominant mechanism for cellular uptake through endocytosis.

A)

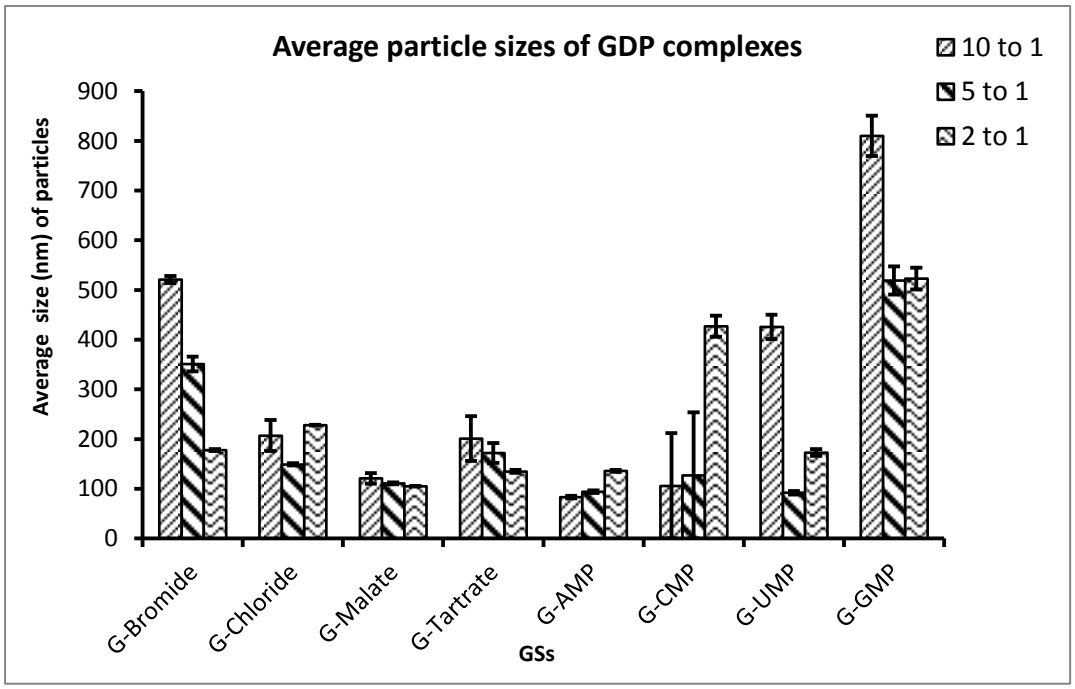

B)

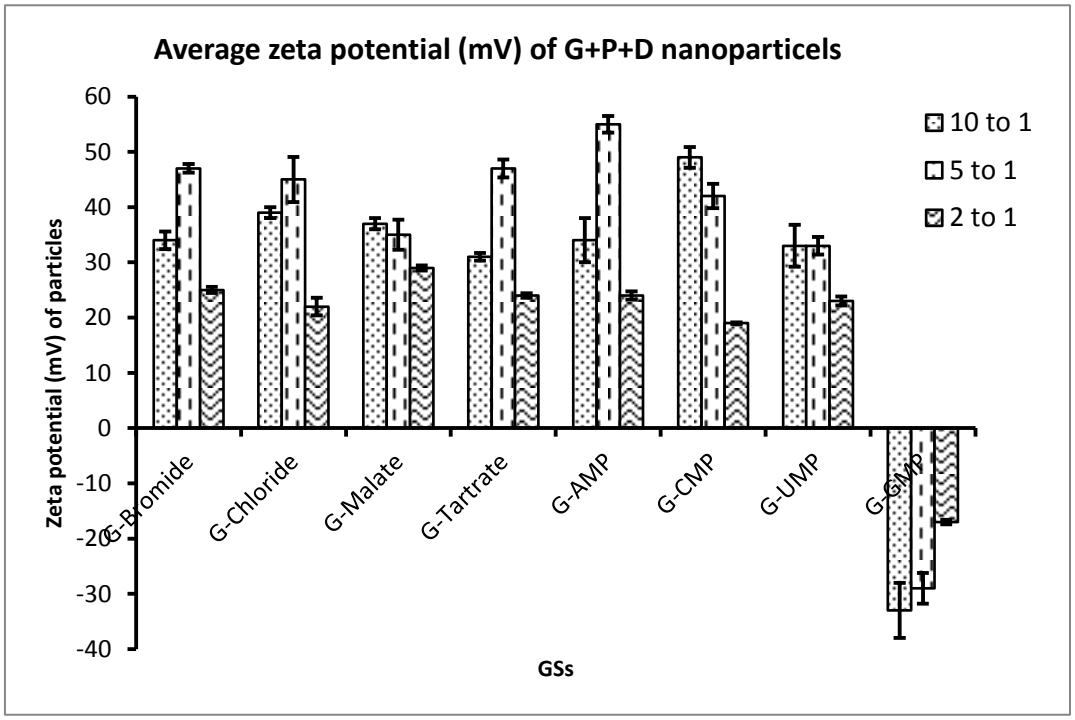

Figure-4.6: Graphical representation illustrating **A)** particle sizes, and **B)** Zeta potentials of GDP nanoparticles at 3 different charge ratios of 16-2-16 gemini surfactants : Plasmid (n = 3, error bar = standard deviation)

Table-4.8 summarizes the average size, polydispersity index and zeta potential for the 16-2-16/DOPE (GD) nanoparticles for the various counterions studied, where at any of the three 16-2-16 : DNA charge ratios, the 16-2-16 : DOPE ratio was always fixed at 2:5. These GD complexes served as a negative control for all the *in vitro* transfection assays. The average sizes of the GD complexes were found at approximately 500 nm range for 16-2-16-Bromide, and at a range of < 300 nm for 16-2-16-Tartrate. Rest of the gemini surfactants produced GD particles possessing the average sizes of >> 1000 nm range. Here, the propensity for 16-2-16 gemini surfactant to form GD micelles/vesicles of varying sizes resulted in the observed high polydispersities as indicated by a PDI value of > ~0.6 in many of the 16-2-16/DOPE systems. In addition, the GD nanoparticles also possess strong positive charges indicating the colloidal stability of the particles which ultimately have the ability to interact with the negatively charged biological membranes.

Table 4.8: Average sizes, polydispersity indices (PDI) and Zeta potentials (ζ) of 16–2–16 gemini/DOPE (GD) nanoparticles

Gemini Surfactants	Nanoparticle charge ratio (+/–)	Size (nm)	PDI	ζ (mV)
16–2–16.2Br $^{-}$	G + D (2 :5)	577 ± 30	0.65	44 ± 2.4
16–2–16.2Cl $^{-}$	G + D (2 :5)	1194 ± 138.6	0.64	41 ± 2.8
16–2–16.Malate $^{--}$	G + D (2 :5)	1594 ± 102.5	0.74	43 ± 3.0
16–2–16.Tartrate $^{--}$	G + D (2 :5)	267 ± 21.8	0.47	41 ± 2.3
16–2–16.2AMP $^{-}$	G + D (2 :5)	1940 ± 219.8	0.50	41 ± 3.8
16–2–16.2CMP $^{-}$	G + D (2 :5)	1288 ± 58.4	0.56	39 ± 8.0
16–2–16.2UMP $^{-}$	G + D (2 :5)	2124 ± 281	0.40	35 ± 5.7
16–2–16.2GMP $^{-}$	G + D (2 :5)	3392 ± 308	0.22	21 ± 2.8

4.4 *In vitro* transfection assays in OVCAR-3 cells

4.4.1 Effect of counterions for *in vitro* transfection assays

An example of the two way scatter plots obtained from the flow cytometer for the controls and treatments are shown in Figure-4.7. Here, the live cells positive for GFP are counted along Y axis (green fluorescence), and are differentiated from the dying or dead cells positive for propidium iodide (PI) counted along X axis (red fluorescence). The upper right quadrant of the plots indicates dying or dead cells expressing GFP (GFP +ve, PI +ve). Negative GFP cells i.e. cells not expressing GFP, but still alive (negative PI) are found in bottom left quadrant. Live cells expressing GFP are found in the upper left quadrant. All dead cells (negative for GFP) found are shown in the bottom right quadrant (PI +ve).

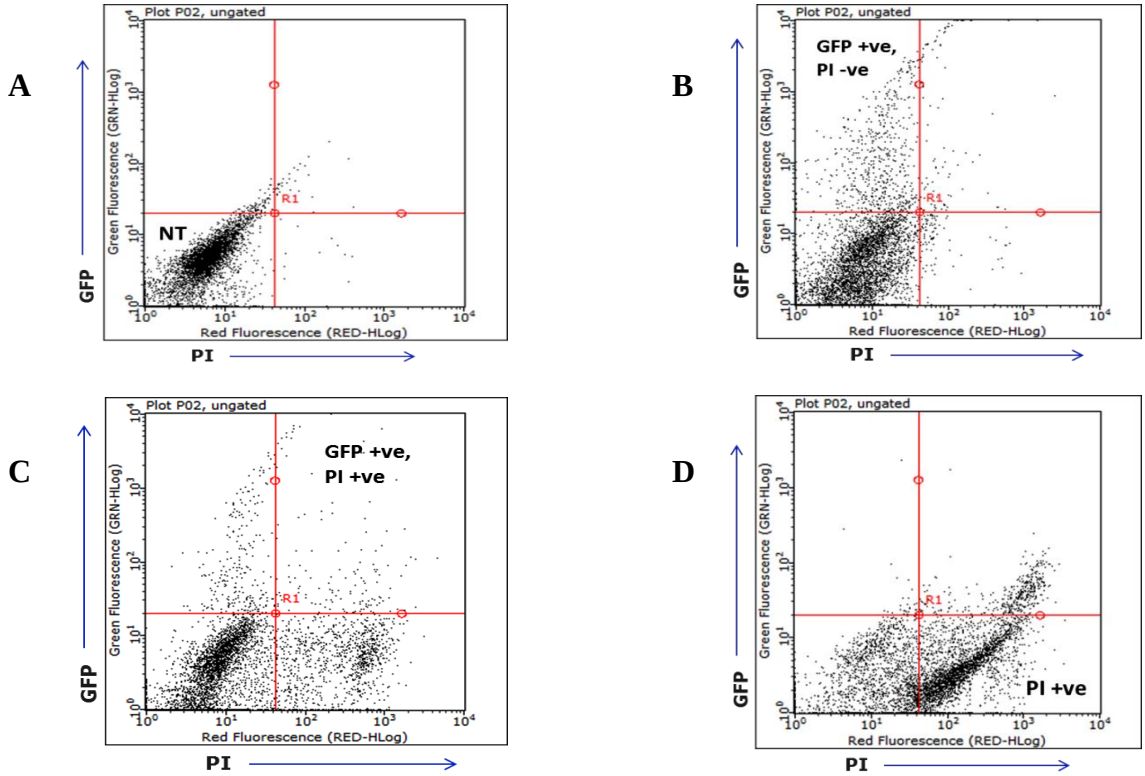

Figure-4.7: An example of two way scatter plots from flow-cytometry indicating **A)** No GFP expression (treated with Opti-MEM media only i.e. no treatment), **B)** Live cells with GFP expression (treated with the control, 'L'), **C)** Dying or dead cells with GFP expression (treated with G-Br based GDP at 10:1), and **D)** Dead cells with no GFP expression (treated with G-UMP based GDP at 10:1). Each dot represents a single OVCAR-3 cell.

4.4.1.1 Effects of counterions on TE: 16-2-16-bromide (G-Br)

The TE and the normalized cell viabilities for cells treated with different nanoparticles based on 16-2-16-bromide are summarized in Table-4.9 and shown graphically in Figure-4.8. Here, the highest TE (10 %) was observed for the charge ratio of 10:1 in case of DOPE complexed nanoparticles (GDP) whereas the TE for Lipofectamine^{TM} 2000 based nanoparticles was 10.7 %. Without the helper lipid i.e. the plasmid complexed with only 16-2-16-bromide (GP), the TE was very close to that observed when DOPE is present, for the same charge ratio. This is in agreement with previous results, which showed that, in a PAM 212 cell line, the gemini surfactants were capable of transfecting plasmids without the need of a helper lipid [106]. The TE for lower charge ratios (5:1 and 2:1) was unexpectedly much lower than that of the charge ratio 10:1 and that of Lipofectamine^{TM} 2000. Whereas, the sizes of GDP particles were much lower for these charge ratio than that of charge ratio 10:1. As expected, the results presented in Table-4.9 demonstrate that the negatively charged plasmid, in the absence of a delivery vector, is unable to transfect the OVCAR-3 cells.

Table-4.9: TE and cell viability for nanoparticles based on 16-2-16-Br (G), Plasmid (P) and Lipofectamine (L):

Parameters	Charge Ratio (GS : P)	Nanoparticle formulations			
		Transfection complexes		Controls	
		G+P+D	G+P	L+P	P
Percentage of transfection* (GFP + ve)	10 : 1	10.0 ± 4.9	9.5 ± 2.3	10.7 ± 0.2	1.3 ± 0.1
	5 : 1	4.0 ± 0.3	2.2 ± 0.6		
	2 : 1	4.3 ± 0.5	7.1 ± 1.4		
Percentage of cell viability* (Normalized)	10 : 1	76.4 ± 14.4	69.8 ± 11.9	93.9 ± 0.9	105.7 ± 8.6
	5 : 1	84.9 ± 2.7	75.9 ± 13.2		
	2 : 1	87.5 ± 12.2	93.4 ± 4.3		

**Mean ± SD (where, n = 6)*

Quaternary ammonium groups, which are present in both the 16-2-16 and also in Lipofectamine, are toxic, thus transfected cells may show lower viabilities, depending upon the composition of the transfection vector. The cell viability for the Lipofectamine was found to be 94 %. For the 16-2-16-bromide, cell viability was found to be inversely proportional to the charge ratio. The larger the charge ratio, the more gemini used in the formulation, and the more the cytotoxic the nanoparticles are. As the plasmids alone are unable to transfect the cells no cell death (relative to control) was observed.

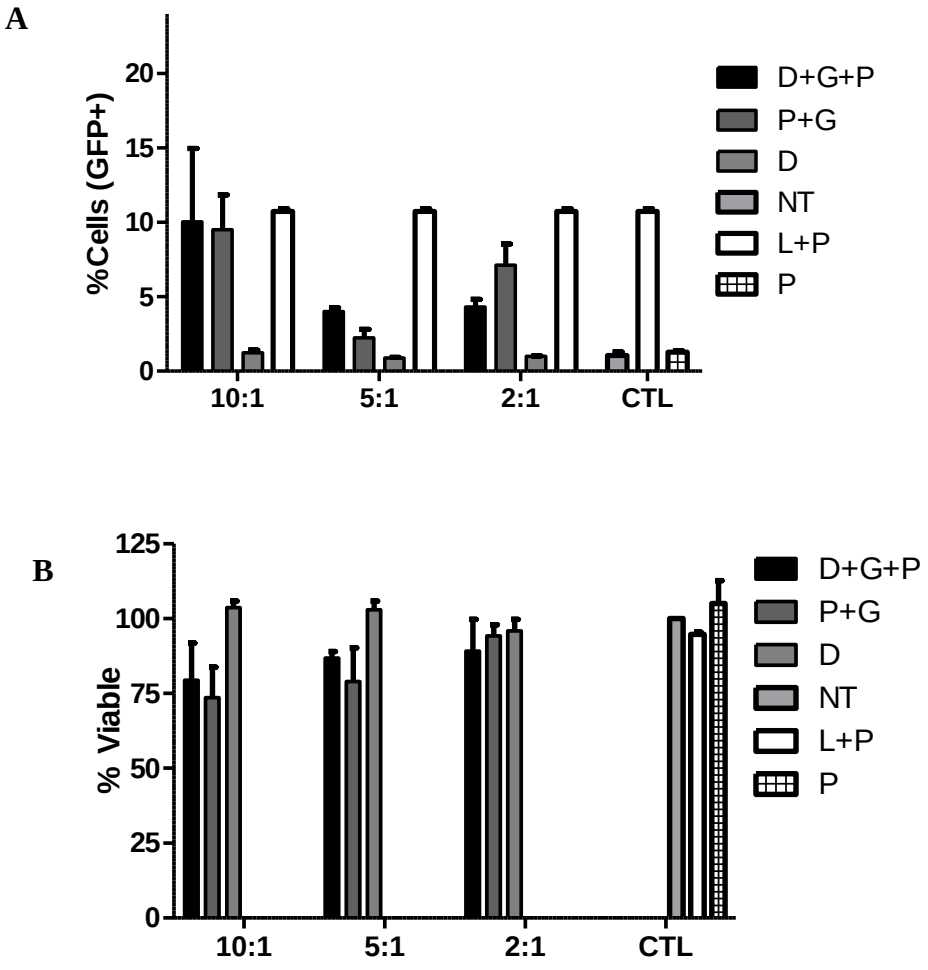

Figure-4.8: Graphical representation illustrating **A)** TE of the resulting aggregates from 16-2-16-Br, L, and P & D only, and **B)** Normalized viability of cells (compared to no treatment, NT) transfected with resulting aggregates from 16-2-16-Br, L, and P & D only (n = 6, error bar = standard deviation).

4.4.1.2 Effects of counterions on TE: 16-2-16-chloride (G-Cl)

The TE and the normalized cell viabilities due to treatment with nanoparticles based on 16-2-16-chloride are summarized in Table-4.10 and shown graphically in Figure-4.9. The nanoparticles produced by this 16-2-16-Cl in the presence of DOPE helper lipids (GDP) for the three charge ratios were all within 230 nm range, but the TE was unexpectedly much lower than for the Lipofectamine^{TM} 2000 formulation (12.4 %). The lowest TE found for the complete 16-2-16-Cl/DOPE/Plasmid (GDP) complex was in case of charge ratio 10:1 where only 1.7 % TE was observed. As the charge ratios were decreased, increased TE was seen for the GDP complexes but none at a level comparable to the TE for Lipofectamine treated cells. As for 16-2-16-Cl, nanoparticles formed without the DOPE (GP), exhibited transfection, but at substantially lower levels than for the complete GDP nanoparticles.

Table-4.10: TE and cell viability by nanoparticles based on 16-2-16-Cl (G), Plasmid (P) and Lipofectamine (L):

Parameters	Charge Ratio (GS : P)	Nanoparticle formulations			
		Transfection complexes		Controls	
		G+P+D	G+P	L+P	P
Percentage of transfection* (GFP + ve)	10 : 1	1.7 ± 0.7	1.9 ± 0.4	12.4 ± 3.8	1.1 ± 0.2
	5 : 1	3.7 ± 0.3	2.7 ± 0.0		
	2 : 1	8.1 ± 1.3	6.2 ± 1.8		
Percentage of cell viability* (Normalized)	10 : 1	69.9 ± 0.3	60.1 ± 10.9	89.2 ± 2.4	99.7 ± 0.5
	5 : 1	90.1 ± 0.6	90.2 ± 2.1		
	2 : 1	94.8 ± 3.5	96.3 ± 2.9		

**Mean ± SD (where, n = 6)*

The cell viabilities for OVCAR-3 cells treated with 16-2-16-Cl formulations were comparable to those observed for Lipofectamine, for charge ratios 5:1 and 2:1. For the

charge ratio 10:1, cell viability was reduced (69.9 %), although the TE was insignificant. Evaluation of the combined TE and cell viability results for 16-2-16-Cl suggest it is less toxic than the 16-2-16-Br, but also less efficient as a transfection vector.

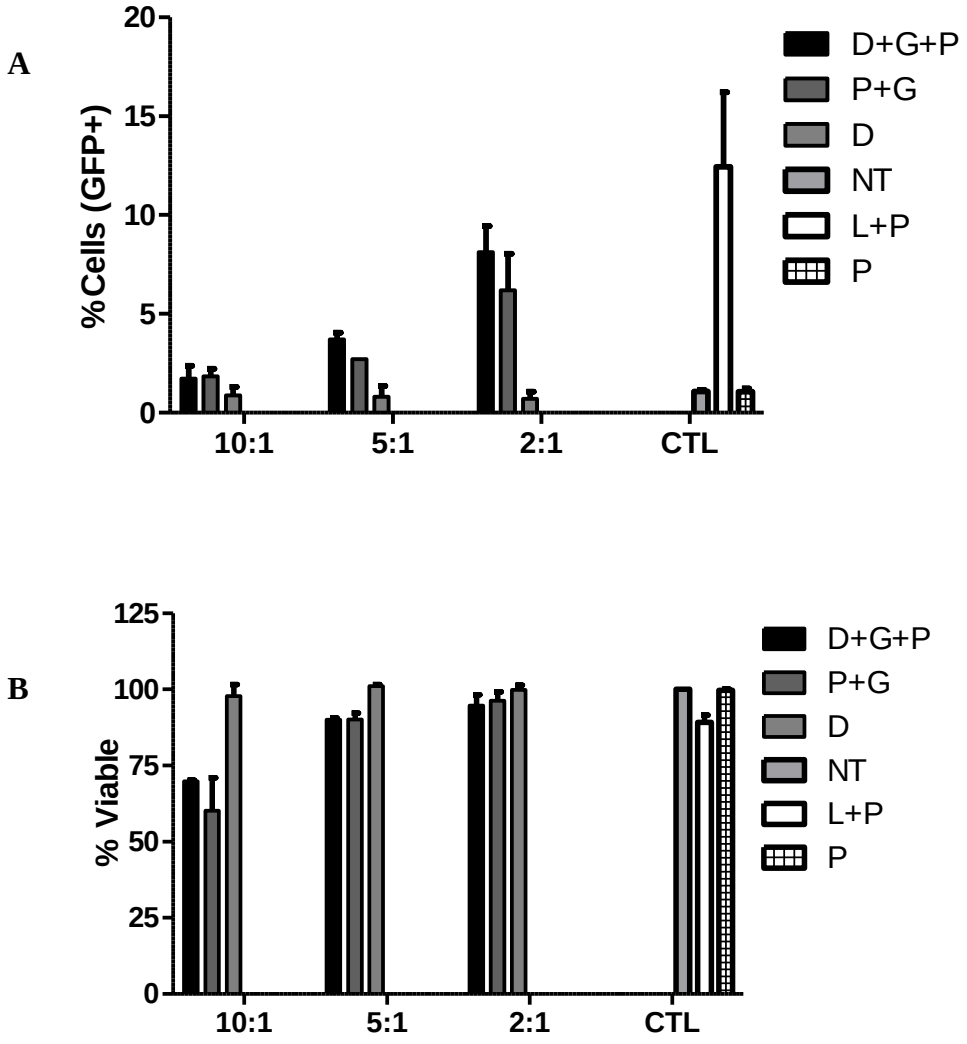

Figure-4.9: Graphical representation illustrating **A)** TE of the resulting aggregates from 16-2-16-Cl, L, and P & D only, and **B)** Normalized viability of cells (compared to no treatment, NT) transfected with resulting aggregates from 16-2-16-Cl, L, and P & D only (n = 6, error bar = standard deviation).

4.4.1.3 Effects of counterions on TE: 16-2-16-malate (G-malate)

The TE and the normalized cell viabilities due to treatment with nanoparticles based on 16-2-16-malate are summarized in Table-4.11 and shown graphically in Figure-4.10. The GDP transfection complexes for 16-2-16-malate showed comparable TE to that of Lipofectamine and 16-2-16 Cl for the charge ratio of 2:1, for which particle size was approximately 230 nm. For the other charge ratios (10:1 and 5:1), the TE was low for the GDP complexes. In the absence of DOPE all the GP complexes exhibited TE greater than that for GDP nanoparticles at all three charge ratios. The highest TE for 16-2-16-malate was observed for the GP complex (11.7 %). Here, the use of helper lipid seemed to decrease the ability of 16-2-16-malate to transfect the OVCAR-3 cells probably due to lower (DOPE mediated) endosomal escape**.** From the resulting sizes, it is evident that the 16-2-16-malate/Plasmid/DOPE (GDP) formed complexes in a much compact manner compared to the sizes of GDP complexes based on 16-2-16-halides. Probably, the transition of DOPE from lamellar (L^{C}_{α}) to inverted hexagonal phase (H^{C}_{II}) was not sufficient enough to release the G+P complexes from the GDP aggregates to enhance the resulting transfection.

Table-4.11: TE and cell viability by nanoparticles based on 16-2-16-malate (G), Plasmid (P) and Lipofectamine (L):

Parameters	Charge Ratio (GS : P)	Nanoparticle formulations			
		Transfection complexes		Controls	
		G+P+D	G+P	L+P	P
Percentage of transfection* (GFP + ve)	10 : 1	6.0 ± 1.7	11.7 ± 6.0	9.9 ± 0.2	1.8 ± 0.1
	5 : 1	4.7 ± 2.0	4.8 ± 1.6		
	2 : 1	7.9 ± 0.5	9.5 ± 0.4		
Percentage of cell viability* (Normalized)	10 : 1	48.0 ± 4.3	52.3 ± 14.3	82.1 ± 2.5	105.8 ± 3.0
	5 : 1	58.7 ± 2.2	73.4 ± 7.9		
	2 : 1	98.3 ± 4.3	95.6 ± 2.2		

**Mean ± SD (where, n = 6)*

From the cell viability results, it can be seen that the 16-2-16-malate counterion is apparently more toxic at increased charge ratios, and more toxic than the 16-2-16-halide surfactants. Aside from the presence of quaternary ammonium groups in the 16-2-16-malate, the elevated cytotoxicity for this vector is probably due to alteration of cytosolic pH as well as osmotic pressure, and due to the presence of toxic metabolites as a result of intracellular metabolism of the exogenous molecules (malate ions).

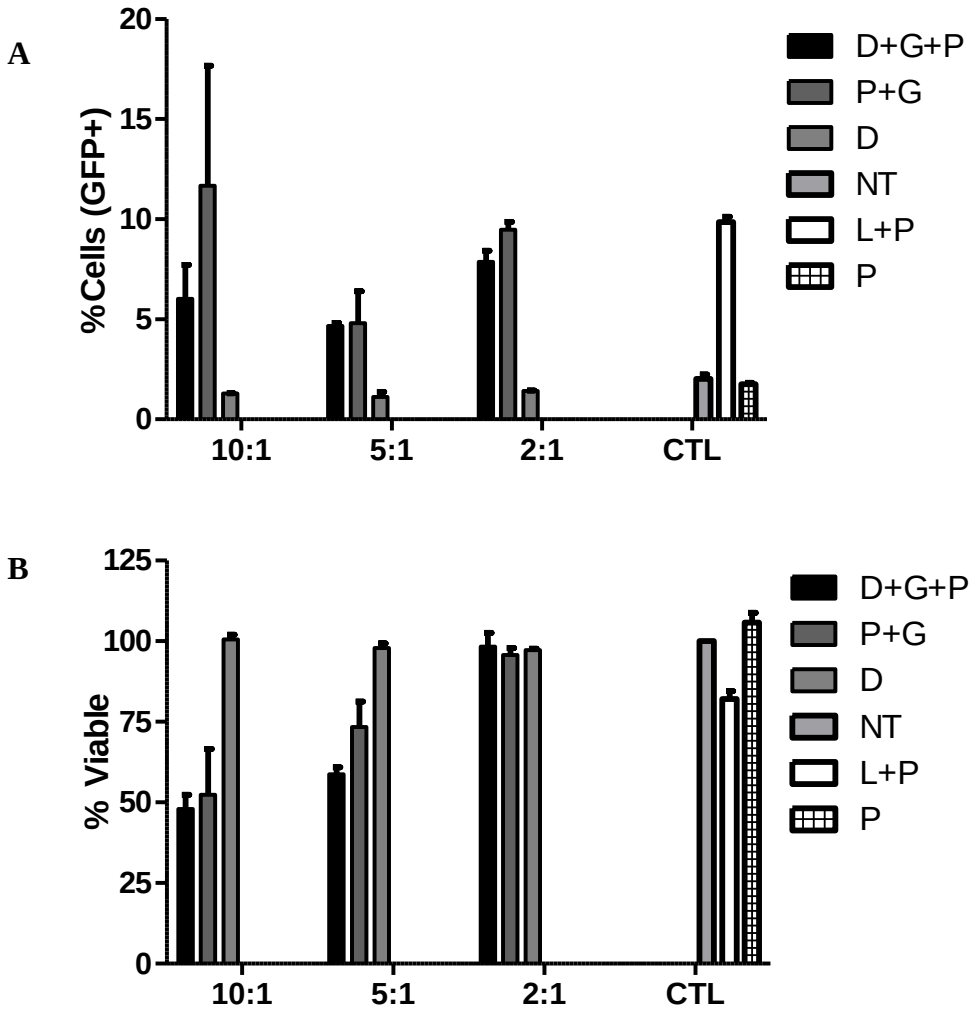

Figure-4.10: Graphical representation illustrating **A)** TE of the resulting aggregates from 16-2-16-malate, L and P & D only, and **B)** Normalized viability of cells (compared to no treatment, NT) transfected with resulting aggregates from 16-2-16-malate, L, and P & D only (n = 6, error bar = standard deviation).

4.4.1.4 Effects of counterions on TE: 16-2-16-tartrate (G-tartrate)

The TE and the normalized cell viabilities due to treatment with different nanoparticles based on 16-2-16-tartrate are summarized in Table-4.12 and shown graphically in Figure-4.11. The nanoparticles produced by this 16-2-16-tartrate in the presence of DOPE helper lipids (GDP) for the three charge ratios were all ≤ 200 nm range, but the TE was much lower than for the Lipofectamine^{TM} 2000 formulation (11.0 %). Here, the lowest TE found for the GDP complex was in case of charge ratio 10:1 where only 4.7 % TE was observed. As the charge ratios were decreased and thus, as the resulting particle sizes decreased, minor increase in the TE was seen for the GDP complexes; but none at a level comparable to the TE for Lipofectamine treated cells. For this 16-2-16-tartrate, the nanoparticles formulated without the DOPE lipid showed transfection which was lower than for the complete GDP nanoparticles in case of the lower charge ratios (5:1 & 2:1). Again, as expected, the results presented in Table-4.18 demonstrate that the negatively charged plasmid, in the absence of a delivery vector, is unable to transfect the OVCAR-3 cells.

Table-4.12: TE and cell viability by nanoparticles based on 16-2-16-tartrate (G), Plasmid (P) and Lipofectamine (L):

Parameters	Charge Ratio (GS : P)	Nanoparticle formulations			
		Transfection complexes		Controls	
		G+P+D	G+P	L+P	P
Percentage of transfection* (GFP + ve)	10 : 1	4.7 ± 0.4	5.7 ± 0.8	11.0 ± 1.3	2.4 ± 0.1
	5 : 1	5.8 ± 0.1	4.8 ± 0.0		
	2 : 1	6.8 ± 0.8	6.3 ± 0.5		
Percentage of cell viability* (Normalized)	10 : 1	55.7 ± 0.4	51.6 ± 1.2	83.4 ± 1.8	101.4 ± 0.6
	5 : 1	63.6 ± 0.7	73.6 ± 5.3		
	2 : 1	96.9 ± 2.9	97.4 ± 2.6		

**Mean ± SD (where, n = 6)*

The cell viabilities of OVCAR-3 cells transfected with 16-2-16-tartrate nanoparticle formulation were comparable to those observed for Lipofectamine^{TM} (83.4 %), for the charge ratio 2:1 only. It is evident from the cell viability data that the tartrate counterions of the 16-2-16-Tartrate vectors are toxic at higher charge ratios, and more toxic than the 16-2-16-halide vectors. Similar trend of viabilities were seen in case of GP nanoparticles. Here the overall pH of the complete nanoparticles (GDP complexes) may be a contributing factor for significant alteration of cytosolic pH, and thus cytotoxicity. As mentioned earlier, the pH of 16-2-16-Tartrate vector itself was found strongly acidic (3.8).

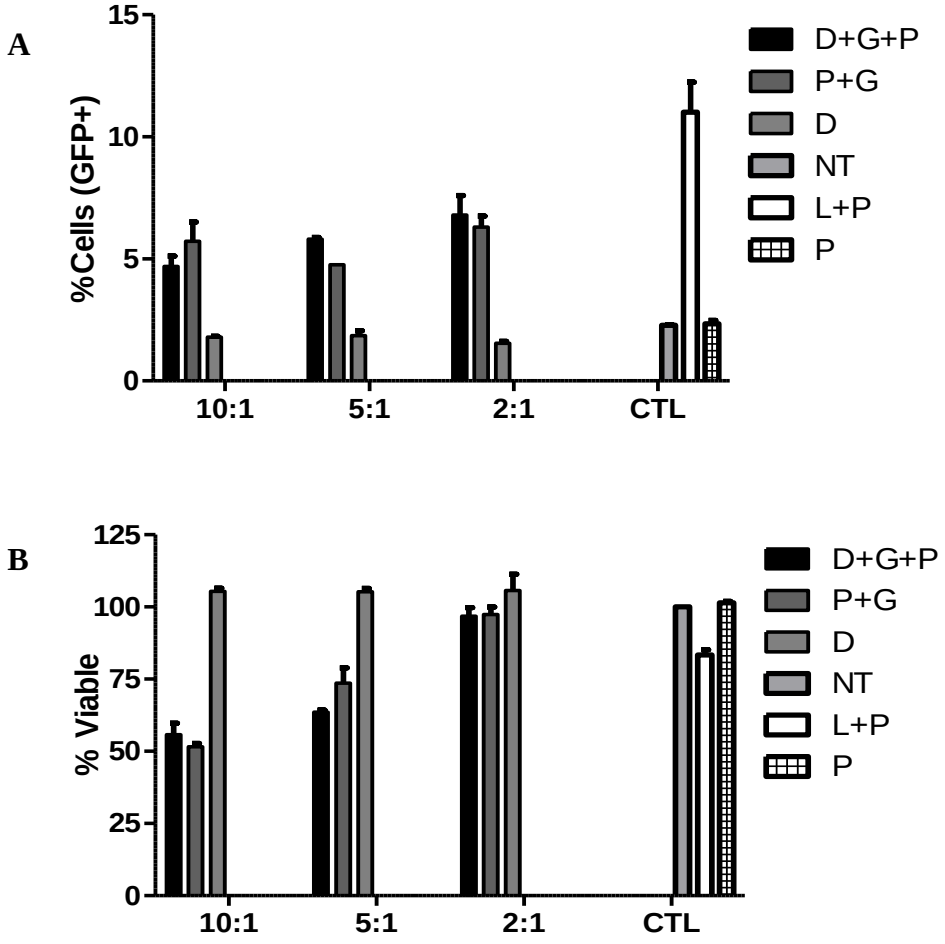

Figure-4.11: Graphical representation illustrating **A)** TE of the resulting aggregates from 16-2-16-tartrate, L, and P & D only, and **B)** Normalized viability of cells (compared to no treatment, NT) transfected with resulting aggregates from 16-2-16-tartrate, L, and P & D only (n = 6, error bar = standard deviation).

4.4.1.5 Effects of counterions on TE: 16-2-16-AMP (G-AMP)

The TE and the normalized cell viabilities due to treatment with different nanoparticles based on 16-2-16-AMP are summarized in Table-4.13 and graphically represented in Figure-4.12. Surprisingly, the TE of the GDP nanoparticles for 16-2-16-AMP was moderate (8.9 %) at the charge ratio of 10:1 which was even higher than the TE for Lipofectamine^{TM} 2000 (8.3 %), and also higher than the TE seen in case of 16-2-16-Cl, 16-2-16-malate and 16-2-16-tartrate GDP systems at any charge ratios. Most interestingly, the TE for the GP nanoparticles were significantly higher for charge ratios 10:1 & 5:1, showing highest TE (14.4%) at charge ratio of 10:1. In this case, the TE of the GP nanoparticles exhibited a decreasing trend, as the charge ratios decreases. Like the 16-2-16-malate systems, for the GDP nanoparticles based on 16-2-16-AMP, the use of helper lipid seemed to decrease the ability of 16-2-16-AMP to transfect the OVCAR-3 cells probably due to the similar reason mentioned in the section 4.4.1.3.

Table-4.13: TE and cell viability by nanoparticles based on 16-2-16-AMP (G), Plasmid (P) and Lipofectamine (L):

Parameters	Charge Ratio (GS : P)	Nanoparticle formulations			
		Transfection complexes		Controls	
		G+P+D	G+P	L+P	P
Percentage of transfection* (GFP + ve)	10 : 1	8.9 ± 1.5	14.4 ± 6.9	8.3 ± 0.6	3.3 ± 1.8
	5 : 1	7.1 ± 0.4	9.5 ± 0.7		
	2 : 1	8.1 ± 0.9	7.9 ± 1.7		
Percentage of cell viability* (Normalized)	10 : 1	48.0 ± 2.9	49.2 ± 19.0	64.7 ± 7.3	91.5 ± 0.0
	5 : 1	51.8 ± 0.1	55.6 ± 25.6		
	2 : 1	84.7 ± 3.1	86.4 ± 11.4		

**Mean ± SD (where, n = 6)*

From the cell viability results it can be seen that the GDP complexes based on 16-2-16-AMP surfactants, are quantitatively similar cytotoxic as seen from the 16-2-16-malate surfactants and increased cytotoxicity was seen at higher charge ratios. Similar trend was also seen in the case of GP nanoparticles. For both of the nanoparticle systems (GDP & GP), the 16-2-16-AMP was found less toxic than those of 16-2-16-tartrate, but significantly more toxic when compared to those of 16-2-16-halides. This increased cytotoxicity may be attributed due to the fact of cytosolic pH and osmotic pressure alteration and presence of toxic metabolites due to intracellular metabolism of the exogenous ions (AMP) in cytosol.

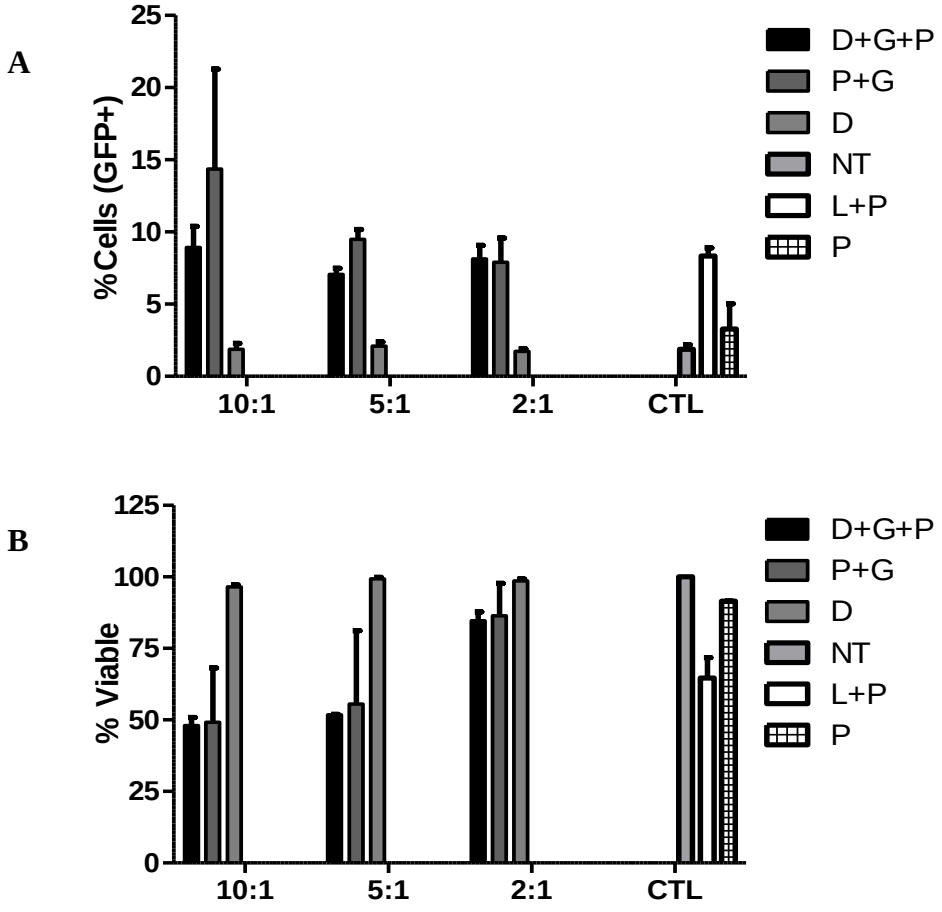

Figure-4.12: Graphical representation illustrating **A)** TE of the resulting aggregates from 16-2-16-AMP, L, and P & D only, and **B)** Normalized viability of cells (compared to no treatment, NT) transfected with resulting aggregates from 16-2-16-AMP, L, and P & D only (n = 6, error bar = standard deviation).

4.4.1.6 Effects of counterions on TE: 16-2-16-CMP (G-CMP)

The TE and the normalized cell viabilities due to treatment with different nanoparticles based on 16-2-16-CMP are summarized in Table-4.14 and shown graphically in Figure-4.13. The nanoparticles produced by this 16-2-16-CMP in presence of DOPE helper lipids (GDP) for the charge ratios of 10:1 and 5:1 were < 200 nm range, but the TE at 5:1 was unexpectedly much lower (3.6 %) than for the Lipofectamine^{TM} 2000 formulation (12.6 %). The highest TE found for the GDP complexes was in case of charge ratio 10:1, whereas, the lowest was observed is the case of charge ratio 2:1, probably due to low cellular uptake of the large sized GDP aggregates (427 nm). Similar trend of TEs were seen in the case of GP nanoparticles, but were significantly lower than those of the GDP complexes. As the charge ratios were increased, increased TE was seen for the GDP complexes but none at a level comparable to the TE for Lipofectamine treated cells. Here, the usage of helper lipid seemed to increase the ability of 16-2-16-CMP to transfect the OVCAR-3 cells.

Table-4.14: TE and cell viability by nanoparticles based on 16-2-16-CMP (G), Plasmid (P) and Lipofectamine (L):

Parameters	Charge Ratio (GS : P)	Nanoparticle formulations			
		Transfection complexes		Controls	
		G+P+D	G+P	L+P	P
Percentage of transfection* (GFP + ve)	10 : 1	7.3 ± 0.2	5.4 ± 0.5	12.6 ± 0.3	1.5 ± 0.4
	5 : 1	3.6 ± 0.1	3.3 ± 0.2		
	2 : 1	2.2 ± 1.0	2.4 ± 0.2		
Percentage of cell viability* (Normalized)	10 : 1	70.5 ± 6.5	61.9 ± 4.9	83.8 ± 3.0	109.9 ± 4.7
	5 : 1	61.5 ± 18.9	45.5 ± 0.3		
	2 : 1	103.3 ± 12.5	90.8 ± 13.5		

**Mean ± SD (where, n = 6)*

The cell viability for the GDP complexes of this 16-2-16-CMP vector was moderate in the case of charge ratios 10:1 & 5:1, but lower than the cell viability for Lipofectamine (83.8%). The cytotoxicity seemed higher at increased charge ratios and this 16-2-16-CMP was found less toxic than those of 16-2-16-malate, 16-2-16-tartrate, and 16-2-16-AMP at any charge ratio. Almost no cell death was found for the GDP complexes of 16-2-16-CMP in case of charge ratio 2:1, compared to control, and again this is probably due to very low cellular uptake of the GDP particles having the mean size of 427 nm at that charge ratio.

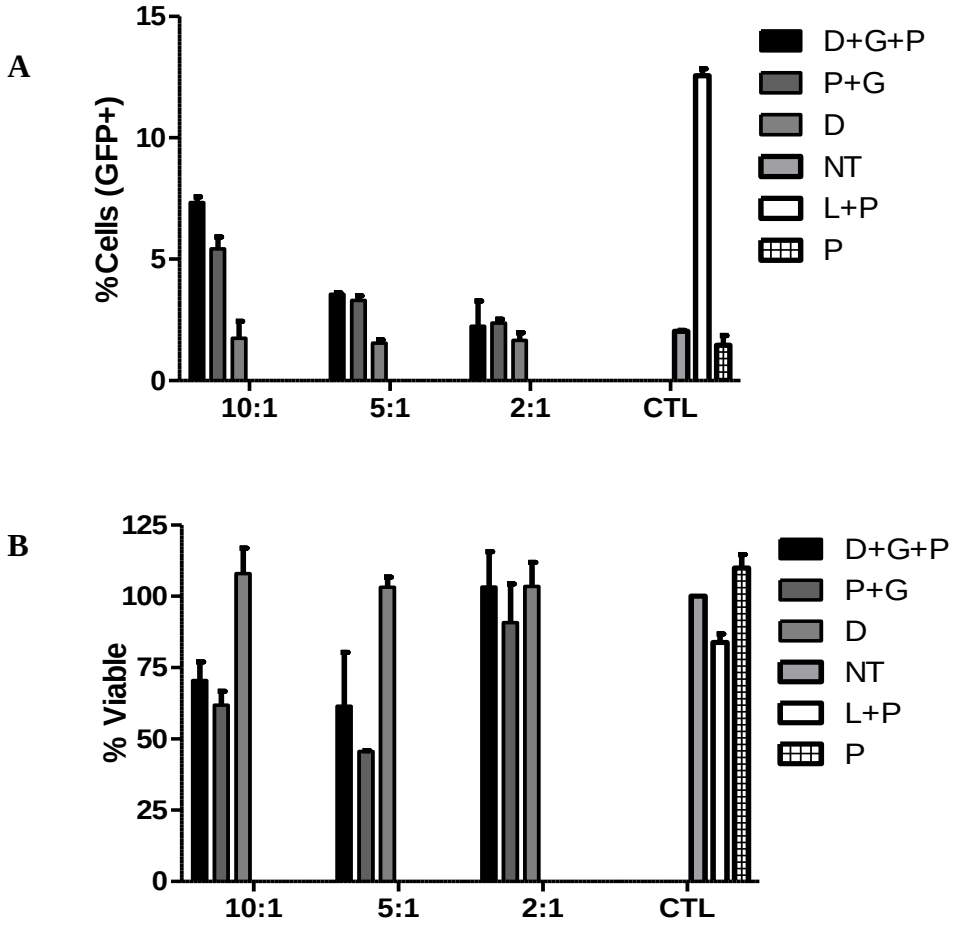

Figure-4.13: Graphical representation illustrating **A)** TE of the resulting aggregates from 16-2-16-CMP, L, and P & D only, and **B)** Normalized viability of cells (compared to no treatment, NT) transfected with resulting aggregates from 16-2-16-CMP, L, and P & D only (n = 6, error bar = standard deviation).

4.4.1.7 Effects of counterions on TE: 16-2-16-UMP (G-UMP)

The TE and the normalized cell viabilities due to treatment with different nanoparticles based on 16-2-16-UMP are summarized in Table-4.15 and shown graphically in Figure-4.14. At the charge ratio of 10:1, the GDP complexes formed by 16-2-16-UMP was large (426 nm), but unexpectedly, significantly higher TE was seen compared to that of 16-2-16-Cl, 16-2-16-malate, and 16-2-16-tartrate. Surprisingly, at charge ratio 5:1, the observed TE suddenly decreased (also in the case of 16-2-16-AMP), although the resulting GDP particles were of lowest size (92 nm) among all the three charge ratios. As the charge ratios were decreased to 2:1, increased TE was seen for the GDP complexes but none at a level comparable to the highest TE for Lipofectamine (14.5 %) treated cells. In case of GP nanoparticles, similar and comparable TE was seen except the fact that, the use of helper lipid for the charge ratio 10:1 seemed to decrease the ability of 16-2-16-UMP to transfect the OVCAR-3 cells.

Table-4.15: TE and cell viability by nanoparticles based on 16-2-16-UMP (G), Plasmid (P) and Lipofectamine (L):

Parameters	Charge Ratio (GS : P)	Nanoparticle formulations			
		Transfection complexes		Controls	
		G+P+D	G+P	L+P	P
Percentage of transfection* (GFP + ve)	10 : 1	7.4 ± 0.3	8.0 ± 0.7	14.5 ± 0.3	2.5 ± 0.2
	5 : 1	4.8 ± 0.3	3.6 ± 0.1		
	2 : 1	8.8 ± 0.2	8.4 ± 0.2		
Percentage of cell viability* (Normalized)	10 : 1	38.9 ± 1.9	34.4 ± 1.7	78.5 ± 2.6	101.7 ±2.9
	5 : 1	58.6 ± 2.8	52.2 ± 0.1		
	2 : 1	92.2 ± 1.1	94.2 ± 1.0		

**Mean ± SD (where, n = 6)*

From the cell viability results, it can be seen that the nanoparticles for both the systems (GDP & GP) based on 16-2-16-UMP vectors are apparently more toxic at increased charge ratios, and the most toxic than all the 16-2-16 gemini vectors discussed so far. This is due to the fact that the UMP counterion of 16-2-16-UMP system contains uracil moiety and these uracil moieties (such as in 5-Fluoro Uracil, 5-FU) showed tumor selective cytotoxicity [195, 196]. Again, this extreme cytotoxicity may also be partly attributed to the alteration of cytosolic pH and osmotic pressure, as the pH of the 16-2-16-UMP alone was found to be most acidic (3.1) among all the 16-2-16 gemini vectors studied.

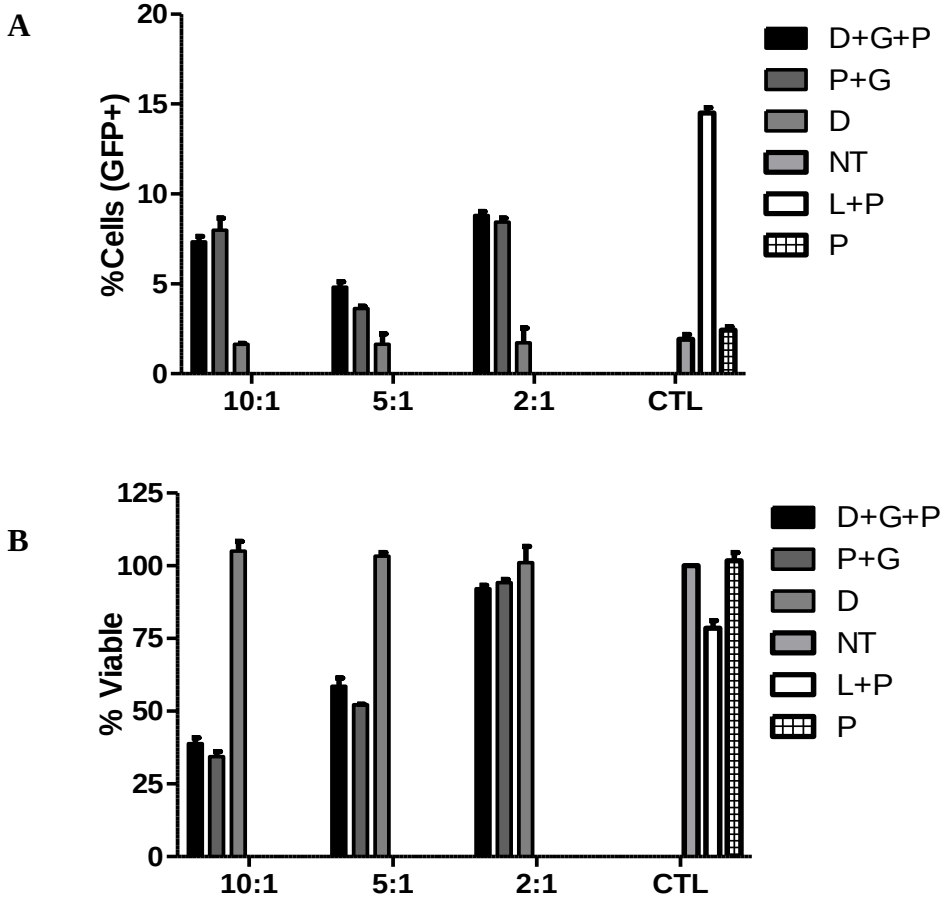

Figure-4.14: Graphical representation illustrating **A)** TE of the resulting aggregates from 16-2-16-UMP, L, and P & D only, and **B)** Normalized viability of cells (compared to no treatment, NT) transfected with resulting aggregates from 16-2-16-UMP, L, and P & D only (n = 6, error bar = standard deviation).

4.4.1.8 Effects of counterions on TE: 16-2-16-GMP (G-GMP)

The TE and the normalized cell viabilities due to treatment with different nanoparticles based on 16-2-16-GMP are summarized in Table-4.16 and shown graphically in Figure-4.15. From the zeta potential characterization results, it was seen that the GDP complexes based on gemini-GMP have a net negative surface charge and was predicted that these high –ve ζ values (especially in the case of charge ratios 10:1 and 5:1) will render the GDP complexes as the lowest effective candidates to transfect the OVCAR-3 cells. Surprisingly, the GDP complexes based on 16-2-16-GMP showed TE to some extent, with the highest TE seen at the charge ratio of 10:1, although the resulting GDP complex size was approximately 1 μm (810 nm) at that charge ratio. As the charge ratios were decreased, this 16-2-16-GMP vector produced GDP complexes of ~ 530 nm size range, and decreased TE was seen for the GDP complexes but none at a level comparable to the highest TE for Lipofectamine^{TM} 2000 (10.7 %) treated cells. In case of GP nanoparticles, similar trend of TE was seen based on charge ratios except the fact that, the use of helper lipid for the charge ratio 2:1 seemed to decrease the ability of 16-2-16-GMP to transfect the OVCAR-3 cells.

Table-4.16: TE and cell viability by nanoparticles based on 16-2-16-GMP (G), Plasmid (P) and Lipofectamine (L):

Parameters	Charge Ratio (GS : P)	Nanoparticle formulations			
		Transfection complexes		Controls	
		G+P+D	G+P	L+P	P
Percentage of transfection* (GFP + ve)	10 : 1	5.4 ± 1.0	4.4 ± 0.1	10.7 ± 0.2	1.8 ± 0.6
	5 : 1	3.5 ± 0.1	3.1 ± 1.2		
	2 : 1	3.4 ± 0.1	4.1 ± 0.4		
Percentage of cell viability* (Normalized)	10 : 1	42.9 ± 0.1	29.5 ± 1.9	71.8 ± 0.8	94.3 ± 4.2
	5 : 1	51.3 ± 0.7	56.8 ± 5.3		
	2 : 1	86.6 ± 1.6	88.8 ± 0.1		

**Mean ± SD (where, n = 6)*

The cell viability for OVCAR-3 cells treated with 16-2-16-GMP nanoparticles (both GDP & GP) were comparable to those observed for the 16-2-16-AMP systems, for all the three charge ratios. The results suggest that 16-2-16-GMP vector is more toxic at increased charge ratios, and viability due to treatment with GDP/GP was found higher than that of Lipofectamine (71.8 %) at the charge ratio of 2:1.

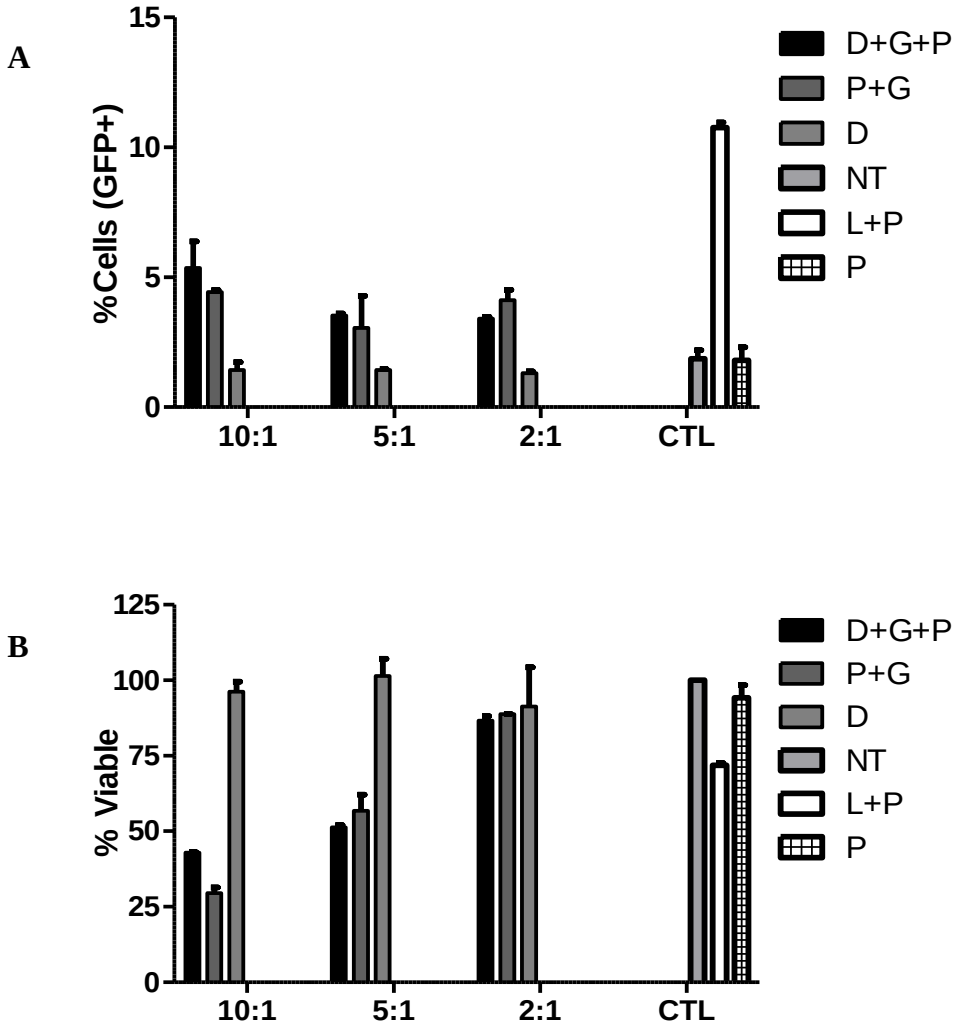

Figure-4.15: Graphical representation illustrating **A)** TE of the resulting aggregates from 16-2-16-GMP, L, and P & D only, and **B)** Normalized viability of cells (compared to no treatment, NT) transfected with resulting aggregates from 16-2-16-GMP, L, and P & D only (n = 6, error bar = standard deviation).

4.4.2 Summary of the effects of counterions on TE

The following table (Table-4.17) summarizes the transfection efficiencies (TE) and cell viabilities (%viability) for nanoparticles formed from all eight 16-2-16 surfactants, in combination with plasmid alone (GP formulations) or plasmid and DOPE (GDP formulations). Although no generalized relation or pattern is observed, overall, the TE was found to be moderate at the lowest charge ratio (2:1), as the GDP particle sizes formed from all the GSs was within nanoparticle range (~500 nm) at that charge ratio. In few cases, the TE was exceptionally higher at the charge ratio (10:1).

Particle size significantly affects the cellular and tissue uptake of nanoparticles in non-viral transfection formulations [197]. In one of the studies, Manisha *et al.* reported that the polylactic-polyglycolic acid co-polymer (PLGA 50:50) nanoparticles of 100 nm sizes showed 2.5 fold greater uptake compared to 1 μm particles, and 6 fold higher uptake compared to 10 μm microparticles in human epithelial colorectal adenocarcinoma (Caco-2) cell line [198]. Similar trend of results were attained when these formulations of nano- and microparticles were tested in a rat in situ intestinal loop model. The efficiency of cellular uptake of 100 nm size particles was seen 15–250 fold greater than larger size (1 and 10 μm) microparticles [199]. Moreover, Prabha *et al.* (2002) reported that smaller sized nanoparticles can give rise to a 27-fold higher TE (analysed by luciferase protein levels) than that of the larger-sized nanoparticles, in COS-7 cells [197]. But in our study, the impact of particle size was not that prominent as few of the gemini surfactants, namely 16-2-16-bromide, 16-2-16-CMP, 16-2-16-UMP, and 16-2-16-GMP formed particles of ~500 nm sizes (for 16-2-16-GMP, particle sizes was > 500 nm) at either 10:1 or 2:1 charge ratios, while exerting moderate TE at the charge ratio of 10:1.

Table 4.17: Summary of transfection efficiencies (TEs) and cell viabilities (% viable) due to treatment with GDP and GP nanoparticles based on all 16-2-16.X surfactants

Formulation	TE* (%)			% Viable*		
	10:1	5:1	2:1	10:1	5:1	2:1
Lipofectamine**		11.3 ± 0.9			86.6 ± 2.7	
GDP (Br)	10.0 ± 4.9	4.0 ± 0.3	4.3 ± 0.3	76.4 ± 14.4	84.9 ± 2.7	87.5 ± 12.2
GP (Br)	9.5 ± 2.3	2.2 ± 0.6	7.1 ± 1.4	69.8 ± 11.9	75.9 ± 13.2	93.4 ± 4.3
GDP (Cl)	1.7 ± 0.7	3.7 ± 0.3	8.1 ± 1.3	69.9 ± 0.3	90.1 ± 0.6	94.8 ± 3.5
GP (Cl)	1.9 ± 0.4	2.7 ± 0.0	6.2 ± 1.8	60.1 ± 10.9	90.2 ± 2.1	96.3 ± 2.9
GDP (Malate)	6.0 ± 1.7	4.7 ± 2.0	7.9 ± 0.5	48.0 ± 4.3	58.7 ± 2.2	98.3 ± 4.3
GP (Malate)	11.7 ± 6.0	4.8 ± 1.6	9.5 ± 0.4	52.3 ± 14.3	73.4 ± 7.9	95.6 ± 2.2
GDP (Tartrate)	4.7 ± 0.4	5.8 ± 0.1	6.8 ± 0.8	55.7 ± 0.4	63.6 ± 0.7	96.9 ± 2.9
GP (Tartrate)	5.7 ± 0.8	4.8 ± 0.0	6.3 ± 0.5	51.6 ± 1.2	73.6 ± 5.3	97.4 ± 2.6
GDP (AMP)	8.9 ± 1.5	7.1 ± 0.4	8.1 ± 0.9	48.0 ± 2.9	51.8 ± 0.1	84.7 ± 3.1
GP (AMP)	14.4 ± 6.9	9.5 ± 0.7	7.9 ± 1.7	49.2 ± 19.0	55.6 ± 25.6	86.4 ± 11.4
GDP (CMP)	7.3 ± 0.2	3.6 ± 0.1	2.2 ± 1.0	70.5 ± 6.5	61.5 ± 18.9	103.3 ± 12.5
GP (CMP)	5.4 ± 0.5	3.3 ± 0.2	2.4 ± 0.2	61.9 ± 4.9	45.5 ± 0.3	90.8 ± 13.5
GDP (UMP)	7.4 ± 0.3	4.8 ± 0.3	8.8 ± 0.2	38.9 ± 1.9	58.6 ± 2.8	92.2 ± 1.1
GP (UMP)	8.0 ± 0.7	3.6 ± 0.1	8.4 ± 0.2	34.4 ± 1.7	52.2 ± 0.1	94.2 ± 1.0
GDP (GMP)	5.4 ± 1.0	3.5 ± 0.1	3.4 ± 0.1	42.9 ± 0.1	51.3 ± 0.7	86.6 ± 1.6
GP (GMP)	4.4 ± 0.1	3.1 ± 1.2	4.1 ± 0.4	29.5 ± 1.9	56.8 ± 5.3	88.8 ± 0.1

**Mean ± SD (where, n = 6), **Mean ± SD (where, n = 16)*

In general, between the 16-2-16-halide, the 16-2-16-bromide showed better TE at 10:1 but, the 16-2-16-chloride showed moderate TE at 2:1. Between the 16-2-16-carboxylates, the GDP particles of based on both the 16-2-16–tartrate and 16-2-16–malate showed better TE at 2:1. Lastly, among the 16-2-16-NMPs, the 16-2-16-AMP showed moderate TE at 10:1 and 2:1; the 16-2-16-CMP showed good TE at 10:1; the 16-2-16-UMP showed TE at 10:1 and 2:1; and gemini-GMP showed poor TE at 10:1. Except in the cases of 16-2-16-Br, 16-2-16-AMP, 16-2-16-CMP, and 16-2-16-GMP, the TE was found to increase with the progression of charge ratios from higher (10:1) to lower (2:1). These results were in agreement with previous reports by Wang *at el.* [145] where it was reported that TE in OVCAR-3 cell line decreased with increasing charge ratios.

Besides, irrespective of charge ratios, 16-2-16-halides (bromide) and 16-2-16-NMPs (except 16-2-16-GMP) are more efficient vectors to transfect OVCAR-3 cells, compared to the 16-2-16-malate/tartrate vectors. In relation to DOPE, the TE due to GP nanoparticles were found significantly higher than the TE due to GDP particles of 16-2-16-malate (d_{GP} = 211 nm & d_{GDP} = 121 nm; where d = size/diameter) and 16-2-16-AMP (d_{GP} = 81 nm & d_{GDP} = 83 nm; where d = size/diameter) at the charge ratio of 10:1, and thus, inferred that the role of DOPE lipid was ineffectual for both of these cases. As discussed earlier, the probable reason for this phenomena was during endosomal escape, the release of the GP complexes from the GDP complexes was not sufficient enough, upon transition of DOPE from lamellar (L^{C}_{α}) to inverted hexagonal phase (H^{C}_{II}).

The GP complexes were found to consistently exhibit low TEs compared to GDP lipoplexes (except few cases as discussed above) most likely due to their inability to undergo structural polymorphisms, for endosomal escape and DNA release, in absence of DOPE

[200]. From our results, it is also evident that, the TE of the Lipofectamine^{TM} 2000 (positive control) was drastically lower than previous reports (11.3 % vs 32.2 %) [94, 145], which may be attributed to cellular senescence caused by high passage number (12-18), during which transfections took place. Further studies, using OVCAR-3 as well as other cell lines, may justify the complete analysis of the differences in TE attained from lipoplexes generated from 16-2-16 gemini systems.

For all the 16-2-16-gemini systems, the normalized cell viability was approximately 95 % on average (compared to control) in the case of charge ratio of 2:1 and more toxicity was seen as the charge ratios increased in general. Eventually, the evaluation of the combined TE and cell viability results for all the 16-2-16-gemini surfactants suggest that, irrespective of charge ratio, the 16-2-16-bromide (halide family of counterion) is the lowest toxic in nature, but also the most efficient as a transfection vector among the eight 16-2-16-gemini vectors studied in this project.

The following figures (Figure-4.16 & Figure-4.17) depict the comparative summary of TE & cell viability due to treatment with (GDP & GP) nanoparticles respectively, based on all the 16-2-16 series of gemini surfactants with different counterions.

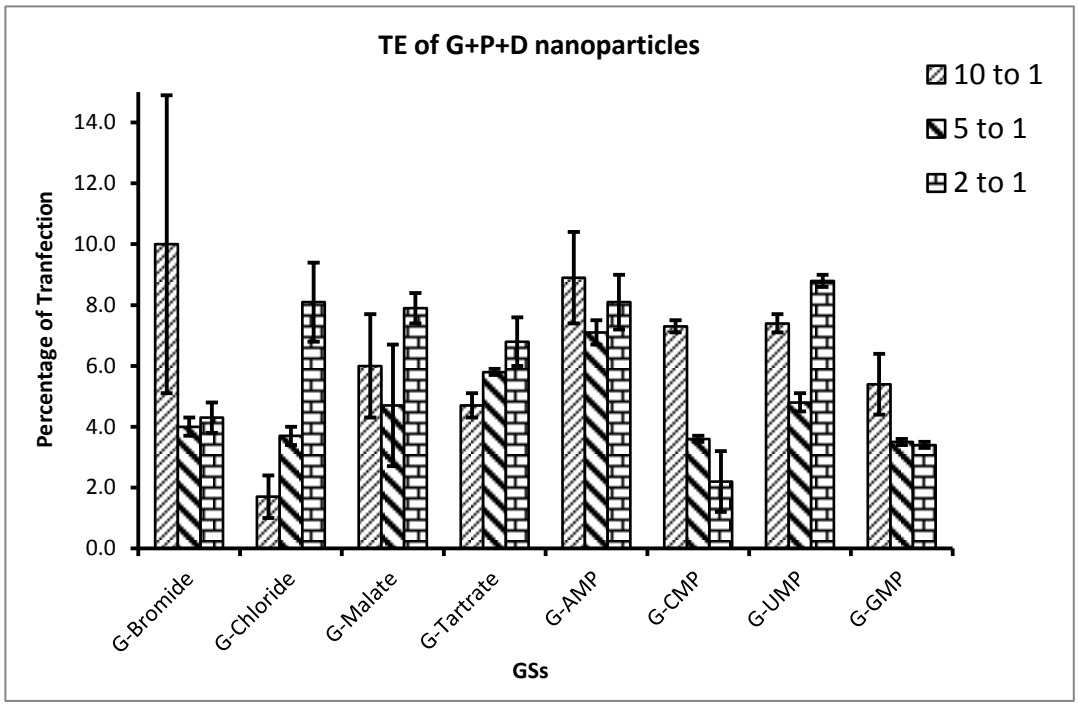

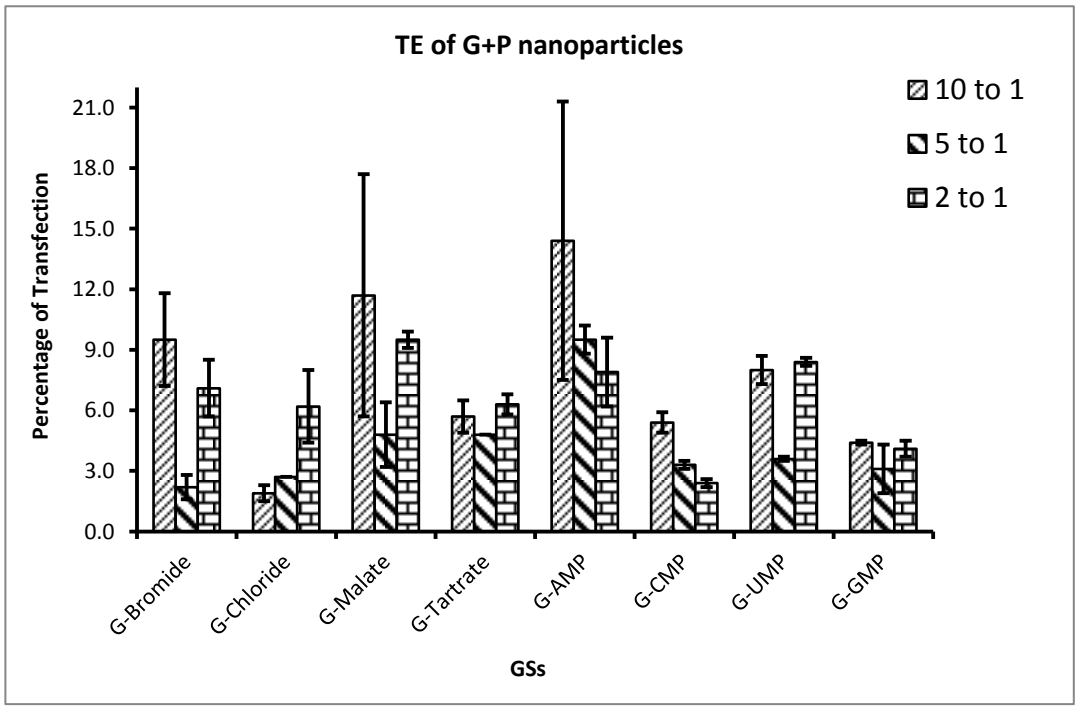

Figure-4.16: Graphical representation illustrating TE of particles, based on 16-2-16 series of gemini surfactants associated with eight different counterions, for all the three charge ratios: **A)** For GDP nanoparticles, and **B)** For GP nanoparticles (n = 6, error bar = standard deviation)

A)

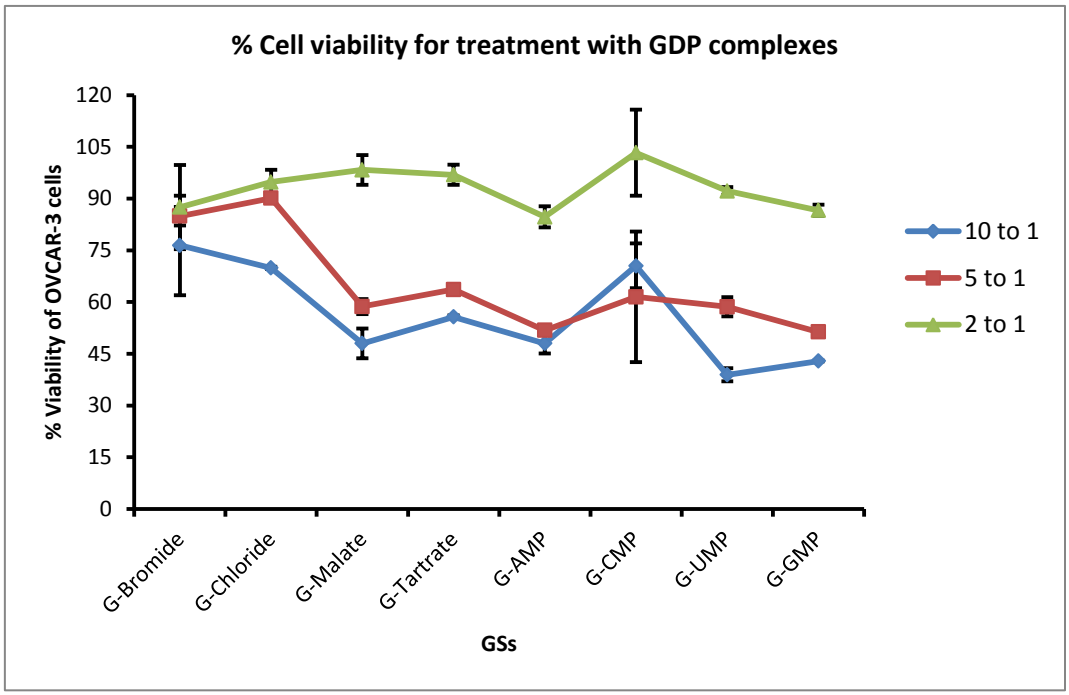

B)

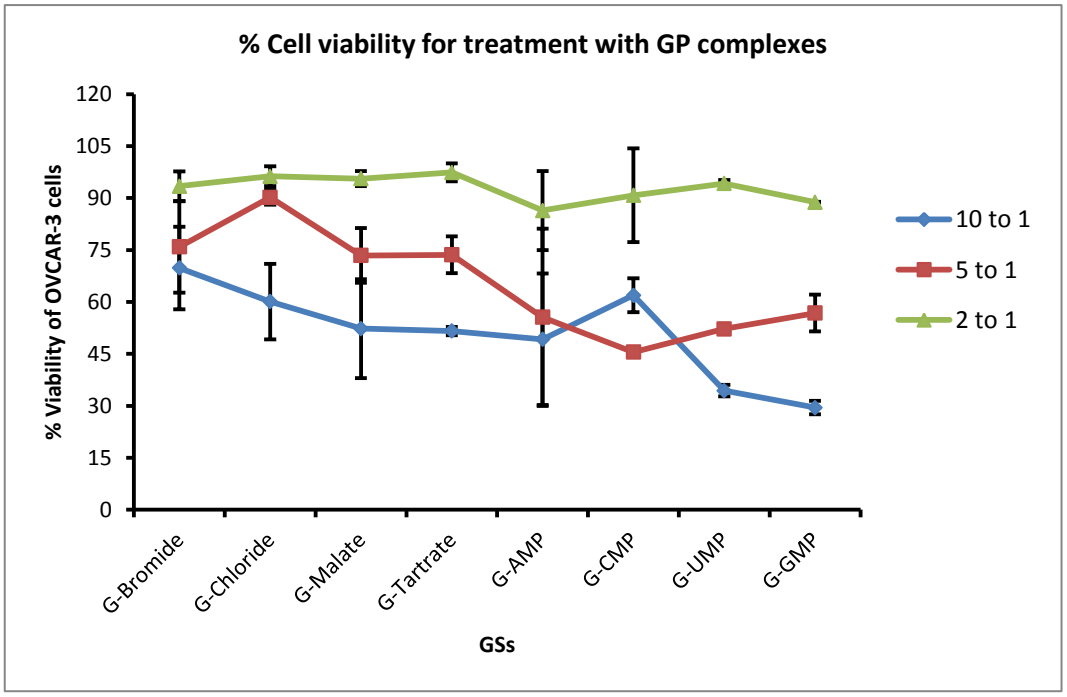

Figure-4.17: Variation of OVCAR-3 percentage cell viability at three different charge ratios when treated with **A)** GDP nanoparticles, and **B)** GP nanoparticles, generated from 16-2-16 series of gemini associated with eight different counterions (n = 6, error bar = standard deviation).

5. Summary and Future Directions

We report the results of the systematic investigation of the effect of associated counterions on the micellization of a novel series of quaternary ammonium 16-2-16 gemini surfactants, in aqueous solution. Our focus regarding the solution properties, aggregation, and micellization of GSs, clearly suggests that ionic hydration, ion polarizability, hydrophobic interactions, counterion dissociation, and intra/inter-molecular hydrogen bonds cooperatively influence the micellization process and the propensity of the counterions to form ion pairs with the oppositely charged head groups of gemini in solution. The results of our study provide new insight to understand the diversified effects of counterions on the intriguing properties of these novel and green surfactants "The Gemini". For all the anions, it was found that, hydrophilicity, polarizability, and hydration numbers of the ions are the dominant factors determining micellization.

In summary, the critical micellar concentration (CMC), degree of micellization (α), as well as degree of binding of counterions to the micelles (β) and other surface properties such as surface excess concentration (Γ_{max}), surface pressure, and minimum area per molecule (A_{min}) at the air/water interface of these bis-cationic dimeric GSs strongly depend on the associated counterions of the respective gemini. Moreover, from our study it was revealed that, the counterions have massive impact on the solubilities and the Krafft temperatures of the individual gemini, mainly due to electrostatic interactions as described earlier. As a part of unique behavior in solution, counterions also play a role for change in density and viscosity due to their micellar packing volume and matrix type aggregation in aqueous solution. Lastly, the foam stability of the gemini is governed by the stable micellar packing in

the adsorbed foam lamellae, and the higher the micellar stability, the greater is the foam stability.

For this project, to investigate the TE we are reporting the transfection ability of 16-2-16 series of GSs associated with different counterions among which the transfectability of those GS with organic counterions are being reported for the first time ever. Considering both the average TE and cytotoxicity, from our investigation it was revealed that the optimal charge ratio of GSs to DNA for good to moderate transfection was found to be 2:1. Furthermore, the particle size characterization of the GDP transfection complexes indicates that particles generated from any of the 16-2-16 gemini surfactants at any charge ratios are within submicron sized. None of the associated counterions showed significantly better TEs than that of the commercially available lipid based reagent Lipofectamine^{TM} 2000. By changing the associated counterions, our primary goal was to develop efficient GSs as transgene delivery vectors for ovarian cancer gene therapy. With the disagreement as we hypothesized, the change in counterions for GSs as a parameter for vector design did not enhance the TE in OVCAR-3 cells at all in comparison to that of Lipofectamine (11.3 ± 0.9) , but we found moderate transfection ability for few 16-2-16 gemini associated with few counterions as discussed in the results section. In terms of cytotoxicity, the counterions seemed well tolerated on average by the cells, eliminating the considerations of effect of mechanical rigors (such as aggressive handling, unexpected contaminations, pH effects of the overall transfection complexes) on cytotoxicity. Our results proved and reinforced that smaller sized particles (i.e. < 200 nm) are not a 'mandatory' requirement for transfection *in vitro* in OVCAR-3 cell line, and our finding is also consistent with results reported by Foldvari *et al.* [201]. However, these micro-sized particles would not be the good candidates

for *in vivo* TE studies, because larger particles may be rapidly degraded by phagocytic cells and the reticuloendothelial systems (RES) as mentioned in the "Introduction" section.

Although we report the morphology (see "Appendix" section) of the GSs only based on CPP values, this project could be expanded using TEM or atomic force microscopy (AFM) imaging to investigate the effect of change in the associated counterions on aggregate morphology of these novel GSs, considering the importance of micellar morphology. Also, this study could be expanded to investigate the aggregation number of the resulting micelles of the GSs as part of important physical characterization data using fluorescence quenching (FQ) technique.

The interaction between the gemini molecules and DNA is another potential study to be explored. Since the GSs associated with different counterions are designed for DNA delivery to be considered as efficient vectors, it would be questionable if the existing interactions of the cationic GSs and the polyelectrolyte DNA is not studied to reveal how the solution properties of GSs are moulded by the addition of DNA and also the effect of changing the counterions on the this GS-DNA interaction. Thus this project could be expanded to investigate this through the application of experimental tools like the isothermal titration calorimetry (ITC) for thermodynamic investigations & critical aggregate concentration (CAC) determination, and Brewster angle microscopy (BAM) for pre-/post images of the interactions.

In terms of transfection, future studies using animal models should be explored for all the charge ratios to investigate the actual resulting influence in reality on gene delivery. Additionally, stability of transfection complexes may be increased by modifying transfection complexes with the attachment of polyethylene glycol (PEG) to the GSs since no studies

involving PEGylation of GSs based DNA delivery have been carried out. Apart from this PEG conjugation approach, pluronic co-polymer or functionalized pluronics with biodegradable moieties (such as PAGA i.e. poly-[α-(4-aminobutyl)-L-glycolic acid]) based gene delivery could also be considered to be studied which has enormous potential for efficient gene delivery [202]. To battle cancers via gene therapy approach, cell-specific targeting is one of the crucial considerations which could be a paramount sector for further research. Thus, another fact to consider for this project in future will be the modification of GSs by attaching a targeting group (i.e. folate if the treatment is for OCs) which will allow increased cellular uptake and cell specificity, when transfection studies will be done with these GSs conjugated with a target ligand both at *in vitro* and *in vivo* situations.

Bibliography

[1] F. Ledley, Pharmaceutical Approach to Somatic Gene Therapy, Pharm Res, 13 (1996) 1595-1614.
[2] W.F. Anderson, Human gene therapy, Nature, 392 (Suppl.) (1998) 25-30.
[3] C.Y.M. Hsu, H. Uludağ, Nucleic-acid based gene therapeutics: delivery challenges and modular design of nonviral gene carriers and expression cassettes to overcome intracellular barriers for sustained targeted expression, Journal of Drug Targeting, 20 (2012) 301-328.
[4] T. Wirth, N. Parker, S. Ylä-Herttuala, History of gene therapy, Gene, 525 (2013) 162-169.
[5] I.M. Verma, M.D. Weitzman, Gene therapy: twenty-first century medicine, Ann. Rev. Biochem., 74 (2005) 711-738.
[6] M. Kumar, K. Jinturkar, M.R. Yadav, A. Misra, Gemini Amphiphiles: A Novel Class of Nonviral Gene Delivery Vectors, Crit Rev Ther Drug Carrier Syst., 27 (2010) 237-278.
[7] S.D. Wettig, R.E. Verrall, M. Foldvari, Gemini surfactants: a new family of building blocks for non-viral gene delivery systems, Current gene therapy, 8 (2008) 9-23.
[8] S.L. Ginn, I.E. Alexander, M.L. Edelstein, M.R. Abedi, J. Wixon, Gene therapy clinical trials worldwide to 2012 – an update, J. Gene. Med., 15 (2013) 65-77.
[9] Gene Therapy Clinical Trials worldwide, http://www.wiley.com/legacy/wileychi/genmed/clinical/, (2014).
[10] D.V. Schaffer, J.T. Koerber, K.-i. Lim, Molecular Engineering of Viral Gene Delivery Vehicles, Annual Review of Biomedical Engineering, 10 (2008) 169-194.
[11] H. Jia, Gene therapy finds welcoming environment in China, Nature medicine, 12 (2006) 263-264.
[12] L.M. Bryant, D.M. Christopher, A.R. Giles, C. Hinderer, J.L. Rodriguez, J.B. Smith, E.A. Traxler, J. Tycko, A.P. Wojno, J.M. Wilson, Lessons learned from the clinical development and market authorization of Glybera, Human gene therapy. Clinical development, 24 (2013) 55-64.
[13] D. Melchiorri, L. Pani, P. Gasparini, G. Cossu, J. Ancans, J.J. Borg, C. Drai, P. Fiedor, E. Flory, I. Hudson, H.G. Leufkens, J. Muller-Berghaus, G. Narayanan, B. Neugebauer, J. Pokrotnieks, J.L. Robert, T. Salmonson, C.K. Schneider, Regulatory evaluation of Glybera in Europe - two committees, one mission, Nature reviews. Drug discovery, 12 (2013) 719.
[14] C.E. Thomas, A. Ehrhardt, M.A. Kay, Progress and problems with the use of viral vectors for gene therapy, Nature reviews. Genetics, 4 (2003) 346-358.
[15] M.A. Kay, J.C. Glorioso, L. Naldini, Viral vectors for gene therapy: the art of turning infectious agents into vehicles of therapeutics, Nature medicine, 7 (2001) 33-40.
[16] L.S. Young, P.F. Searle, D. Onion, V. Mautner, Viral gene therapy strategies: from basic science to clinical application, The Journal of pathology, 208 (2006) 299-318.
[17] R. Waehler, S.J. Russell, D.T. Curiel, Engineering targeted viral vectors for gene therapy, Nature reviews. Genetics, 8 (2007) 573-587.
[18] M. Donkuru, I. Badea, S. Wettig, R. Verrall, M. Elsabahy, M. Foldvari, Advancing nonviral gene delivery: lipid- and surfactant-based nanoparticle design strategies, Nanomedicine (London, England), 5 (2010) 1103-1127.
[19] M. Al-Dosari, X. Gao, Nonviral Gene Delivery: Principle, Limitations, and Recent Progress, AAPS J, 11 (2009) 671-681.

[20] M.A. Mintzer, E.E. Simanek, Nonviral Vectors for Gene Delivery, Chem. Rev., 109 (2008) 259-302.
[21] A. Mountain, Gene therapy: the first decade, Trends in Biotechnology, 18 (2000) 119-128.
[22] J. Douglas, Adenoviral vectors for gene therapy, Mol Biotechnol, 36 (2007) 71-80.
[23] M.A. Kay, State-of-the-art gene-based therapies: the road ahead, Nature reviews. Genetics, 12 (2011) 316-328.
[24] E. Marshall, What to do when clear success comes with an unclear Risk?, Science, 298 (2002) 510-511.
[25] A. Fischer, S. Hacein-Bey-Abina, M. Cavazzana-Calvo, 20 years of gene therapy for SCID, Nature immunology, 11 (2010) 457-460.
[26] S. Lehrman, Virus treatment questioned after gene therapy death, Nature, 401 (1999) 517-518.
[27] N. Somia, I.M. Verma, Gene therapy: trials and tribulations, Nature reviews. Genetics, 1 (2000) 91-99.
[28] S.E. Raper, N. Chirmule, F.S. Lee, N.A. Wivel, A. Bagg, G.-p. Gao, J.M. Wilson, M.L. Batshaw, Fatal systemic inflammatory response syndrome in a ornithine transcarbamylase deficient patient following adenoviral gene transfer, Molecular Genetics and Metabolism, 80 (2003) 148-158.
[29] S.E. Raper, Gene therapy: the good, the bad, and the ugly, Surgery, 137 (2005) 487-492.
[30] J.M. Wilson, Lessons learned from the gene therapy trial for ornithine transcarbamylase deficiency, Molecular Genetics and Metabolism, 96 (2009) 151-157.
[31] M. Donkuru, I. Badea, S. Wettig, R. Verrall, M. Elsabahy, M. Foldvari, Advancing nonviral gene delivery: lipid- and surfactant-based nanoparticle design strategies, Nanomedicine, 5 (2010) 1103-1127.
[32] Y. Seow, M.J. Wood, Biological gene delivery vehicles: beyond viral vectors, Mol Ther, 17 (2009) 767-777.
[33] S.-D. Li, L. Huang, Non-viral is superior to viral gene delivery, J. Control. Release., 123 (2007) 181-183.
[34] B. Dalby, S. Cates, A. Harris, E.C. Ohki, M.L. Tilkins, P.J. Price, V.C. Ciccarone, Advanced transfection with Lipofectamine 2000 reagent: primary neurons, siRNA, and high-throughput applications, Methods (San Diego, Calif.), 33 (2004) 95-103.
[35] L.B. Jacobsen, S.A. Calvin, K.E. Colvin, M. Wright, FuGENE 6 Transfection Reagent: the gentle power, Methods (San Diego, Calif.), 33 (2004) 104-112.
[36] A.S. Arnold, V. Laporte, S. Dumont, A. Appert-Collin, P. Erbacher, G. Coupin, R. Levy, P. Poindron, J.P. Gies, Comparing reagents for efficient transfection of human primary myoblasts: FuGENE 6, Effectene and ExGen 500, Fundamental & clinical pharmacology, 20 (2006) 81-89.
[37] H. Pollard, J.S. Remy, G. Loussouarn, S. Demolombe, J.P. Behr, D. Escande, Polyethylenimine but not cationic lipids promotes transgene delivery to the nucleus in mammalian cells, J Biol Chem, 273 (1998) 7507-7511.
[38] D.J. Glover, H.J. Lipps, D.A. Jans, Towards safe, non-viral therapeutic gene expression in humans, Nature reviews. Genetics, 6 (2005) 299-310.
[39] M. Ruponen, S. Arkko, A. Urtti, M. Reinisalo, V.P. Ranta, Intracellular DNA release and elimination correlate poorly with transgene expression after non-viral transfection, Journal of controlled release : official journal of the Controlled Release Society, 136 (2009) 226-231.
[40] X.-X. Zhang, T.J. McIntosh, M.W. Grinstaff, Functional lipids and lipoplexes for improved gene delivery, Biochimie, 94 (2012) 42-58.

[41] C. Wang, X. Li, S.D. Wettig, I. Badea, M. Foldvari, R.E. Verrall, Investigation of complexes formed by interaction of cationic gemini surfactants with deoxyribonucleic acid, Phys. Chem. Chem. Phys., 9 (2007) 1616-1628.
[42] B.D. Chithrani, A.A. Ghazani, W.C. Chan, Determining the size and shape dependence of gold nanoparticle uptake into mammalian cells, Nano letters, 6 (2006) 662-668.
[43] M. Breunig, U. Lungwitz, R. Liebl, A. Goepferich, Fluorescence resonance energy transfer: evaluation of the intracellular stability of polyplexes, European journal of pharmaceutics and biopharmaceutics : official journal of Arbeitsgemeinschaft fur Pharmazeutische Verfahrenstechnik e.V, 63 (2006) 156-165.
[44] S.D. Li, L. Huang, Gene therapy progress and prospects: non-viral gene therapy by systemic delivery, Gene Ther, 13 (2006) 1313-1319.
[45] M.E. Ferrari, D. Rusalov, J. Enas, C.J. Wheeler, Synergy between cationic lipid and co-lipid determines the macroscopic structure and transfection activity of lipoplexes, Nucleic Acids Research, 30 (2002) 1808-1816.
[46] S. Patil, D. Rhodes, D. Burgess, DNA-based therapeutics and DNA delivery systems: A comprehensive review, AAPS J, 7 (2005) E61-E77.
[47] M. Mintzer, E. Simanek, Nonviral vectors for gene delivery, Chem Rev, 109 (2008) 259 - 302.
[48] A.J. Kirby, P. Camilleri, J.B. Engberts, M.C. Feiters, R.J. Nolte, O. Soderman, M. Bergsma, P.C. Bell, M.L. Fielden, C.L. Garcia Rodriguez, P. Guedat, A. Kremer, C. McGregor, C. Perrin, G. Ronsin, M.C. van Eijk, Gemini surfactants: new synthetic vectors for gene transfection, Angewandte Chemie (International ed. in English), 42 (2003) 1448-1457.
[49] S.Y. Wong, J.M. Pelet, D. Putnam, Polymer systems for gene delivery—Past, present, and future, Prog. Polym. Sci., 32 (2007) 799-837.
[50] H. Yin, R.L. Kanasty, A.A. Eltoukhy, A.J. Vegas, J.R. Dorkin, D.G. Anderson, Non-viral vectors for gene-based therapy, Nature reviews. Genetics, 15 (2014) 541-555.
[51] P.L. Felgner, T.R. Gadek, M. Holm, R. Roman, H.W. Chan, M. Wenz, J.P. Northrop, G.M. Ringold, M. Danielsen, Lipofection: a highly efficient, lipid-mediated DNA-transfection procedure, Proc. Natl. Acad. Sci., 84 (1987) 7413-7417.
[52] K. Kasireddy, S.M. Ali, M.U. Ahmad, S. Choudhury, P.-Y. Chien, S. Sheikh, I. Ahmad, Synthesis of cationic cardiolipin analogues, Bioorganic Chemistry, 33 (2005) 345-362.
[53] R. Srinivas, S. Samanta, A. Chaudhuri, Cationic amphiphiles: promising carriers of genetic materials in gene therapy, Chemical Society reviews, 38 (2009) 3326-3338.
[54] K. Kasireddy, M.U. Ahmad, S.M. Ali, I. Ahmad, Synthesis of novel cationic cardiolipin analogues for the optimal delivery of therapeutic agents, Tetrahedron Letters, 45 (2004) 2743-2746.
[55] C. Bombelli, L. Giansanti, P. Luciani, G. Mancini, Gemini surfactant based carriers in gene and drug delivery, Current medicinal chemistry, 16 (2009) 171-183.
[56] Y.K. Song, F. Liu, S. Chu, D. Liu, Characterization of cationic liposome-mediated gene transfer in vivo by intravenous administration, Human gene therapy, 8 (1997) 1585-1594.
[57] R. Labas, F. Beilvert, B. Barteau, S. David, R. Chevre, B. Pitard, Nature as a source of inspiration for cationic lipid synthesis, Genetica, 138 (2010) 153-168.
[58] R. Marty, C.N. N'soukpoé-Kossi, D. Charbonneau, C.M. Weinert, L. Kreplak, H.-A. Tajmir-Riahi, Structural analysis of DNA complexation with cationic lipids, Nucleic Acids Research, 37 (2009) 849-857.

[59] S. Zhang, Y. Xu, B. Wang, W. Qiao, D. Liu, Z. Li, Cationic compounds used in lipoplexes and polyplexes for gene delivery, Journal of Controlled Release, 100 (2004) 165-180.
[60] C. Dong, Characterization of Gemini Nanoparticle Assembly by Fluorescence Correlation Spectroscopy, in: School of Pharmacy, University of Waterloo, Waterloo, Ontario, Canada, 2013, pp. 134.
[61] C. Pichon, L. Billiet, P. Midoux, Chemical vectors for gene delivery: uptake and intracellular trafficking, Current opinion in biotechnology, 21 (2010) 640-645.
[62] C.M. Wiethoff, C.R. Middaugh, Barriers to nonviral gene delivery, J. Pharm. Sci., 92 (2003) 203-217.
[63] I. Zuhorn, J.F.N. Engberts, D. Hoekstra, Gene delivery by cationic lipid vectors: overcoming cellular barriers, Eur Biophys J, 36 (2007) 349-362.
[64] L.F. Gottfried, D.A. Dean, Extracellular and Intracellular Barriers to Non-Viral Gene Transfer, in: Ming Wei, David Good (Eds), Novel Gene Therapy Approaches, InTech, Croatia, 2013, pp. 75-88.
[65] M. Giacca, Methods for Gene Delivery, in: Gene therapy, Springer Milan, 2010, pp. 47-137.
[66] K. Miyata, N. Nishiyama, K. Kataoka, Rational design of smart supramolecular assemblies for gene delivery: chemical challenges in the creation of artificial viruses, Chem. Soc. Rev., 41 (2012) 2562-2574.
[67] S. Xiang, H. Tong, Q. Shi, J.C. Fernandes, T. Jin, K. Dai, X. Zhang, Uptake mechanisms of non-viral gene delivery, J. Control. Release., 158 (2012) 371-378.
[68] C. Scholz, E. Wagner, Therapeutic plasmid DNA versus siRNA delivery: Common and different tasks for synthetic carriers, J. Control. Release., 161 (2012) 554-565.
[69] F.C. Perez-Martinez, J. Guerra, I. Posadas, V. Cena, Barriers to non-viral vector-mediated gene delivery in the nervous system, Pharm Res, 28 (2011) 1843-1858.
[70] T. Wang, J.R. Upponi, V.P. Torchilin, Design of multifunctional non-viral gene vectors to overcome physiological barriers: dilemmas and strategies, Int J Pharm, 427 (2012) 3-20.
[71] M. Elsabahy, A. Nazarali, M. Foldvari, Non-viral nucleic acid delivery: key challenges and future directions, Curr Drug Deliv, 8 (2011) 235-244.
[72] Y.W. Won, K.S. Lim, Y.H. Kim, Intracellular organelle-targeted non-viral gene delivery systems, Journal of controlled release : official journal of the Controlled Release Society, 152 (2011) 99-109.
[73] A. Pathak, S. Patnaik, K.C. Gupta, Recent trends in non-viral vector-mediated gene delivery, Biotechnology journal, 4 (2009) 1559-1572.
[74] M. Ruponen, P. Honkakoski, S. Rönkkö, J. Pelkonen, M. Tammi, A. Urtti, Extracellular and intracellular barriers in non-viral gene delivery, Journal of Controlled Release, 93 (2003) 213-217.
[75] Z. Rehman, I.S. Zuhorn, D. Hoekstra, How cationic lipids transfer nucleic acids into cells and across cellular membranes: recent advances, Journal of controlled release : official journal of the Controlled Release Society, 166 (2013) 46-56.
[76] I. Lentacker, R.E. Vandenbroucke, B. Lucas, J. Demeester, S.C. De Smedt, N.N. Sanders, New strategies for nucleic acid delivery to conquer cellular and nuclear membranes, Journal of controlled release : official journal of the Controlled Release Society, 132 (2008) 279-288.
[77] M. Sui, W. Liu, Y. Shen, Nuclear drug delivery for cancer chemotherapy, Journal of controlled release : official journal of the Controlled Release Society, 155 (2011) 227-236.

[78] E.V. Batrakova, A.V. Kabanov, Pluronic block copolymers: evolution of drug delivery concept from inert nanocarriers to biological response modifiers, Journal of controlled release : official journal of the Controlled Release Society, 130 (2008) 98-106.
[79] C.H. Sum, Optimized Production and Purification of LCC DNA Minivectors for Applications in Gene Therapy and Vaccine Development, in: School of Pharmacy, University of Waterloo, Waterloo, Ontario, Canada, 2014, pp. 163.
[80] S. Noori, A. Naqvi, W. Ansari, M. Akram, D. Kabir ud, Synthesis and Investigation of Surface Active Properties of Counterion Coupled Gemini Surfactants, J Surfact Deterg, (2013) 1-9.
[81] M.S. Borse, S. Devi, Importance of head group polarity in controlling aggregation properties of cationic gemini surfactants, Advances in colloid and interface science, 123-126 (2006) 387-399.
[82] H. Akbaş, A. Elemenli, M. Boz, Aggregation and Thermodynamic Properties of Some Cationic Gemini Surfactants, J Surfact Deterg, 15 (2012) 33-40.
[83] R. TAMOTO, Chiral Nano/Micro Self-Assemblies of Cationic Surfactants: from dynamic behavior of supramolecular architectures towards hybrid nanomaterials., in: Biophysical Chemistry, University of Bordeaux, Bordeaux, France, 2011, pp. 222.
[84] F. Khan, U.S. Siddiqui, I.A. Khan, D. Kabir ud, Physicochemical study of cationic gemini surfactant butanediyl-1,4-bis(dimethyldodecylammonium bromide) with various counterions in aqueous solution, Colloids and Surfaces A: Physicochemical and Engineering Aspects, 394 (2012) 46-56.
[85] F.M. Menger, J.S. Keiper, Gemini Surfactants, Angew. Chem. Int. Edit., 39 (2000) 1906-1920.
[86] F.M. Menger, C.A. Littau, Gemini-surfactants: synthesis and properties, Journal of the American Chemical Society, 113 (1991) 1451-1452.
[87] Y.-p. Zhu, A. Masuyama, M. Okahara, Preparation and surface active properties of amphipathic compounds with two sulfate groups and two lipophilic alkyl chains, J Am Oil Chem Soc, 67 (1990) 459-463.
[88] K.M. Layn, P.G. Debenedetti, R.K. Prud'homme, A theoretical study of Gemini surfactant phase behavior, The Journal of Chemical Physics, 109 (1998) 5651-5658.
[89] S.K. Hait, S.P. Moulik, Gemini surfactants: A distinct class of self-assembling molecules, Curr. Sci., 82 (2002) 1101-1111.
[90] M. Rosen, D. Tracy, Gemini surfactants, J Surfact Deterg, 1 (1998) 547-554.
[91] M. Borse, V. Sharma, V.K. Aswal, P.S. Goyal, S. Devi, Effect of head group polarity and spacer chain length on the aggregation properties of gemini surfactants in an aquatic environment, Journal of colloid and interface science, 284 (2005) 282-288.
[92] J.R. Akbar, R. Deubry, D.G. Marangoni, S.D. Wettig, Interactions between gemini and nonionic pharmaceutical surfactants, Canadian Journal of Chemistry, 88 (2010) 1262-1270.
[93] J.R. Akbar, Pharmaceutical Applications of Gemini Surfactants, in: School of Pharmacy, University of Waterloo, Waterloo, Ontario, Canada, 2010, pp. 122.
[94] H. Wang, S.D. Wettig, Synthesis and aggregation properties of dissymmetric phytanyl-gemini surfactants for use as improved DNA transfection vectors, Physical chemistry chemical physics : PCCP, 13 (2011) 637-642.
[95] F.M. Menger, C.A. Littau, Gemini-surfactants: synthesis and properties, J. Am. Chem. Soc., 113 (1991) 1451-1452.
[96] P. Renouf, C. Mioskowski, L. Lebeau, D. Hebrault, J.-R. Desmurs, Dimeric surfactants: First synthesis of an asymmetrical gemini compound, Tetrahedron Letters, 39 (1998) 1357-1360.

[97] R. Oda, S. J. Candau, R. Oda, I. Huc, Gemini surfactants, the effect of hydrophobic chain length and dissymmetry, Chemical Communications, (1997) 2105-2106.
[98] J. Akbar, N. Tavakoli, D. Gerrard Marangoni, S.D. Wettig, Mixed aggregate formation in gemini surfactant/1,2-dialkyl-sn-glycero-3-phosphoethanolamine systems, Journal of colloid and interface science, 377 (2012) 237-243.
[99] S.D. Wettig, C. Wang, R.E. Verrall, M. Foldvari, Thermodynamic and aggregation properties of aza- and imino-substituted gemini surfactants designed for gene delivery, Physical Chemistry Chemical Physics, 9 (2007) 871-877.
[100] X. Huang, Y. Han, Y. Wang, M. Cao, Y. Wang, Aggregation properties of cationic gemini surfactants with dihydroxyethylamino headgroups in aqueous solution, Colloids and Surfaces A: Physicochemical and Engineering Aspects, 325 (2008) 26-32.
[101] A.K. Tiwari, Sonu, S.K. Saha, Aggregation properties and thermodynamics of micellization of gemini surfactants with diethyl ether spacer in water and water–organic solvent mixed media, The Journal of Chemical Thermodynamics, 70 (2014) 24-32.
[102] C. Wang, S.D. Wettig, M. Foldvari, R.E. Verrall, Synthesis, Characterization, and Use of Asymmetric Pyrenyl-Gemini Surfactants as Emissive Components in DNA−Lipoplex Systems, Langmuir : the ACS journal of surfaces and colloids, 23 (2007) 8995-9001.
[103] M. Donkuru, Non-viral Gene Delivery with pH-sensitive Gemini Nanoparticles: Synthesis of Gemini Surfactant Building Blocks, Characterization and In-Vitro Screening of Transfection Efficiency and Toxicity in: Pharmacy and Nutrition, University of Saskatchewan, Saskatoon, Saskatchewan, Canada, 2008, pp. 205.
[104] M. Hajy Alimohammadi, S. Javadian, H. Gharibi, A.r. Tehrani-Bagha, M.R. Alavijeh, K. Kakaei, Aggregation behavior and intermicellar interactions of cationic Gemini surfactants: Effects of alkyl chain, spacer lengths and temperature, The Journal of Chemical Thermodynamics, 44 (2012) 107-115.
[105] X. Pei, Y. You, J. Zhao, Y. Deng, E. Li, Z. Li, Adsorption and aggregation of 2-hydroxyl-propanediyl-alpha,omega-bis(dimethyldodecyl ammonium bromide) in aqueous solution: effect of intermolecular hydrogen-bonding, Journal of colloid and interface science, 351 (2010) 457-465.
[106] I. Badea, R. Verrall, M. Baca-Estrada, S. Tikoo, A. Rosenberg, P. Kumar, M. Foldvari, In vivo cutaneous interferon-gamma gene delivery using novel dicationic (gemini) surfactant-plasmid complexes, J Gene Med, 7 (2005) 1200-1214.
[107] L. Karlsson, M.C.P. Van Eijk, O. Söderman, Compaction of DNA by gemini surfactants: Effects of surfactant architecture, Journal of colloid and interface science, 252 (2002) 290-296.
[108] D. Myers, Surfactant Science and Technology, 3rd ed., John Wiley & Sons, Inc. , Hoboken, New Jersey, 2006.
[109] Z. Raoul, Gemini (Dimeric) Surfactants in Water, in: Gemini Surfactants, CRC Press, 2003.
[110] C. Wang, X. Li, S.D. Wettig, I. Badea, M. Foldvari, R.E. Verrall, Investigation of complexes formed by interaction of cationic gemini surfactants with deoxyribonucleic acid, Physical chemistry chemical physics : PCCP, 9 (2007) 1616-1628.
[111] K.K. Ewert, A. Ahmad, H.M. Evans, C.R. Safinya, Cationic lipid-DNA complexes for non-viral gene therapy: relating supramolecular structures to cellular pathways, Expert opinion on biological therapy, 5 (2005) 33-53.

[112] A.J. Lin, N.L. Slack, A. Ahmad, C.X. George, C.E. Samuel, C.R. Safinya, Three-Dimensional Imaging of Lipid Gene-Carriers: Membrane Charge Density Controls Universal Transfection Behavior in Lamellar Cationic Liposome-DNA Complexes, Biophys. J., 84 (2003) 3307-3316.
[113] I. Badea, Gemini Cationic Surfactant-Based Delivery Systems for Non-Invasive Cutaneous Gene Therapy, in: College of Pharmacy and Nutrition, University of Saskatchewan, Saskatoon, Saskatchewan, Canada, 2006, pp. 237.
[114] T. Alejo, M.D. Merchán, M.M. Velázquez, Specific ion effects on the properties of cationic Gemini surfactant monolayers, Thin Solid Films, 519 (2011) 5689-5695.
[115] D. Yu, X. Huang, M. Deng, Y. Lin, L. Jiang, J. Huang, Y. Wang, Effects of inorganic and organic salts on aggregation behavior of cationic gemini surfactants, The journal of physical chemistry. B, 114 (2010) 14955-14964.
[116] N. Jiang, P. Li, Y. Wang, J. Wang, H. Yan, R.K. Thomas, Micellization of Cationic Gemini Surfactants with Various Counterions and Their Interaction with DNA in Aqueous Solution, J. Phys. Chem. B, 108 (2004) 15385-15391.
[117] S. Manet, Y. Karpichev, D. Dedovets, R. Oda, Effect of Hofmeister and alkylcarboxylate anionic counterions on the Krafft temperature and melting temperature of cationic gemini surfactants, Langmuir : the ACS journal of surfaces and colloids, 29 (2013) 3518-3526.
[118] C. Aimé, S. Manet, T. Satoh, H. Ihara, K.-Y. Park, F. Godde, R. Oda, Self-Assembly of Nucleoamphiphiles: Investigating Nucleosides Effect and the Mechanism of Micrometric Helix Formation, Langmuir : the ACS journal of surfaces and colloids, 23 (2007) 12875-12885.
[119] A. Brizard, C. Aimé, T. Labrot, I. Huc, D. Berthier, F. Artzner, B. Desbat, R. Oda, Counterion, Temperature, and Time Modulation of Nanometric Chiral Ribbons from Gemini-Tartrate Amphiphiles, Journal of the American Chemical Society, 129 (2007) 3754-3762.
[120] A. Brizard, R.K. Ahmad, R. Oda, Control of nano-micrometric twist and helical ribbon formation with gemini-oligoalanine via interpeptidic [small beta]-sheet structure formation, Chemical Communications, (2007) 2275-2277.
[121] Y. Wang, B. Desbat, S. Manet, C. Aime, T. Labrot, R. Oda, Aggregation behaviors of gemini nucleotide at the air-water interface and in solutions induced by adenine-uracil interaction, Journal of colloid and interface science, 283 (2005) 555-564.
[122] W. Kunz, P. Lo Nostro, B.W. Ninham, The present state of affairs with Hofmeister effects, Current Opinion in Colloid & Interface Science, 9 (2004) 1-18.
[123] S. Manet, Y. Karpichev, D. Bassani, R. Kiagus-Ahmad, R. Oda, Counteranion effect on micellization of cationic gemini surfactants 14-2-14: Hofmeister and other counterions, Langmuir : the ACS journal of surfaces and colloids, 26 (2010) 10645-10656.
[124] R. Oda, I. Huc, J.-C. Homo, B. Heinrich, M. Schmutz, S. Candau, Elongated Aggregates Formed by Cationic Gemini Surfactants, Langmuir : the ACS journal of surfaces and colloids, 15 (1999) 2384-2390.
[125] Y. Kim, T. Kim, H. Chung, I. Kwon, S. Jeong, Counterion effects on transfection activity of cationic lipid emulsion, Biotechnol. Bioprocess Eng., 6 (2001) 279-283.
[126] A.M. Aberle, M.J. Bennett, R.W. Malone, M.H. Nantz, The counterion influence on cationic lipid-mediated transfection of plasmid DNA, Biochimica et Biophysica Acta (BBA) - Lipids and Lipid Metabolism, 1299 (1996) 281-283.
[127] S. Franceschi, O. Bordeau, C. Millerioux, E. Perez, P. Vicendo, I. Rico-Lattes, A. Moisand, Highly Compacted DNA-Polymer Complexes Obtained via New Polynorbornene Polycationic

Latexes with Lactobionate Counterion, Langmuir : the ACS journal of surfaces and colloids, 18 (2002) 1743-1747.
[128] T. Noël, S. Franceschi, E. Perez, P. Vicendo, I. Rico-Lattes, High Compacted DNA−Polymer Complexes via New Polynorbornene Polycationic Latexes with Acetate Counterion, Langmuir : the ACS journal of surfaces and colloids, 16 (2000) 8980-8983.
[129] E. Serres, P. Vicendo, E. Perez, T. Noel, I. Rico-Lattes, DNA Condensation and Transfection of Cells in Culture by a New Polynorbornane Polycationic Polymer, Langmuir : the ACS journal of surfaces and colloids, 15 (1999) 6956-6960.
[130] S. Asgatay, S. Franceschi-Messant, E. Perez, P. Vicendo, I. Rico-Lattes, E. Phez, M.P. Rols, Polynorbornene polycationic polymers as gene transfer agents: Influence of the counterion for in vitro transfection, International Journal of Pharmaceutics, 285 (2004) 121-133.
[131] R. Oda, I. Huc, S.J. Candau, Gemini Surfactants as New, Low Molecular Weight Gelators of Organic Solvents and Water, Angewandte Chemie International Edition, 37 (1998) 2689-2691.
[132] N. Nafissi, R. Slavcev, Construction and characterization of an in-vivo linear covalently closed DNA vector production system, Microbial cell factories, 11 (2012) 154.
[133] F.M. Menger, J.S. Keiper, Gemini Surfactants, Angewandte Chemie (International ed. in English), 39 (2000) 1906-1920.
[134] N. Jiang, P. Li, Y. Wang, J. Wang, H. Yan, R.K. Thomas, Micellization of Cationic Gemini Surfactants with Various Counterions and Their Interaction with DNA in Aqueous Solution, The Journal of Physical Chemistry B, 108 (2004) 15385-15391.
[135] J. Aslam, U. Siddiqui, W. Ansari, D. Kabir ud, Micellization Studies of Dicationic Gemini Surfactants (m-2-m Type) in the Presence of Various Counter- and Co-Ions, J Surfact Deterg, 16 (2013) 693-707.
[136] A. Brizard, D. Berthier, C. Aime, T. Buffeteau, D. Cavagnat, L. Ducasse, I. Huc, R. Oda, Molecular and supramolecular chirality in gemini-tartrate amphiphiles studied by electronic and vibrational circular dichroisms, Chirality, 21 Suppl 1 (2009) E153-162.
[137] C. Aime, S. Manet, T. Satoh, H. Ihara, K.Y. Park, F. Godde, R. Oda, Self-assembly of nucleoamphiphiles: investigating nucleosides effect and the mechanism of micrometric helix formation, Langmuir : the ACS journal of surfaces and colloids, 23 (2007) 12875-12885.
[138] E. Fisicaro, C. Compari, F. Bacciottini, N. Barbero, G. Viscardi, P. Quagliotto, Is the counterion responsible for the unusual thermodynamic behaviour of the aqueous solutions of gemini bispyridinium surfactants?, Colloids and Surfaces A: Physicochemical and Engineering Aspects, 443 (2014) 249-254.
[139] C. Huh, S.G. Mason, A rigorous theory of ring tensiometry, Colloid Polym Sci, 253 (1975) 566-580.
[140] D.N. Furlong, P.A. Freeman, I.M. Metcalfe, L.R. White, Wall effects in du Nouy ring tensiometry. Theory and experiment, Journal of the Chemical Society, Faraday Transactions 1: Physical Chemistry in Condensed Phases, 79 (1983) 1701-1719.
[141] P.Y. Lee, J. Costumbrado, C.Y. Hsu, Y.H. Kim, Agarose gel electrophoresis for the separation of DNA fragments, Journal of visualized experiments : JoVE, (2012).
[142] P.R.R.a.N. Raju, Gel-Electrophoresis and Its Applications (Chapter-2), in: S. Magdeldin (Ed.) Gel Electrophoresis – Principles and Basics, In Tech, Croatia, 2012.
[143] S. Wettig, I. Badea, M. Donkuru, R. Verrall, M. Foldvari, Structural and transfection properties of amine-substituted gemini surfactant-based nanoparticles, J Gene Med, 9 (2007) 649 - 658.

[144] A. Laouini, C. Jaafar-Maalej, I. Limayem-Blouza, S. Sfar, C. Charcosset, H. Fessi, Preparation, Characterization and Applications of Liposomes: State of the Art, Journal of Colloid Science and Biotechnology, 1 (2012) 147-168.
[145] H. Wang, T. Kaur, N. Tavakoli, J. Joseph, S. Wettig, Transfection and structural properties of phytanyl substituted gemini surfactant-based vectors for gene delivery, Phys. Chem. Chem. Phys., 15 (2013) 20510-20516.
[146] A.L. Barran-Berdon, S.K. Misra, S. Datta, M. Munoz-Ubeda, P. Kondaiah, E. Junquera, S. Bhattacharya, E. Aicart, Cationic gemini lipids containing polyoxyethylene spacers as improved transfecting agents of plasmid DNA in cancer cells, Journal of Materials Chemistry B, 2 (2014) 4640-4652.
[147] R.N.B. Robert T. Morrison, Organic Chemistry, Sixth Edition, Prentice-Hall Inc., USA, 1992.
[148] H.-P. Lin, C.-P. Kao, C.-Y. Mou, S.-B. Liu, Counterion Effect in Acid Synthesis of Mesoporous Silica Materials, The Journal of Physical Chemistry B, 104 (2000) 7885-7894.
[149] L. Gaillon, J. Lelièvre, R. Gaboriaud, Counterion Effects in Aqueous Solutions of Cationic Surfactants: Electromotive Force Measurements and Thermodynamic Model, Journal of colloid and interface science, 213 (1999) 287-297.
[150] M.M. Knock, C.D. Bain, Effect of Counterion on Monolayers of Hexadecyltrimethylammonium Halides at the Air−Water Interface, Langmuir : the ACS journal of surfaces and colloids, 16 (2000) 2857-2865.
[151] L. Abezgauz, K. Kuperkar, P.A. Hassan, O. Ramon, P. Bahadur, D. Danino, Effect of Hofmeister anions on micellization and micellar growth of the surfactant cetylpyridinium chloride, Journal of colloid and interface science, 342 (2010) 83-92.
[152] L. Wattebled, A. Laschewsky, Effects of Organic Salt Additives on the Behavior of Dimeric ("Gemini") Surfactants in Aqueous Solution, Langmuir : the ACS journal of surfaces and colloids, 23 (2007) 10044-10052.
[153] Y. He, Y. Shang, S. Shao, H. Liu, Y. Hu, Micellization of cationic gemini surfactant and its interaction with DNA in dilute brine, J. Colloid Interface Sci., 358 (2011) 513-520.
[154] R. Zana, H. Lévy, D. Danino, Y. Talmon, K. Kwetkat, Mixed Micellization of Cetyltrimethylammonium Bromide and an Anionic Dimeric (Gemini) Surfactant in Aqueous Solution, Langmuir : the ACS journal of surfaces and colloids, 13 (1997) 402-408.
[155] K. Tsubone, Y. Arakawa, M.J. Rosen, Structural effects on surface and micellar properties of alkanediyl-α,ω-bis(sodium N-acyl-β-alaninate) gemini surfactants, Journal of colloid and interface science, 262 (2003) 516-524.
[156] F. Li, M.J. Rosen, S.B. Sulthana, Surface Properties of Cationic Gemini Surfactants and Their Interaction with Alkylglucoside or -maltoside Surfactants, Langmuir : the ACS journal of surfaces and colloids, 17 (2001) 1037-1042.
[157] T. Lu, Y. Lan, C. Liu, J. Huang, Y. Wang, Surface properties, aggregation behavior and micellization thermodynamics of a class of gemini surfactants with ethyl ammonium headgroups, Journal of colloid and interface science, 377 (2012) 222-230.
[158] M. Akram, S. Yousuf, T. Sarwar, D. Kabir ud, Micellization and interfacial behavior of 16-E2-16 in presence of inorganic and organic salt counterions, Colloids and Surfaces A: Physicochemical and Engineering Aspects, 441 (2014) 281-290.

[159] S. Kolay, K.K. Ghosh, P. Quagliotto, Micellization behavior of [C16-12-C16], 2Br− gemini surfactant in binary aqueous-solvent mixtures, Colloids and Surfaces A: Physicochemical and Engineering Aspects, 348 (2009) 234-239.
[160] P. Ajmal Koya, D. Kabir ud, K. Ismail, Micellization and Thermodynamic Parameters of Butanediyl-1,4-bis(tetradecyldimethylammonium Bromide) Gemini Surfactant at Different Temperatures: Effect of the Addition of 2-Methoxyethanol, J Solution Chem, 41 (2012) 1271-1281.
[161] R. Nagarajan, C.-C. Wang, Theory of Surfactant Aggregation in Water/Ethylene Glycol Mixed Solvents, Langmuir : the ACS journal of surfaces and colloids, 16 (2000) 5242-5251.
[162] X. Wang, J. Wang, Y. Wang, H. Yan, Salt effect on the complex formation between cationic gemini surfactant and anionic polyelectrolyte in aqueous solution, Langmuir : the ACS journal of surfaces and colloids, 20 (2004) 9014-9018.
[163] S.D. Wettig, R.E. Verrall, Thermodynamic Studies of Aqueous m–s–m Gemini Surfactant Systems, Journal of colloid and interface science, 235 (2001) 310-316.
[164] K.D. Collins, M.W. Washabaugh, The Hofmeister effect and the behaviour of water at interfaces, Quarterly reviews of biophysics, 18 (1985) 323-422.
[165] N. Vlachy, B. Jagoda-Cwiklik, R. Vácha, D. Touraud, P. Jungwirth, W. Kunz, Hofmeister series and specific interactions of charged headgroups with aqueous ions, Advances in colloid and interface science, 146 (2009) 42-47.
[166] Y. Zhang, P.S. Cremer, Interactions between macromolecules and ions: the Hofmeister series, Current Opinion in Chemical Biology, 10 (2006) 658-663.
[167] A. Renoncourt, N. Vlachy, P. Bauduin, M. Drechsler, D. Touraud, J.M. Verbavatz, M. Dubois, W. Kunz, B.W. Ninham, Specific Alkali Cation Effects in the Transition from Micelles to Vesicles through Salt Addition, Langmuir : the ACS journal of surfaces and colloids, 23 (2007) 2376-2381.
[168] B. Thalody, G.G. Warr, The selective binding of anions to gemini and trimeric surfactants at air/solution interfaces, Aust. J. Chem., 57 (2004) 193-196.
[169] L. Zhou, X. Jiang, Y. Li, Z. Chen, X. Hu, Synthesis and Properties of a Novel Class of Gemini Pyridinium Surfactants, Langmuir : the ACS journal of surfaces and colloids, 23 (2007) 11404-11408.
[170] Q. Zhang, Z. Gao, F. Xu, S. Tai, X. Liu, S. Mo, F. Niu, Surface tension and aggregation properties of novel cationic gemini surfactants with diethylammonium headgroups and a diamido spacer, Langmuir : the ACS journal of surfaces and colloids, 28 (2012) 11979-11987.
[171] A. Laschewsky, L. Wattebled, M. Arotçaréna, J.-L. Habib-Jiwan, R.H. Rakotoaly, Synthesis and Properties of Cationic Oligomeric Surfactants, Langmuir : the ACS journal of surfaces and colloids, 21 (2005) 7170-7179.
[172] S.D. Wettig, X. Li, R.E. Verrall, Thermodynamic and Aggregation Properties of Gemini Surfactants with Ethoxylated Spacers in Aqueous Solution, Langmuir : the ACS journal of surfaces and colloids, 19 (2003) 3666-3670.
[173] K.M. Jenkins, S.D. Wettig, R.E. Verrall, Studies of the Aggregation Behavior of Cyclic Gemini Surfactants, Journal of colloid and interface science, 247 (2002) 456-462.
[174] S.D. Wettig, P. Nowak, R.E. Verrall, Thermodynamic and Aggregation Properties of Gemini Surfactants with Hydroxyl Substituted Spacers in Aqueous Solution, Langmuir : the ACS journal of surfaces and colloids, 18 (2002) 5354-5359.
[175] R. Zana, Critical Micellization Concentration of Surfactants in Aqueous Solution and Free Energy of Micellization, Langmuir : the ACS journal of surfaces and colloids, 12 (1996) 1208-1211.

[176] P. Carpena, J. Aguiar, P. Bernaola-Galván, C. Carnero Ruiz, Problems Associated with the Treatment of Conductivity−Concentration Data in Surfactant Solutions: Simulations and Experiments, Langmuir : the ACS journal of surfaces and colloids, 18 (2002) 6054-6058.
[177] D. Tikariha, B. Kumar, N. Singh, K. Ghosh, P. Quagliotto, Micellization Behavior of Cationic Gemini Surfactants in Aqueous-Ethylene Glycol Solution, J Surfact Deterg, 14 (2011) 555-562.
[178] Q. Zhang, Z. Gao, F. Xu, S. Tai, Effect of hydrocarbon structure of the headgroup on the thermodynamic properties of micellization of cationic gemini surfactants: An electrical conductivity study, Journal of colloid and interface science, 371 (2012) 73-81.
[179] R. Zana, M. In, H. Lévy, G. Duportail, Alkanediyl-α,ω-bis(dimethylalkylammonium bromide). 7. Fluorescence Probing Studies of Micelle Micropolarity and Microviscosity, Langmuir : the ACS journal of surfaces and colloids, 13 (1997) 5552-5557.
[180] X. Li, S.D. Wettig, C. Wang, M. Foldvari, R.E. Verrall, Synthesis and solution properties of gemini surfactants containing oleyl chains, Physical Chemistry Chemical Physics, 7 (2005) 3172-3178.
[181] B.L. Bales, M. Benrraou, R. Zana, Krafft Temperature and Micelle Ionization of Aqueous Solutions of Cesium Dodecyl Sulfate, The Journal of Physical Chemistry B, 106 (2002) 9033-9035.
[182] J. Roy, M.N. Islam, G. Aktaruzzaman, The Effect of NaCl on the Krafft Temperature and Related Behavior of Cetyltrimethylammonium Bromide in Aqueous Solution, J Surfact Deterg, 17 (2014) 231-242.
[183] C. Vautier-Giongo, B.L. Bales, Estimate of the Ionization Degree of Ionic Micelles Based on Krafft Temperature Measurements, The Journal of Physical Chemistry B, 107 (2003) 5398-5403.
[184] Z. Chu, Y. Feng, Empirical Correlations between Krafft Temperature and Tail Length for Amidosulfobetaine Surfactants in the Presence of Inorganic Salt, Langmuir : the ACS journal of surfaces and colloids, 28 (2011) 1175-1181.
[185] H. Eagle, The effect of environmental pH on the growth of normal and malignant cells, Journal of Cellular Physiology, 82 (1973) 1-8.
[186] T. Sato, T. Ishii, Y. Okahata, In vitro gene delivery mediated by chitosan. effect of pH, serum, and molecular mass of chitosan on the transfection efficiency, Biomaterials, 22 (2001) 2075-2080.
[187] A. Colomer, A. Pinazo, M.T. García, M. Mitjans, M.P. Vinardell, M.R. Infante, V. Martínez, L. Pérez, pH-Sensitive Surfactants from Lysine: Assessment of Their Cytotoxicity and Environmental Behavior, Langmuir : the ACS journal of surfaces and colloids, 28 (2012) 5900-5912.
[188] M. Munoz-Ubeda, S.K. Misra, A.L. Barran-Berdon, C. Aicart-Ramos, M.B. Sierra, J. Biswas, P. Kondaiah, E. Junquera, S. Bhattacharya, E. Aicart, Why is less cationic lipid required to prepare lipoplexes from plasmid DNA than linear DNA in gene therapy?, J Am Chem Soc, 133 (2011) 18014-18017.
[189] M. Muñoz-Úbeda, S.K. Misra, A.L. Barrán-Berdón, S. Datta, C. Aicart-Ramos, P. Castro-Hartmann, P. Kondaiah, E. Junquera, S. Bhattacharya, E. Aicart, How Does the Spacer Length of Cationic Gemini Lipids Influence the Lipoplex Formation with Plasmid DNA? Physicochemical and Biochemical Characterizations and their Relevance in Gene Therapy, Biomacromolecules, 13 (2012) 3926-3937.
[190] J. Akbar, N. Tavakoli, D. Gerrard Marangoni, S.D. Wettig, Mixed aggregate formation in gemini surfactant/1,2-dialkyl-sn-glycero-3-phosphoethanolamine systems, J. Colloid Interface Sci., 377 (2012) 237-243.

[191] J. Panyam, V. Labhasetwar, Biodegradable nanoparticles for drug and gene delivery to cells and tissue, Advanced Drug Delivery Reviews, 64, Supplement (2012) 61-71.
[192] J. Rejman, V. Oberle, I.S. Zuhorn, D. Hoekstra, Size-dependent internalization of particles via the pathways of clathrin- and caveolae-mediated endocytosis, Biochem J, 377 (2004) 159-169.
[193] S. Honary, F. Zahir, Effect of Zeta Potential on the Properties of Nano-Drug Delivery Systems - A Review (Part 1), Trop. J. Pharm. Res., 12 (2013) 255-264.
[194] S. Patil, A. Sandberg, E. Heckert, W. Self, S. Seal, Protein adsorption and cellular uptake of cerium oxide nanoparticles as a function of zeta potential, Biomaterials, 28 (2007) 4600-4607.
[195] A. Eisenthal, K. Eytan, E. Brazowski, G. Gitstein, R. Greenberg, Y. Skornick, Effects of 5-FU on DNA synthesis and cytotoxicity of human lymphocytes induced by IL-2, TGF-beta3 and PGE2, Anticancer research, 29 (2009) 3925-3930.
[196] T. Shirasaka, Y. Shimamato, H. Ohshimo, M. Yamaguchi, T. Kato, K. Yonekura, M. Fukushima, Development of a novel form of an oral 5-fluorouracil derivative (S-1) directed to the potentiation of the tumor selective cytotoxicity of 5-fluorouracil by two biochemical modulators, Anti-cancer drugs, 7 (1996) 548-557.
[197] S. Prabha, W.Z. Zhou, J. Panyam, V. Labhasetwar, Size-dependency of nanoparticle-mediated gene transfection: studies with fractionated nanoparticles, Int J Pharm, 244 (2002) 105-115.
[198] M. Desai, V. Labhasetwar, E. Walter, R. Levy, G. Amidon, The Mechanism of Uptake of Biodegradable Microparticles in Caco-2 Cells Is Size Dependent, Pharm Res, 14 (1997) 1568-1573.
[199] M. Desai, V. Labhasetwar, G. Amidon, R. Levy, Gastrointestinal Uptake of Biodegradable Microparticles: Effect of Particle Size, Pharm Res, 13 (1996) 1838-1845.
[200] M. Foldvari, Wettig, S., Badea, I., Verrall, R., Bagonluri, M., Dicationic gemini surfactant gene delivery complexes contain cubic-lamellar mixed polymorphic phase., NSTI-Nanotech, 2 (2006) 400-403.
[201] M. Foldvari, I. Badea, S. Wettig, R. Verrall, M. Bagonluri, Structural characterization of novel gemini non-viral DNA delivery systems for cutaneous gene therapy, J Exp Nanosci, 1 (2006) 165 - 176.
[202] Q. Wang, P. Liu, Y. Sun, H. Wu, X. Li, Y. Duan, Z. Zhang, Pluronic-poly[alpha-(4-aminobutyl)-1-glycolic acid] polymeric micelle-like nanoparticles as carrier for drug delivery, Journal of nanoscience and nanotechnology, 14 (2014) 4843-4850.
[203] H. Li, C. Yu, R. Chen, J. Li, J. Li, Novel ionic liquid-type Gemini surfactants: Synthesis, surface property and antimicrobial activity, Colloids and Surfaces A: Physicochemical and Engineering Aspects, 395 (2012) 116-124.
[204] A.R. Tehrani-Bagha, K. Holmberg, Cationic Ester-Containing Gemini Surfactants: Physical−Chemical Properties, Langmuir : the ACS journal of surfaces and colloids, 26 (2010) 9276-9282.

Appendix

A-1.1: Atomic details and ^{1}H NMR spectral analysis of 1-halohexadecane:

The structure of the 1-halohexadecane (Cetyl halide) is as following –

$$CH_3 - CH_2 - (CH_2)_{12} - CH_2 - {}^+CH_2 - X^-$$

Atomic details:

Total Carbon, (C) = 16

Total Hydrogen, (H) = 33

Total Halide, (X^-) = 1 **(X^- = Bromide or Chloride)**

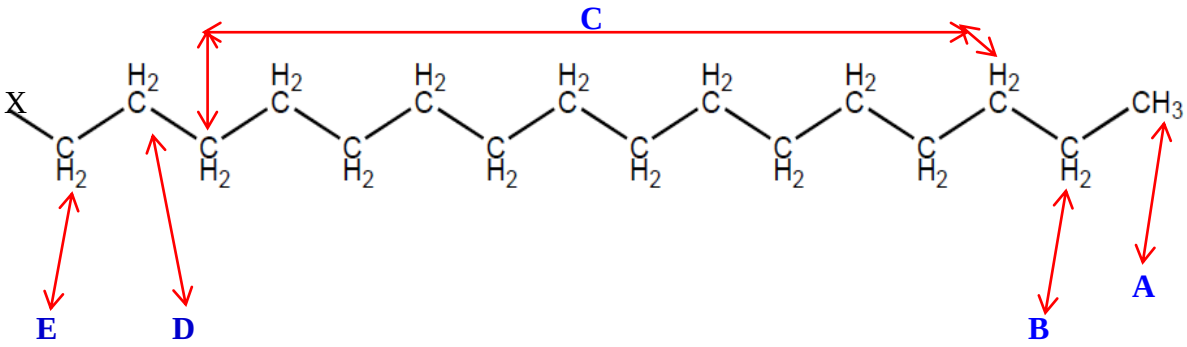

Figure-A-1.1: Assignment of protons in the 1-Halohexadecane structure used in the interpretation of ^{1}H NMR spectra.

Category / Name of the Proton	Total number of proton for that category
A	3
B	2
C	24
D	2
E	2
TOTAL for all category	33 Protons

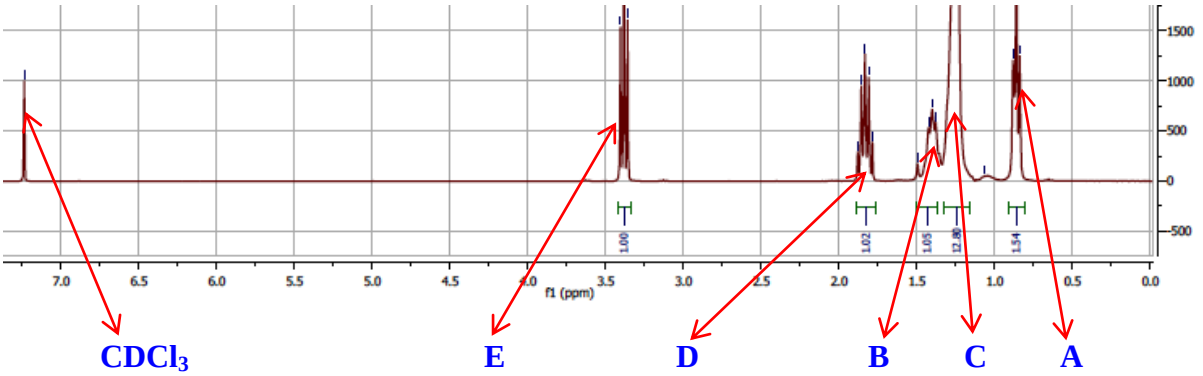

Figure-A-1.2: Identification of ^{1}H NMR peaks of protons of 1-halohexadecane (in $CDCl_3$)

A-1.3: Atomic details and ^{1}H NMR spectral analysis of TMEDA:

The structure of the *N,N,N′,N′*-tetra–methyl–ethylene–1,2-di-amine (TMEDA) is as following –

$$(CH_3)_2N - CH_2 - CH_2 - N(CH_3)_2$$

Atomic details:

Total Carbon, (C) = 6
Total Hydrogen, (H) = 16
Total Nitrogen, (N) = 2

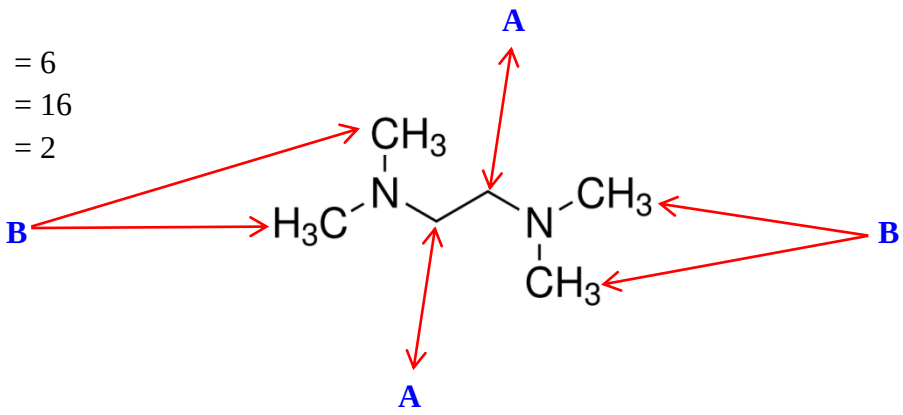

Figure-A-1.3: Assignment of protons in the *N,N,N′,N′*-Tetramethylethylene–1,2-diamine (TMEDA) structure used in the interpretation of ^{1}H NMR spectra.

Category / Name of the Proton	Total number of proton for that category
A	4
B	12
TOTAL for all category	16 Protons

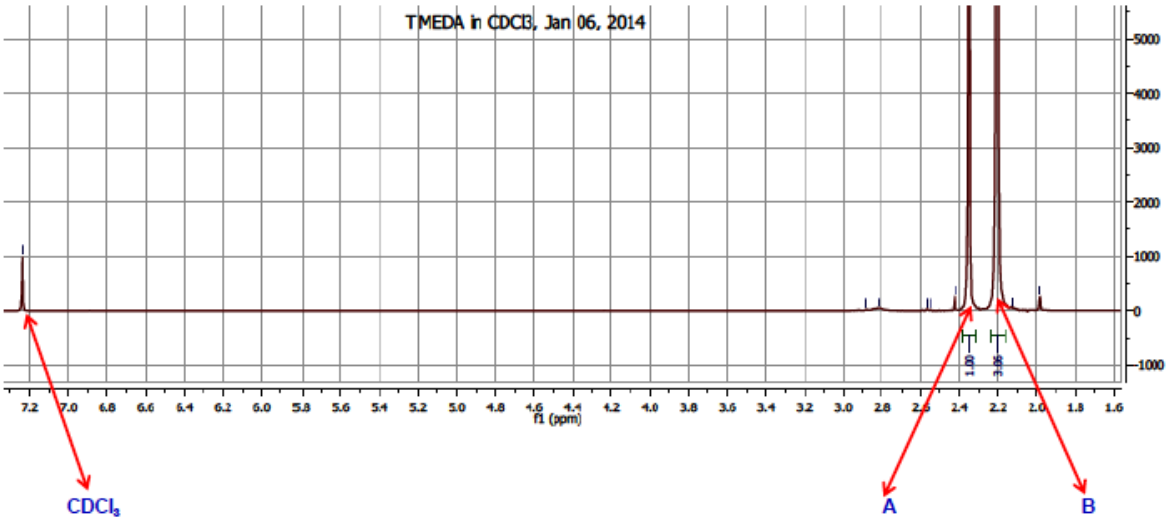

Figure-A-1.4: Identification of ^{1}H NMR peaks of protons of TMEDA (in $CDCl_3$)

A-1.3: Atomic details and ^{1}H NMR spectral analysis of Tartaric Acid:

The structure of the Tartaric Acid (MW = 150.01; Molecular formula: $C_4H_6O_6$) is –

Atomic details:

Total Carbon, (C) = 4
Total Hydrogen, (H) = 6
Total oxygen, (O) = 6

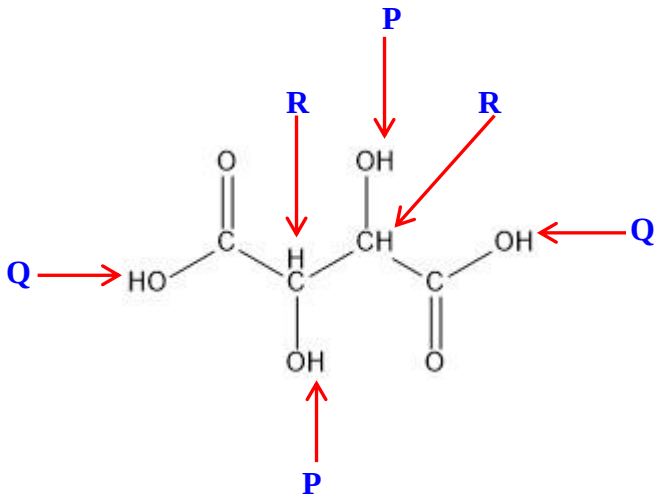

Figure-A-1.5: Assignment of protons in the Tartaric Acid structure used in the interpretation of ^{1}H NMR spectra.

Category / Name of the Proton	Total number of proton for that category
P*	2
Q*	**2 (*^{1}H NMR peaks will be missing in gemini-tartrate*)
R	2
TOTAL for all category	6 Protons

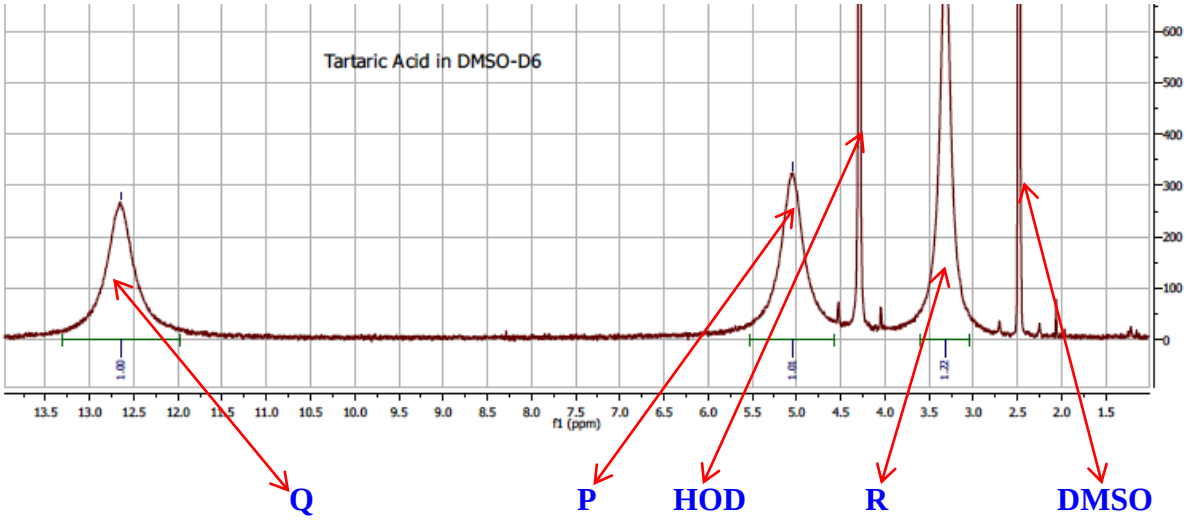

Figure-A-1.6: Identification of ^{1}H NMR peaks of protons of Tartaric acid (in DMSO-D_6)

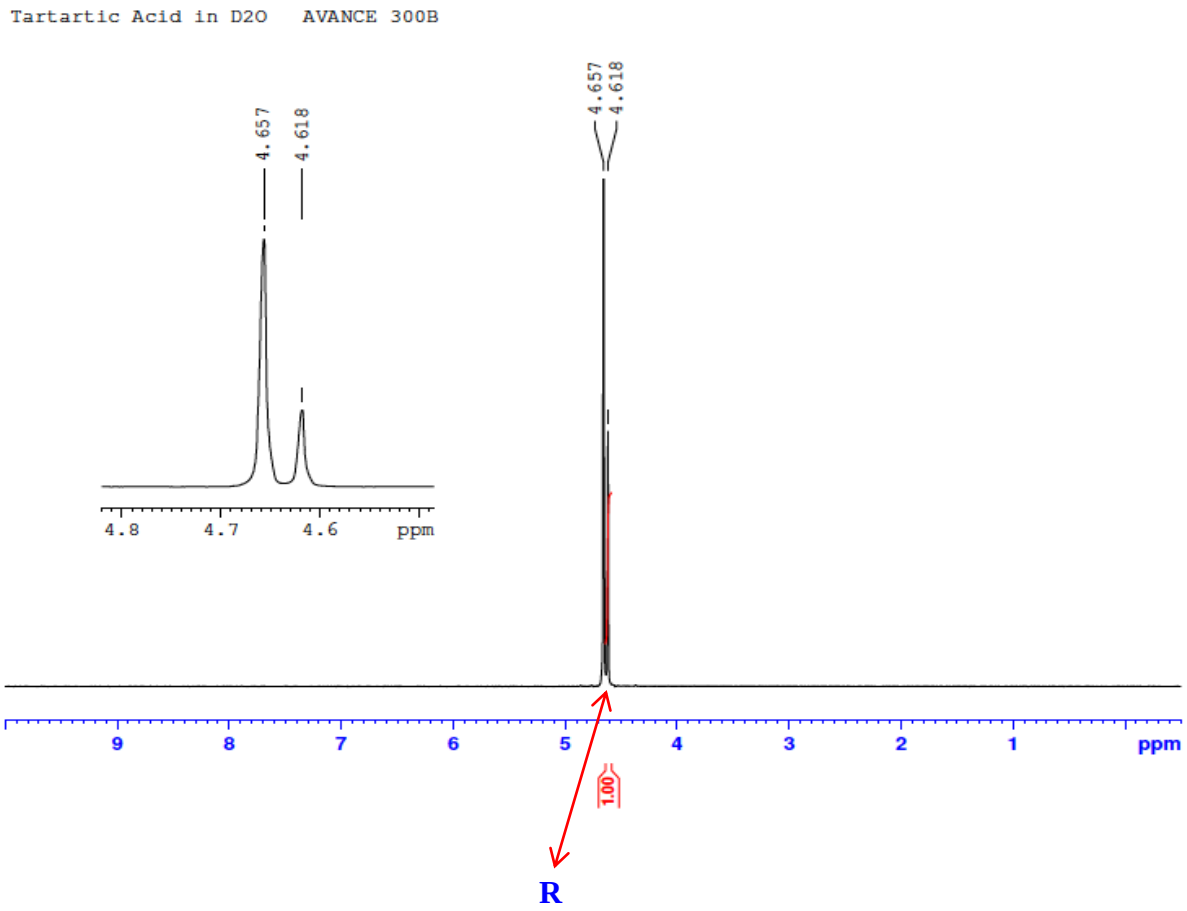

Figure-A-1.7: Identification of ^{1}H NMR peaks of protons of Tartaric acid (in D_2O).

N.B.:

***** All the '**P'** protons and '**Q'** protons were displaced by deuterium when dissolved in D_2O. Thus no peak was seen in the spectra obtained from the solution of Tartaric acid in D_2O. Same applies to the spectra of 16 – 2 – 16.Tartrate solution in D_2O.

**During synthesis of the 16 – 2 – 16.Tartrate molecule, both of the protons from the two carboxylate group was ionized and gets attached with each of the quaternary ammonium head group. Thus the ^{1}H NMR peak represents no proton for both of the carboxylate groups (ionized form) for this gemini solution in D_2O.

A-1.4: Atomic details and ^{1}H NMR spectral analysis of Malic Acid:

The structure of the Malic Acid (MW = 134.09; Molecular formula: $C_4H_6O_5$) is –

Atomic details:

Total Carbon, (C) = 4
Total Hydrogen, (H) = 6
Total oxygen, (O) = 5

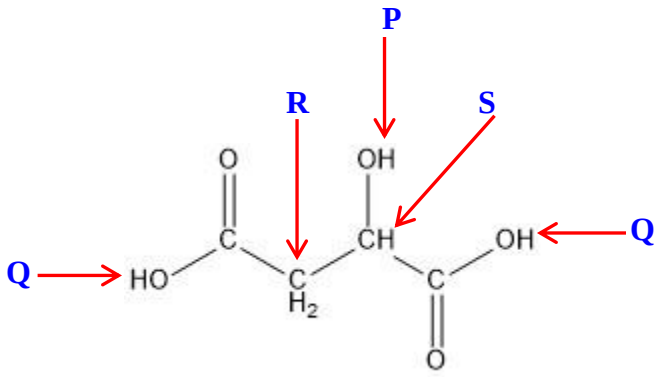

Figure-A-1.8: Assignment of protons in the Malic Acid structure used in the interpretation of ^{1}H NMR spectra.

Category / Name of the Proton	Total number of proton for that category
P*	1
Q*	**2 (*^{1}H NMR peaks will be missing in gemini-malate*)
R	2
S	1
TOTAL for all category	6 Protons

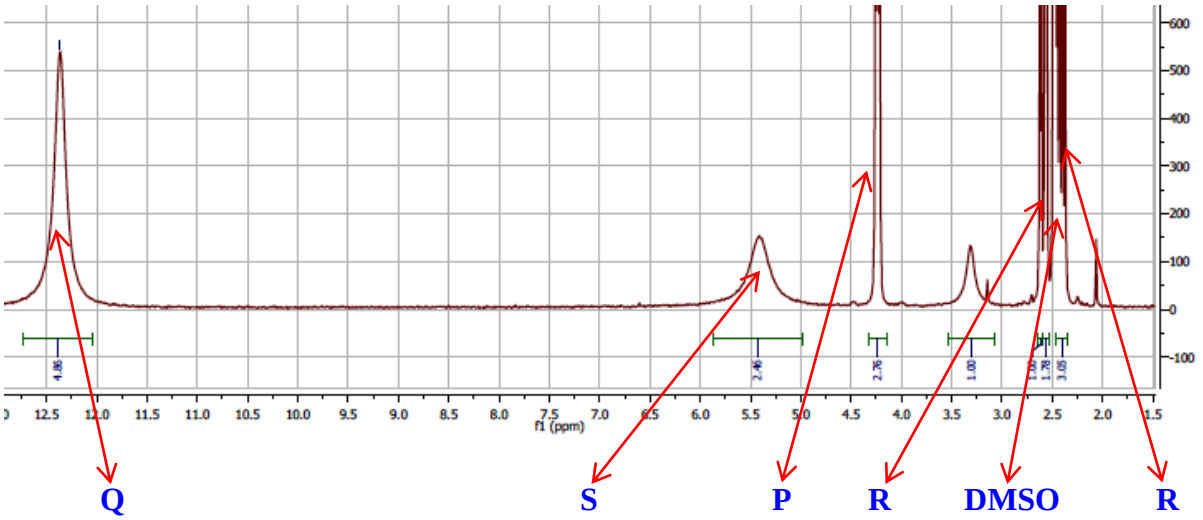

Figure-A-1.9: Identification of ^{1}H NMR peaks of protons of Malic acid (in DMSO-D_6)

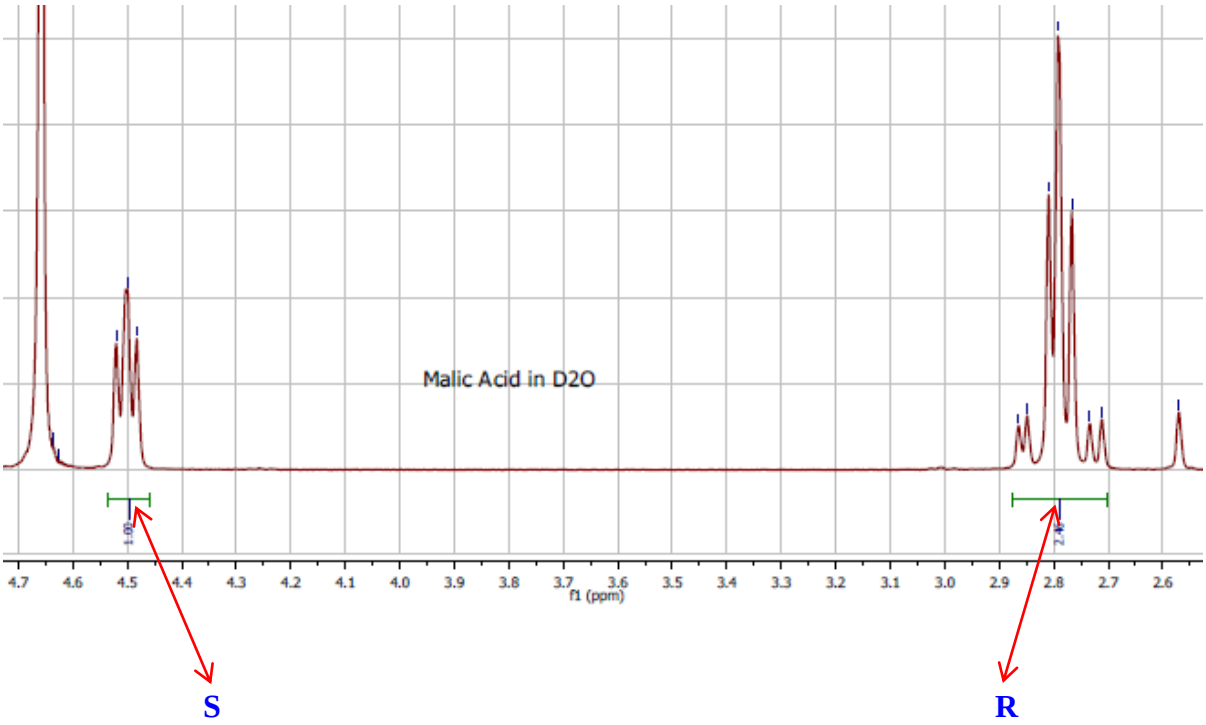

Figure-A-1.10: Identification of ^{1}H NMR peaks of protons of Malic acid (in D_2O).

N.B.:

***** All the '**P'** proton and '**Q'** protons were displaced by deuterium when dissolved in D_2O. Thus no peak was seen in the spectra obtained from the solution of Tartaric acid in D_2O. Same applies to the spectra of 16 – 2 – 16.Malate solution in D_2O.

**During synthesis of the 16 – 2 – 16.Malate molecule, both of the protons from the two carboxylate group was ionized and gets attached with each of the quaternary ammonium head group. Thus the ^{1}H NMR peak represents no proton for both of the carboxylate groups (ionized form) for this gemini solution in D_2O.

A-1.5: Atomic details and ^{1}H NMR spectral analysis of Adenylic Acid (AMP):

The structure of the AMP (MW = 347.2, & Molecular formula: $C_{10}H_{14}N_5O_7P$) is as following –

Atomic details:

Total Carbon, (C) = 10
Total Hydrogen, (H) = 14
Total Nitrogen, (N) = 5
Total oxygen, (O) = 7
Total Phosphorus, (P) = 1

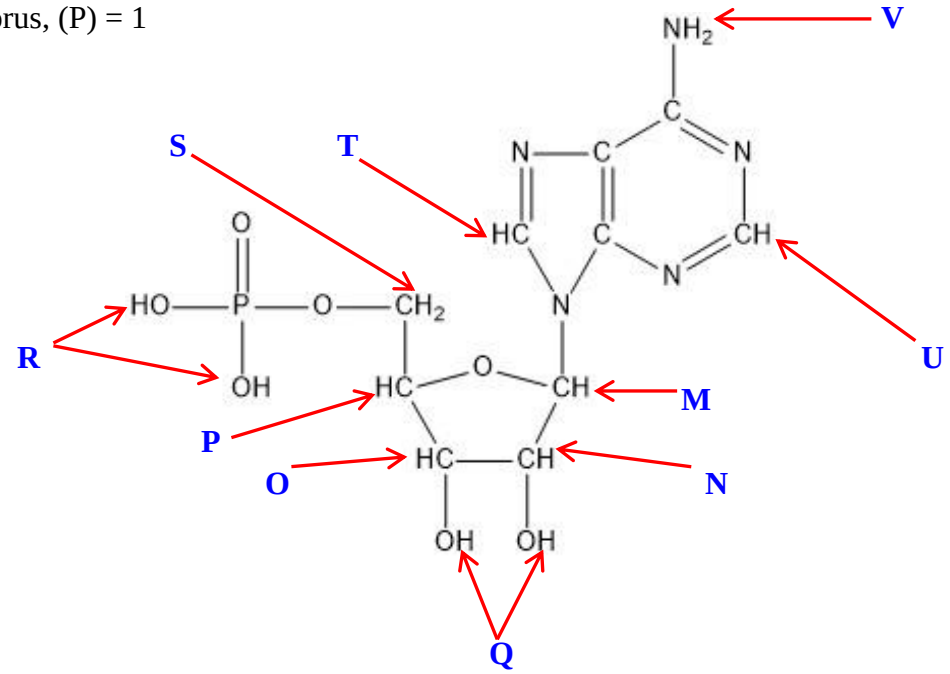

Figure-A-1.11: Assignment of protons in the Adenylic Acid (AMP) structure used in the interpretation of ^{1}H NMR spectra.

Category / Name of the Proton	Total number of proton for that category
M	1
N	1
O	1
P	1
Q*	2
R*	**2
S	2
T	1
U	1
V*	2
TOTAL for all category	14 Protons

**All the protons (^{1}H) of Q, R, and V are displaced by deuterium (D) in the ^{1}H NMR spectra of AMP (acid) in D_2O*

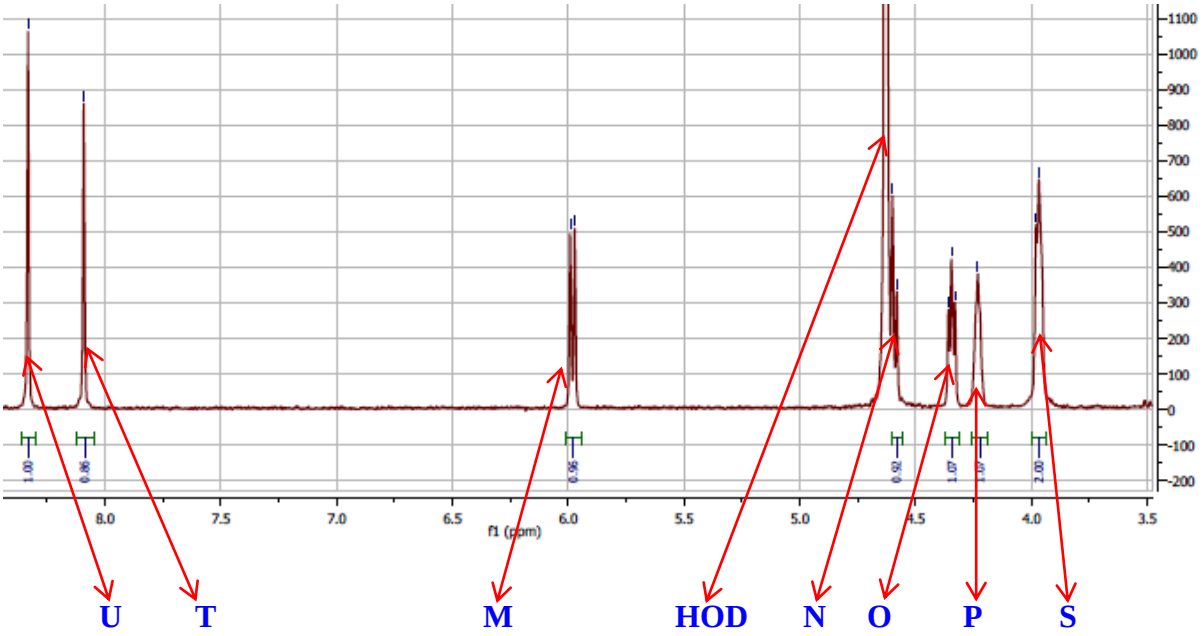

Figure-A-1.12: Identification of ^{1}H NMR peaks of protons of Adenylic acid (in D_2O).

****N.B. :**

During synthesis of the 16 – 2 – 16.2AMP molecule, only one proton from the phosphate group was ionized and gets attached with each of the quaternary ammonium head group. Thus, when the 16 – 2 – 16.2AMP was dissolved D_2O, the remaining proton of the phosphate group of the dissociated counterion was displaced by deuterium. As a result, in the ^{1}H NMR spectra, no peak was found for the phosphate group (ionized form) for this gemini solution in D_2O.

A-1.6: Atomic details and ^{1}H NMR spectral analysis of Cytidylic Acid (CMP):

The structure of the CMP (MW = 323.20, & Molecular formula: $C_9H_{14}N_3O_8P$) is as following –

Atomic details:

Total Carbon, (C) = 9
Total Hydrogen, (H) = 14
Total Nitrogen, (N) = 3
Total oxygen, (O) = 8
Total Phosphorus, (P) = 1

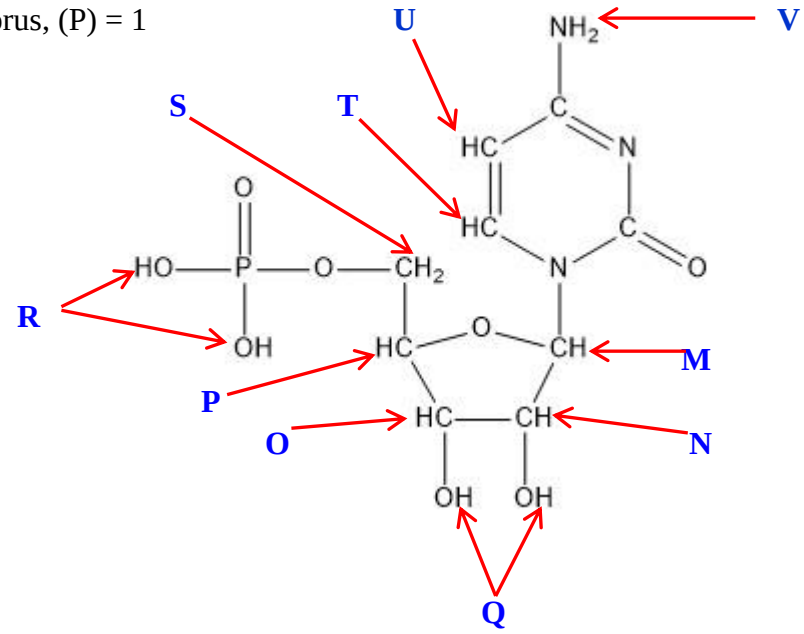

Figure-A-1.13: Assignment of protons in the Cytidylic Acid (CMP) structure used in the interpretation of ^{1}H NMR spectra.

Category / Name of the Proton	Total number of proton for that category
M	1
N	1
O	1
P	1
Q*	2
R*	**2
S	2
T	1
U	1
V*	2
TOTAL for all category	14 Protons

** All the protons (^{1}H) of Q, R, and V are displaced by deuterium (D) in the ^{1}H NMR spectra of CMP (acid) in D_2O*

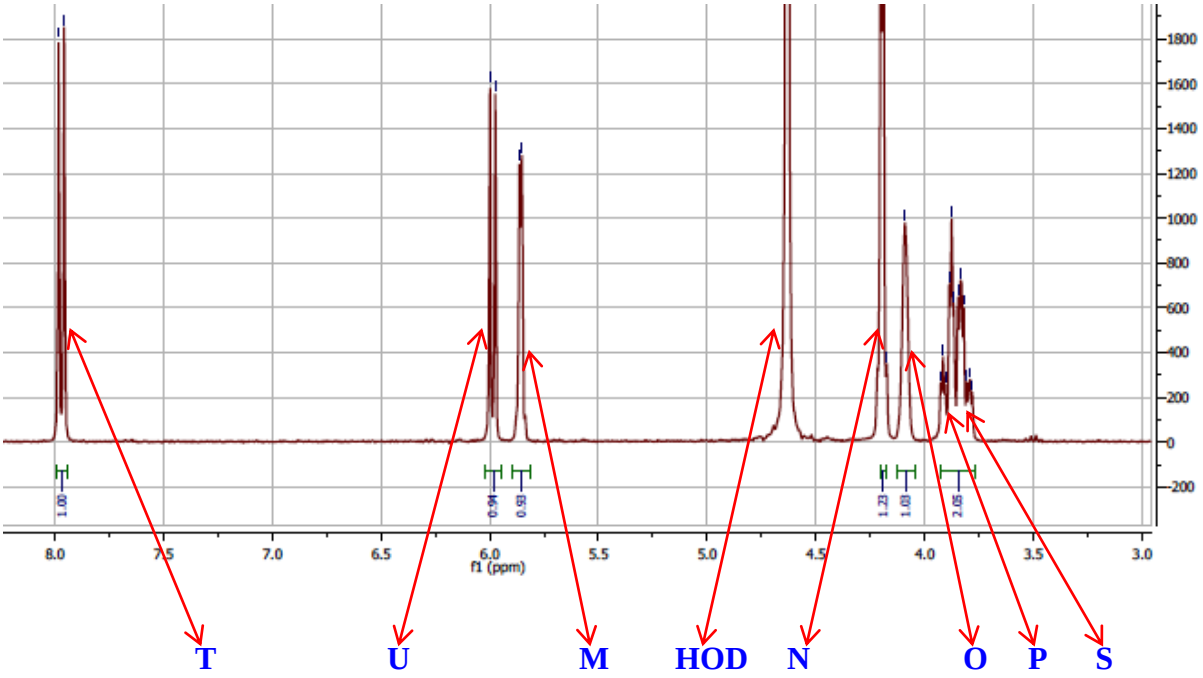

Figure-A-1.14: Identification of ^{1}H NMR peaks of protons of Cytidylic acid (in D_2O).

****N.B. :**

During synthesis of the 16 – 2 – 16.2CMP molecule, only one proton from the phosphate group was ionized and gets attached with each of the quaternary ammonium head group. Thus, when the 16 – 2 – 16.2CMP was dissolved D_2O, the remaining proton of the phosphate group of the dissociated counterion was displaced by deuterium. As a result, in the ^{1}H NMR spectra, no peak was found for the phosphate group (ionized form) for this gemini solution in D_2O.

A-1.7: Atomic details and HNMR spectral analysis of Uridylic Acid (UMP):

The structure of the UMP (MW = 324.18, & Molecular formula: $C_9H_{13}N_2O_9P$) is as following –

Atomic details:

Total Carbon, (C) = 9
Total Hydrogen, (H) = 13
Total Nitrogen, (N) = 2
Total oxygen, (O) = 9
Total Phosphorus, (P) = 1

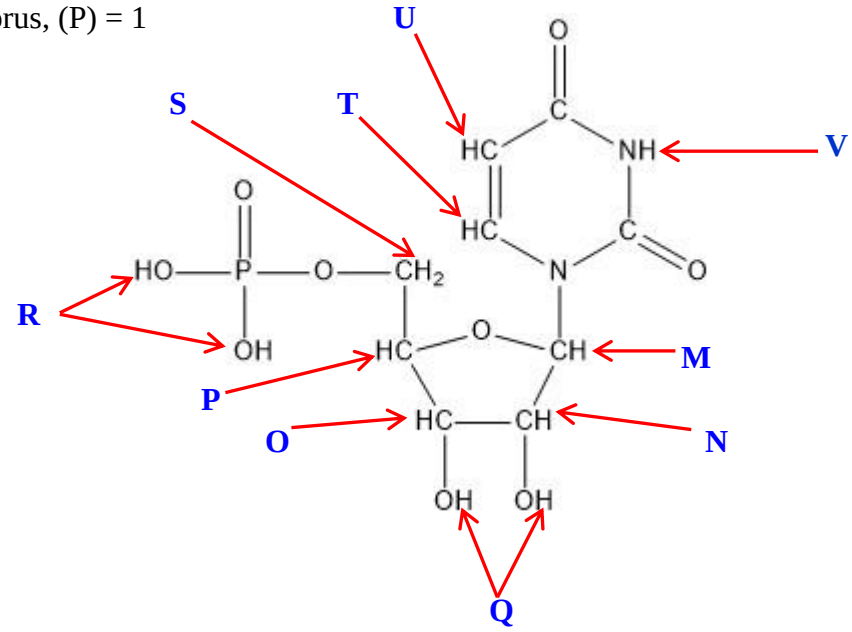

Figure-A-1.15: Assignment of protons in the Uridylic Acid (UMP) structure used in the interpretation of ^{1}H NMR spectra.

Category / Name of the Proton	Total number of proton for that category
M	1
N	1
O	1
P	1
Q*	2
R*	**2
S	2
T	1
U	1
V*	1
TOTAL for all category	13 Protons

** All the protons (^{1}H) of Q, R, and V are displaced by deuterium (D) in the ^{1}H NMR spectra of UMP (acid) in D_2O*

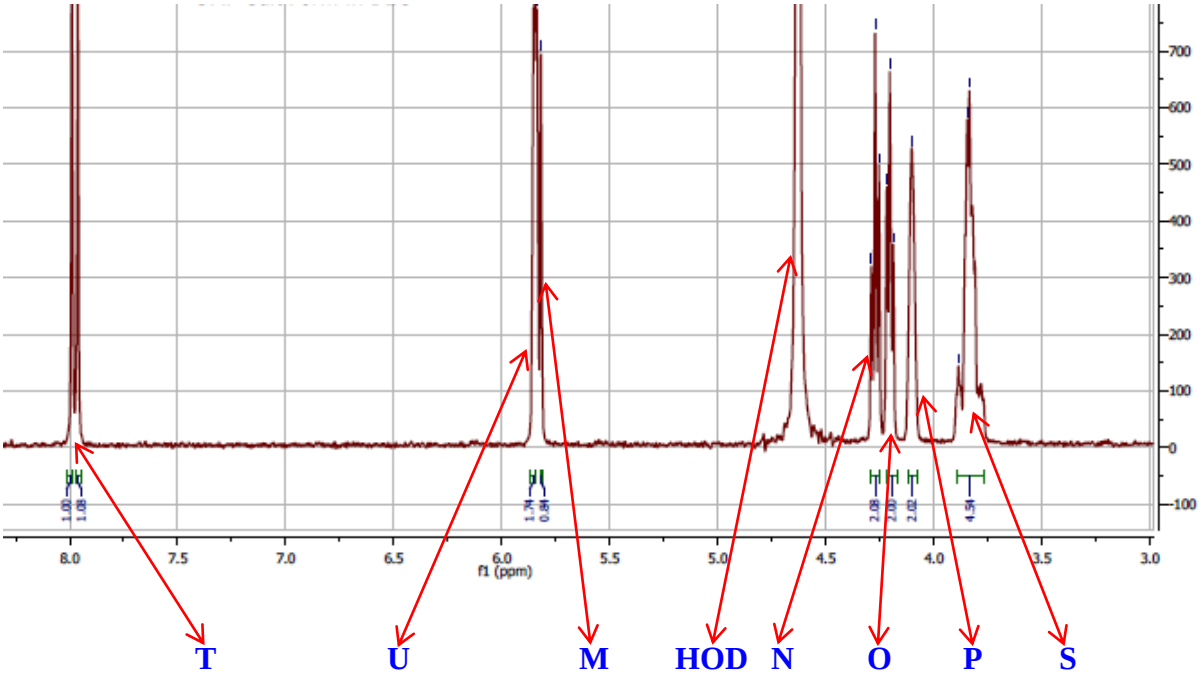

Figure-A-1.16: Identification of ^{1}H NMR peaks of protons of Uridylic acid (in D_2O).

****N.B. :**

During synthesis of the 16 – 2 – 16.2UMP molecule, only one proton from the phosphate group was ionized and gets attached with each of the quaternary ammonium head group. Thus, when the 16 – 2 – 16.2UMP was dissolved D_2O, the remaining proton of the phosphate group of the dissociated counterion was displaced by deuterium. As a result, in the ^{1}H NMR spectra, no peak was found for the phosphate group (ionized form) for this gemini solution in D_2O.

A-1.8: Atomic details and ^{1}H NMR spectral analysis of Guanylic Acid (GMP):

The structure of the GMP (MW = 363.2, & Molecular formula: $C_{10}H_{14}N_5O_8P$) is as following –

Atomic details:

Total Carbon, (C) = 10
Total Hydrogen, (H) = 14
Total Nitrogen, (N) = 5
Total oxygen, (O) = 8
Total Phosphorus, (P) = 1

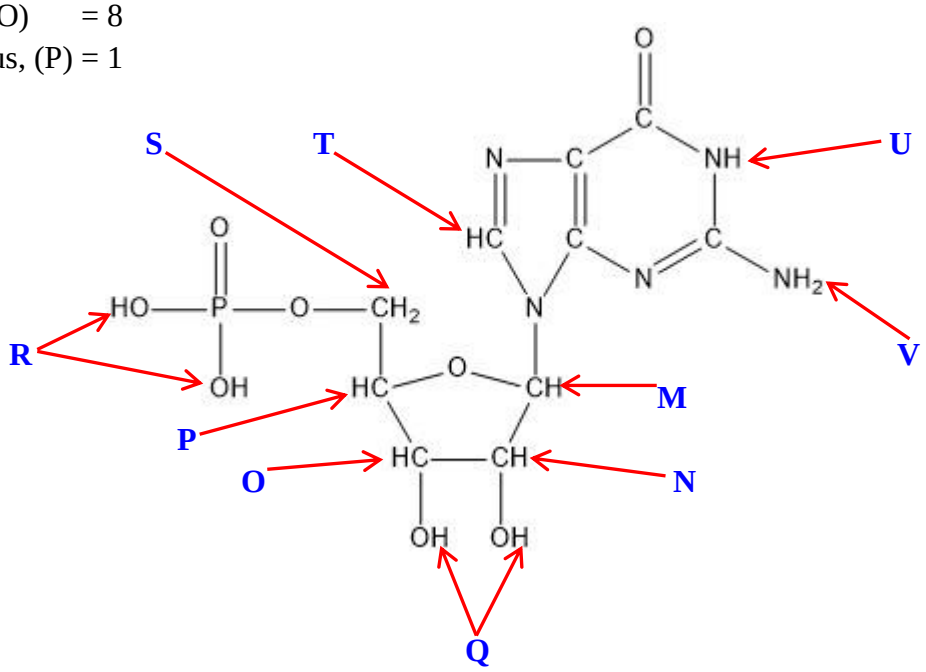

Figure-A-1.17: Assignment of protons in the Guanylic Acid (GMP) structure used in the interpretation of ^{1}H NMR spectra.

Category / Name of the Proton	Total number of proton for that category
M	1
N	1
O	1
P	1
Q*	2
R*	**2
S	2
T	1
U*	1
V*	2
TOTAL for all category	14 Protons

** All the protons (^{1}H) of Q, R, U, and V are displaced by deuterium (D) in the ^{1}H NMR spectra of UMP (acid) in D_2O*

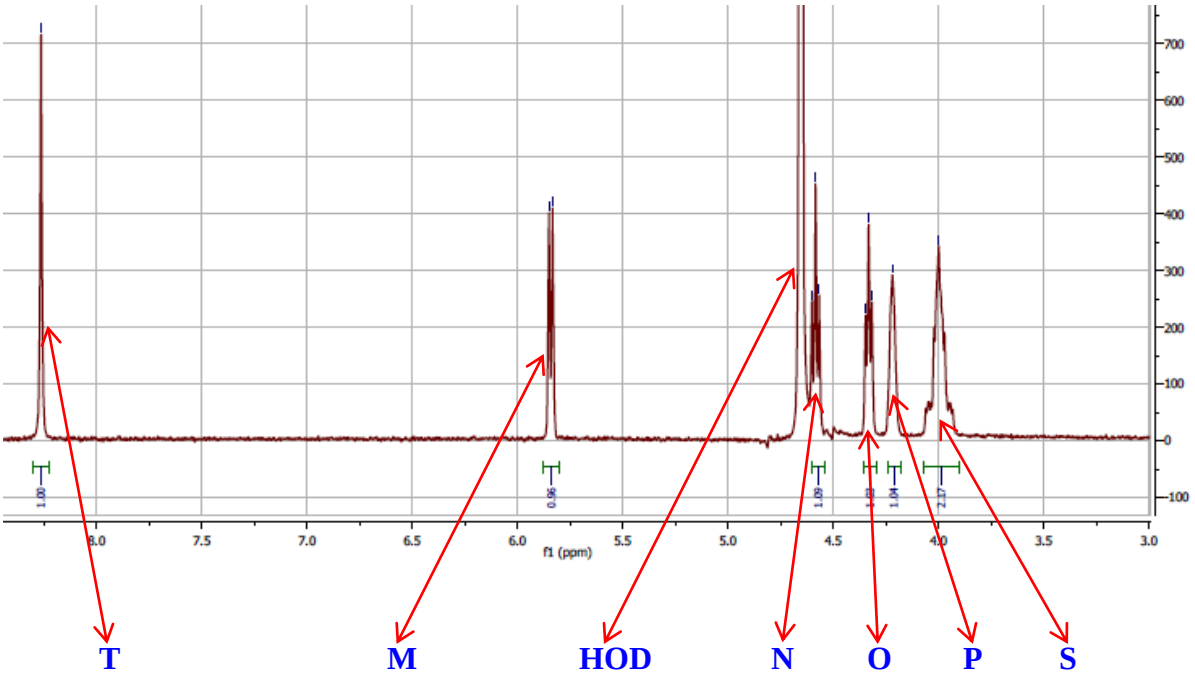

Figure-A-1.18: Identification of ^{1}H NMR peaks of protons of Guanylic acid (in D_2O).

****N.B. :**

During synthesis of the 16 – 2 – 16.2GMP molecule, only one proton from the phosphate group was ionized and gets attached with each of the quaternary ammonium head group. Thus, when the 16 – 2 – 16.2GMP was dissolved D_2O, the remaining proton of the phosphate group of the dissociated counterion was displaced by deuterium. As a result, in the ^{1}H NMR spectra, no peak was found for the phosphate group (ionized form) for this gemini solution in D_2O.

A-1.9: Atomic details and ^{1}H NMR spectral analysis of 16–2–16.2X^{-} (X^{-} = Br^{-}/Cl^{-}):

The structure of the 16–2–16.2X^{-} (MW = 726.9 (Br^{-}) & 638 (Cl^{-}), & Molecular formula: $C_{38}H_{82}N_2X_2$) is as following –

Atomic details:

Total Carbon, (C) = 38
Total Hydrogen, (H) = 82
Total Nitrogen, (N) = 2
Total Halide, (X^{-}) = 2 (X^{-} = Bromide or Chloride)

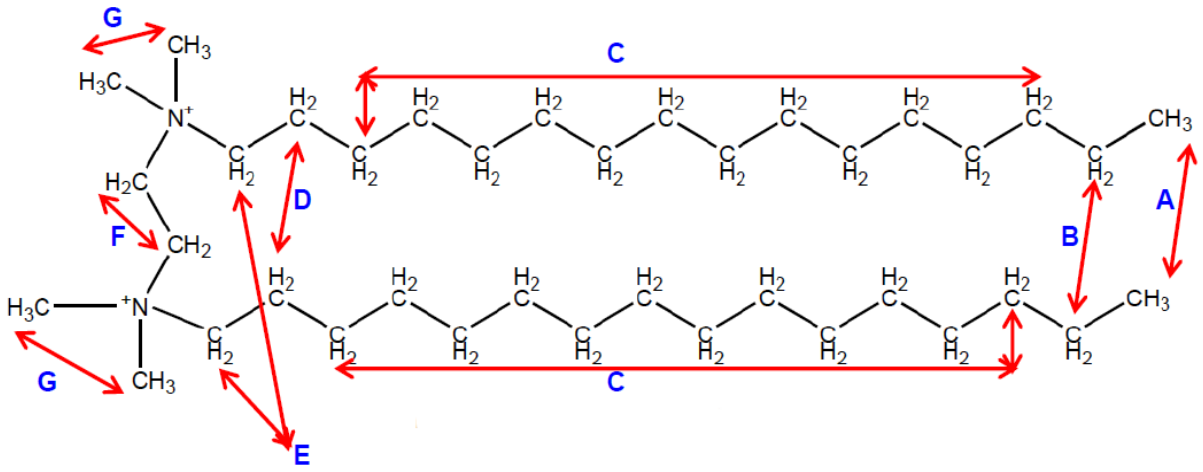

Figure-A-1.17: Assignment of protons in the 16–2–16.2X^{-} gemini surfactants structure (where, X^{-} = Br^{-}/Cl^{-}) used in the interpretation of ^{1}H NMR spectra.

Category / Class of the Proton	Total number of proton for that category
A	6
B	4
C	48
D	4
E	4
F	4
G	12
TOTAL for all categories	82 Protons

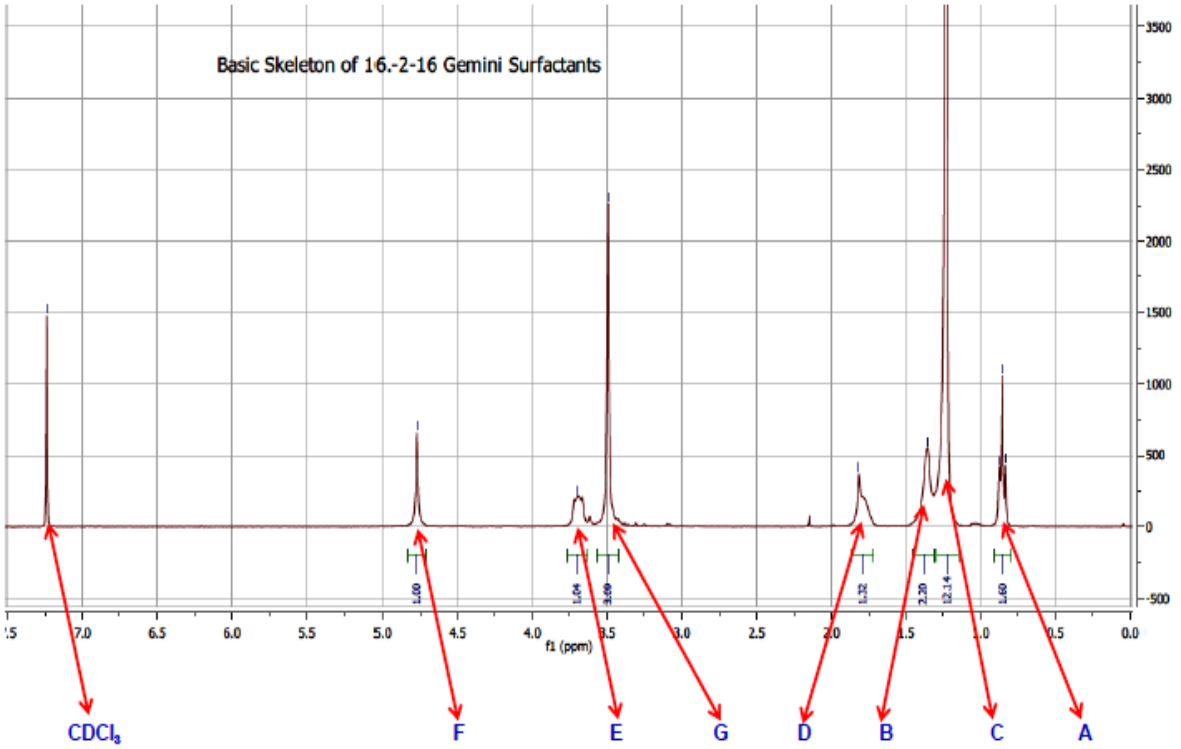

Figure-A-1.18: Identification of ^{1}H NMR peaks of protons of 16–2–16.2X^{-} gemini surfactants (where, $X^{-} = Br^{-}/Cl^{-}$)

A-2.1: Complete ^{1}H NMR Spectra of 16-2-16 series of GSs with various counterions:

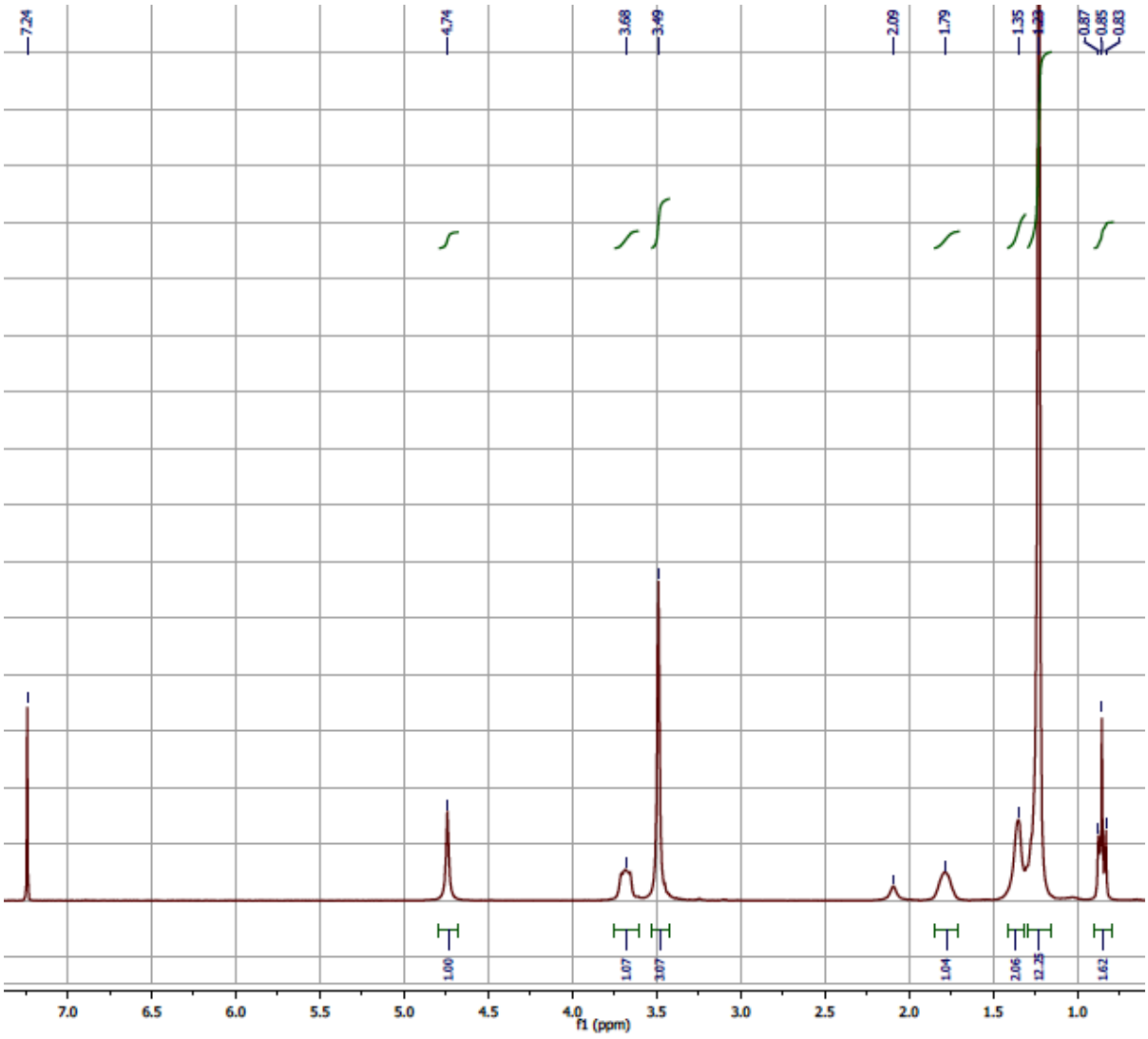

Figure-A-2.1: ^{1}H NMR spectra of 16-2-16.2Br $^{-}$

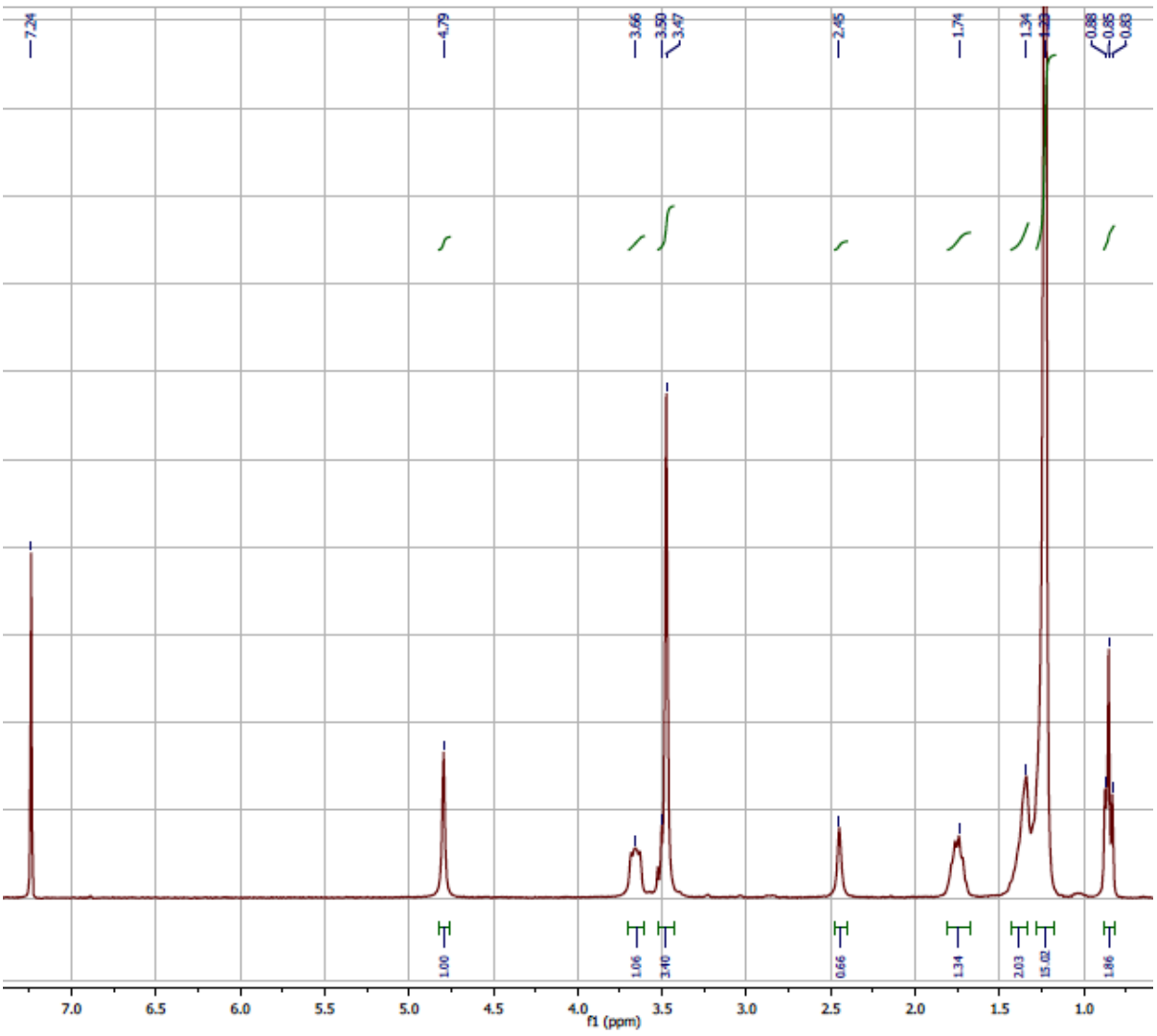

Figure-A-2.2: ^{1}H NMR spectra of 16-2-16.2Cl $^{-}$

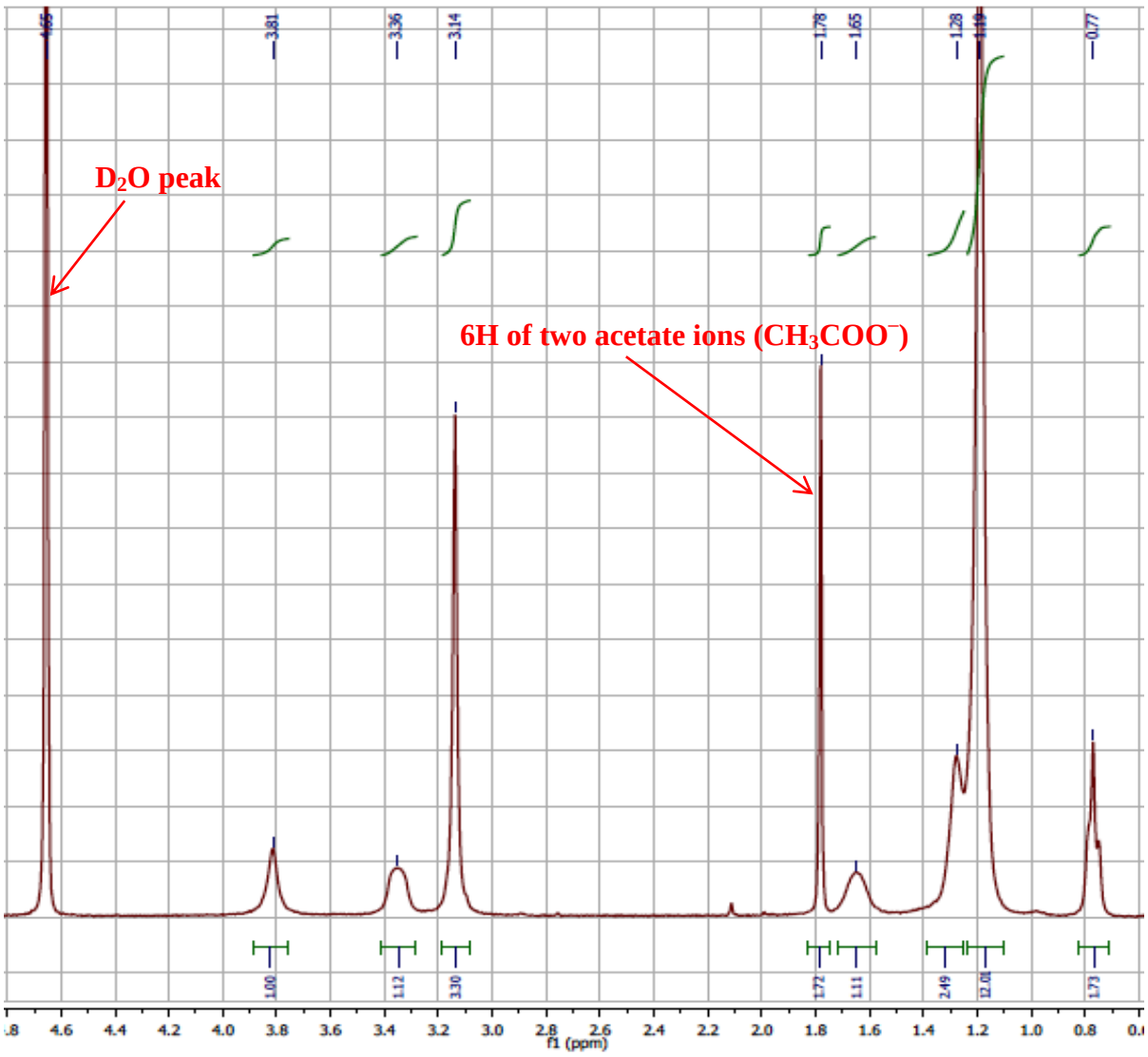

Figure-A-2.3: ^{1}H NMR spectra of 16-2-16.2Ac $^{-}$

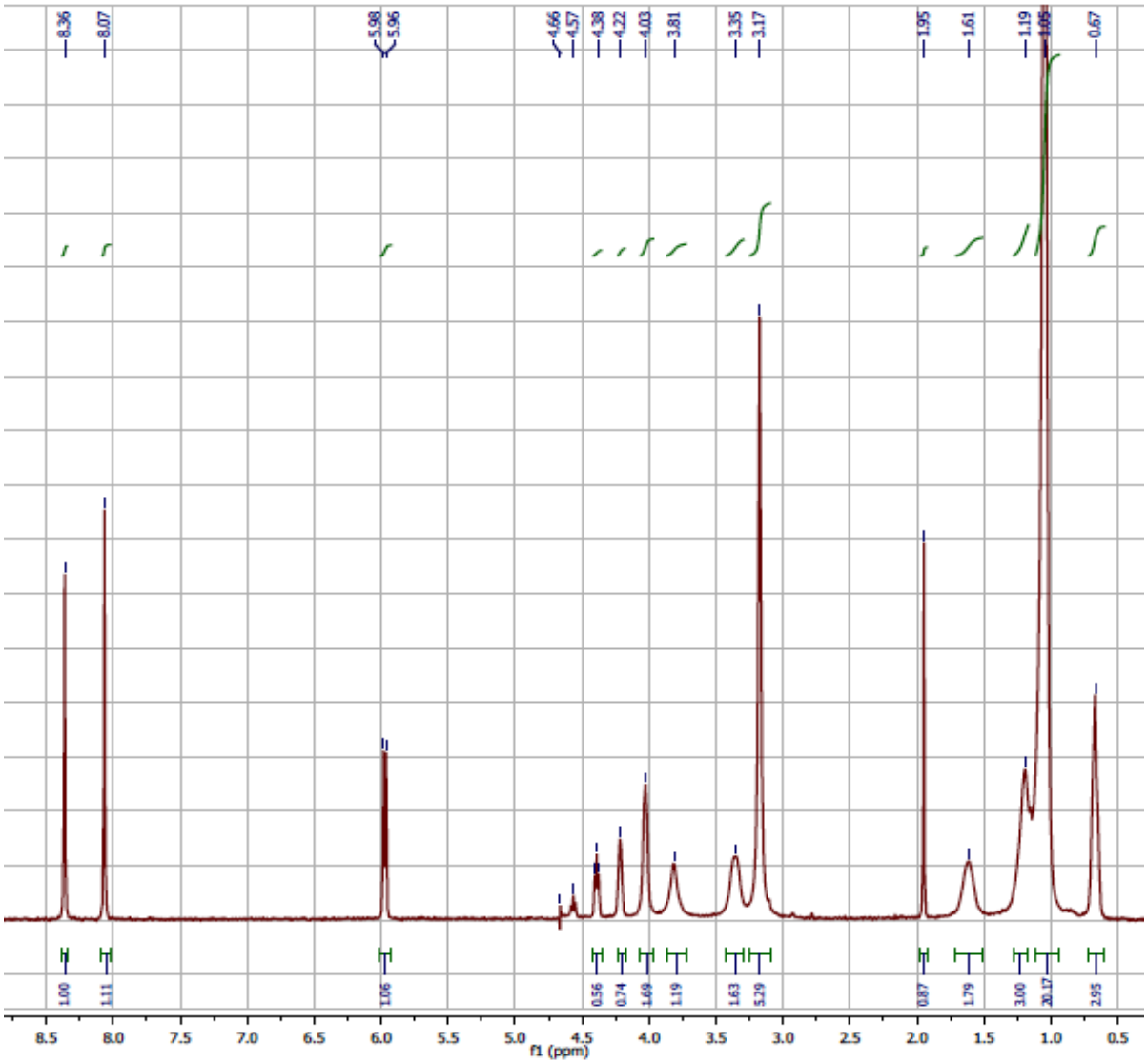

Figure-A-2.4: ^{1}H NMR spectra of 16-2-16.2AMP $^{-}$

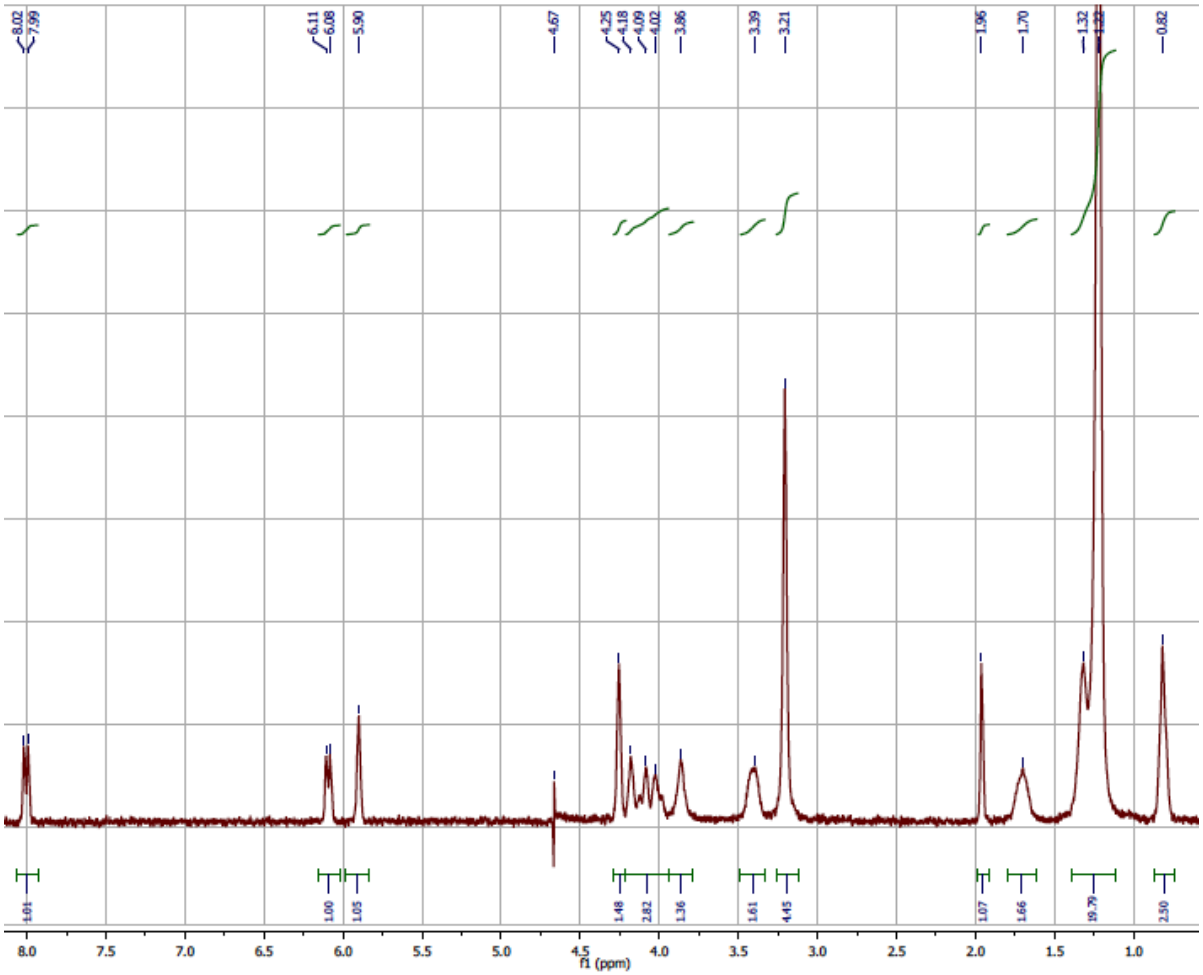

Figure-A-2.5: ^{1}H NMR spectra of 16-2-16.2CMP $^{-}$

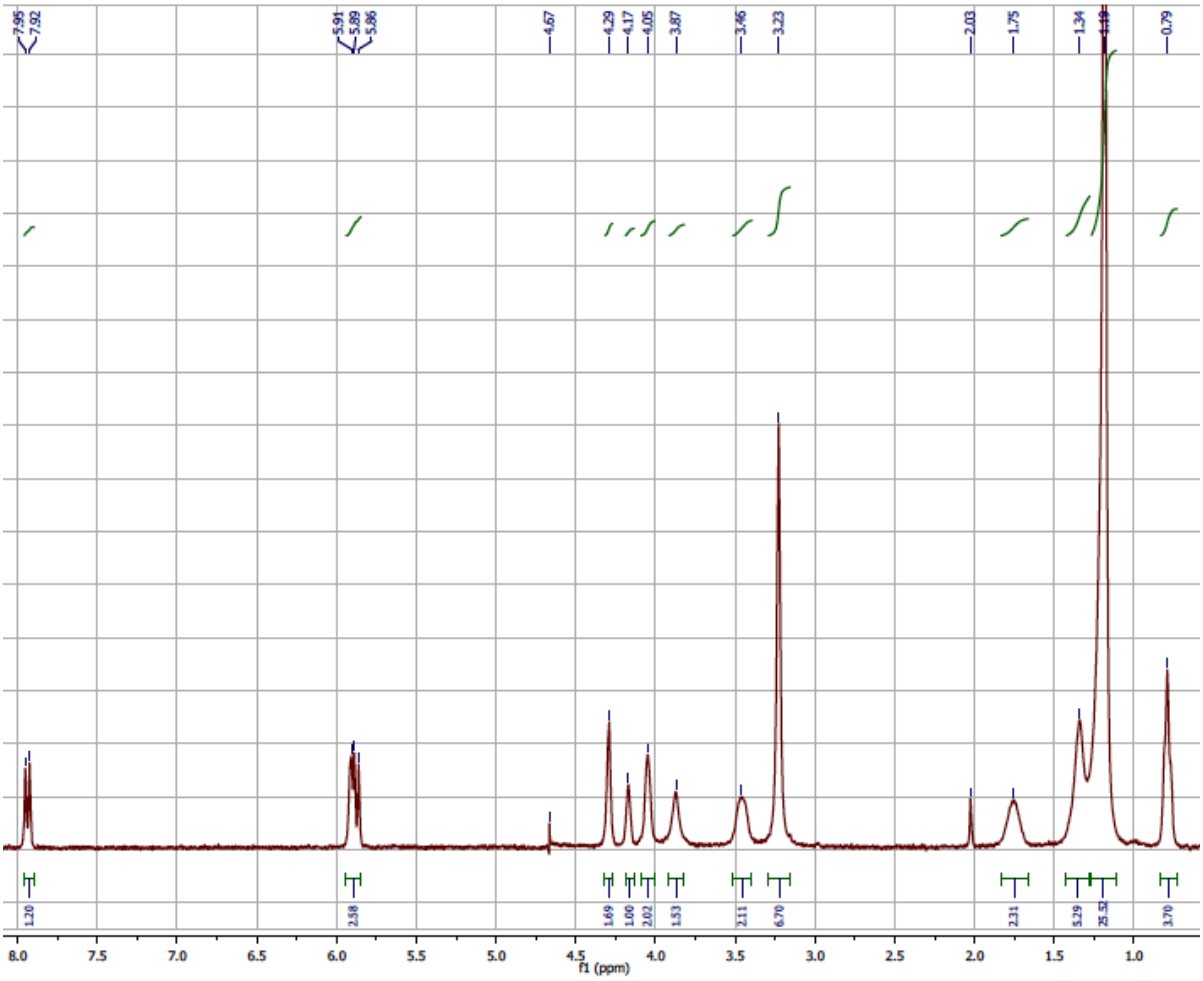

Figure-A-2.6: ^{1}H NMR spectra of 16-2-16.2UMP $^{-}$

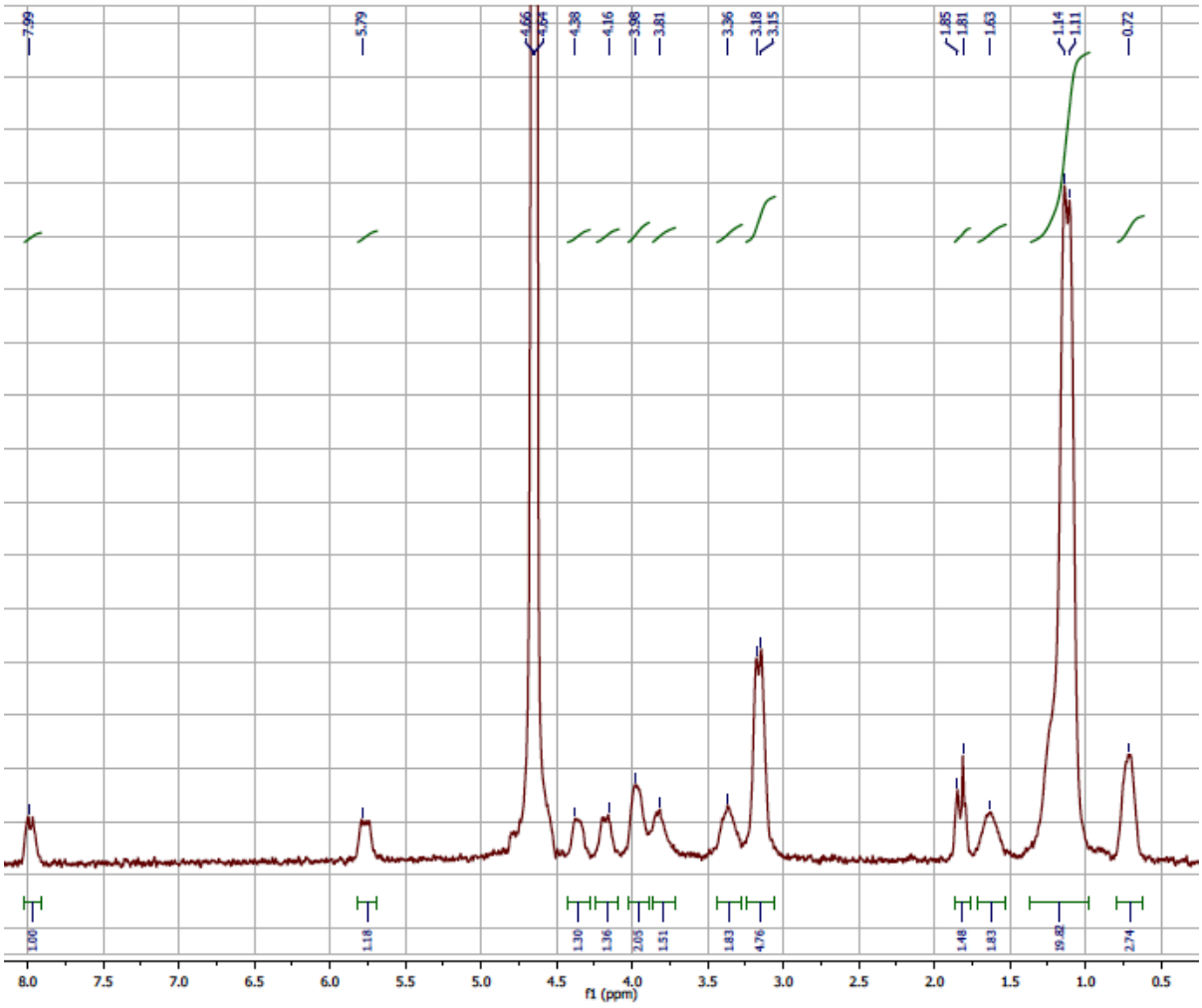

Figure-A-2.7: ^{1}H NMR spectra of 16-2-16.2GMP $^{-}$

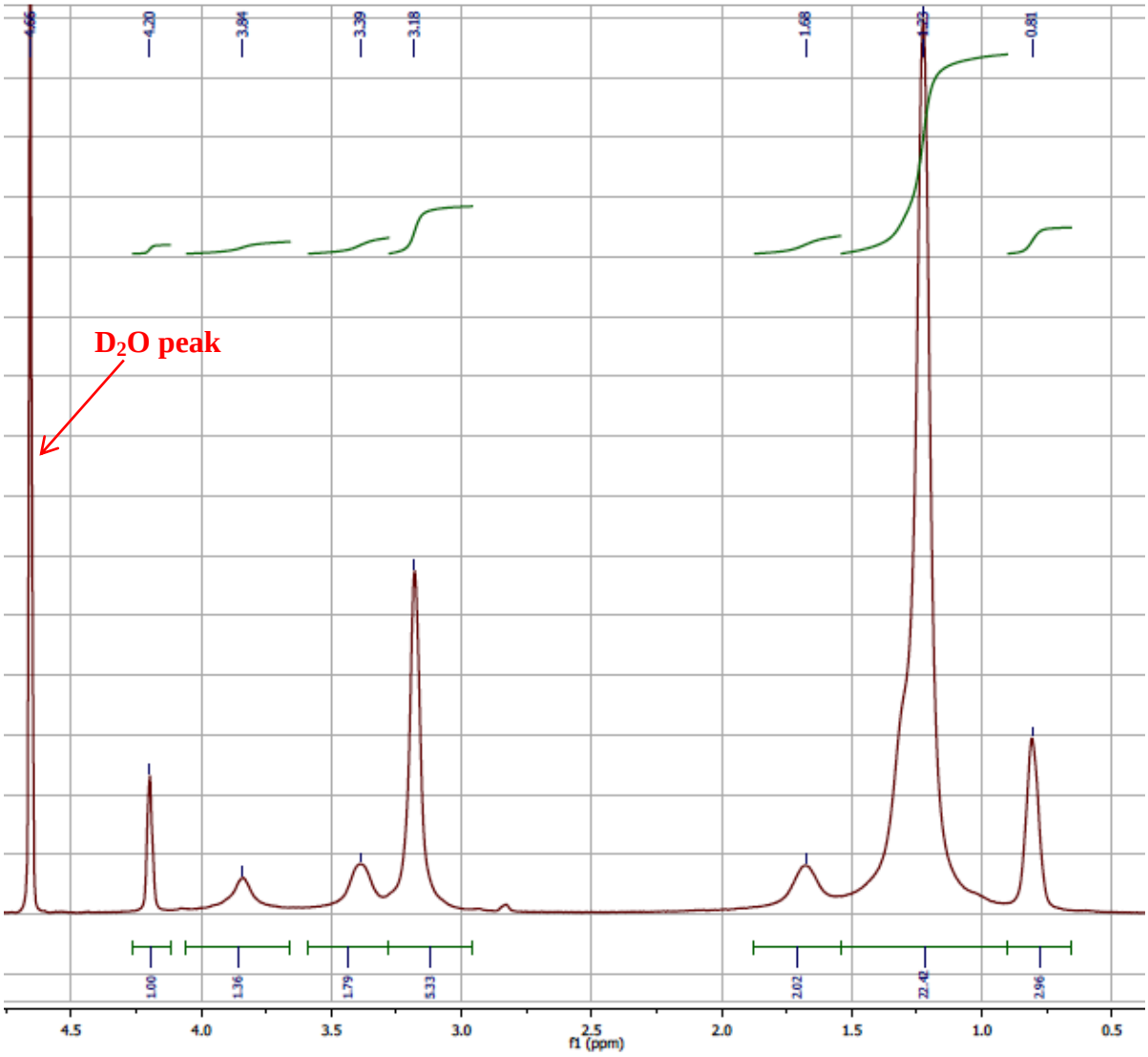

Figure-A-2.8: ^{1}H NMR spectra of 16-2-16.Tartrate $^{--}$

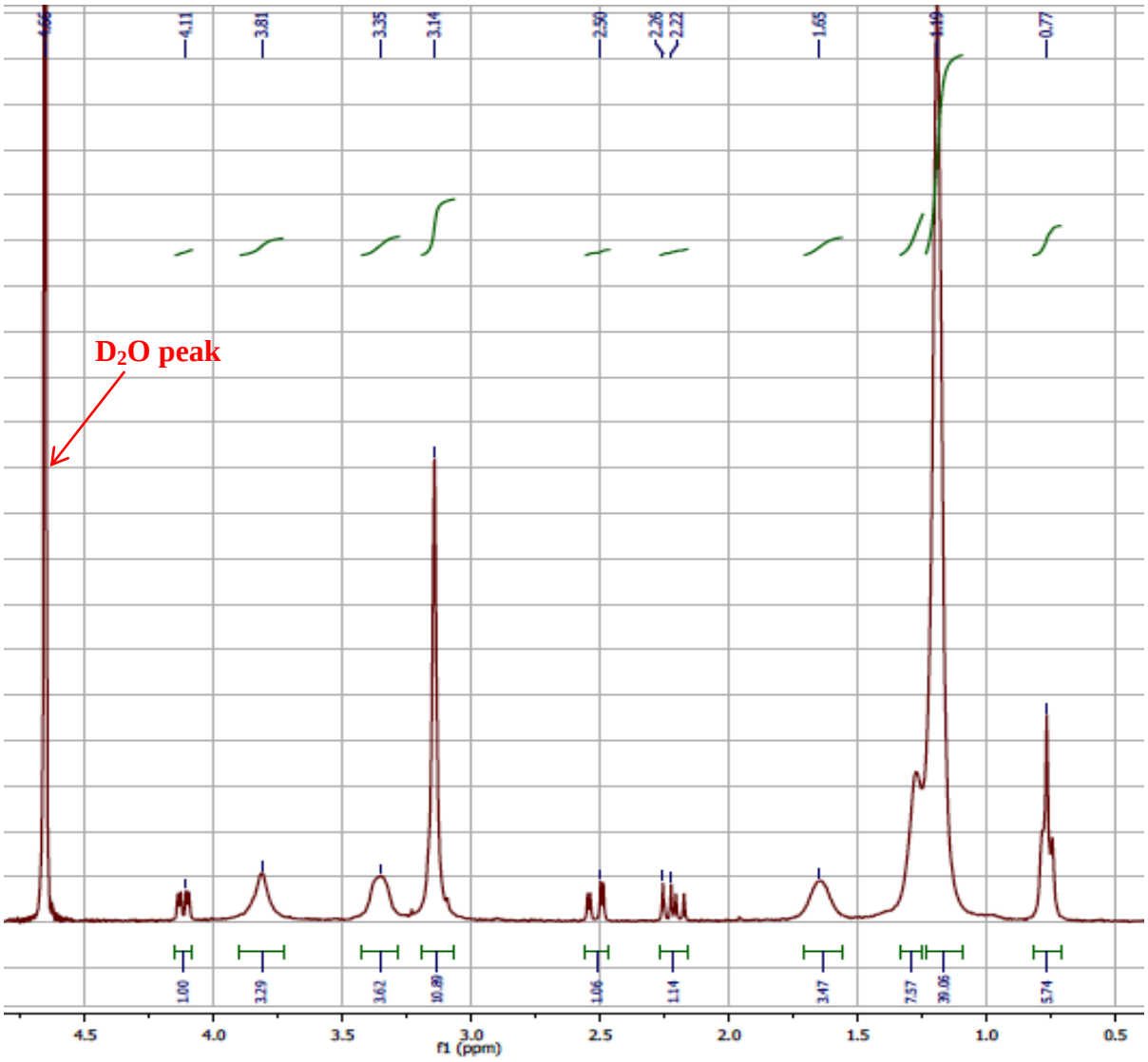

Figure-A-2.9: ^{1}H NMR spectra of 16-2-16.Malate $^{--}$

Table-A-3.1: Solubility test data for organic counterions

Properties	Counterion (ACIDIC form)*					
	Tartaric Acid	**Malic Acid**	**AMP.H_2O**	**CMP**	**UMP**	**GMP**
Molar Mass (g/mole)	150.08	134.09	365.24	323.20	324.18	363.20
Solubility in water ('x' mg / 100 µL)	167 mg @ 40^0C	58.8 mg @ 25^0C	33 mg @ 40^0C	10 mg @ 35^0C	40 mg @ 25^0C	6.7 mg @ 60^0C
# Hydroxyl Group	2	1	2	2	2	2

***** *AMP.H_2O: Adenylic acid, CMP: Cytidylic acid, UMP: Uridylic acid, GMP: Guanidylic acid*

Table-A-3.2: Results of comparative solubility conditions for 16-2-16 series of GSs

Gemini Solutions (1.5 mM, 10 mL)	Sonication time required for the GSs to get dissolved from solid crystals @ 55^0C (minutes)	Inference / Verdict
16 – 2 – 16 . $2Br^-$	50	Soluble
16 – 2 – 16 . $2Cl^-$	25	Soluble
16 – 2 – 16 . $2AMP^-$	30	Soluble
16 – 2 – 16 . $2CMP^-$	25	Soluble
16 – 2 – 16 . $2UMP^-$	< 1, at 25^0C, no sonication required	Readily Soluble
16 – 2 – 16 . $2GMP^-$	75 (+ Vortexing)	Sparingly Soluble
16 – 2 – 16 . $Tartrate^{--}$	40	Soluble
16 – 2 – 16 . $Malate^{--}$	< 10 (Was soluble in 25^0C)	Readily Soluble

Table-A-3.3: Critical Packing Parameters of 16-2-16 series of GS with different counterions

Gemini Surfactants	Average Critical Packing Parameter, CPP = V / $a_0.l_C$	Aggregate Structure according to CPP
16-2-16.$2Br^-$	0.34	Spherical micelles
16-2-16.$2Cl^-$	0.32	Spherical micelles
16-2-16.$2AMP^-$	0.33	Spherical micelles
16-2-16.$2CMP^-$	0.39	Cylindrical or rod shape micelles
16-2-16.$2UMP^-$	0.34	Spherical micelles
16-2-16.$2GMP^-$	0.53	Cylindrical or rod shape micelles
16-2-16.$Tartrate^{--}$	0.43	Cylindrical or rod shape micelles
16-2-16.$Malate^{--}$	0.50	Cylindrical or rod shape micelles

A-3.4.1 Viscosity measurement

The viscosity of the gemini solutions were measured using a Gilmont Falling ball viscometer (size #2, GV 2200, Thermo Scientific, USA) at 55^0C. The temperature was controlled at a precision of $\pm 0.05^0$C using an immersion circulating water bath (VWR, USA). Saturated aqueous solutions (~1.5 mM, >> CMC for all surfactants) were prepared, separately, for each gemini surfactant, by sonication at 55^0C and the gemini solutions were inserted in the viscometer assembly along with the stainless steel ball, and the time (in milliseconds) required for the ball to travel across the start and stop points of the viscometer was recorded. All viscosity measurements were repeated in triplicate and the average is reported. Viscosities were calculated according to (Equation-A-3.1) as following:

Viscosity of a liquid (in centipoise units), $\mu = K(D_b - D_W) / t$ A-3.1

Where,

K = Viscometer constant (for viscometer size #2, K = 3.3 was used as provided)

D_b = Density of the stainless steel ball (8.02 g/mL)

D_W = Density of Milli Q water at experimental temperature (0.98 g/mL @ 55^0C)

t = Required time (in minutes) for the ball to travel across the start – stop points

A-3.4.2 Foam ability and foam stability measurement

Foamability and foam-stability of the gemini surfactants were studied using a previously reported method [80, 81, 203, 204]. Twenty milliliters of gemini solution (1.5 mM >> CMC for all surfactants) at 55^0C was placed into a calibrated 100 mL graduated cylinder equipped with a stopper. The solution was shaken in the cylinder uniformly and vigorously for 10 seconds and the volume of foam produced was recorded at 0 min, 10 min and 20 min. The initial volume (0 min) of the foam produced was measured as foamability of the surfactant, while foam stability was determined from the remaining foam at 10 and 20 minutes [204]. All the measurements of foamability and foam stability were repeated in duplicate for each gemini.

Table-A-3.4: Viscosity, foam-ability & foam stability data of 16-2-16 series of gemini surfactant solutions with eight different counterions

Name of the GS solution (0.1 % or 1.5 mM)	Average Viscosity* (cP)	Ave. of the Initial volume of the foam produced (mL)	Ave. Foam stability after 10 mins (%)	Ave. Foam stability after 20 mins (%)
16-2-16.2Br $^{-}$	1.09	6.7	49.6	20.3
16-2-16.2Cl $^{-}$	1.06	13	82.4	53.3
16-2-16.2AMP $^{-}$	0.98	10.6	89.9	46.7
16-2-16.2CMP $^{-}$	0.94	12.4	90.1	50.1
16-2-16.2UMP $^{-}$	0.97	11.3	88.7	52.3
16-2-16.2GMP $^{-}$	0.96	10	85.8	38.8
16-2-16.Tartrate $^{--}$	0.97	9.4	84.3	33
16-2-16.Malate $^{--}$	1.03	10.7	86.7	62.6

***** *Viscosity of milli Q water was found 0.47 cP*

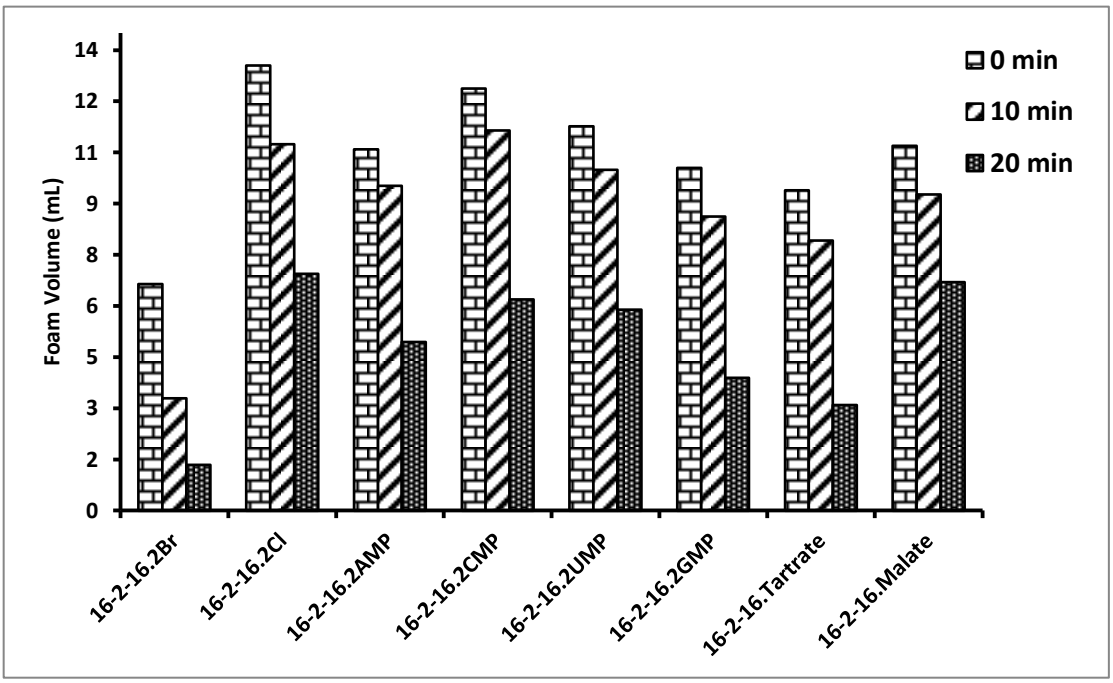

Figure-A-3.1: Graphical representations of the foaming volume (foamability) produced by the 16-2-16 series of gemini at different time intervals

Table-A-3.5: Recorded values & parameters of all the extractions for pNN9 plasmid

Extraction Number	Extracted Sample	Extraction Kit Used	Sample conc. (ng/ µL)	$A_{260/280}$ (Nano-drop)
Extraction-1 OD_{600} = 1.66	Sample – 1	E.Z.N.A.® Maxi	179.2	1.81
	Sample – 2	E.Z.N.A.® Maxi	193.2	1.83
Extraction-2 OD_{600} = 1.54	Sample – 1	E.Z.N.A.® Maxi	104.4	1.85
	Sample – 2	E.Z.N.A.® Maxi	92.5	1.80
	Sample – 3	E.Z.N.A.® Maxi	97.1	1.82
Extraction-3 OD_{600} = 1.82	Sample – 1	E.Z.N.A.® Endo-Free Maxi	523.3	1.88
	Sample – 2	E.Z.N.A.® Endo-Free Maxi	656.1	1.91

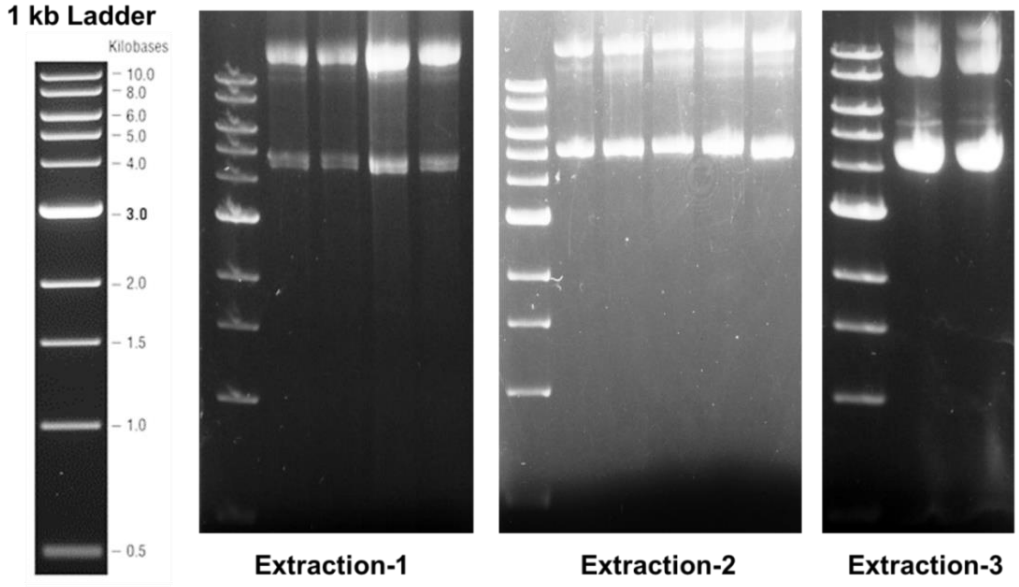

Figure-A-3.2: UV image of the agarose gel after AGE for size confirmation of pNN9 plasmid

Letters of copyright permission

1. Copyright permission for Figure-1.3 to reuse/reprint:

ELSEVIER LICENSE
TERMS AND CONDITIONS

Dec 11, 2014

This is a License Agreement between Muhammad Shahidul Islam ("You") and Elsevier ("Elsevier") provided by Copyright Clearance Center ("CCC"). The license consists of your order details, the terms and conditions provided by Elsevier, and the payment terms and conditions.

All payments must be made in full to CCC. For payment instructions, please see information listed at the bottom of this form.

Supplier	Elsevier Limited The Boulevard,Langford Lane Kidlington,Oxford,OX5 1GB,UK
Registered Company Number	1982084
Customer name	Muhammad Shahidul Islam
Customer address	10A Victoria Street S Kitchener, ON N2G 2B2
License number	3526200095977
License date	Dec 11, 2014
Licensed content publisher	Elsevier
Licensed content publication	Bioorganic Chemistry
Licensed content title	Synthesis of cationic cardiolipin analogues
Licensed content author	None
Licensed content date	October 2005
Licensed content volume number	33
Licensed content issue number	5
Number of pages	18
Start Page	345
End Page	362
Type of Use	reuse in a thesis/dissertation

ELSEVIER LICENSE
TERMS AND CONDITIONS

Dec 11, 2014

This is a License Agreement between Muhammad Shahidul Islam ("You") and Elsevier ("Elsevier") provided by Copyright Clearance Center ("CCC"). The license consists of your order details, the terms and conditions provided by Elsevier, and the payment terms and conditions.

All payments must be made in full to CCC. For payment instructions, please see information listed at the bottom of this form.

Supplier	Elsevier Limited The Boulevard,Langford Lane Kidlington,Oxford,OX5 1GB,UK
Registered Company Number	1982084
Customer name	Muhammad Shahidul Islam
Customer address	10A Victoria Street S Kitchener, ON N2G 2B2
License number	3526200277884
License date	Dec 11, 2014
Licensed content publisher	Elsevier
Licensed content publication	Journal of Controlled Release
Licensed content title	Cationic compounds used in lipoplexes and polyplexes for gene delivery
Licensed content author	Shubiao Zhang,Yingmei Xu,Bing Wang,Weihong Qiao,Dongliang Liu,Zongshi Li
Licensed content date	24 November 2004
Licensed content volume number	100
Licensed content issue number	2
Number of pages	16
Start Page	165
End Page	180
Type of Use	reuse in a thesis/dissertation

2. Copyright permission for Figure-1.9, 1.10 & 1.12 to reuse/reprint:

Copyright Clearance Center RightsLink®

Home | Account Info | Help

ACS Publications
Most Trusted. Most Cited. Most Read.

Title: Counteranion Effect on Micellization of Cationic Gemini Surfactants 14-2-14: Hofmeister and Other Counterions

Author: Sabine Manet, Yevgen Karpichev, Dario Bassani, et al

Publication: Langmuir

Publisher: American Chemical Society

Date: Jul 1, 2010

Copyright © 2010, American Chemical Society

Logged in as:
Muhammad Islam
Account #:
3000844155

LOGOUT

PERMISSION/LICENSE IS GRANTED FOR YOUR ORDER AT NO CHARGE

This type of permission/license, instead of the standard Terms & Conditions, is sent to you because no fee is being charged for your order. Please note the following:

- Permission is granted for your request in both print and electronic formats, and translations.
- If figures and/or tables were requested, they may be adapted or used in part.
- Please print this page for your records and send a copy of it to your publisher/graduate school.
- Appropriate credit for the requested material should be given as follows: "Reprinted (adapted) with permission from (COMPLETE REFERENCE CITATION). Copyright (YEAR) American Chemical Society." Insert appropriate information in place of the capitalized words.
- One-time permission is granted only for the use specified in your request. No additional uses are granted (such as derivative works or other editions). For any other uses, please submit a new request.

If credit is given to another source for the material you requested, permission must be obtained from that source.

3. Copyright permission for Figure-1.13 to reuse/reprint:

SPRINGER LICENSE
TERMS AND CONDITIONS

Dec 11, 2014

This is a License Agreement between Muhammad Shahidul Islam ("You") and Springer ("Springer") provided by Copyright Clearance Center ("CCC"). The license consists of your order details, the terms and conditions provided by Springer, and the payment terms and conditions.

All payments must be made in full to CCC. For payment instructions, please see information listed at the bottom of this form.

License Number	3525831135504
License date	Dec 11, 2014
Licensed content publisher	Springer
Licensed content publication	Biotechnology and Bioprocess Engineering
Licensed content title	Counterion effects on transfection activity of cationic lipid emulsion
Licensed content author	Young Jin Kim
Licensed content date	Jan 1, 2001
Volume number	6
Issue number	4
Type of Use	Thesis/Dissertation
Portion	Figures
Author of this Springer article	No
Order reference number	None
Original figure numbers	Figure 2
Title of your thesis / dissertation	Characterization of Counter-ion Effects of Gemini Surfactants and In Vitro Studies of Transfection Efficiency for Gene Therapy in Ovarian Cancer
Expected completion date	Dec 2014
Estimated size(pages)	200
Total	0.00 USD

4. Copyright permission for Figure-1.14 & 1.15 to reuse/reprint:

ELSEVIER LICENSE
TERMS AND CONDITIONS

Dec 11, 2014

This is a License Agreement between Muhammad Shahidul Islam ("You") and Elsevier ("Elsevier") provided by Copyright Clearance Center ("CCC"). The license consists of your order details, the terms and conditions provided by Elsevier, and the payment terms and conditions.

All payments must be made in full to CCC. For payment instructions, please see information listed at the bottom of this form.

Supplier	Elsevier Limited The Boulevard,Langford Lane Kidlington,Oxford,OX5 1GB,UK
Registered Company Number	1982084
Customer name	Muhammad Shahidul Islam
Customer address	10A Victoria Street S Kitchener, ON N2G 2B2
License number	3525831383584
License date	Dec 11, 2014
Licensed content publisher	Elsevier
Licensed content publication	International Journal of Pharmaceutics
Licensed content title	Polynorbornene polycationic polymers as gene transfer agents Influence of the counterion for in vitro transfection
Licensed content author	None
Licensed content date	5 November 2004
Licensed content volume number	285
Licensed content issue number	1-2
Number of pages	13
Start Page	121
End Page	133
Type of Use	reuse in a thesis/dissertation

5. Copyright permission for Figure-1.16 to reuse/reprint:

ELSEVIER LICENSE
TERMS AND CONDITIONS

Dec 11, 2014

This is a License Agreement between Muhammad Shahidul Islam ("You") and Elsevier ("Elsevier") provided by Copyright Clearance Center ("CCC"). The license consists of your order details, the terms and conditions provided by Elsevier, and the payment terms and conditions.

All payments must be made in full to CCC. For payment instructions, please see information listed at the bottom of this form.

Supplier	Elsevier Limited The Boulevard,Langford Lane Kidlington,Oxford,OX5 1GB,UK
Registered Company Number	1982084
Customer name	Muhammad Shahidul Islam
Customer address	10A Victoria Street S Kitchener, ON N2G 2B2
License number	3525840068021
License date	Dec 11, 2014
Licensed content publisher	Elsevier
Licensed content publication	Journal of Colloid and Interface Science
Licensed content title	Aggregation behaviors of gemini nucleotide at the air–water interface and in solutions induced by adenine–uracil interaction
Licensed content author	None
Licensed content date	15 March 2005
Licensed content volume number	283
Licensed content issue number	2
Number of pages	10
Start Page	555
End Page	564
Type of Use	reuse in a thesis/dissertation

JOHN WILEY AND SONS LICENSE TERMS AND CONDITIONS

Dec 11, 2014

This is a License Agreement between Muhammad Shahidul Islam ("You") and John Wiley and Sons ("John Wiley and Sons") provided by Copyright Clearance Center ("CCC"). The license consists of your order details, the terms and conditions provided by John Wiley and Sons, and the payment terms and conditions.

All payments must be made in full to CCC. For payment instructions, please see information listed at the bottom of this form.

License Number	3525840358582
License date	Dec 11, 2014
Licensed content publisher	John Wiley and Sons
Licensed content publication	Angewandte Chemie International Edition
Licensed content title	Gemini Surfactants as New, Low Molecular Weight Gelators of Organic Solvents and Water
Licensed copyright line	© 1998 WILEY-VCH Verlag GmbH, Weinheim, Fed. Rep. of Germany
Licensed content author	Reiko Oda,Ivan Huc,Sauveur J. Candau
Licensed content date	Dec 17, 1998
Start page	2689
End page	2691
Type of use	Dissertation/Thesis
Requestor type	University/Academic
Format	Print and electronic
Portion	Figure/table
Number of figures/tables	1
Original Wiley figure/table number(s)	Figure-0
Will you be translating?	No
Title of your thesis / dissertation	Characterization of Counter-ion Effects of Gemini Surfactants and In Vitro Studies of Transfection Efficiency for Gene Therapy in Ovarian Cancer
Expected completion date	Dec 2014
Expected size (number of pages)	200